A.A. Molenaar

STRUCTURAL PERFORMANCE AND DESIGN OF FLEXIBLE ROAD CONSTRUCTIONS AND ASPHALT CONCRETE OVERLAYS

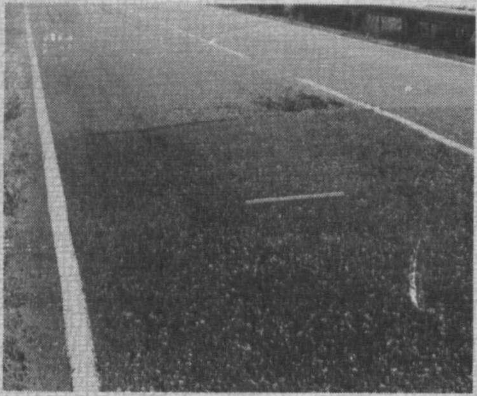

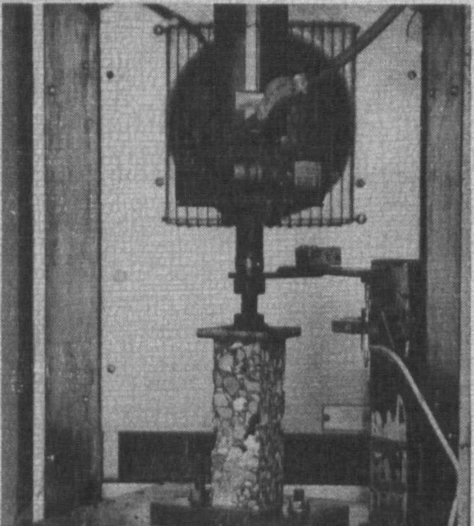

STRUCTURAL PERFORMANCE AND DESIGN OF FLEXIBLE ROAD CONSTRUCTIONS AND ASPHALT CONCRETE OVERLAYS

PROEFSCHRIFT ter verkrijging van
de graad van doctor in de
technische wetenschappen
aan de Technische Hogeschool Delft,
op gezag van de rector magnificus,
prof. ir. B.P.Th. Veltman,
voor een commissie aangewezen
door het college van dekanen
te verdedigen op
dinsdag 10 mei 1983
te 16.00 uur door
ANDREAS ADRIANUS ANTHONIUS MOLENAAR
civiel ingenieur
geboren te Hoorn

Dit proefschrift is goedgekeurd door
de promotor: PROF. IR. H.J.Th. SPAN
en de copromotor: PROF. R.L. LYTTON, BSc MSc PhD

Acknowledgement

The author wishes to thank all the members of the Laboratory for Road and Railroad Research for their collaboration, support and encouragement. Especially the interest, valuable support and stimulating discussions of ir. Ch.A.P.M. van Gurp are gratefully acknowledged.
The author also likes to thank all the students who worked on the "Pavement Management" Project for their enthusiasm and contributions.
The Board of the Delft University is gratefully acknowledged for the special grant ("Beleidsruimte") by which part of the research could be financed.
Furthermore the author likes to thank mrs. Jongeleen, mrs. Kros and mrs. Zalm for their careful typing of the manuscript.
Last but certainly not least, the author likes to thank his wife and children for their love, support, inspiration and remarkable good humour during the 1½ year he was working on the manuscript.

Samenvatting

Dit rapport beschrijft een systeem voor de dimensionering, evaluatie en herdimensionering van flexibele verhardingsconstructies. Dit systeem is opgedeeld in een vijftal subsystemen welke zijn:

a. een systeem waarmee wegverhardingen kunnen worden gedimensioneerd en waarmee de achteruitgang van de structurele conditie (draagcapaciteit) in de tijd kan worden beschreven,
b. een systeem van visuele inspectie waarmee de conditie van wegverhardingen kan worden vastgesteld en op basis waarvan onderhoud kan worden gepland,
c. een systeem waarmee, onder gebruikmaking van deflectiemetingen, de structurele restwaarde van wegconstructies kan worden bepaald,
d. een systematiek voor de bepaling van de breuk en scheurgroei eigenschappen van asfaltbetonmengsels,
e. een dimensioneringsysteem voor overlagen.

De subsystemen zijn gebaseerd op een theoretische analyse van elastische meerlagensystemen, op in situ metingen aan wegverhardingen, en op een karakterisering van de breuk en scheurkarakteristieken van asfaltmengsels met behulp van principes uit de breukmechanica.
Bij de ontwikkeling van de subsystemen is speciaal aandacht geschonken aan de praktische toepasbaarheid ervan. Tevens is nadruk gelegd op de wijze waarop deze subsystemen kunnen worden gebruikt bij de planning van onderhoudsmaatregelen zowel naar aard als in de tijd.
Elk subsysteem is in een apart hoofdstuk beschreven. Verder is voor een zodanige rapportagevorm gekozen dat de hoofdstukken onafhankelijk van elkaar kunnen worden gelezen.
In het hierna volgende zal derhalve het rapport hoofdstuksgewijs worden samengevat.

Hoofdstuk 3 beschrijft een *nieuwe ontwerpmethodiek voor flexibele verhardingsconstructies*. Deze methode is gebaseerd op een karakterisering van de draagcapaciteit van wegverhardingen met behulp van de equivalente laagdikte theorie van Odemark, en op relaties welke zijn ontwikkeld tussen aan de ene kant de equivalente laagdikte en aan de andere kant de maximale rek in bitumineuze lagen van wegconstructies ten gevolge van een aslast van 100 kN.
Daarnaast is een model ontwikkeld waarmee de *achteruitgang van de structurele conditie van de gehele verharding* kan worden beschreven. Dit model is op zijn juistheid gecontroleerd met behulp van in situ metingen aan de draagcapaciteit van wegverhardingen.
Verder is een model ontwikkeld waarmee de *toekomstige permanente deformatie (spoorvorming)* van wegverhardingen kan worden bepaald.
Het hoofdstuk besluit met een aantal voorbeelden waarmee de modellen en methoden worden geïllustreerd.

Hoofdstuk 4 beschrijft allereerst het *visueel inspectiesysteem* dat in deze studie is gebruikt teneinde de conditie van wegverhardingen en de achteruitgang ervan in de tijd vast te kunnen leggen. Daarna is ingegaan op de *gedragsmodellen* welke op basis van inspectieresultaten zijn opgesteld. Hiervoor zijn inspectiedata gebruikt zoals die over een periode van vijf jaar op een aantal wegen in de provincie Zuid Holland zijn verzameld.
Verder zijn *normen* ten aanzien van de nog toelaatbare verhardingsconditie gegeven. Deze normen zijn gerelateerd aan het risico voor extra onderhoud ten gevolge van winterschade.
Tot slot is aangegeven hoe het inspectiesysteem tezamen met de gedragsmodellen kan worden gebruikt in de *planning van het onderhoud*. Een en ander is geïllustreerd met behulp van voorbeelden.

In *hoofdstuk 5* is beschreven hoe de *structurele conditie-index* en de *structurele levensduur* van wegverhardingen kan worden bepaald met behulp van *deflectiemetingen*. In dit hoofdstuk is aangetoond dat de beschikbaarheid van gegevens met betrekking tot de verkeershistorie in termen van gepasseerd aantal equivalente 100 kN enkel assers geen absolute voorwaarde is om de restlevensduur te kunnen berekenen.
Verder is aangetoond op welke wijze de *snelheid van achteruitgang van de structurele conditie*, of met andere woorden de vorm van het structurele gedragsmodel, kan worden bepaald met behulp van deflectiemetingen.
Veel aandacht is verder geschonken aan die condities waarbij de structurele conditie-index niet met behulp van deflectiemetingen kan worden bepaald. Getoond is hoe in voorkomende gevallen deze index uit de visuele inspectieresultaten kan worden berekend.
Een model is gepresenteerd waarmee de *toekomstige permanente deformatie (spoorvorming)* onder gebruikmaking van *deflectiemetingen* kan worden bepaald. Naast een min of meer klassieke methode, is een meer algemeen toepasbare methodiek gepresenteerd waarmee een in situ model voor de permanente deformatie kan worden opgesteld.
Ook dit hoofdstuk is afgesloten met een aantal voorbeelden.

In *hoofdstuk 6* zijn de resultaten gepresenteerd van een studie naar de *breuk en scheurgroeikarakteristieken van asfaltbetonmengsels*. In de inleiding van dit hoofdstuk is aangegeven dat de problematiek van reflectiescheuren in wegverhardingen alleen naar behoren kan worden geanalyseerd met behulp van principes uit de breukmechanica. Vervolgens is een korte beschrijving van deze principes gegeven, waarna is ingegaan op de modellen waarmee de scheurgroei kan worden beschreven. Speciale aandacht is hierbij gegeven aan de theorie van Schapery. Met behulp van deze theorie is aangetoond dat de constanten uit de scheurgroeirelatie van Paris kunnen worden bepaald met behulp van nomogrammen en eenvoudige statische proeven.
Verder zijn in dit hoofdstuk de resultaten gegeven en besproken van de uitgevoerde breuktaaiheids en scheurgroei-experimenten. Aangetoond is dat er een grote verwantschap bestaat tussen de constanten uit de op de aangebrachte spanning cq rek gebaseerde vermoeiingsrelaties en de constanten uit de scheurgroeirelatie.
Tot slot is getoond hoe de *constanten uit de scheurgroeirelatie* kunnen worden bepaald met behulp van *nomogrammen* voor de berekening van de mengselstijfheid, en *splijtproeven*.

De methoden die zijn ontwikkeld voor de dimensionering van *overlagen welke al dan niet zijn gehecht aan de onderliggende constructie* zijn beschreven in *hoofdstuk 7*. Aangetoond is dat de dimensionering van niet gehechte overlagen gebaseerd moet zijn op de rek welke optreedt onderin de overlaag. Tevens is getoond dat bij toepassing van dit type overlaag, de reductie van het rekniveau in de bestaande constructie slechts beperkt is.
Bij het ontwerpen van een aan de bestaande constructie *gehechte overlaag* moet onderscheid worden gemaakt in de dikte die nodig is om een bepaalde *rekreductie in de bestaande constructie* te realiseren, en in de overlaagdikte welke nodig is om *vroegtijdig doorscheuren (reflectiescheuren) van de overlaag* te voorkomen.
Alle drie ontwerp opties zijn geïllustreerd met behulp van een voorbeeld.

Table of Contents

Chapter 1

INTRODUCTION AND SCOPE OF THIS STUDY

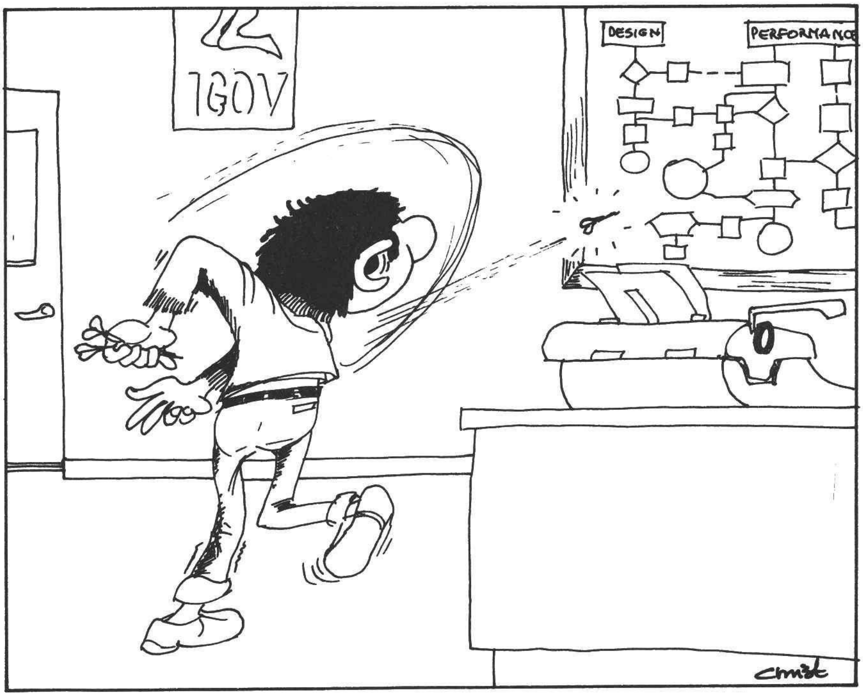

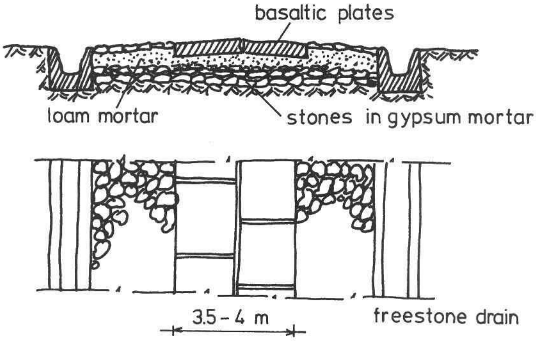

Figure 1.1 *Example of Pavements built on Crete during the Monoian Period*

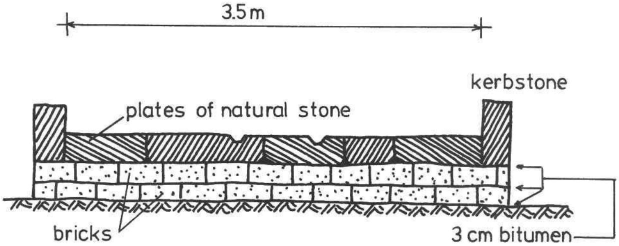

Figure 1.2 *Construction of the Procession Road to the Isjtar Temple*

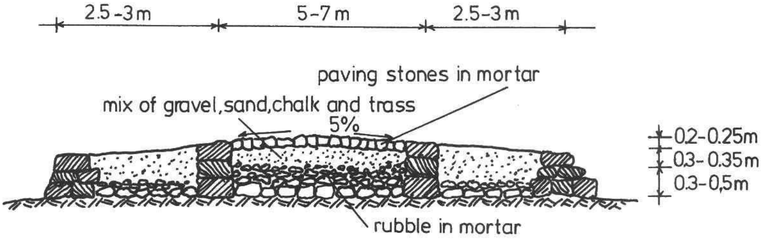

Figure 1.3 *Road Construction as built by the Romans*

1.1 Introduction

From the beginning of mankind, transportation has been a main aspect in human live. Communication, trade and wars between nations would not have been possible without it.

Already in the early days, mankind recognized the importance of a paved transportation surface. Some excellent examples of these early pavements will be given here.
Figure 1 for instance shows the pavements built on Crete during the Minoian period (2600 - 1150 B.C.). Figure 2 shows the construction used for the procession road to the Isjtar temple of Assoer as built by Nebuchadnezzer II (605 - 562 B.C.). Finally figure 3 shows the famous road construction as built by the Romans. It should be noted that these pavements were already remarkably well designed. The Roman pavements are, in five aspects, an improvement of the other ancient pavements.

a. the application of wooden mattresses under the stone base in marshy areas
b. the heavy construction layer which consisted of rubble, debris of bricks, and gravel; these materials were used in such a way that the fine materials were used in the upper part of the layer, while the coarse materials were used in the lower part.
c. the stone base was luted by means of loam or chalk mortar
d. the paving stones were of high durability
e. the types of construction were standardized over the entire Roman empire.

In the modern western world, one accepts the existance of a well developed transportation system as something normal. Often it is forgotten that the social, cultural and economic society would collapse if no road transportation would be possible.
In the developing countries, road transportation is even more important since there the existance of this type of transportation very often means whether or not one is able to survive.

Concentrating oneself to the Netherlands, one could ask: "what is the size of the road network", "what is its value", and "how much does it cost to keep it on an acceptable level of service".
The information needed to answer these questions was obtained from |2|.
Tables 1.1 and 1.2 give an indication of the size of the road network in the Netherlands. It should be noted that the building and maintenance of the state roads is fully subsidized by the government. This is partly the case for the secondary and tertiary road network, while no governmental subsidy is obtained for the other roads (city roads etc.).
Table 1.3 shows which authorities are responsible for the maintenance of certain parts of the road network. Table 1.4 shows the amount of money which has been spent by the various authorities on the maintenance of the road network in 1980. Table 1.5 gives an indication of how this maintenance budget has been devided over the various items.

Little information is available on the replacement value of the road network in its present state. However an estimation made by Wester |3| does indicate that this value might be over 100 billion guilders (this includes replacement of pavements, bridges and flyovers but not of embankements and other earth works).

From the above mentioned arguments it will be obvious that one should design and maintain pavements in such a way that a safe and fast public transportation surface is guarenteed over a large number of years.

Table 1.1 Size of the Road Network in the Netherlands

Paved Area	Size $\|km^2\|$
Roads	520
Residential Areas x	3
Bicycle Lanes	110
Parking Lots	15
Other	2
Total (2 % of country area)	650

x by these "woonerven" are meant

Table 1.2 Length of the Road Network in the Netherlands

Road System		Length |km|
State Roads (Total)		4562
State Highways	1755	
Secondary Roads		3494
Tertiary Roads		5133
Other		80356
Unpaved		15800
Total		109345

Table 1.3 Overall Picture of the Authorities responsible for the Maintenance of the Road Network

	Percentage of Total Area to be Maintained
State	9.6
Provinces	12.1
Cities and Others	78.3

Table 1.4 Maintenance Budget in 1980

	Guilders x10^6
State	506
Provinces	202
Cities	1364
Others	96
Total	2168

Table 1.5 Maintenance Budget as devided over the various Items

	Percentage
Overlays and Surface Courses	30.3
Illumination	14.5
Traffic Signs	6.7
Bridges	6.2
Other	42.3

Due to the complexity of the problem, pavement design and planning of maintenance has always heavily relied on the experience and skill of the highway engineers in charge.

The recent economic recession however has put large demands on these engineers in this sense, that they have to allocate the available budget even more precisely than they did before. Furthermore the engineers must be able to give a good argumentation why a certain budget is needed, and what the effects are in terms of loss in safety and accelerated deterioration if the budget request is not granted. This will only be possible if one is able to determine the behavior of new designs, existing pavements and the effect of maintenance activities like for instance overlays.

Unfortunately the existing methods and techniques for designing pavements and assessing maintenance priorities are not developed so far that the highway engineer can solve the above mentioned problems completely by means of these methods and techniques.

The shortcomings of the existing methods have been recognized at the Chair of Highway Engineering of the Delft University in 1974. This has resulted in the initiation of two research programs:

a. a research program on the development of a pavement management system
b. a research program on the development of structural performance models and a (overlay) design method for flexible road constructions.

The results of this latter research program are presented in this report.

1.2 Scope of the Study

This Study is dealing with the *"Structural Performance and Design of Flexible Road Constructions and Asphalt Concrete Overlays"*. The words "flexible road constructions" are used instead of "flexible pavements" since these latter might be understood as pavements that are mainly built up from asphalt concrete layers. This has certainly not been the intention of this study. From the beginning of the research project, emphasis has been placed on the importance of covering also pavements that are mainly built up from unbound granular materials, with a thin bituminous bound top layer, the main purpose of which is to seal the granular base layers. This latter type of pavement was the most important construction type a few decades ago and it is still used for farm to market roads. Although this type of pavement has mainly been replaced by pavement types having thicker asphalt layers, one still has to deal with it in the planning and design of maintenance and reconstructions.

Now attention is paid to the various aspects covered by this report.

a. First of all a *new design method* is developed. This method is, like all existing mechanistic design methods, based on a theoretical analysis of three layered pavement systems. This analysis is made assuming that the pavement materials behave like linear elastic, homogeneous and isotropic materials. Normally such analyses are made by means of computer programs to determine the stresses and strains in the pavement system due to wheel loads.
Although well known and well accepted techniques have been used, the method is considered to be new since equations have been developed which allow the assessment of stresses and strains in the pavement in a very simple way. These types of equations have not been presented before.
Furthermore the method is considered to be new since it incorporates a model which enables the determination of the pavement strength deterioration in time. This model has been tested and validated by means of in situ measurements on pavement strength.
The development of this model is thought to be one of the major achievements of this study, because now the highway engineer will have a tool that can be used to determine when maintenance activities should be carried out. In other words, a tool has been provided by which pavement designs can be made in relation to future maintenance.
The development of the new design method is described in chapter 3.

b. The next item which is dealt with in this report is the *visual condition survey of pavements and the planning of maintenance activities by means of the results of these surveys*. It needs no argumentation that one should perform condition surveys regularly in order to determine whether or not the construction behaves as designed. The results of these surveys can be used to make time projections on when predefined minimum acceptance levels will be reached. In other words, the results of these condition surveys can be used in the planning of maintenance and rehabilitation.
The visual condition survey system as used in this research program is described. It is also shown how visual condition performance models have been developed from data which were gathered during a five year period on a number of roads. These performance models are thought to be another major

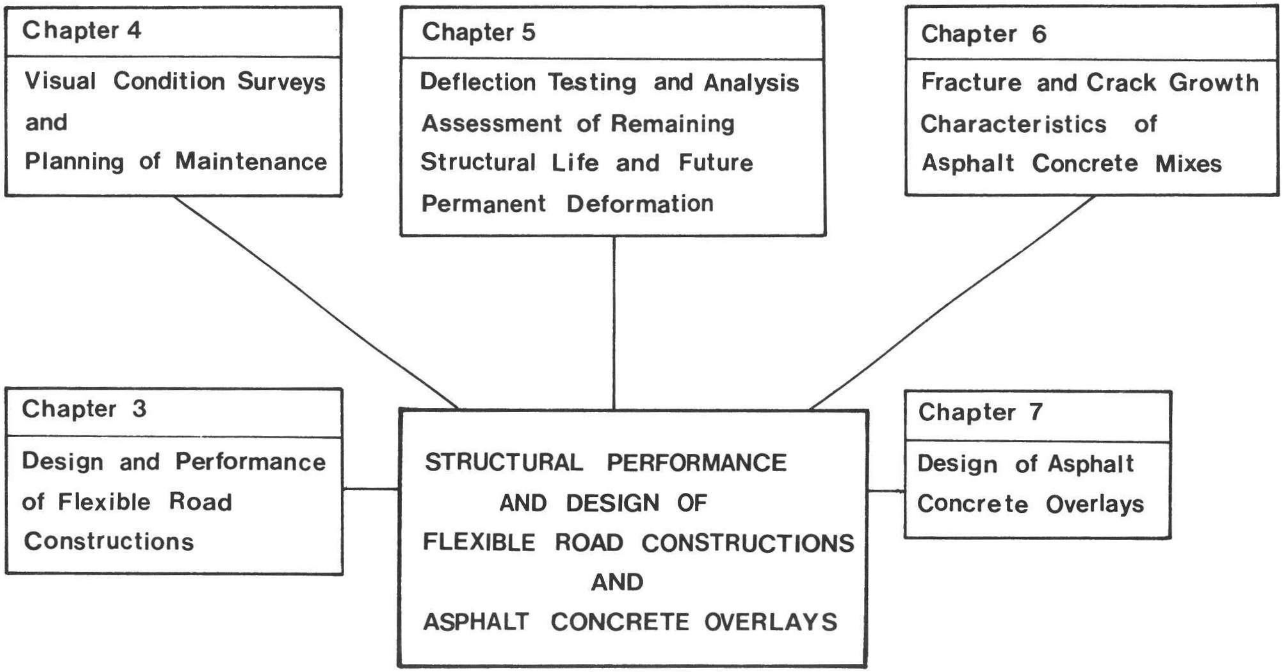

Figure 1.4 *Schematical Representation of the Organisation of this Report*

accomplishment of this study since by these it is possible to predict the future visual conditions of pavements.
It is shown that planning of maintenance in time can be done rather easily by means of these models and the empirically developed minimum acceptance levels.
Since the adopted survey technique as well as the performance models do have a large practical value, this part of the study should be of special interest to those engineers who are in charge of the planning of maintenance activities.
Chapter 4 describes this part of the study.

c. Although visual condition surveys are a very simple and powerful tool to assess the pavement condition, deflection measurements and material testing need to be performed in order to obtain a detailed insight into the structural pavement condition.
One could state that visual condition surveys should be used as a broad survey technique for a pavement network, while deflection measurements and material testing are diagnostic survey techniques which should be used on sites selected by means of the visual condition surveys.
Therefore a considerable amount of attention has been paid in this study to *deflection measurements and the assessment of the remaining structural life of the pavement by means of these measurements*. It is shown how the structural condition index of the pavement as well as the shape of the curve which describes the structural performance, can be assessed by means of these measurements.
An important result of this study is that for the remaining life assessment, the traffic history in terms of applied number of load repetitions, needs not to be known in absolute values. This is in contradistinction with exisying methods where such information is a vital part in the calculation of the remaining life.
Furthermore attention is paid to those conditions where it is troublesome to assess the remaining structural life and the actual structural condition by means of deflection measurements. It is shown how in these conditions, both values can be determined from the results of visual condition surveys.
This study is not only dealing with the assessment of the structural condition in terms of cracking, but also with the assessment of the condition in terms of permanent deformation. It is shown how future permanent deformation can be calculated from deflection measurements. Besides a rather classical method a new, more generally applicable, method is presented.
Chapter 5 describes this part of the study.

d. As mentioned before, material testing is an important part in the structural evaluation of pavements. In this study special emphasis is placed on the *fracture and crack growth characteristics of asphalt concrete mixes*.
It is discussed that especially the cracking behavior of overlays is hard to describe by means of the classical approach which is based on limiting the maximum tensile strain in the asphalt layer(s) of both the existing pavement and the overlay.
Furthermore a discussion is given on the applicability of the fracture mechanics principles to solve the reflection cracking problem of overlays.
Then the report continues with a description of, and a discussion on the results of fracture toughness and crack growth tests as carried out on several asphalt concrete mixes.
A major accomplishment of this study is thought to be the equations which have been developed to assess the constants in the Paris' crack growth law from nomographs and simple static tests. It is thought that these relations do promote the application of fracture mechanics for overlay design purposes. In chapter 6, this part of the study is described.

e. After it has been shown how pavements can be designed, how their condition can be monitored, how maintenance can be planned, and how the remaining life can be assessed, attention is paid to the design of overlays.

A *new overlay design method* is presented in which two types of overlay are discerned viz. the unbonded and bonded overlay.
A calculation method is provided for the assessment of the strain level in the overlay as well as in the existing structure.
Considering the bonded overlays, two approaches of design are discerned. The first one is based on the preservation of the total construction. Here the aim of the overlay is to reduce the stress and strain level in the existing pavement.
The second approach is based on the reduction of reflection cracking in the overlay due to wheel loads. In this approach the results of the material testing performed to determine the crack growth characteristics of asphalt concrete mixes are used.
The overlay design method is described in chapter 7.

1.3 Organization of the Report

From the description of the scope of the various chapters of this study, it can be observed that five main aspects are discerned in the structural performance and design of flexible road constructions and asphalt concrete overlays. These aspects are all strongly interrelated with each other; nevertheless they can be treated as separate subsystems of the overall design and performance system.
In order to promote the readableness of the report, the author has decided to write it in such a way that each aspect is covered in a separate chapter. Furthermore the various chapters have been written in such a way that they can be read independently from the other chapters. Therefore it is not necessary for the reader who is interested only in one aspect of this study, to go through the entire report
Figure 1.4 schematizes the organization of this report.

References

|1| SCHREIBER, H.
From Caravan Route to Highway (in Dutch)
Elsevier Publishing Comp.
Amsterdam - 1961

|2| CENTRAL BUREAU OF STATISTICS
Statistics on the Road Network (in Dutch)
Staatsuitgeverij
the Hague - 1982

|3| WESTER, K.
Personal Communication
Study Centre for Road Construction
Arnhem - 1982

Chapter 2

PAVEMENT CONSTRUCTIONS, ENVIRONMENTAL CONDITIONS AND EXAMPLES OF PAVEMENT PERFORMANCE IN THE NETHERLANDS

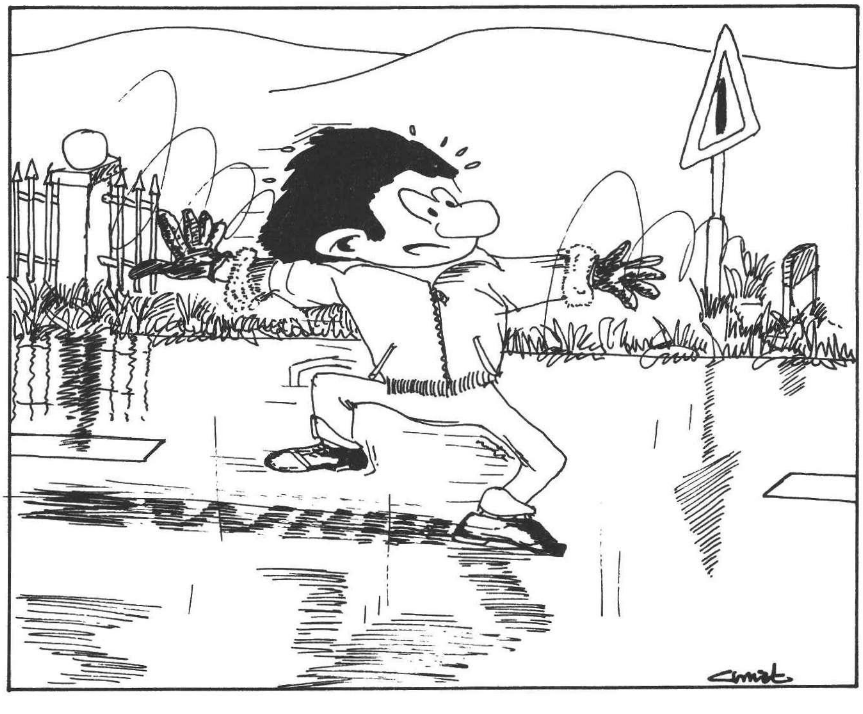

TABLE OF CONTENTS

2.1 Introduction

Before one goes into the development of pavement design and performance models, one needs to have some general information on, e.g. subsoil conditions, pavement construction types, environmental conditions, traffic etc..
The intention of this chapter is to give this type of information and to provide in this way a background for the theoretical aspects of pavement design and performance which will be dealt with in the chapters to follow.
The information that will be given, can be considered to be typical for the conditions that were observed in the province of Zuid Holland of the Netherlands.

2.2 Types of Construction

Most of the data that are used in this study to develop the performance models described in the various chapters of this report, are obtained on pavement sections of the road network of the province of Zuid Holland. The location of the sections is shown in figure 2.1, while their constructions are given in figure 2.2
As can be observed from this latter figure, this report deals with a wide variety of constructions and materials.
In the recent years however, the province of Zuid Holland is standardizing the construction for new pavements to the one with a 0.3 m thick base of blast furnance slag, 0.07 m gravel sand asphalt, 0.04 m open asphaltic concrete, and a 0.04 m thick surface course of dense asphaltic concrete |1|.

In the following part of this section, information is given on the characteristics of the materials used in the various parts of the pavement, and the specifications set for them.

2.2.1 Subsoil

Figure 2.3 is a schematic geotechnical profile through the Netherlands. The profile is representative for the conditions one encounters going from the Hague eastward to the German border. One will notice that in the western part of the Netherlands (left hand side of figure 2.3), the subsoil consists of a wide variety of weak layers (notice the low cone penetrometer values).

In order to improve the bearing capacity of the subsoil, usually a sand layer with a thickness of about 1 m is applied. For secondary and less important roads, this sand layer is placed directly on the weak subsoil. Fore state highways, the weak layers are normally dredged out and replaced by a hydraulic sand fill. This sand layer can be assumed to be the pavement subgrade.

As can be expected, the application of a sand layer on the weak subsoil will result in settlements. In order to assess the amount of settlement, commonly use is made of Koppejan's formula |2|:

$$S_t = h\left(\frac{1}{C_p} + \frac{1}{C_s} \log t \right) \log\left(\frac{P_i + \Delta P}{P_i} \right) \qquad \text{eq. 2.1}$$

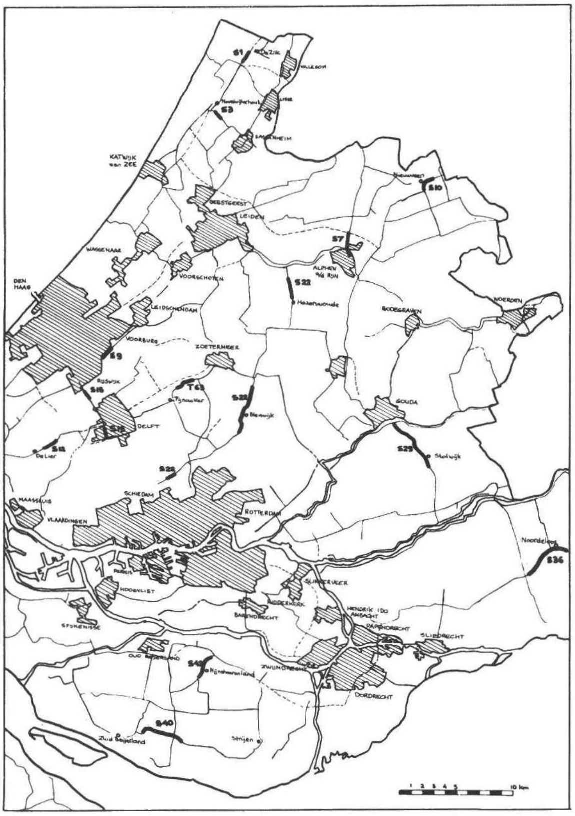

Figure 2.1 *Location of the Test Sections in the Province of Zuid Holland*

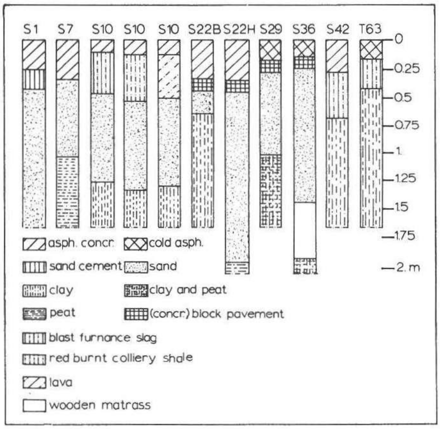

Figure 2.2 *Construction of the Test Sections*

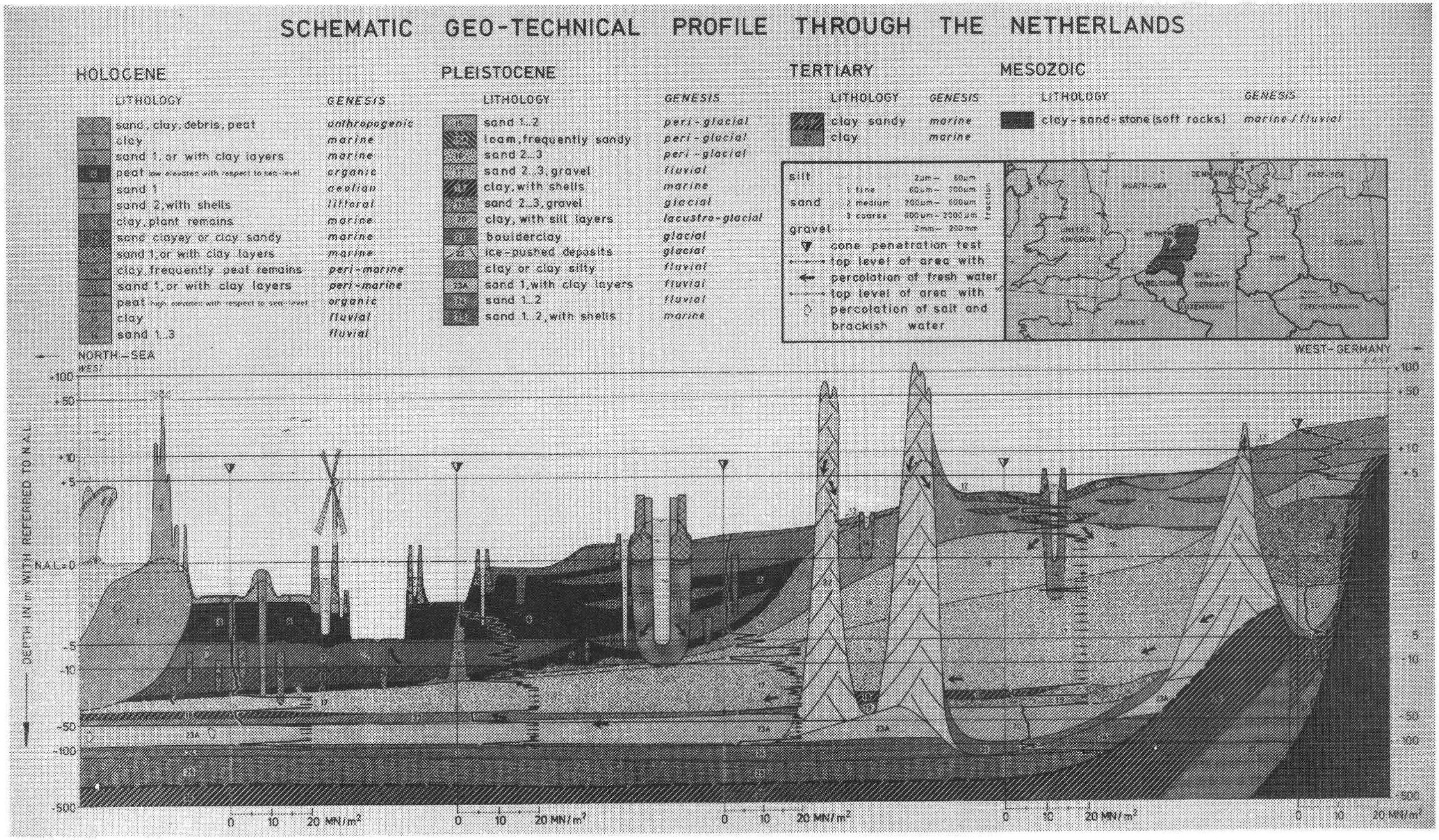

Figure 2.3 Geo-Technical Profile through the Netherlands (courtesy Lab. for Soil Mechanics)

where S_t = settlement at time t |m|
h = thickness compressible layer |m|
C_p = constant which indicates the magnitude of the primary settlement (consolidation)
C_s = constant which indicates the magnitude of the secondary settlemant (creep)
P_i = soil pressure before the overload is applied
t = time |days|
ΔP = increase in soil pressure due to the overload

Typical values for C_p and C_s are given in table 2.1.

Table 2.1 Typical Values for C_p and C_s

	C_p	C_s
Clay	5 - 10	20 - 100
Peat	2 - 5	10 - 20

Normally the groundwater table is rather high. Since most roads are built in polders, the groundwater level is controlled artificially and shows only little variation during the year. Typical information on the groundwater table is given in table 2.2.

Table 2.2 Variation of the Groundwater Table during the Year in the Region of the S_{10} Road Sections

	Depth below Ground Level |m|
Summer (June, July, August, Sept.)	0.7 - 1.0
Winter (December, January, Febr.)	0.2 - 0.4

Of course these subsoil conditions have their implications on the selection of the pavement type. In general it can be stated that the weaker the subgrade, the more flexible the pavement structure should be. This means that very often concrete block pavements or pavements built up from cold asphalt layers (cold asphalt exhibits a large flexibility) are used in areas with a very weak subsoil. Some of this is reflected in the constructions shown in figure 2.2.

2.2.2 Subgrade

As mentioned before, the subgrade usually consists of a sand layer with a thickness of about 1 m. This sand is obtained by means of suction dredging or dry excavation. Table 2.3 gives an overall picture of the sands which are available in the Netherlands for road construction |3|.
Typical information on gradation, CBR values, and moisture - density relations of the Oosterschelde estuarine sand, which is often used in the western part of the Netherlands, is given in figure 2.4.

The sand used in the subgrade should fulfil the specifications set by the State Authority for Roads, Bridges, and Waterworks (Rijkswaterstaat) |4|. Specifications are developed for the gradation, degree of compaction, and amount of organic material.
Although these specifications are developed for state highways, they are also used by the provincial and city road authorities.

Table 2.3 Classification and Identification of Available Sands

no.	place of origin	type of sand (classification according to the genesis)	manner of winning (suction dredging: wet; dry excav.: dry)	parameters on which designation and classification are based: coarseness modulus	loam percentage	uniformity coefficient of sand fraction
1	Echteld (test sections R.W. 15	river sand	wet	1.66	1.7	2.00''
2	Angerlo	river sand	dry	1.41	2.8	2.54'''
3	Oosterschelde	estuarine sand	wet	0.73	0.3	1.71'
4	Medemblik	marine sand	wet	0.78	1.0	1.65'
5	Deurne	aeolian sand	dry	0.10	20.0	2.00''
6	Donderen	aeolian sand (mixture)	dry	0.31	21.7	3.12'''
7	Voorthuizen	aeolian sand	dry	0.06	15.9	2.07'''

Note: ' poorly graded
'' moderately graded
''' well graded

Places of origin of the available sands

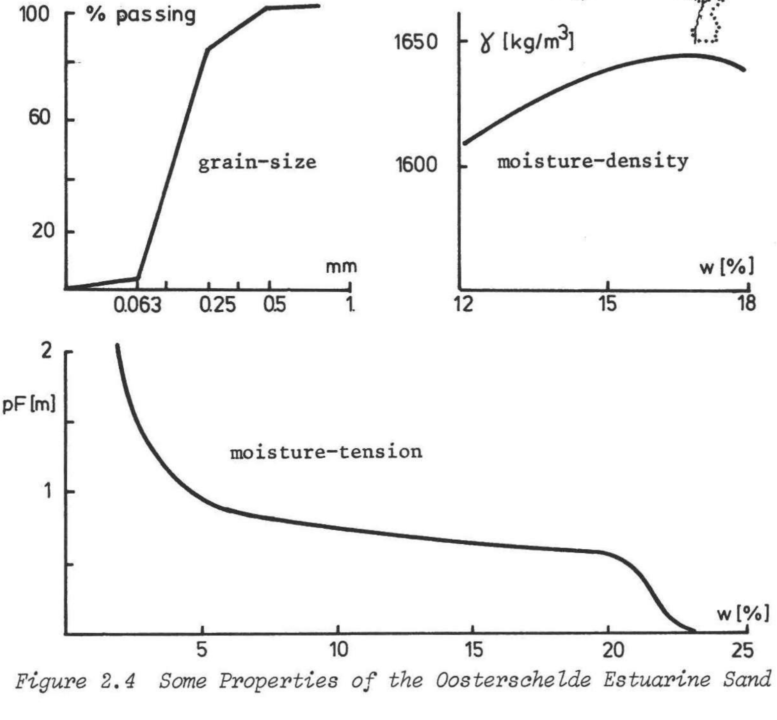

Figure 2.4 Some Properties of the Oosterschelde Estuarine Sand

2.2.3 Base

Distinction is made in the following base types:
a. unbound bases
b. unbound bases showing some cementation
c. cement bound bases
d. bituminous bound bases

Re a,b. The specifications set in |4| for the grainsize distribution of an unbound base and for unbound bases showing some cementation are given in table 2.4. For this latter base type also specifications are set for the degree of cementation in time.
No specifications are given for the required density and required CBR values.

Re c. In |4| specifications are given for the sand, cement, and water which is used in the preparation of cement stabilizied sand bases. Also specifications are given for the degree of compaction and compressive strength. These latter specifications are given in table 2.5.

Re d. Sand asphalt and gravel sand asphalt mixtures are used as bituminous bound base in pavement constructions. Again ref. |4| gives specifications for the bitumen type and content, the grainsize distribution of the granular material, and the degree of compaction. Also specifications are given for the mechanical properties of the mix. These specifications are related to 4 traffic classes.
Table 2.6 gives the traffic classes, while table 2.7 gives the required mechanical properties of the sand asphalt and gravel sand asphalt mixes.

2.2.4 Top Layers

Normally dense asphaltic concrete is used as top layer material. Open asphaltic concrete is another mix that is used in the upper part of bituminous road constructions. This type of mix is usually used as so called binder layer between the top layer and the bituminous base. Regularly it is used as a temporary top layer.
Reference |4| contains a set of specifications for the mechanical characteristics of these mixes. They are summarized in table 2.8.

2.3 Environmental Conditions

Environmental conditions have a large influence on the behavior of pavement systems. Temperature for instance, has a large influence on the stiffness of asphalt mixes. Temperatures below 0^oC will influence the behavior of the total construction if frost susceptible material is used in the base and/or subgrade (frost heave). During the following thaw period, weakening of the base and subgrade might occur.
Precipitation will influence the moisture conditions in the base and subgrade and in this way the deformation characteristics of these layers are influenced.
In this section, typical temperature and moisture data will be given for the Delft region.

2.3.1 Temperature

Figure 2.5 shows the annual air temperature variation as determined for the Delft region. The data presented are taken from |5| and are based on observations taken during the period 1931 - 1960.

Table 2.4 Specifications on Grainsize and Cementation of Unbound Bases

Nominal Grading	0/40		0/80		20/80	
On Sieve (Percentage by Mass)	min.	max.	min.	max.	min.	max.
C 90	-	-	0	10	0	10
C 45	0	10	-	-	20	50
C 31.5	-	-	10	40	-	-
C 16	10	40	-	-	90	-
C 8	-	-	40	70	-	-
C 4	40	70	-	-	-	-
2 mm	50	80	55	85	-	-
63 μm	92	-	92	-	92	-

Unbound Bases

Nominal Grading	0/40		0/60	
On Sieve (percentage by Mass)	min.	max.	min.	max.
C 90	-	-	-	-
C 63	-	-	0	10
C 45	0	10	-	-
C 31.5	-	-	-	-
C 22.4	-	-	10	40
C 16	10	40	-	-
C 8	-	-	-	-
C 4	30	70	35	75
2 mm	50	80	50	80

Unbound Bases showing some Cementation

Specification Degree of Cementation:
CBR after 7 days of hardening should be at least 125% of the CBR directly after preparation

Table 2.5 Strength Requirements for Cement Stabilized Bases

$\bar{\sigma}$ of cores prepared according to Proctor method	5 MPa (after 28 days of hardening)
σ_{min} of cores taken from base	1.5 MPa (after 90 days of hardening)

Note: $\bar{\sigma}$ = mean compressive strength, σ_{min} = minimum compressive strength

Table 2.6 Traffic Classes

Traffic Class	Traffic Intensity (mean number of vehicles per working day)	Number of Lanes
1	< 1000	1 or 2
2	1000 - 10000	2
	< 20000	4 or more
3	10000 - 20000	2
	20000 - 50000	4 or more
4	> 20000	2
	> 50000	4 or more

Table 2.7 Required Mechanical Properties of Base Course Mixes

	Traffic Class	1		2		3		4	
Mix Type	Mechanical Property	min.	max.	min.	max.	min.	max.	min.	max.
Sand	Marshall Stab. at 40°C |N|	4000	-	4000	-	5000	-	5000	-
Asphalt	Marshall Flow at 40°C |mm|	1.5	3.5	1.5	3.5	1.5	3.5	1.5	3.5
	Marsh. Quotient |N/mm|	2000	-	2000	-	2500	-	2500	-
Gravel	Marshall Stab. at 60°C |N|	3000	-	4500	-	5000	-	6000	-
Sand	Marshall Flow at 60°C |mm|	1.5	3.0	1.5	3.0	1.5	3.0	1.5	3.0
Asphalt	Marsh. Quotient |N/mm|	1500	-	2000	-	2500	-	3000	-

Table 2.8 Required Mechanical Properties of Top Layer and Binder Mixes

	Traffic Class	1		2		3		4	
Mix Type	Mechanical Property	min.	max.	min.	max.	min.	max.	min.	max.
Dense	Marshall Stab. at 60°C |N|	4000	-	5500	-	6500	-	7500	-
Asphalt.	Marshall Flow at 60°C |mm|	2.0	4.0	2.0	4.0	2.0	4.0	2.0	4.0
Concrete	Marsh. Quotient |N/mm|	1500	-	2000	-	2500	-	3000	-
Open	Marshall Stab. at 60°C |N|	4000	-	5500	-	6500	-	7000	-
Asphalt.	Marshall Flow at 60°C |mm|	2.0	4.0	2.0	4.0	2.0	4.0	2.0	4.0
Concrete	Marsh. Quotient |N/mm|	1500	-	2000	-	2500	-	3000	-

The temperature distribution in the pavement is not only influenced by the air temperature but also by the amount of solar energy. Figure 2.6 shows the variation of the solar energy during a summer day in July, in relation to different degrees of cloudiness.

The severity of a winter is usually expressed by means of the freezing index. This index is defined as the negative sum of the mean negative daily temperatures during the frost period.
An example of this index is given in figure 2.7 |6|. It should be noted that the winter of '78 - '79 was, according to Dutch circumstances, a severe winter while the winter of '62 - '63 was a very severe one.
Figure 2.8 |6| shows the freezing index which might occur once per 10 years.
Figure 2.9 |6| shows the frost penetration which might occur once per 50 years.

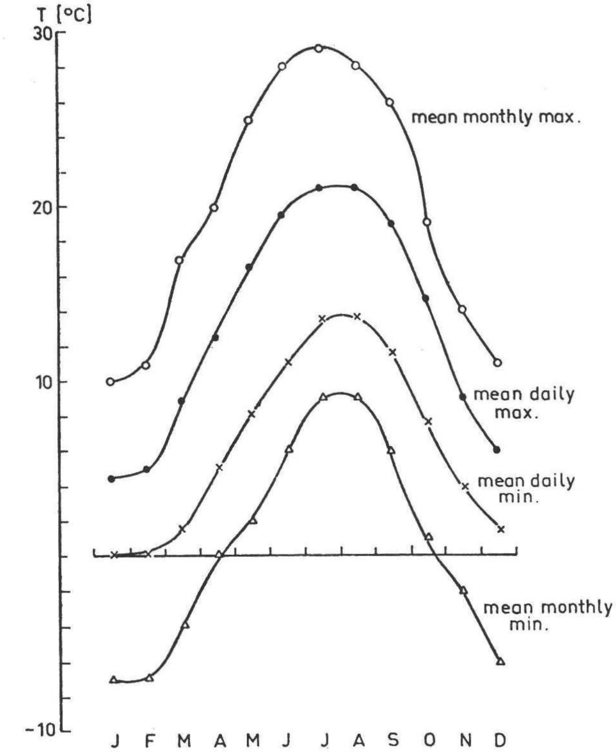

Figure 2.5 *Annual Temperature Variation*

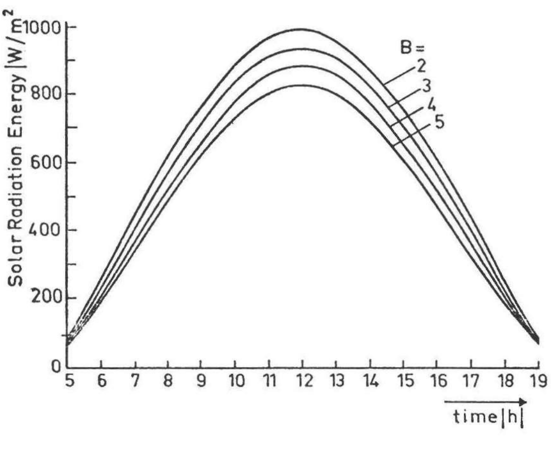

Figure 2.6 *Daily Variation of the Solar Radiation Energy during a Summer Day in July in relation to different Cloudiness Levels (B)*

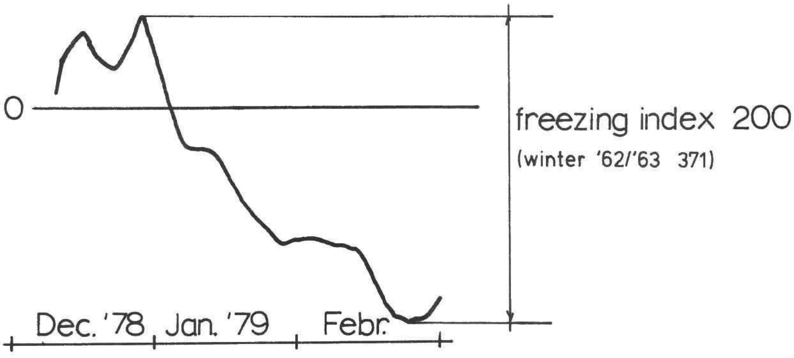

Figure 2.7 Freezing Index on the Airfield Deelen during the 1978-1979 Winter

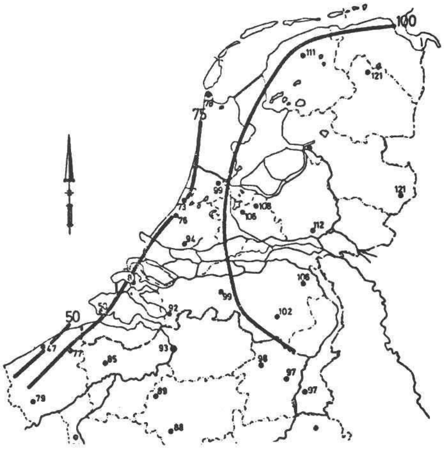

Figure 2.8 Freezing Index which might occur once per 10 years

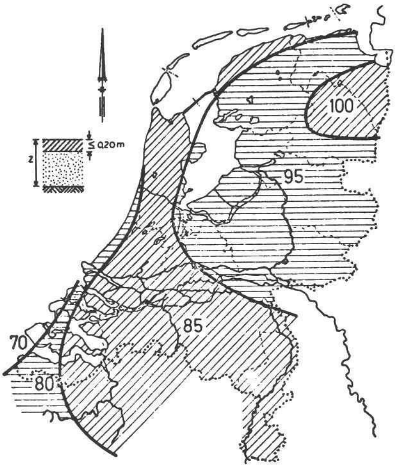

Figure 2.9 Frost penetration which might occur once per 50 year under pavements with an asphalt layer thickness of less than 200 mm

2.3.2 Precipitation

The variation of the moisture content of the base and subgrade will be influenced to a large extent by the precipitation and evaporation. Figure 2.10, which is obtained from data presented in |5|,shows the annual variation of the precipitation. Also the annual variation of the precipitation minus the evaporation |5| is given in figure 2.10. The effect of this difference on the subgrade modulus is illustrated in figure 2.11.

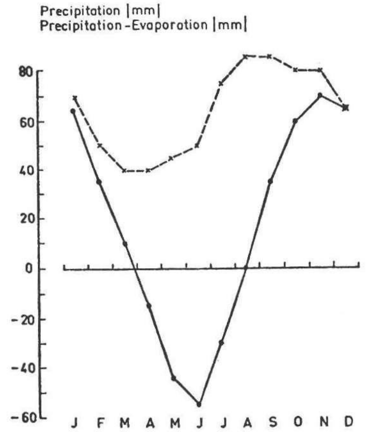

Figure 2.10 *Annual Variation of Precipitation and Precipitation minus Evaporation*

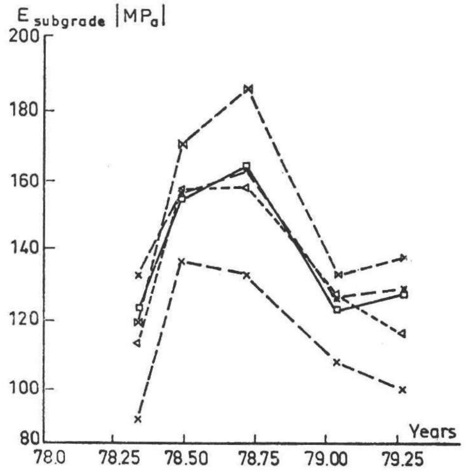

Figure 2.11 *Seasonal Variation of the Stiffness of the Sand Subgrade of the S_1 Sections*

2.4 Pavement Performance

As mentioned before, also some data on pavement performance will be given in this chapter in order to give the reader an idea of the type of data one is dealing with in this report.
Pavement performance is influenced by the following main factors:

a. skid resistance
b. road roughness
c. pavement strength

Re a. In the Netherlands, skid resistance is the most important maintenance criterion. Based on the results of a research program on the relation between the lack of skid resistance and traffic accidents, minimum skid resistance acceptance levels have been defined.
Each year the skid resistance of the state highways, the secondary, and partly the tertiary road network, is measured by the state road laboratory. Maintenance is applied on those sections where the skid resistance requirements are not met.

Re b. Although road roughness is regularly measured, it is seldom a cause for maintenance. In this respect it is doubted whether the present serviceability index which is used in other countries to determine maintenance needs, is applicable to Dutch conditions (as will be known, the present serviceability index is mainly determined by road roughness).

Re c. Pavement Strength is another major maintenance criterion. Although a lack of strength will ultimately influence the safety conditions, structural maintenance to restore the pavement strength is mainly performed to preserve the structural condition and so the invested capital.

This report is only dealing with the structural performance of pavements, therefore no examples will be given of the deterioration of the skid resistance and the development of road roughness in time.

The deterioration of pavement strength can be observed by means of visual condition surveys, and deflection measurements. In the remaining part of this section examples will be given of the structural deterioration of pavements as determined by means of these two evaluation techniques.

2.4.1 Structural Deterioration as observed by means of Visual Condition Surveys

In chapter 4 of this report, the visual condition survey technique and the processing of the data obtained in this way, will be discussed extensively. Here these items will be discussed in a more general way.

A large number of defects are observed on pavements. These defects are categorized into three classes.

a. surface defects
b. cracking
c. permanent deformations

Re a. Typical surface defects are raveling (loss of aggregate particles from the pavement surface), bleeding (appearance of a bitumen film at the top of the pavement surface), and potholes. These types of defects are influencing the safety and riding comfort conditions of the pavement. There appearance is not necessarely a sign of structural deterioration.

Re b. Basicly three types of cracking can be discerned. They are: longitudinal, transverse, and alligator cracking. Transverse cracking is mainly due to environmental effects. Longitudinal and alligator cracking are usually the result of the detrimental effect of traffic loads.

Re c. Permanent deformations of the pavement are a result of traffic loads (rutting and corrugations) and uneven settlements of the subsoil. The latter type of deformation can be easily recognized because of its long wave length.

In order to be able to quantify and qualify the observed defects systematically, several condition survey techniques have been developed. In most of these techniques, the combinations of severity and extent are transformed into deduct points. Such a system was also used in this study.
Figures 2.12 and 2.13, give examples of the cracking development and the deterioration of the overall pavement condition, as determined for a specific road section. These types of data were the basis for the development of the visual condition performance model which is described in chapter 4.

2.4.2 Structural Deterioration as observed by means of Deflection Measurements

In the Netherlands, deflection measurements are taken by means of four devices. They are:

a. Benkelman beam
b. Dynaflect
c. Lacroix Deflectograph
d. Falling weight deflectometer

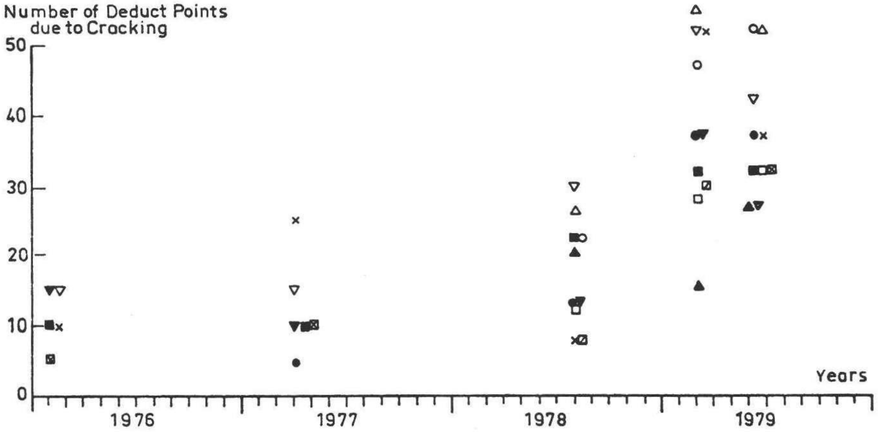

Figure 2.12 *Deterioration in terms of Cracking of the S_{10} Road Sections*

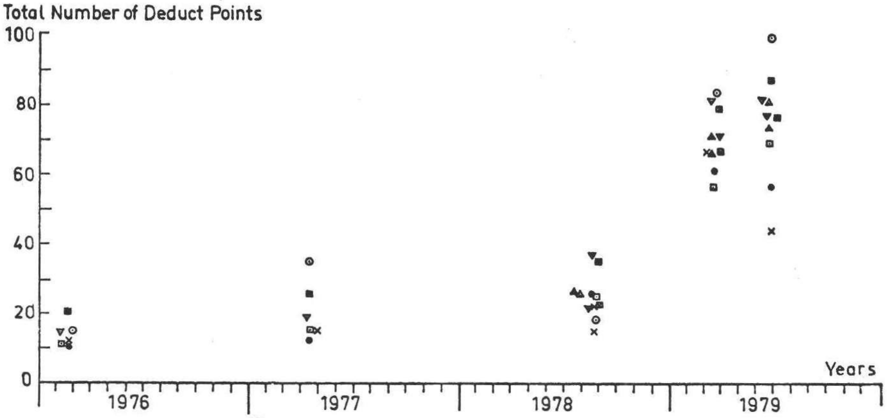

Figure 2.13 *Deterioration of the Overall Condition of the S_{10} Road Sections*

A detailed description of these devices can be found elsewhe~e e.g. |7|. Although these devices do measure the same thing, there are marked differences in the results of the measurements. These differences can be attributed to differences in load magnitude and duration of the load pulse. It will be obvious that using one type of device in conjunction with another will result in transformation problems. Therefore the author believes that if one has selected a type of device, one should stay with it.

Nevertheless it might sometimes be necessary to use different types of device next to each other. In that case one needs to have relations that describe the correlation between the devices. Figures 2.14 |8|, 2.15 |9|, and 2.16 |9|, give examples of these relations as determined by several researchers.

In general these relations show a considerable amount of scatter, and sometimes hardly any relationship can be observed. This leads to the conclusion that one has to be very careful in using correlation equations to transform data obtained by one device into data which would be obtained if another device had been used.

In this study use has been made of a falling weight deflectometer. By means of this device, a large number of measurements have been performed on the pavement sections shown in figure 2.2.

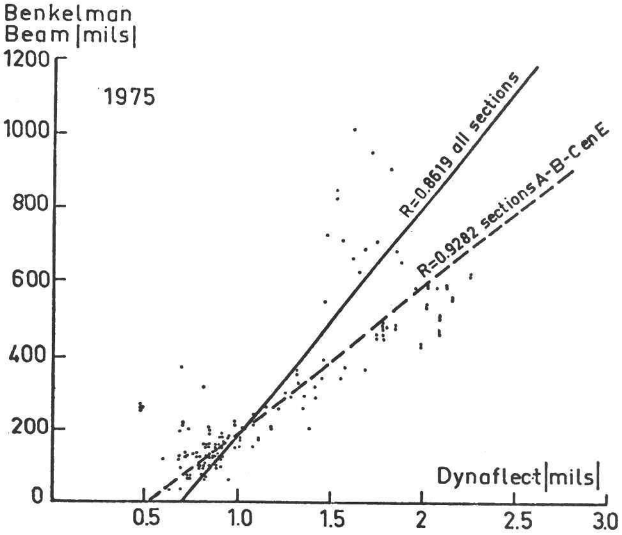

Figure 2.14 Relation between Dynaflect and Benkelman Beam Deflections

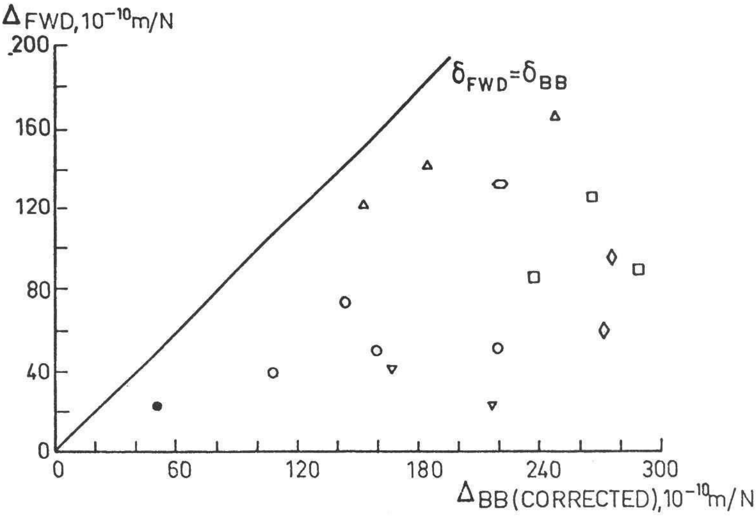

Figure 2.15 Relation between Benkelman Beam and Falling Weight Deflections

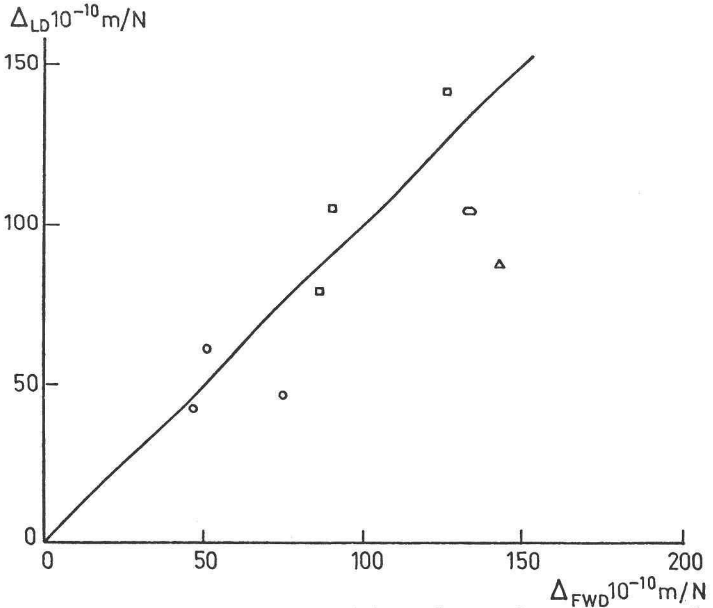

Figure 2.16 Relation between Falling Weight and Lacroix Deflectograph Deflections

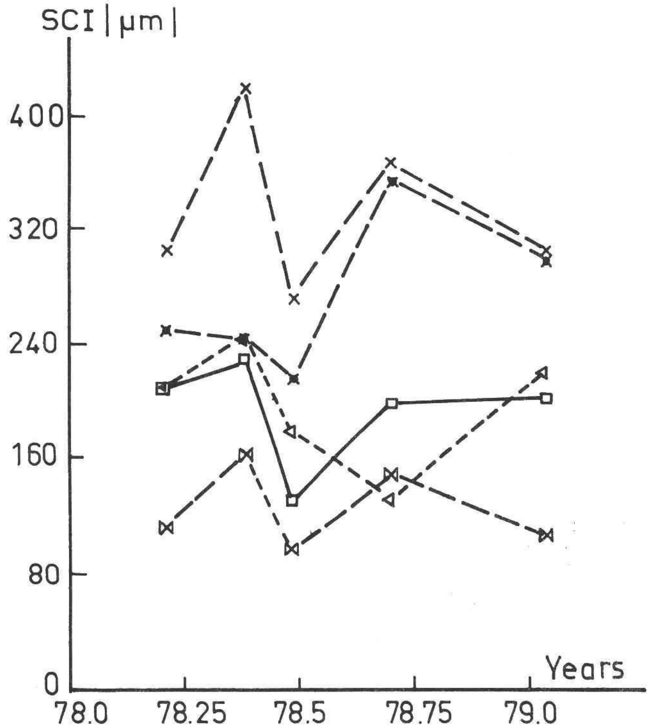

Figure 2.17 Seasonal Variation of the SCI as determined for the S_{10} Road Sections

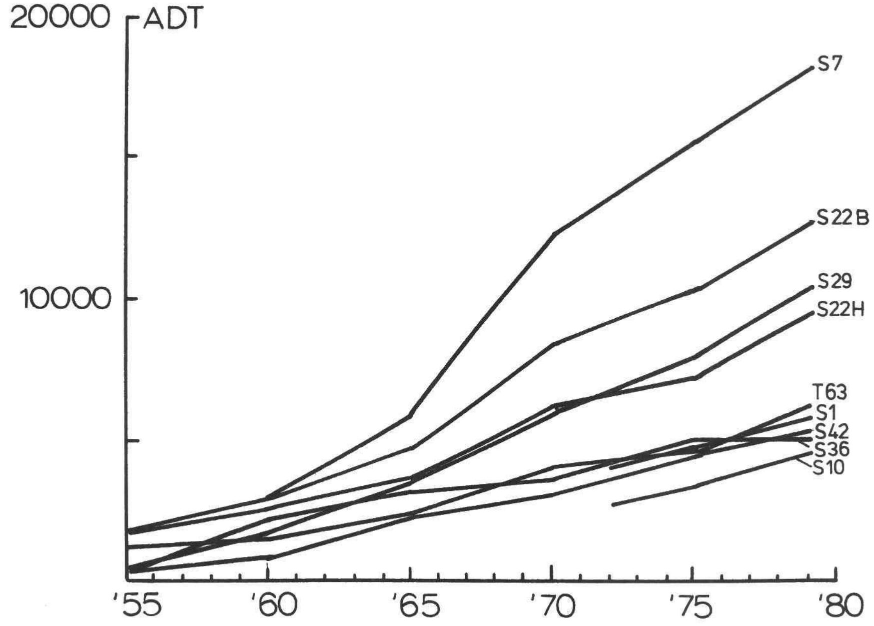

Figure 2.18 *Increase of the Average Daily Traffic (ADT) in Time of the Road Sections considered*

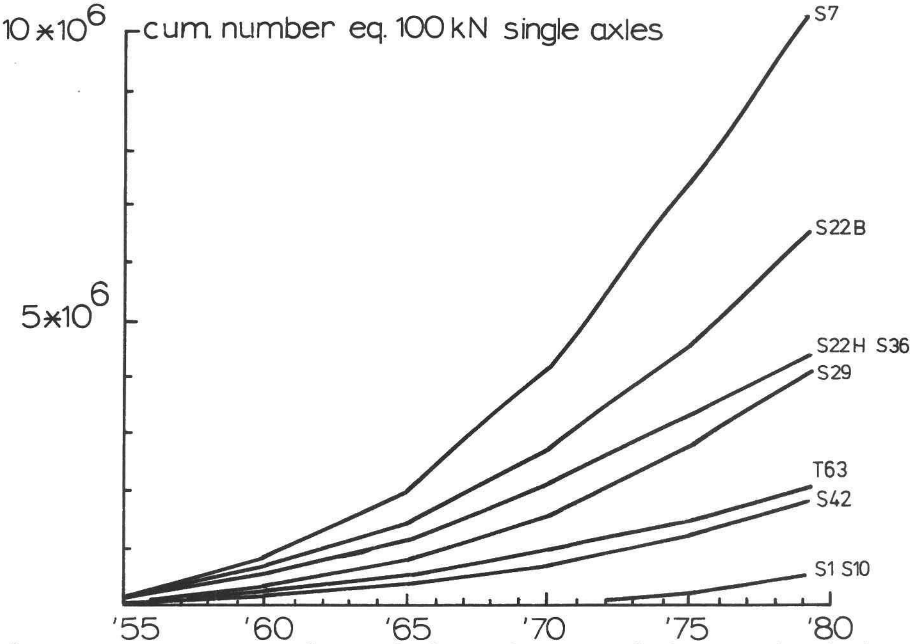

Figure 2.19 *Increase of the Cumulative Number of Equivalent 100 kN Single Axles in Time of the Road Sections considered*

Typical examples of the development of the surface curvature index (SCI) in time as determined by means of this device, are given in figure 2.17. It should be noted that the SCI is defined as

$$SCI = \Delta_0 - \Delta_{0.5} \qquad \text{eq. 2.2}$$

where Δ_0 = deflection as measured at the loading centre
$\Delta_{0.5}$ = deflection as measured at a distance of 0.5 m from the loading centre

Furthermore it should be noted that the SCI values given in figure 2.17 are not corrected for temperature and other influences.

2.5 Traffic

The amount of traffic, and more specifically the number and magnitude of the axle loads, is of importance in order to be able to make proper evaluations of the present-day pavement condition, and to make reasonable estimates of the future condition.
In the Netherlands, information on the amount of traffic in terms of number of vehicles, is readily available for state highways as well as for the secondary road system. There is however very little information on the axle load spectrum on the respective road types. Little to no traffic information is available fore the less important roads.
For the Zuid Holland road sections (figures 2.1 and 2.2), Beuving |10| derived an overview of the average daily traffic development over the years (figure 2.18) and the cumulative number of equivalent 100 kN single axles (figure 2.19). Figure 2.18 is based on traffic counts performed by the provincial highway department. Figure 2.19 is based on relations that seem to exist between the truck silhouette and the number of equivalent 100 kN single axles per truck.
The data given in figure 2.19 were used in the development of a structural performance model.

2.6 Summary

In this chapter, general information has been given on the construction types, materials used in pavement structures, and specifications set for them.
Attention has been paid to the subsoil and environmental conditions that are typical fore the Zuid Holland region.
Furthermore, typical examples are given of structural performance data as obtained by means of visual condition surveys and deflection measurements.
Also information on the amount of traffic and the traffic loads determined for the road sections considered, was given.
This introductory chapter was thought to be necessary in order to give the reader an idea and understanding of the material which is dealt with in this report.

References

|1| VAN DIGGELE, P.
"Application of Slags" (in Dutch)
Application of Waste Materials in Road Construction, Report of the SCW Symposium; Study Centre for Road Construction, Arnhem - 1981

|2| LANGEJAN, A.
Course Notes on Soil Mechanics (in Dutch)
Department of Civil Engineering
Delft University of Technology

|3| STUDY CENTRE FOR ROAD CONSTRUCTION
Various Properties of Natural Sands for Netherlands Highway Engineering
SCW Record 4
Arnhem - 1978

|4| RIJKSWATERSTAAT
Specifications for Materials used in Road Construction (in Dutch)
Staatsuitgeverij, the Hague - 1978

|5| KONINKLIJK NEDERLANDS METEOROLOGISCH INSTITUUT
Climatological Atlas of the Netherlands (in Dutch)
Staatsuitgeverij, the Hague - 1972

|6| VAN DER PLAS, J.J
"Frost Penetration in our Country is not a Constant" (in Dutch)
SCW Publication N
Study Centre for Road Construction, Arnhem - 1980

|7| STUDY CENTRE FOR ROAD CONSTRUCTION
A Guide for Pavement Management (in Dutch)
SCW Publication K
Arnhem - 1977

|8| CARMICHAEL, R.F.; VAN DIGGELE, P.; KREPEL, L.C.
Some Aspects concerning the Maintenance of Road Pavements (in Dutch)
"Wegen", Vol. 50 no. 6 - 1976

|9| CLAESSEN, A.I.M.; VALKERING, C.P.; DITMARSCH, R.
Pavement Evaluation with the Falling Weight Deflectometer
"Proceedings Association of Asphalt Paving Technologists", Vol. 45 - 1976

|10| BEUVING, E.
Calculation of the Traffic Intensities and Number of Equivalent 100 kN Single Axles on 9 Road Sections in the Province of Zuid Holland (in Dutch)
Report WB - 15 (7-80-115-8); Dep. of Civil Engineering; Lab. for Road and Railroad Research; Delft University of Technology - 1980

Chapter 3

DESIGN AND PERFORMANCE OF FLEXIBLE ROAD CONSTRUCTIONS

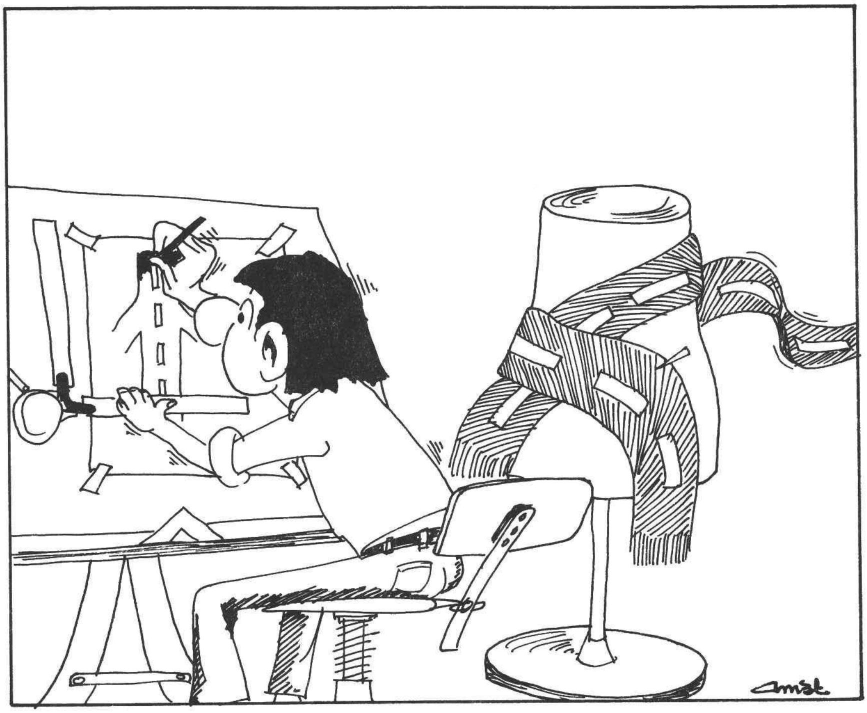

TABLE OF CONTENTS

3.1 Introduction

The design of flexible pavements should be such that a safe, comfortable and fast public and commercial transportation is possible during a large number of years. These demands, made by the road user, mean to the road designer that he should provide a smooth driving surface with a high skid resistance. Also the design of the structure should be such that the longitudinal and transverse deformations as well as surface distress which will be developed during the pavement life, do not exceed predefined minimum acceptance levels.

The development of damage or distress of the pavement depends to a large extent on the quality of the subsoil but to an even larger extent on the quality of the design of the pavement structure. Table 3.1 |1| gives an overview of distress modes, distress manifestations and examples of distress mechanism. Distress which should be contributed to the pavement structure itself, is the result of overstressing parts of the structure or the total structure. Overstressing means that the stresses have reached such a magnitude that relatively large permanent deformations and or cracking of the materials used, will occur. Especially cracking of one of the pavement layers should be of major concern since this may result in large deformations in other layers and finally in the inability of the total structure to transfer loads. Also traffic may pull the broken parts out of the pavement surface which result in potholes which in turn will have a negative influence on the riding comfort and even on the safety conditions.

In order to be able to design pavements in such a way that a high quality driving surface is offered over a large number of years, a large number of methods have been developed in the past. These design methods can roughly be categorized into two groups.

a. empirical design methods
b. mechanistic design methods

ad a. The empirical design methods are based on the observed behavior of pavements related to the thicknesses of the different layers, some simple strength characteristics of the materials used, and the number and magnitude of the loads applied to the pavement. Although these empirical methods do have the large advantage of being based on observed damage developments, the main shortcoming is that they are not based on a proper evaluation of the stresses within the pavement and a proper description of the characteristics of the materials used, such as strength and deformation characteristics. This ties these empirical methods to the materials, climatic and loading conditions for which they are developed. Use of these methods under other circumstances may result in wrong or unreliable designs.

ad b. To overcome the drawbacks of the empirical design methods, mechanistic design methods have been under development during the last twenty years. With the term mechanistic methods, those methods are meant which use a "fundamentally" sound approach to the calculations of the stresses and strains in pavement structures and which are based on a "fundamentally" sound description of the materials characteristics such as deformation and fracture properties. In the previous sentence, the word fundamentally has been placed between quotation marks. This is because up till now all calculations are made under the assumption that the effects of dynamic traffic loads can be evaluated by means of calculation techniques which assume a static loading. The dynamic nature is simulated by using elastic modulus values which are typical for the prevailing dynamic loading conditions.

Table 3.1: *Categories of Pavement Distress*

Distress Mode	Distress Manifestation	Examples of Distress Mechanism
Fracture	Cracking	Excessive loading Repeated loading (i.e. fatigue) Thermal changes Moisture changes Slippage (horizontal forces) Shrinkage
		Excessive loading Repeated loading (i.e. fatigue) Thermal changes Moisture changes
Distortion	Permanent deformation	Excessive loading Time-dependent deformation (e.g. creep) Densification (i.e. compaction) Consolidation Swelling
	Faulting	Excessive loading Densification (i.e. compaction) Consolidation Swelling
Desintegration	Stipping	Adhesion (i.e. loss of bond) Chemical reactivity Abrasion by traffic
	Raveling and Scaling	Adhesion (i.e. loss of bond) Chemical reactivity Abrasion by traffic Degradation of aggregate Durability of binder

Furthermore very often far reaching assumptions need to be made on material properties, such as deformation characteristics, in order to perform the stress and strain calculations within a reasonable time and budget.

The major advantage of these methods is, that they are not bound to certain local conditions but can be applied anywhere at any time.

A major disadvantage of almost all mechanistic methods is, that only the number of load applications to failure can be calculated. No predictions can be made on pavement performance during the time period which lies between construction and failure.
Another disadvantage of these mechanistic methods is, that hardly any verification on the predictive capabilities of these models has been performed.
Although one can consider the above mentioned disadvantages as serious drawbacks of the so-called mechanistic methods, it is believed that their use should be encouraged because they give a better understanding or at least a better insight in why a given design will perform well or not.

This study has been undertaken to improve the prediction capabilities of existing *mechanistic design methods*. Especially emphasis is placed on the prediction of future performance as well as on prediction of cracking. First of all, a short description will be given of the basic principles of existing mechanistic design methods in order to get an understanding of the rationale for this study.

3.2 Mechanistic Design Methods; Basic Principles

A rather complete picture on existing mechanistic design methods can be found in the proceedings of the 4th International Conference Structural Design of Asphalt Pavements |2|. This section summarizes the basic assumptions used in most of the methods presented there.
In all mechanistic design methods the pavement structure is modelled as a number of layers resting on an infinite half space. Mostly the materials are assumed to be linear elastic, homogeneous and isotropic. This is never true for pavement materials but in many cases it is a reasonable assumption. To overcome this problem, sometimes a linear viscoelastic approach or a non-linear elastic approach is adopted. The linear visco elastic approach is attractive to model the deformation characteristics of bituminous materials; granular materials and cohesive soils can be described better by a non-linear elastic approach.
However a better model involves too, that more sophisticated tests should be performed to determine the deformation properties of the materials. This is costly, time consuming, and at the present state of knowledge, a better design is not garanteed by using better material models. This is why usually a linear elastic approach is adopted.
It should be recognized that in many design procedures the linear elastic deformation properties of the materials considered are estimated from rules of the thumb and nomographs to overcome the necessity to perform expensive and time consuming tests. One well known rule of the thumb is the relation to estimate the elastic modulus of the subgrade :

$$E_s = 10^7 \text{ CBR}$$

where E_s = elastic modulus of the subgrade $|N/m^2|$
CBR = California Bearing Ratio of the subgrade |%|

It will be obvious that the application of these types of rule is derationalizing the mechanistic design methods.
Fortunately the nomographs that are used to estimate the elastic deformation characteristics of bituminous materials, are based on extensive laboratory testing of these materials. By using these nomographs usually reliable deformation values are obtained.

In all design methods the pavement structure is loaded by uniformly distributed vertical loads applied on circular areas. Computer codes have been developed to calculate the stresses and strains in a linear elastic, or linear viscoelastic layered pavement structure |3, 4|.
One recent computer code |5| is capable of handling anisotropy and non uniformly distributed vertical and horizontal loads. This latter is important since especially inward shear loads, which have been neglected in most of the design methods, can have a major influence on the stresses and strains near the pavement surface.

Since the magnitude of the wheel loads varies over a broad range, Miner's law is used to determine the overall damage caused by the different wheel loads.
Miner's law is:

$$\sum_{i=1}^{j} \frac{n_i}{N_i} < 1$$

where n_i = number of load applications of magnitude i
N_i = allowable number of load repetitions of magnitude i
j = number of load magnitudes (load classes) considered.

Normally all axle or wheel loads considered are transformed to an equivalent single axle or wheel load in order to overcome the necessity to perform calculations for a large number of load groups. The number of equivalent axle loads (N) is calculated with

$$N = \sum_{i=1}^{j} \left(\frac{P_i}{P_e}\right)^m n_i$$

where P_i = axle load of magnitude i
n_i = number of axle load repetitions of magnitude P_i
P_e = reference axle load or equivalent axle load
m = a constant ranging from 3 to 6

In this study the reference axle load P_e is set a 100 kN being the legal limit for single axles in the Netherlands.

All design methods use two basic design criteria. They are the maximum horizontal tensile strain in the asphalt layer, which is responsible for cracking of the asphalt layer, and the vertical compressive strain at the top of the subgrade, which is responsible for permanent deformation of the subgrade, resulting in permanent deformation of the pavement surface. Some design methods do also take into account the permanent deformation developed in the individual pavement layers.
To check when or whether cracking or permanent deformation occurs, the calculated stresses or strains are put into fatigue relations, which almost all have been developed from laboratory tests, and into permanent deformation models that have been developed in the laboratory too, or that have been derived from observed in situ behavior of pavement.

The laboratory determined fatigue relations that are used, are corrected by a factor, mostly ranging from 2 to 30, to take into account beneficial effects as rest periods, crack propagation and the lateral distribution of the traffic loads over the pavement width.

Only a few design methods incorporate reliability concepts, by taking into account the influence of variability of material and load characteristics, layer thicknesses etc. on the pavement life. The way in which this is done is complicated and a fairly large computer is then needed. This is the reason why the reliability concepts are restricted in their practical use.

3.3 Discussion on the Applicability of the Mechanistic Design Methods; Setting the Scope for a New Design Method

As mentioned before one of the major drawbacks of the mechanistic design methods is the uncertainty of whether theoretical results will match observed pavement behavior. In reality pavement damage (cracking, permanent deformation) develops in time in a gradual way. At the present moment, this can only be simulated by using design methods which are incorporating reliability concepts but they are, as noticed before, in their present form not user friendly.

Another main shortcoming of most of the present design methods is, that the fatigue and permanent deformation relations used, are not, or only to a limited amount, checked on observed pavement behavior.
This is thought to be especially true for fatigue cracking of the asphalt layers. As mentioned before a factor of 2 up to 30 is used to "correct" the fatigue relations determined in the laboratory to simulate the cracking behavior of the pavement. It will be obvious that in this case the introduction of reliability concepts will give some indication on the cracking behavior of the pavement in time, but that the predicted moment of the appearance of cracks at the pavement surface becomes highly unreliable itself due to the inconsistency of the correction factors.
Not only the prediction of the moment of appearance of the cracks at the pavement surface is rather unreliable, also the prediction of the type of cracking as done by means of the existing mechanistic methods gives cause to question marks on the applicability of these methods.
In general, cracking which grows from bottom to top can be very well explained by means of the existing methods. Also it can be explained why the cracks sometimes initiate somewhere within the asphalt layers |6|. In many pavements however a large amount of so called surface cracking can be observed. This type of cracking is defined as cracking which grows from the pavement surface downwards but only to a limited extent. For instance Dauzats et al. |7| showed that in France longitudinal surface cracking contributed to about 25% of the total amount of cracking in thick asphaltic concrete pavements. For overlaid pavements surface cracking contributed to about 90% of the total amount of cracking. Unfortunately this type of cracking cannot be explained by means of the calculation techniques which are commonly used. This is considered to be an imperfection of these methods which should be overcome. One should be able to predict and to recognize the occurence of surface cracking since it will influence the selection of maintenance strategies.

Furthermore a strong need is felt on fairly simple structural performance models. By these, models are meant which can be used by the road engineer to estimate how the proposed designs will most probably behave in time in terms of cracking

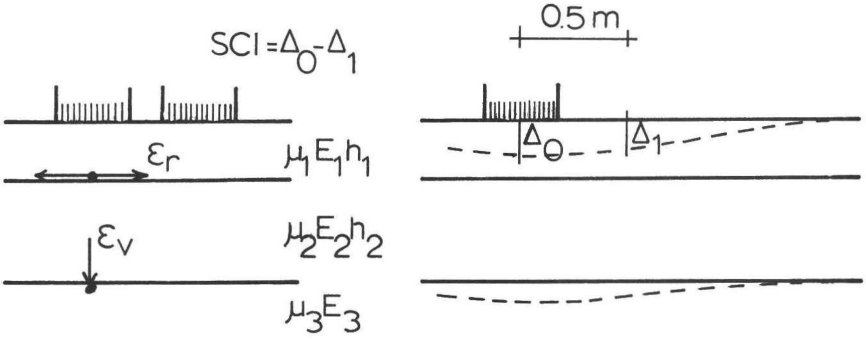

Figure 3.1 *Pavement and Loading Geometry used in the Analysis*

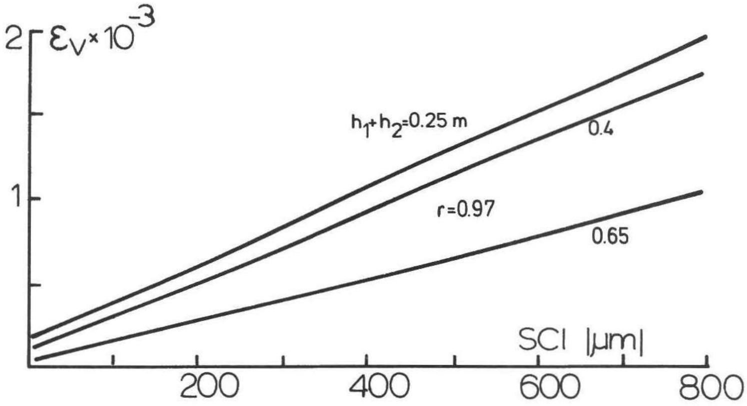

Figure 3.2a *Relation between the Surface Curvature Index (SCI) and the Vertical Compressive Strain at the top of the Subgrade (ε_v)*

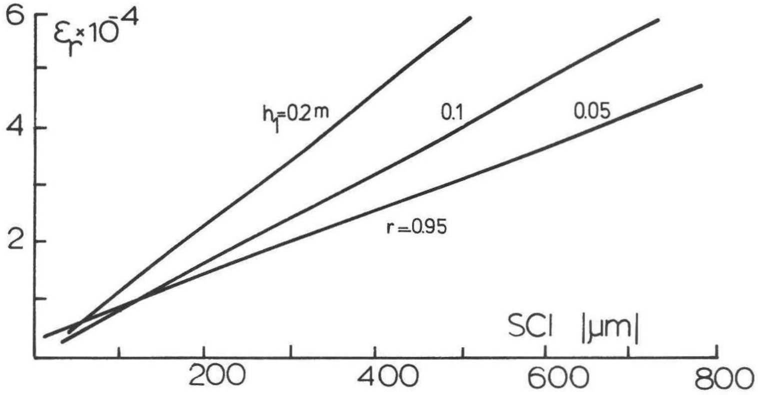

Figure 3.2b *Relation between the Surface Curvature Index (SCI) and the Horizontal Tensile Strain at the bottom of the Asphalt Top Layer*

and permanent deformation. These models must enable the road engineer to check whether an existing road needs to be maintained and when this maintenance activity should take place.
Finally it is recognized that much attention should be paid to the comprehensibility and applicability of methods to be developed, since it has been stated several times that those design methods that already fullfill to some extent these demands, for instance the method presented in |8|, are rather complex and therefore not very attractive to be used by the practising highway engineer.

The above mentioned considerations have led to the conclusion that the existing pavement design methods should be extended. Departing from the same basic principles as used in the existing methods, simplified performance models should be developed which will enable the road engineer to check whether these designs perform as expected and to determine whether maintenance activities should be scheduled or not.
This latter demand means that the design and performance models should be strongly related to data which can be obtained by means of deflection measurements and visual condition surveys. This is because these types of measurements are normally used to assess the pavement condition.

In the subsequent sections of this chapter, the development of such an extended design method will be described in which the requirements mentioned above are, according to this author, met as best as possible.
Since this extended method contains many new and original developments it can be classified, without exaggeration, as a new design method.

3.4 A New Design Method

In the subsequent sections of this chapter on the development of a new design method, attention will be paid to

a. development of simple techniques to assess the design strain levels, which are the tensile strain in the asphalt layer and the vertical compressive strain at the top of the subgrade;
b. development of a structural performance model;
c. development of a permanent deformation model.

Of course none of these subjects were developed from one day to the next so each section will start with a short review of the work executed on each subject by the author and others at the Laboratory of Road and Railroad Research of the Delft University.
After that, the recent developments made by the author will be discussed which have led to the techniques and models as they are at this moment.

3.4.1 Development of Simple Techniques to Assess the Design Strain Levels

3.4.1.1 Review of Previous Work

Already in 1976 evidence was obtained from extensive BISAR |3| calculations on three layer pavement systems, performed by the author |9| that a relation could be derived between the surface curvature index (SCI) of the pavement caused by a dual wheel loading (fig. 3.1), and the two major design criteria which are:

a. the horizontal tensile strain at the bottom of the asphalt layer;
b. the vertical compressive strain at the top of the subgrade.

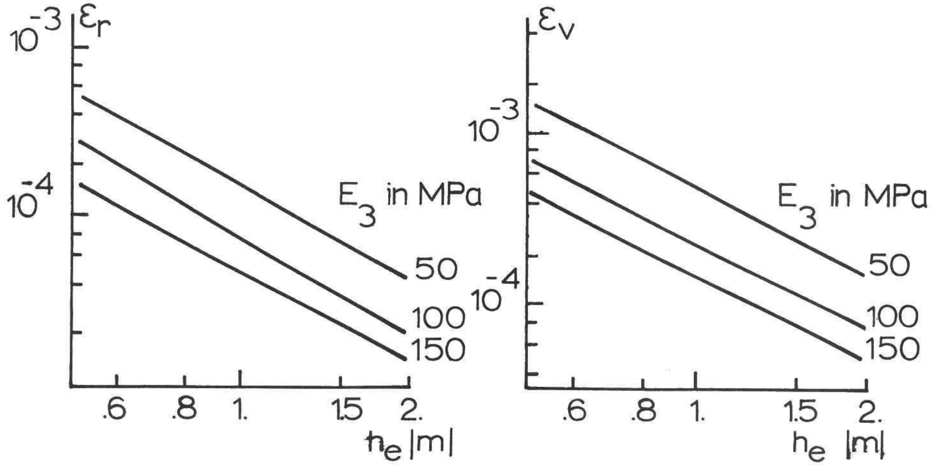

Figure 3.4 *Relations between the Equivalent Layer Thickness (h_e) on one hand and the Horizontal Tensile Strain at the bottom of the Asphalt Layer (ε_r) or the Vertical Compressive Strain at the top of the Subgrade (ε_v) on the other.*

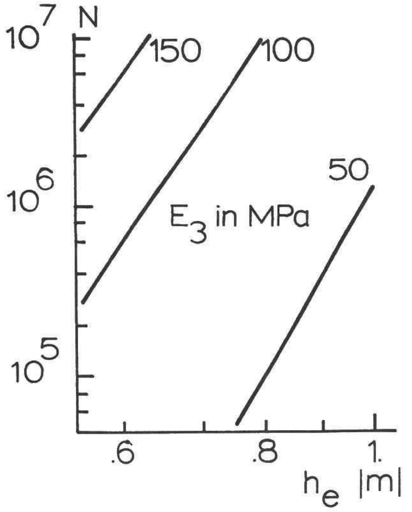

Figure 3.5 *Pavement Design Curves based on the Equivalent Layer Thickness (h_e)*

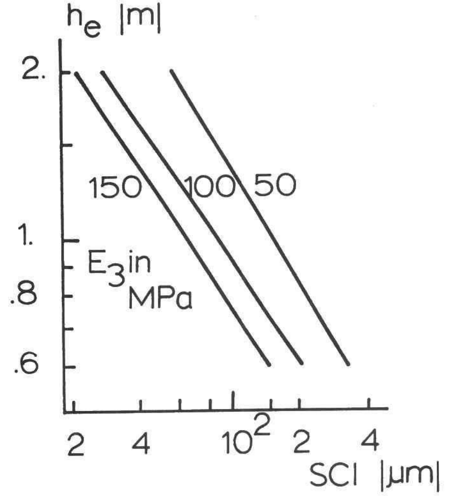

Figure 3.6 *Relation between the Surface Curvature Index (SCI) and the Equivalent Layer Thickness (h_e)*

This work has been extended by Zijlstra |10|. In 1977 the author presented relations between the surface curvature index on one hand and both strain values on the other |11| (fig. 3.2). As can be seen from figure 3.2, both strain values can be estimated with a rather high accuracy provided the total pavement thickness (base plus top layer) and the thickness of the asphaltic top layer are known. By using fatigue relations derived by Shell researchers for different asphalt mixes |12|, and a subgrade fatigue relation also developed by Shell |13|, the author has derived relations between the surface curvature index and the pavement life based upon both design criteria (fig. 3.3).

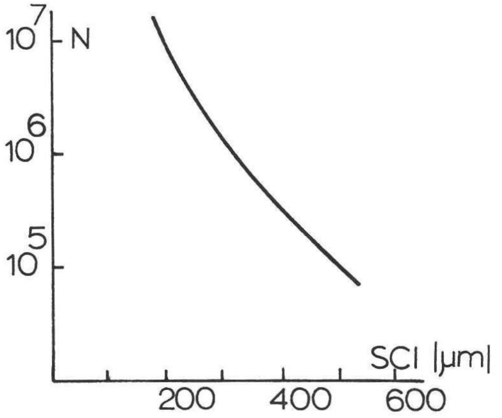

Figure 3.3 *Example of a Pavement Design Curve based on the Surface Curvature Index (SCI)*

Although these relations are fortunately independent of any layer modulus, they are dependent on layer thicknesses. This means that quite a lot of cores should be taken from pavements in order to be able to determine the strain values. This was thought not to be attractive. Also it was thought that designing pavements based on a surface curvature index is not very practical. This curvature index must still be translated into layer thicknesses and elastic modulus values. Therefore this basic work was extended further by the author and Van Gurp |14, 15, 16, 17, 18, 19, 20| in the following way. First of all relations were derived between the equivalent layer thickness, calculated according to Odemark, |21| and both basic design criteria, i.e. the horizontal tensile strain at the bottom of the asphalt layer and the vertical compressive strain at the top of the subgrade (fig. 3.4).
The equivalent layer thickness (h_e) is calculated by

$$h_e = 0.9 \sum_{i=1}^{L-1} h_i \sqrt[3]{\frac{E_i}{E_s}} \qquad \text{eq. 3.1}$$

where h_i = thickness of layer i |m|
E_i = elastic modulus of layer i $|N/m^2|$
E_s = elastic modulus of the subgrade $|N/m^2|$
L = Number of layers

Odemark's equivalency theory was used since the equivalent layer thickness is a magnitude which is meaningful and easily to be understood. A pavement with a high h_e will last longer than a pavement with a low h_e.

SCI = surface curvature index (as defined in figure 3.1)
N = number of load repetitions to failure

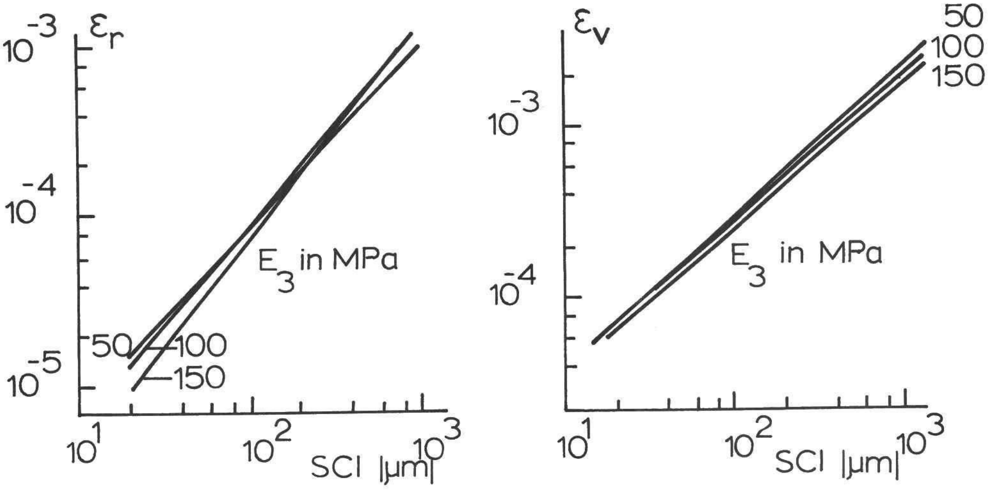

Figure 3.7 *Relations between the SCI on one hand and the ε_r and ε_v on the other*

Examples of these design curves are given in figure 3.8

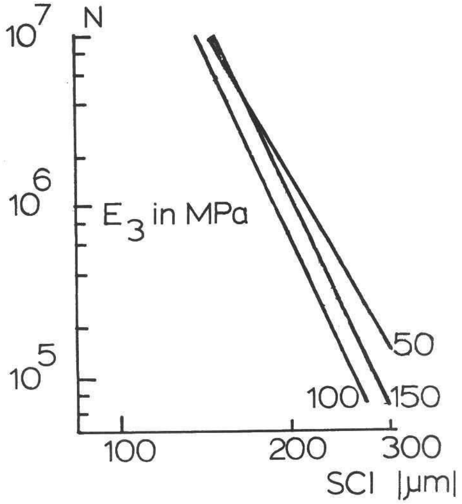

Figure 3.8 *Pavement Design Curves based on the SCI*

By means of the relations between the h_e and the design strain levels, and by applying appropriate fatigue relations, pavement design curves like those given in figure 3.5 were developed.
Each design curve can be described with

$$\log N = a_0 + a_1 b_0 + a_1 b_1 \log h_e \qquad \text{eq. 3.2}$$

where a_0, a_1 = constants from the fatigue relation which is $\log N = a_0 + a_1 \log \varepsilon$
b_0, b_1 = constants from the relation $\log \varepsilon = b_0 + b_1 \log h_e$
h_e = equivalent layer thickness
N = number of load repetitions to failure

The big advantage of this type of design curves is, that once a design equivalent layer is selected, it can be broken down very simple to layer thicknesses and elastic moduli values by using equation 3.1. This makes it possible to select alternative designs. It could be argued that the elastic modulus of the subgrade still needs to be known in order to be able to select a proper h_e value. This modulus value can be selected by using the well known rule of the thumb.

$E_s = 10^7$ CBR
$|E_s| = |N/m^2|$
$|CBR| = |\%|$

It has been stated in section 3.3 that it is desirable to have relations between the magnitude, which is used in the design method to describe the load carrying capacity of the pavement, and deflection data.
Therefore the surface curvature index of the deflection bowl caused by the dual wheel loading which is a measurable quantity, and the equivalent layer thickness were correlated with each other.
The result is shown in figure 3.6.

It is obvious that relations between the SCI and the design strain levels are preferred over the SCI vs h_e and h_e vs ε relations when one needs to know the strain level in existing pavements. Therefore the relations given in figure 3.2 were somewhat simplified in order to get relations of the same shape as the h_e vs ε relations. These simplified relations are shown in figure 3.7.
A logarithm based relation was used since this type of relation had a somewhat higher coefficient of correlation than the straight forward linear relation which was used before.
The unknown subgrade modulus can directly be calculated from deflection measurements. For a dual wheel load this relation is developed in |11|, for a falling weight load this relation is given in |22|. This latter relation is

$$\log E_s = 9.87 - \log \Delta_2 \qquad \text{eq. 3.3}$$

where E_s = elastic modulus of the subgrade $|N/m^2|$
Δ_2 = deflection measured at 2 m from the loading center ($P = 50$ kN, $t = 0{,}02$ s) $|\mu m|$

By means of these relations and appropriate fatigue relations, design curves based on the SCI could be developed. These curves can be described with

$$\log N = a_0 + a_1 c_0 + a_1 c_1 \log SCI \qquad \text{eq. 3.4}$$

where a_0, a_1 = as defined earlier (eq. 3.2)
c_0, c_1 = constants from the relation $\log \varepsilon = c_0 + c_1 \log SCI$

The relations given so far were the base of further work in this field and of the development of a structural performance model which will be discussed later on.

3.4.1.2 Recent Developments

Recently the author has made several modifications to the relations presented in the previous section. These modifications were thought to be necessary due to a number of reasons which are listed below.

a. In the derivation of the presented relations, it is assumed that the maximum asphalt strain occurs at the bottom of the asphalt layer. It has been shown at several locations that this is not always true. Also perfect adhesion between the layers was assumed. There is no doubt adhesion is absent in a relatively large number of occasions, especially in overlay conditions. The question therefore remains, will it be possible to estimate the tensile strain, which occurs in these conditions, by means of the earlier developed SCI vs ε relations.

b. The uniqueness of the h_e vs ε and SCI vs h_e relations has been questioned in a few occasions when it was discovered that ranking different pavement sections according to surface curvature index and equivalent layer thickness, resulted in incompatible maintenance priorities. Solving this problem is thought to be important since the equivalent layer thickness is an ideal yardstick to compare the condition of pavement sections, because it is significant, easy to understand, and therefore very attractive to be used for these purposes.

c. The question how to explain surface cracking that has been observed in a number of occasions,is not solved by the relations presented in the previous section. From the available literature on this subject, it could be concluded that there are two possible causes for this type of cracking. Yandell and Lytton |23| have indicated that surface cracking might be the result of residual stresses which are at their maximum just after the passage of a load and which will relax gradually. On the other hand Wardle and Gerrard |24| have shown that longitudinal surface cracking can be explained by taking into account radial shear stresses acting under rolling as well as standing wheels.
Considering the fact that most of the surface cracking observed in this study was longitudinal cracking, it was decided by the author to perform additional calculations to quantify and qualify the effects of the above mentioned radial shear stresses.

In order to solve the above mentioned question marks, a number of calculations on three layered pavement systems were performed by using the CIRCLY computer program |5|.
The loading geometry as well as the pavement characteristics are shown in figure 3.9.
From figure 3.9 it can be observed that three base stiffnesses were considered.
a. a low stiffness base, representing an unbound base ($E_2 = kE_3$)
b. a moderate stiff base, representing an unbound base showing some cementation as is for instance the case with bases built of blast furnance slags (E_2 = 1200 MPa)
c. a stiff base, representing a typical sand cement stabilized base ((E_3 = 6000 MPa).
Also it can be observed that full slip as well as full adhesion conditions were assumed at the interface between the top layers and the base.

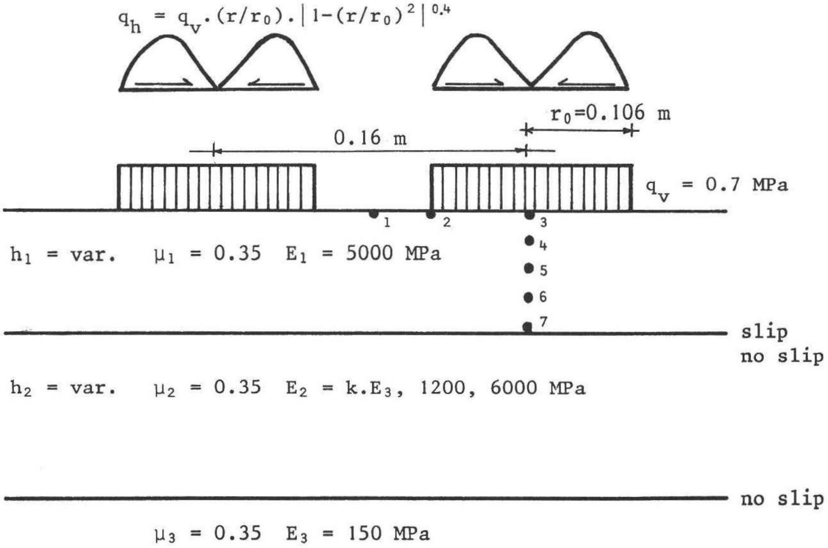

Figure 3.9 *Input for the CIRCLY Calculations*

A detailed discussion on the results of these calculations is given in appendix 3A. In this section only the main findings from the analyses will be given.

First of all attention will be paid to the location of the maximum tensile strain in the asphalt layer.
From the results of the calculations, it is concluded that the location of the maximum tensile strain within the asphaltic top layer was dependent on the ratio of base stiffness to top layer stiffness and the thickness of the asphaltic top layer. The rule of thumb developed by Claessen |6| to determine the location of the maximum strain was confirmed.
Furthermore the calculations showed that in most cases the tensile strain at the bottom of the asphalt layer or the strain at some depth below the surface, is smaller than the tensile strain at the pavement surface occuring at the tire edge, caused by inward shear forces.
Also it could be concluded that for the given loading configuration the magnitude of the tensile strain at the pavement surface is solely dependent on the stiffness of the top layer.

The following practical conclusions on the cracking behavior of flexible pavements could be drawn from the results of the performed analysis.

a. Cracking observed on pavements having an unbound base and an asphalt top layer thickness less than 0.2 m, can be judged as cracking which has grown from bottom to top.
b. Longitudinal cracking observed on pavements having an unbound base and an asphalt top layer thicker than 0.2 m, can be judged as cracking which has grown from top to bottom.
c. Longitudinal cracking observed on pavements having a stiff base is most probably cracking which has initiated at the top of the pavement.
d. Transverse cracking observed on pavements having a stiff base might be due to environmental effects or due to fatigue of the stabilized base; in both

cases the observed transverse cracking in the asphalt layer is reflection cracking.

Now the uniqueness of the relations between the equivalent layer thickness on one hand and the maximum tensile strain in the asphalt layer will be considered. Again all the details of the analysis carried out on these relations are presented in appendix 3A. From this analysis the following conclusions have been drawn.

a. If one wants to estimate the tensile strain in the asphalt layer from the equivalent layer thickness (h_e) with a high degree of accuracy, the thickness as well as the base stiffness should be taken into account.

b. Also the stiffness of the top layer influences the h_e vs ε relation but since this influence is limited, it can be neglected for practical purposes.

c. For practical design purposes it is recommended to use the h_e vs ε relation developed for pavement having an unbound base with a thickness of 0.3 m. This relation is shown in figure 3.10.

d. The new h_e vs ε relation produces more conservative results than the old h_e vs ε relation.

On the theoretically derived relation between the surface curvature index and the maximum tensile strain in the asphalt layer, the following commentary can be given.

a. The SCI correlates rather well with the tensile strain in the asphalt layer both in cases where full adhesion exists, and in cases where full slip between the top layer and the base occurs (fig. 3.11).

b. There is a good relation between the SCI and the tensile strain at the bottom of the base (fig. 3.11).

c. The new relation between the SCI and the maximum strain in the asphalt layer produces more conservative results than the old relation.

d. It has been shown that the SCI is almost independent of the subgrade modulus.

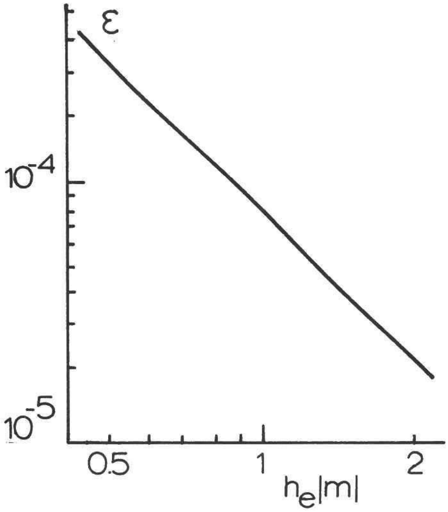

Figure 3.10 Relation between the Equivalent Layer Thickness (h_e) and the Maximum Tensile Strain in the Asphalt Layer (ε)

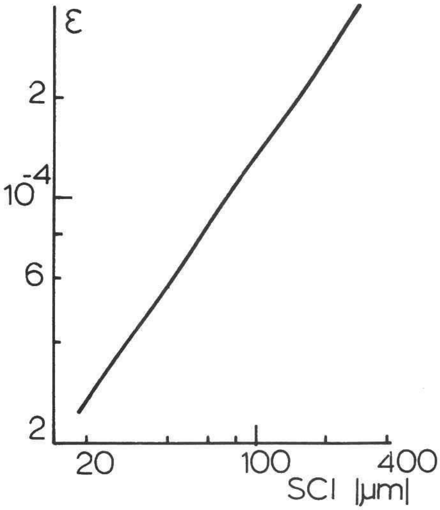

Figure 3.11 Relation between the Surface Curvature Index (SCI) and the Maximum Tensile Strain in the Asphalt Layer (ε)

Furthermore it is strongly recommended to take cores if pavement evaluation is done by means of deflection measurements. The purpose of taking cores is not only to get samples for the material testing but also because it enables the pavement engineer to check the degree of adhesion between the pavement layers. It has been shown that this is important because a low SCI will not always mean a low strain level in the asphalt layer.

Finally some comments will be made on the relation between the SCI and h_e. Also this relation is influenced by the thickness and stiffness of the base. However for pavements with stiff bases, the relation between SCI and h_e is not influenced by the properties of the base.
Furthermore it can be concluded that the old relation between SCI and h_e produced more conservative results (i.e. lower h_e values) than the new relations.

Although the previous given relations between h_e and ε as well as between SCI and h_e need to be modified to a considerable extent, one should know what the net effect of these modifications is. For instance if one wants to express the load carrying capacity of an existing pavement by means of h_e, one has to calculate h_e from the SCI which in turn can be determined by means of deflection measurements. For further evaluation purposes one has to translate h_e into a strain level. One could ask now what the difference is in the strain value estimated by means of the old equations and the strain value estimated by the new equations. Table 3.2 gives the results of such a comparison. The comparison is based on a base thickness of 0.3 m since this is a commonly used thickness.

Table 3.2 Equivalent Layer Thickness and Strain Estimations by means of the Original and Revised Equations.

	New Relations						Original Relations	
$E_2\ \vert\mathrm{MPa}\vert$	400		1200		6000			
SCI $\vert\mu\mathrm{m}\vert$	$h_e\ \vert\mathrm{m}\vert$	ε	$h_e\ \vert\mathrm{m}\vert$	ε	$h_e\ \vert\mathrm{m}\vert$	ε	$h_e\ \vert\mathrm{m}\vert$	ε
200	0.68	$1.7 . 10^{-4}$	0.58	$2.3 . 10^{-4}$	0.36	$1.3 . 10^{-4}$	0.51	$1.7 . 10^{-4}$
100	1	$8.6 . 10^{-5}$	0.91	$8.5 . 10^{-5}$	1	$1.7 . 10^{-5}$	0.73	$8.7 . 10^{-5}$
50	1.43	$4.3 . 10^{-5}$	1.49	$3.1 . 10^{-5}$	1.75	$2.2 . 10^{-5}$	1.05	$4.5 . 10^{-5}$

As can be seen from table 3.2 the agreement between the strain values estimated by means of the old equations and the strain values determined by means of the new equations is good for pavements with an unbound base. The agreement is reasonable for pavements with a moderate stiff base (E_2 = 1200 MPa) but poor for pavements with a stiff stabilized base (E_2 = 6000 MPa).

3.4.2 Development of a Structural Performance Model

In this section the development of a structural performance model will be described. As mentioned before such a model should describe how the pavement will deteriorate in time. It is obvious that such a model is important if an overall economic analysis of the pavement structure (design plus maintenance) has to be made. As mentioned before a structural performance model is also an important tool in the planning and design of maintenance activities.

The structural performance model developed in this study, has been built around the relations between h_e or SCI on one hand and ε on the other. These were described in the previous section.

3.4.2.1 Review of Previous Work

The work done at the Laboratory of Road and Railroad Research of the Delft University on the development of a structural performance model has started in 1979. The original developments have been reported in |14| while further developments have been published in |15, 16, 17, 18, 19, 20|. The basic idea behind these performance curves is that designs made by using equations 3.2 or 3.4 have a reliability of 50% since all factors used are set at their mean value. Departing from this mean value of the number of load repetitions to failure, the number of load repetitions N_p to a certain reliability level P can be calculated by

$$\log N_p = a_0 + a_1 b_0 + a_1 b_1 \log h_e - u.S_{\log N} \qquad \text{eq. 3.5}$$

where a_0, a_1, b_0, b_1 = as defined before
u = standardised normal deviate associated to a probability P
$S_{\log N}$ = standard deviation of the logarithm of the expected number of load repetitions to failure.

It is obvious that a same type of relation can be derived based on the measured surface curvature index.
As can be seen, the governing factor in the determination of log N_p is the factor $S_{\log N}$, this parameter can be determined using the partial derivative method for determining the variance of a multivariate |25, 26|.
First of all the variance of the equivalent layer thickness ($S^2_{h_e}$) is calculated in the following way

$$S^2_{h_e} = \sum_{i=1}^{L-1} \left(\frac{\delta f}{\delta h_i}\right)^2 S^2_{h_i} + \sum_{i=1}^{L} \left(\frac{\delta f}{\delta E_i}\right)^2 S^2_{E_i} \qquad \text{eq. 3.6}$$

where $S^2_{h_i}$ = variance of layer thickness i
$S^2_{E_I}$ = variance of the elastic modulus of layer i
L = number of layers
$f = 0.9 \sum_{i=1}^{L-1} h_i \sqrt[3]{\frac{E_i}{E_s}}$
h_i = thickness of layer i
E_s = elastic modulus of the subgrade
E_i = elastic modulus of layer i

From the relation

$$\log \varepsilon = b_0 + b_1 \log h_e \qquad \text{eq. 3.7}$$

the variance of the strains is calculated by

$$S^2_{\log \varepsilon} = b_1^2 S^2_{\log h_e} \qquad \text{eq. 3.8}$$

using the first order second moment approach. A detailed description of the calculation of $S^2_{\log h_e}$ is given in appendix 3D.

From the relation

$$\log N = a_0 + a_1 \log \varepsilon \qquad \text{eq. 3.9}$$

the variance of log N is calculated in the same way, which results in

$$S^2_{\log N} = a_1^2 S^2_{\log \varepsilon} = a_1^2 b_1^2 S^2_{\log h_e} + S^2_{\text{l.o.f.}(\log N - \log \varepsilon)} \qquad \text{eq. 3.10}$$

where $S_{\text{l.o.f.}}$ = lack of fit of the equation describing the fatigue relation.

In equation 3.10 a lack of fit term has been introduced because of the large amount of scatter which is normally observed in the results of fatigue tests. A value of 0.16 can be used for the lack of fit term |17| while a value of 0.0035 can be adopted for $S^2_{\log h_e}$ (see also appendix 3D).
As can be observed from eq. 3.10 the value of $S^2_{\log N}$ is mainly determined by the variance in material properties and layer thicknesses as well as the slope of fatigue relation and the slope of the h_e vs ε relation.

Using the same approach to determine the dependency of $S_{\log N}$ on the variance of measured surface curvature index values resulted in

$$S^2_{\log N} = a_1^2 c_1^2 S^2_{\log SCI} + S^2_{\text{l.o.f.}\ (\log N - \log \varepsilon)} \qquad \text{eq. 3.11}$$

This is an important relation since it means that the variance of the pavement life, expressed in a number of load applications N, can be derived from deflection measurements. The importance of this will be described in detail later on. Based on the pavement design curves given in figure 3.5, probability of survival curves were derived for a few values of $S_{\log N}$ and a given value for h_e. These curves are shown in figure 3.12. Also probability of survival curves were derived for several values of h_e and a given value of $S_{\log N}$. These curves are given in figure 3.13. The probability of survival P is defined as the chance the pavement will sustain a certain number of load applications without failure.
As can be seen from figure 3.12, low values of $S_{\log N}$ mean that after a rather long period in which no damage to the pavement can be expected, an abrupt and rather steep decrease of the probability of survival might be expected. This is also illustrated in figure 3.14 where the decrease of P is shown in respect with the ratio applied number of load applications to allowable number of load applications n/N. Since figure 3.14 shows in a basic form the decrease of P in respect of n/N , or in other words the structural deterioration of the pavement in respect of n/N , this figure is defined as the basic structural performance model which can be used for pavement design and pavement evaluation purposes.

3.4.2.2 Further Developments

This section deals with the developments made by the author on the original structural performance model which has been described in the previous section. These developments are mainly concerned with the transformation of the parameter P into other parameters which have a physical meaning. For instance P should give information on the area which exhibits cracking or on to what extent the equivalent layer thickness of the pavement as constructed originally, has deteriorated. These aspects as well as the verification and validation of the nature of the structural performance model, as has been performed by analysing the results of in situ tests on the load carrying capacity of pavements (falling weight deflectometer tests), will be discussed in this section.

3.4.2.2.1 Formulation of an Equivalent Layer Thickness Deterioration Model

If one considers the decrease of h_e with respect to the number of load applications, one will observe that this decrease can be described by an S shaped curve (fig. 3.15).

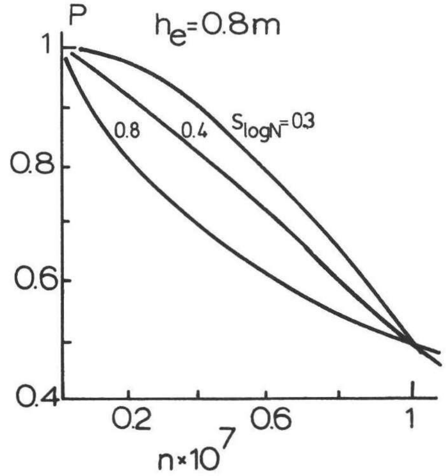

Figure 3.12 Survival Curves for a given value of the Equivalent Layer Thickness (h_e) and different Values of $S_{log\ N}$

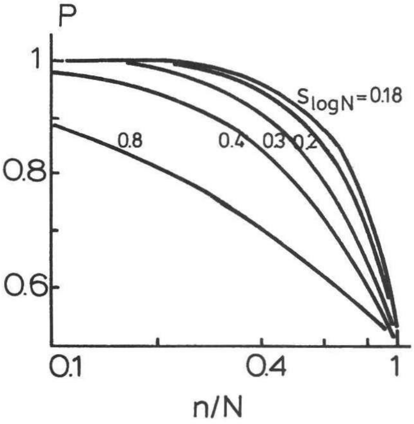

Figure 3.14 Basic Structural Performance Curves

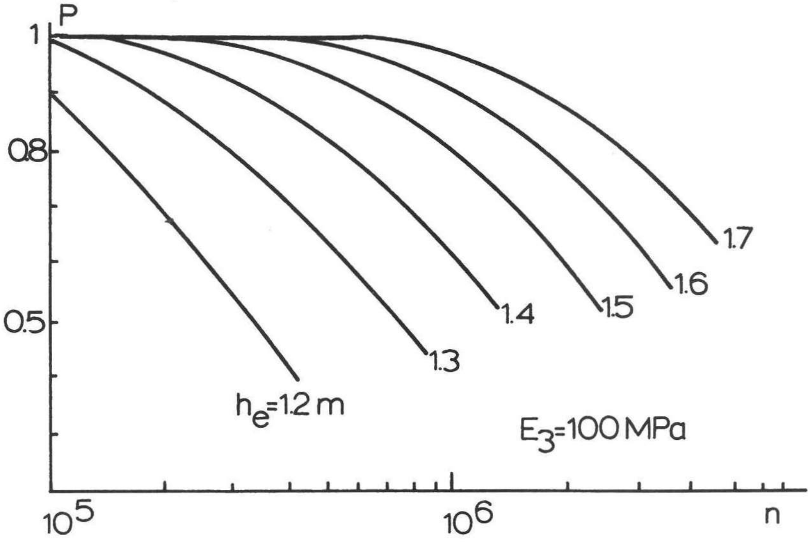

Figure 3.13 Decrease of the Probability of Survival as a function of the number of Load Repetitions and the Equivalent Layer Thickness (h_e)

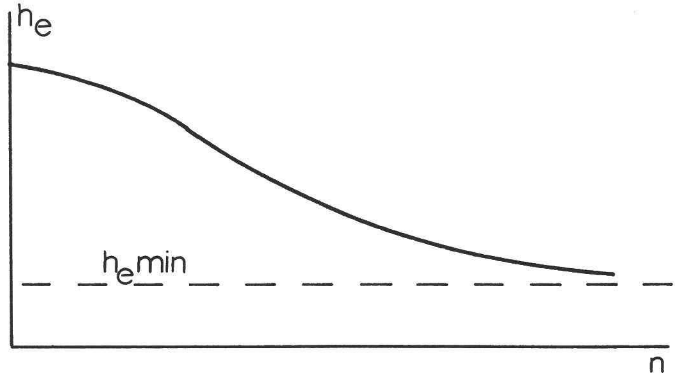

Figure 3.15 *Hypothesized Decrease of the Equivalent Layer Thickness (h_e) with respect to the Number of Load Applications (n)*

The maximum level of h_e is determined by the thickness of the top layer and base and the ratio of the elastic modulus of the top layer resp. base to the elastic modulus of the subgrade. The minimum level of h_e is equal to the sum of the thickness of the top layer and the thickness of the base, assuming that both top layer and base have been ruined so far that the elastic modulus of those layers is the same as the elastic modulus of the subgrade.
Another minimum level of h_e ($h_{e\ min}$) can be defined by assuming that the elastic modulus of the top layer and base deteriorates to that of an unbound base. In this case $h_{e\ min}$ is equal to

$$h_{e\ min} \simeq 1.3\ (h_1 + h_2) \qquad \text{eq. 3.12}$$

where $h_{e\ min}$ = minimum equivalent layer thickness |m| assuming $E_1 = E_2 = 3E_3$
h_1 = thickness of the top layer |m|
h_2 = thickness of the base |m|
E_1 = stiffness of the top layer |MPa|
E_2 = stiffness of the base |MPa|
E_3 = stiffness of the subgrade |MPa|

Although minimum values for h_e can be defined in this way, they are not considered to be applicable to the definition of the end of the pavement life.
A usable minimum h_e level can be defined by considering the condition of the pavement where a crack has propagated through all bound pavement layers and where no transfer of load due to aggregate interlocking across the crack takes place. In other words the pavement has reached its minimum h_e if the original "interior" loading conditions have changed to "free edge" loading conditions. This condition of a fully developed crack coïncides with the condition where n/N = 1 (fig. 3.14).
By using Westergaard's solutions |27| for stresses and displacements at the interior and free edge of plates supported by a Winkler foundation, it can easily be shown that in case of a fully developed crack, the equivalent layer thickness is decreased to 70% (if based on the stress analysis) or 37% (if based on the displacement analysis) of its original value. From this it seems reasonable to define the end of the pavement life as the moment at which the equivalent layer

thickness has decreased to 50% of its original value.

From the foregoing it was concluded that the decrease of h_e with respect to n could be described by

$$h_{e_n} = \frac{h_{e_o}}{1 + e^{\beta \log (n/N)}} \qquad \text{eq. 3.13}$$

where h_{e_n} = equivalent layer thickness after n load repetitions
h_{e_o} = equivalent layer thickness at n = 0
β = a constant
n = number of load repetitions
N = number of load repetitions to failure ($h_{e_n} = 0.5\ h_{e_o}$)

Emphasis is placed on the fact that the shape of the performance curves as defined by equation 3.13 is almost the sȧme as the shape of the performace curves shown in figure 3.14. A comparison between both types of curves is given in figure 3.16.

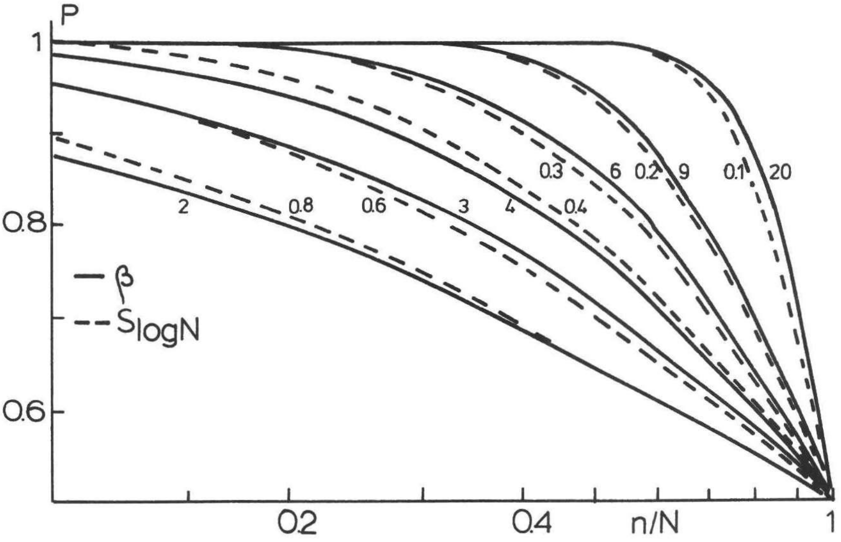

Figure 3.16 *Comparison of the Theoretically Derived Structural Performance Model and the Equivalent Layer Thickness Deterioration Model*

The agreement between the theoretically developed structural performance model and the equivalent layer thickness deterioration model which is hypothesized here, is thought to be of importance since it would mean that the probability of survival of the pavement can be determined from the ratio h_{e_n}/h_{e_o}. This ratio in turn can be estimated by means of deflection measurements.

Considering the properties of equation 3.13 it can be seen that they fullfill the requirements set in the beginning of this section.
The h_{e_n} as described by equation 3.13 varies between a starting value h_{e_o} and some threshold value.
According the equation 3.13, this threshold value is zero. However if one plots the decrease of h_e with respect to n instead of log n, one will observe that af-

ter $h_{en} = 0.5\ h_{eo}$ the decrease will be very gradually and a pratical minimum value for h_e will be observed (fig. 3.17).

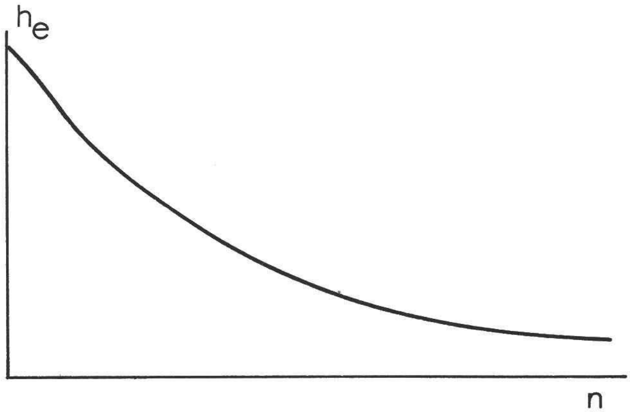

Figure 3.17 *Decrease of the Equivalent Layer Thickness (h_e) with respect to the Number of Load Applications (n)*

In order to check the validity of equation 3.13, it was decided to carry out an experimental program on a number of road sections. This program should consist of deflection measurements taken on a regular base over a number of years. These measurements should be complemented with visual condition surveys in order to qualify and quantify the visual deterioration of the pavement.

The validation of equation 3.13 by means of deflection measurements will be described in the next subsection. The results of the visual condition surveys will be discussed in chapter four.

3.4.2.2.2 Validation of the Equivalent Layer Thickness Deterioration Model by Means of Deflection Measurements

As indicated in the previous subsection, deflection measurements were carried out on a number of road sections over a number of years to verify the validity of equation 3.13. Eleven different road sections were selected which varied in construction as well as in traffic loading.
The construction details of the road sections tested, are given in figure 3.18. The deflection measurements were done by means of a falling weight deflectometer. If available, Benkelman beam data were used too in the analysis.

As will be understood from the previous subsection, the aim of the deflection measurements was to determine the equivalent layer thickness, the decrease of this value in time, and to verify whether this decrease could be modelled by means of equation 3.13. Although this procedure seems rather straight forward, it is not that simple due to the fact that the deflection measurements are influenced by the temperature conditions in the pavement as well as the moisture conditions in the base and subgrade. It is a well known fact that higher deflections will be measured at higher temperatures. This is because the elastic modulus of the asphaltic top layer decreases with increasing temperature. Furthermore the elastic modulus of the subgrade will be influenced by the moisture content of the subgrade material. This moisture content depends on the

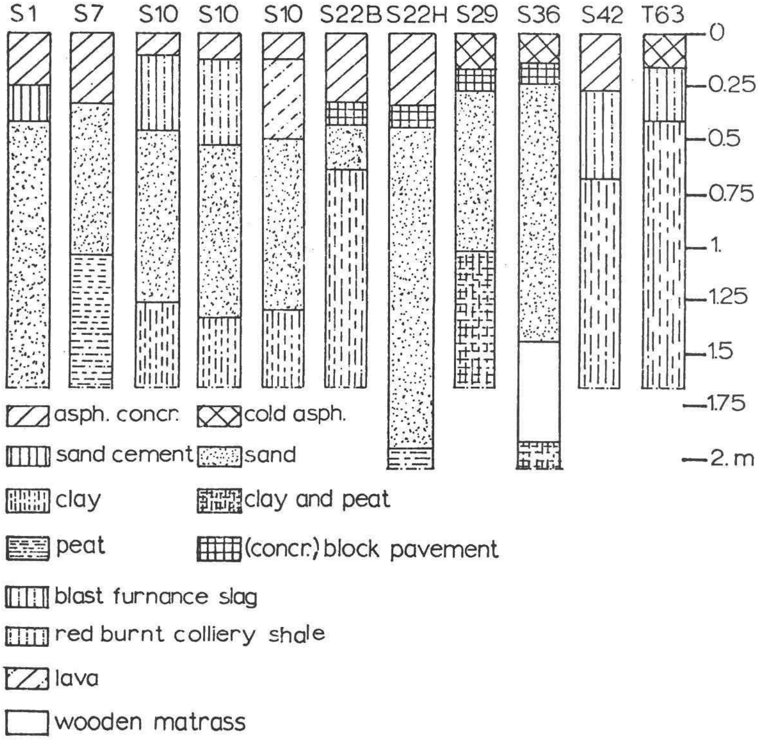

Figure 3.18 Construction Details of the Road Sections evaluated in this Study

moisture supply which in turn is not constant during the year (see also chapter 2).
The first step was therefore to develop a technique which could be used to correct the equivalent layer thickness for influences of varying the stiffness of the top layer, base and subgrade. This has resulted in a so called corrected equivalent layer thickness h_{ec} |20, 29, 30|. The graph which has been developed to calculate h_{ec} from the deflection measurements is given in figure 3.19 |20|. Appendix 3B contains all the details of the development of this correction method.

It should be emphasized that the above mentioned correction method is only applicable to pavements having a hot mix asphalt top layer and should only be used in environmental conditions which are the same as those occuring in the Netherlands.

The h_{ec} values which were derived in this way for the different road sections, were plotted against the number of load applications that were applied to the sections considered. These latter data were obtained from |28, 31, 32|. Subsequently equation 3.13 was used to fit the data. A detailed description of the analysis which has been carried out, is given in appendix 3C.

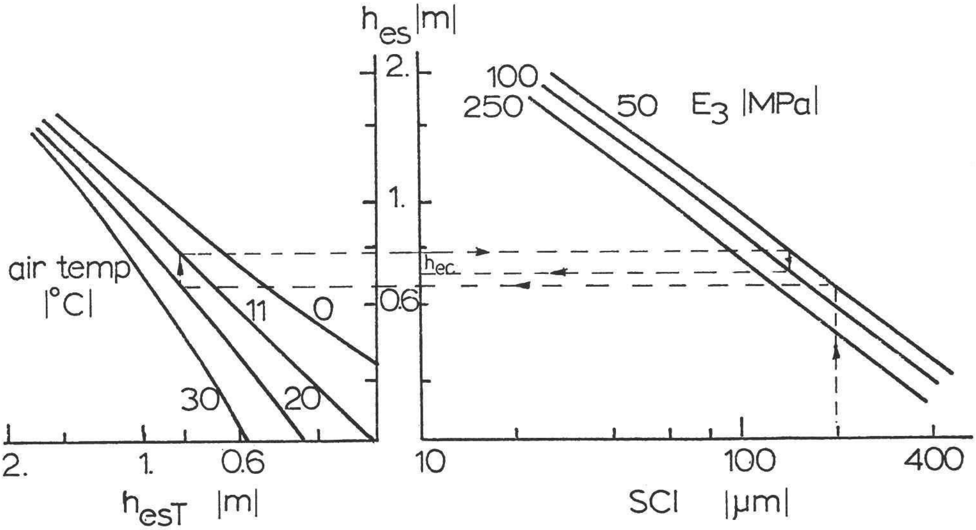

Figure 3.19 Chart to Determine the Corrected Equivalent Layer Thickness h_{e_c}

From this curve fitting proces three conclusions have been drawn:

a. The equivalent layer thickness deterioration model (eq. 3.13) describes rather well the deterioration which have been observed in the field (table 3.3) on flexible pavements having a hot mix asphalt concrete top layer.

b. The equivalent layer thickness deterioration model cannot be used on pavements having a cold asphalt top layer. In fact no decrease of the equivalent layer thickness could be detected on these pavements. This might have been caused by the fact that hardening of the bitumen in the cold asphalt mix balances the deterioration of the layer.

c. In order to obtain reliable estimates for h_{eco} (eq. 3.13) it is strongly recommended to take deflection measurements immediately after construction of a road section has completed.

From the results of the deflection testing program it was concluded that there were no reasons to reject the equivalent layer thickness deterioration model which is represented by equation 3.13. Therefore this model is used in the remaining part of this study to characterize the structural behavior of flexible pavements having a hot mix asphalt concrete top layer.

3.4.3 Development of a Permanent Deformation Model

As has been mentioned before, permanent deformation of the individual layers resulting in permanent deformation of the total construction, is another major aspect which should be considered in the design of new pavements and the evaluation and overlay design of existing pavements.
The type of permanent deformation which will be discussed here is that which occurs in the wheeltracks and which is known as rutting.
Two types of rutting can be discerned (fig. 3.20).

Table 3.3 *Results of the Regression Analysis fitting the Equivalent Layer Thickness Deterioration Model to the observed Data.*

Road Number	Section Number	r^2	β	N
S_1	2L	0.54	2.72	$3.98 * 10^5$
	3L	0.9	3.41	$4.31 * 10^5$
	1R	0.81	5.7	$1.35 * 10^6$
	2R	0.84	2.43	$2.01 * 10^6$
	3R	0.42	3.3	$9.9 * 10^5$
S_7	1L	0.82	2.9	$4.17 * 10^6$
	2L	0.88	3.1	$2.24 * 10^6$
	3L	0.73	2.43	$5.97 * 10^6$
	1R	0.98	2.64	$2.04 * 10^6$
	2R	0.60	1.84	$2.52 * 10^6$
	3R	0.94	2.64	$1.86 * 10^6$
S_{10}	1L	0.32	9.5	$5.75 * 10^5$
	2L	0.44	3.1	$2.95 * 10^5$
	4L	0.66	4.4	$3.23 * 10^5$
	5L	0.75	3.41	$2.06 * 10^5$
	1R	0.91	3.1	$3.13 * 10^5$
	2R	0.80	4.	$1.57 * 10^5$
	3R	0.99	3.	$2.12 * 10^5$
	4R	0.96	3.4	$2.14 * 10^5$
	5R	0.87	3.3	$3.49 * 10^5$
S_{22} B	1L	0.45	2.89	$3.04 * 10^6$
	2L	0.23	1.29	$2.69 * 10^6$
	5L	0.81	1.32	$3.93 * 10^6$
	1R	0.62	0.88	$2.8 * 10^6$
	2R	0.05	0.94	$7.63 * 10^6$
	5R	0.95	2.8	$2.09 * 10^6$
S_{42}	1L	0.43	2.69	$2.45 * 10^6$
	3L	0.79	2.69	$2.14 * 10^6$
	4L	1.	2.55	$5.62 * 10^6$
	5L	0.99	2.82	$2.05 * 10^6$
	1R	0.41	4.3	$1.35 * 10^6$

Note: N is the number of load repetitions to $h_{ecn} = 0.5\ h_{eco}$; h_{ecn} is the corrected equivalent layer thickness after n load repetitions

a. Rutting without lateral displacement of the material. This type of rutting is due to densification of the material and will be called type A rutting.
b. Rutting with lateral displacement of the material. Now the rutting can be judged to be a Prandtl type of shear deformation. This type of rutting will be called type B.

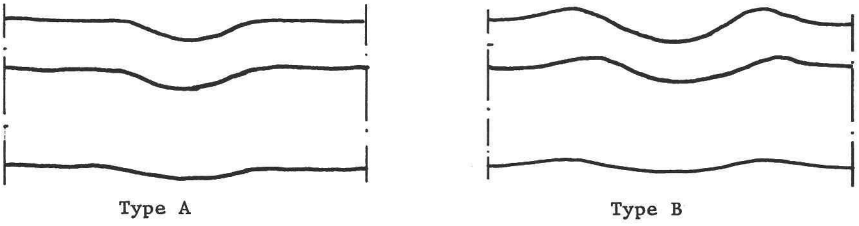

Figure 3.20 Types of Rutting which can be discerned

This section deals with models which can be used to predict the occurrence and magnitude of type A rutting and models which can be used to design pavements in such a way that the occurrence of type B rutting will be prevented.
The presented equations to assess the stresses and displacements in a pavement system are developed by the author while the model which is used to describe the permanent deformation behavior of pavement materials is developed at the Belgian Road Research Centre.

3.4.3.1 Prediction of Type A Rutting

As discussed before, most design methods use a subgrade strain criterion in order to limit the deformations at the top of the subgrade and so the permanent deformation at the pavement surface. This approach was originally developed by Dorman and Metcalf in their analysis of the behavior of the test sections of the AASHO Road test (33). In fact they related the calculated strain level in the subgrade to the number of load applications, that the pavement could sustain to a present serviceability index of 2.5 (fig. 3.21). Since the present serviceability index is an overall pavement performance indicator, the subgrade strain criterion developed by Dorman and Metcalf is not strictly focussed on the prevention of rutting.
The same type of analysis which was carried out by researchers at the Waterways Experiment Station (WES) |34|, in order to obtain subgrade strain criteria to prevent rutting in airfield pavements, resulted in a similar subgrade strain criterion.
Although these simple subgrade strain criteria are very easy to use and therefore very attractive, they are nevertheless thought to cover only a part of the permanent deformation of the pavement structure because each layer can exhibit some permanent deformation itself.

In order to get a better understanding of the permanent deformation characteristics of pavement materials, extensive research has been carried out in the recent past at several research institutes. This research has resulted in models and methods which can be used to make rut depth predictions for a given pavement design.
One rather simple method, which is based on the equivalent layer thickness con-

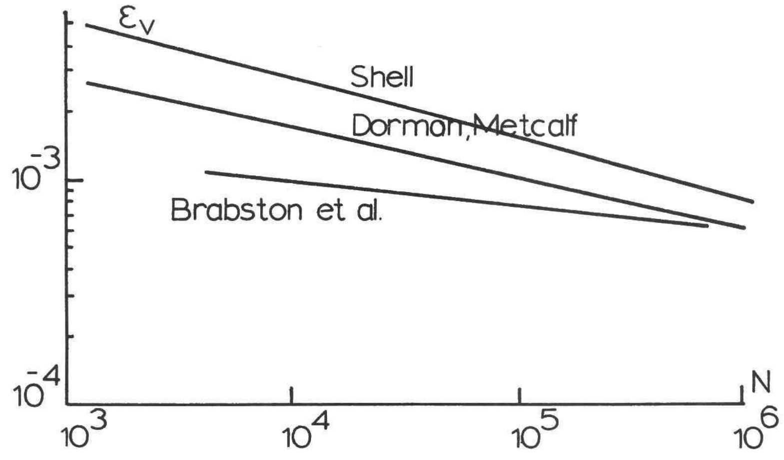

Figure 3.21 *Subgrade Strain Criterion as developed by Dorman and Metcalf*

cept and which is therefore compatible with the approach used in this study, has been reported by Veverka |35|. Veverka's method is based on the concept that the permanent deformation can be estimated from the elastic deformation using.

$$u_p = u_{el}.b_0 n^{b_1} \qquad \text{eq. } 3.14$$

where u_p = permanent deformation |m|
u_{el} = elastic deformation |m|
b_0, b_1 = constants
n = number of repetitions of elastic deformation u_{el}

This basic model has been developed after extensive testing of asphaltic and granular materials, carried out at the Belgium Road Research Center |36, 37|. Veverka showed that for asphaltic concrete the constant b_0 is about 4.49 while b_1 is about 0.25. For granular materials like sand and crushed stone, b_0 is about 2, while b_1 varies between 0.2 and 0.3. Furthermore it was shown |38|, that for fine grained soils the permanent deformation could be estimated by

$$u_p = u_{el}\ (1.3 + 0.7 \log n) \qquad \text{eq. } 3.15$$

Veverka used Odemark's equivalent layer thickness concept and Boussinesq's equation to estimate u_{el} in different parts of the pavement structure. This procedure is represented schematically in figure 3.22.

Verstraeten et al. |39| have shown that a rather good agreement exists between the rut depth as measured and the rut depth as predicted by means of Veverka's method. Figure 3.23 |39| shows the results as reported by Verstraeten et al. It will be obvious that this permanent deformation model, if used together with the equivalent layer thickness deterioration model which was described in the previous sections, forms a simple but comprehensive prediction technique.

The only modification that has been introduced by the author to the method proposed by Veverka is that the deflection factor was calculated for a dual wheel loading by using the tables developed by Ahlvin and Ulery |40|. Also a value of 0.35 was used as Poisson's ratio instead of 0.5 as used by Veverka.

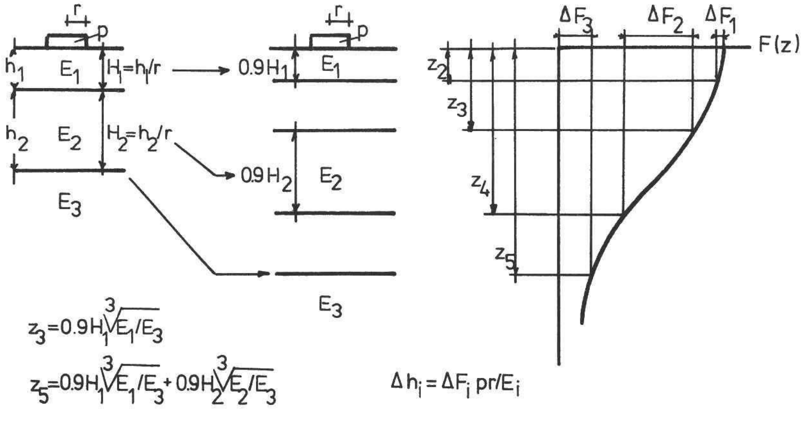

Figure 3.22 *Schematical Representation of the calculation of the Elastic Deformation*

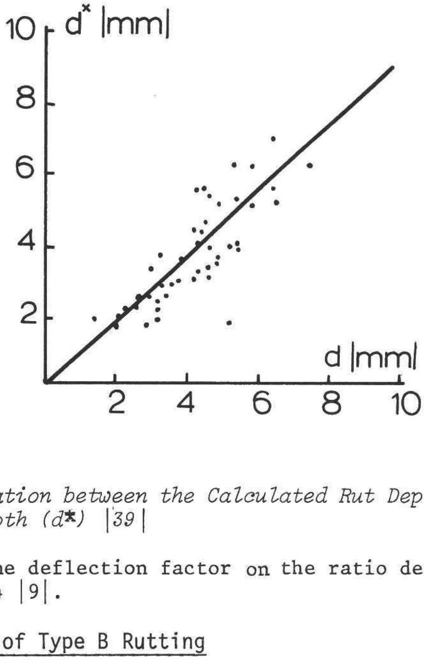

Figure 3.23 *Correlation between the Calculated Rut Depth (d) and the Observed Rut Depth (d^*)* |39|

The dependency of the deflection factor on the ratio depth over load radius is shown in figure 3.24 |9|.

3.4.3.2 Prediction of Type B Rutting

The permanent deformation prediction method presented in the previous section is a very attractive one due to its simplicity in use. However it should be used with caution especially if flexible pavements with rather thin asphaltic top layers are considered. In those cases the load carrying capacity of the

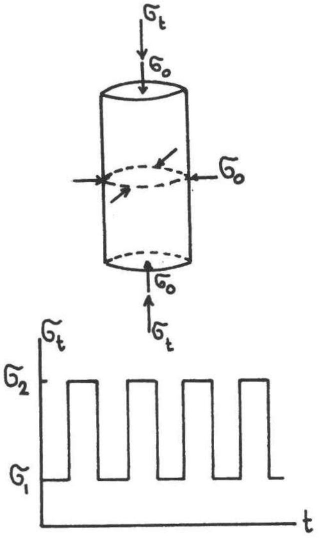

Figure 3.25 *Stress Conditions used in Descornet's Triaxial Tests*

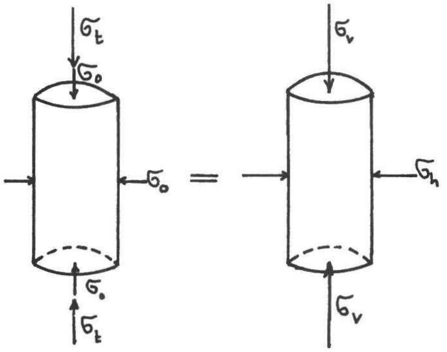

Figure 3.26 *Transformation of Descornet's Stress Conditions into in situ Stress Conditions*

From a closer observation of Descornet's data, this author concluded that R^* was strongly dependent on the dry density and the water content (fig. 3.27).

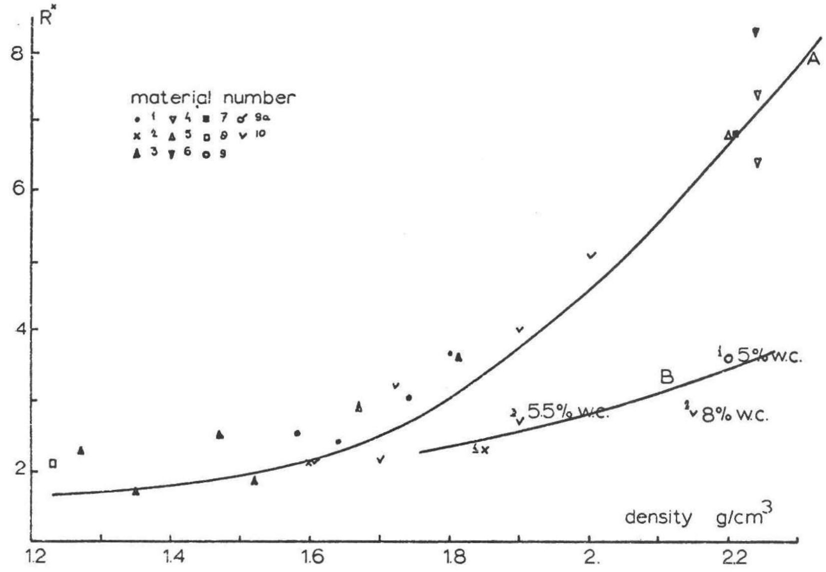

Figure 3.27 *Dependency of R* on the Material Density*

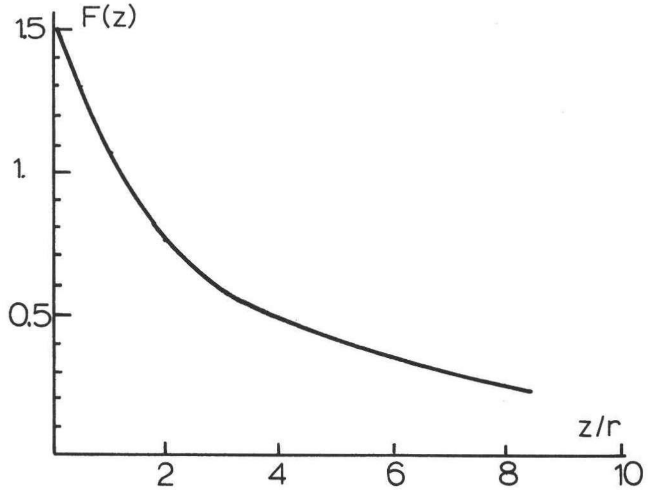

Figure 3.24 Displacement Factors calculated for a Dual Wheel Loading.

pavement comes mainly from the unbound base and subbase and a stress analysis might be necessary to determine whether rutting of type B might occur or not. In other words, such pavement types should be designed in such a way that the permanent deformation of the unbound base layer is due to post compaction of this layer. Preferably the permanent vertical deformation should not be accompanied by permanent horizontal deformations, since then a shear failure type of deformation has taken place. For the shear failure analysis of unbound granular bases, the author has used the limiting deformation model developed by Descornet of the Belgian Road Research Laboratory.
Descornet |36| has shown that no horizontal permanent deformation occurs if

$$R < R^* \qquad \text{eq. 3.16}$$

where $R = 1 + \sigma_1/\sigma_0$
R^* = resistance value of the material
σ_1, σ_0 = definition of the stress conditions used by Descornet in his triaxial tests (fig. 3.25)

The expression for R can be rewritten to the vertical and horizontal stresses that occur in the pavement under a circular load (figure 3.26). This results into

$$R = 1 + \frac{\sigma_v - \sigma_h}{\sigma_h} \qquad \text{eq. 3.17}$$

The values for σ_v and σ_h in the base layer due to traffic loads can be easily determined by means of Odemark's equivalency theory and by using Boussinesq's equations. This procedure is compatible to the procedure of estimating the elastic deformations in the pavement system.
The value of σ_v due to the weight of the overlaying layers can easily be calculated from the volumetric weight and the thickness of the overlaying layers. The value of σ_h due to the overburden pressure can be calculated from

$$\sigma_h = (1 - \sin \phi)\ \sigma_v \qquad \text{eq. 3.18}$$

where ϕ = angle of internal friction

From figure 3.27 the influence of the material density on R^* can easily be observed. The influence of moisture can be observed by taking into account the outliers marked with indices 1 to 4. Points 1, 2 and 3 were obtained on stony materials with rather high water contents. It is believed that due to these high water contents, these materials did not behave like the other materials. From figure 3.27 it can be concluded that a good compaction, a good drainage, and a sealing of the base against intrusion of water, are important factors in the prevention of distortion of the granular base.

It is believed that in this way a rather practical approach to the evaluation of the behavior of unbound granular base layers is obtained.
From knowledge of the equivalent layer thickness and by using Boussinesq's theory, R can be calculated.
A value of R^* can be estimated from figure 3.27, using density measurements as input. If the water content is considered to be high it is recommended to use line B for the estimation of R^* instead of line A.

3.5 Summary

In this chapter a description has been given of a new design method for flexible road constructions.
The method takes into account cracking as well as rutting of the pavement. It is based on simple and meaningful relations that exist between the load carrying capacity of the pavement, quantified by the equivalent layer thickness, and the maximum tensile strain in the asphalt layer and the vertical compressive strain at the top of the subgrade.
The rutting prediction method is based on relations between the equivalent layer thickness and the elastic deformation in the pavement layers, and the relation between the elastic deformation and permanent deformation in pavement layers which has been developed at the Belgian Road Research Laboratory.
In order to be able to predict the future behavior of the pavement, a structural performance model has been developed. It is shown how the structural deterioration depends on the variability of the properties of the materials used and on the variability of the layer thicknesses.
This structural performance model has been verified and validated by means of deflection measurements taken on a relatively limited amount of pavement sections. From this analysis it has been concluded that at this moment the developed model can only be used for pavements with hot mix asphalt concrete top layers. Also it has been shown that the structural condition of the pavement can be quantified by the ratio h_{ecn}/h_{eco}.
Furthermore attention has been paid to the development of surface cracking. It has been shown that this cracking can be explained by taking into account the detrimental effect of inward shear forces which are normally neglected in the design of pavements.
In order to illustrate the use of the design method that has been presented in this chapter, an example will be given in the next section.

3.6 Example

A pavement has to be designed for a tertiary road with a traffic load of $5 * 10^5$ equivalent single 100 kN axles. The subgrade is a sand layer with an elastic modulus of 150 MPa. Unbound granular materials are available to be used

in the base course. Also a blast furnance slag is available for this purpose. This material exhibits some puzzolanic reaction which makes the blast furnance slag to behave like a bound base having an elastic modulus of 1200 MPa. The design should be such that after 10^7 load repetitions the probability of survival is 0.6 or higher. The rut depth should be limited to 18 mm.
From laboratory tests it was determined that the fatigue behavior of the asphalt mix to be used, could be characterized by

$$\log N = -5.345 \log \varepsilon - 15.819 \qquad \text{eq. 3.18}$$

It was decided to use a shift factor of 4 to take into account the benificial effects of rest periods, transverse distribution of traffic etc. This means that only 1 out of 4 load repetitions is contributing to the damage development.
The stiffness of the mix was assumed to be 5000 MPa.

The first step is to calculate the value of $S_{\log N}$ for constructions having a base thickness of 0.15, 0.3 and 0.6 m. These values are given in table 3.4. The necessary h_e vs ε relations are given in table 3.5.

Table 3.4 Values for $S_{\log N}$ used in the Example Problem

Base Type Thickness |m|	Unbound $E_2 = k\ E_3$	Bound $E_2 = 1200$ MPa
0.15	0.64	0.638
0.3	0.738	0.769
0.6	0.996	1.029

Note: $S_{\log N} = \sqrt{a_1{}^2 b_1{}^2 S^2_{\log h_e} + S^2_{l.o.f.(\log N - \log \varepsilon)}}$

$a_1 = -5.345$
b_1 = see table 3.5
$S_{l.o.f.} = 0.4$

Table 3.5 Values of b_0 and b_1 of the Relation $\log \varepsilon = b_0 + b_1 \log h_e$

Base Type Thickness |m|	Unbound $E_2 = k\ E_3$ b_0	 b_1	Bound $E_2 = 1200$ MPa b_0	 b_1
0.15	-4.183	-1.581	-4.294	-1.572
0.30	-4.070	-1.963	-4.158	-2.079
0.60	-3.674	-2.617	-3.617	-2.998

The next step is to calculate the needed equivalent layer thicknesses. For this equation 3.5 is used.
We recall:

$$\log N_p = a_0 + a_1 b_0 + a_1 b_1 \log h_e - u.S_{\log N} \qquad \text{eq. 3.19}$$

where $\log N = a_0 + a_1 \log \varepsilon$
$\log \varepsilon = b_0 + b_1 \log h_e$
$a_0 = -15.819$
$a_1 = -5.345$
b_0, b_1 = see table 3.5

$S_{\log N}$ = see table 3.4
u = 0.255 (for normal distributions; $P = 0.6$)
$N_p = 1.25 \star 10^5$

The calculated h_e values are given in table 3.6

Table 3.6 Calculated Values for the Equivalent Layer Thickness (h_e)

Base Type Thickness |m|	Unbound $E_2 = k\ E_3$	Bound E_2 = 12oo MPa
0.15	0.71	0.61
0.30	0.88	0.80
0.60	1.27	1.31

These h_e values are translated into layer thicknesses using Odemark's equation. The results of this transformation are given in table 3.7.

Table 3.7 Possible Construction Alternatives

Base Type	Unbound		Bound	
Thickness |m|	E_2 |MPa|	h_1 |m|	E_2 |MPa|	h_1 |m|
0.15	300	0.19	1200	0.12
0.30	400	0.18	1200	0.09
0.60	500	0.16	1200	0.08

By using the approach described in section 3.4.3, the permanent deformation was calculated from the elastic deformations which were determined by means of the equivalent layer thickness and Boussinesq's equation.
The results of this analysis are given in table 3.8.
The used permanent deformation laws are given in table 3.9.

Table 3.8 Permanent Deformation predicted for the different Constructions.

Base		Permanent Deformations |m| $\star 10^{-2}$			
Type	Thickness |m|	Top layer	Base	Subgrade	Total
	0.15	0.11	0.06	1.44	1.56
	0.3	0.11	0.12	1.15	1.38
	0.6	0.10	0.13	0.85	1.08
	0.15	0.08		1.27	1.35
	0.3	0.07		1.07	1.14
	0.6	0.05		0.85	0.90

Table 3.9 Permanent Deformation Laws used in the Analysis.

	Permanent Deformation Law
Top layer	$u_p = u_{el} \star 4.49\ n^{0.25}$
Base layer	$u_p = u_{el} \star 2\ n^{0.2}$
Subgrade	$u_p = u_{el} \star 2\ n^{0.3}$

It was assumed that no permanent deformation would occur in the cemented blast furnance slag base.
The calculation procedure has been illustrated in figure 3.28 for the construction having a top layer thickness of 0.19 m and an unbound base thickness of 0.15m.

From the results given in table 3.8 one can observe that each design satifies the permanent deformation constraint. It should be noted however that the structural deterioration was not taken into account in the calculation of the rut depths.

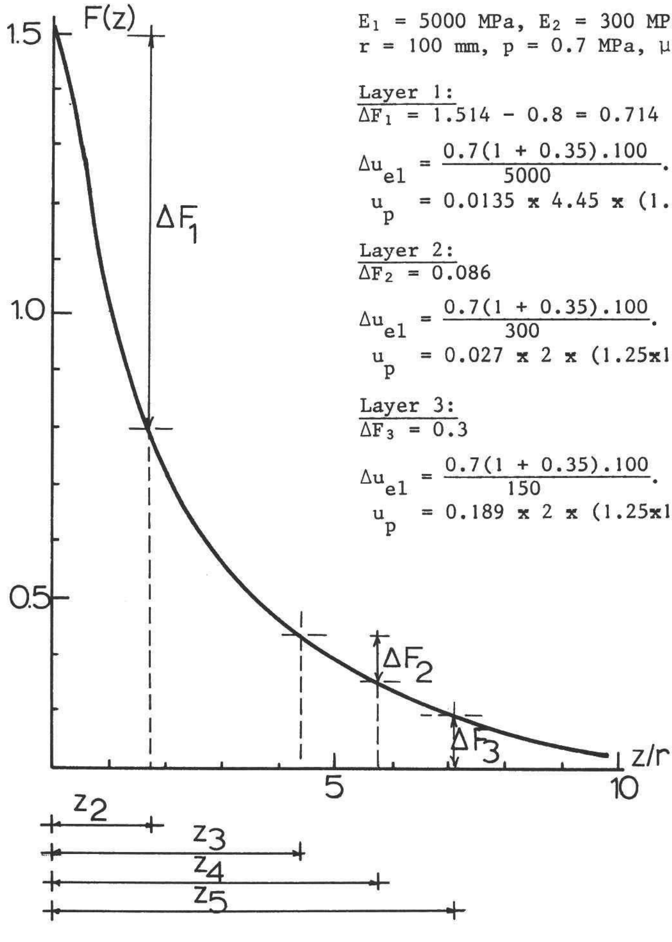

E_1 = 5000 MPa, E_2 = 300 MPa, E_3 = 150 MPa
r = 100 mm, p = 0.7 MPa, μ = 0.35

Layer 1:
$\Delta F_1 = 1.514 - 0.8 = 0.714$

$$\Delta u_{el} = \frac{0.7(1 + 0.35).100}{5000}. 0.714 = 0.0135 \text{ mm}$$

$$u_p = 0.0135 \times 4.45 \times (1.25\times10^5)^{0.25} = 1.1 \text{ mm}$$

Layer 2:
$\Delta F_2 = 0.086$

$$\Delta u_{el} = \frac{0.7(1 + 0.35).100}{300}. 0.086 = 0.027 \text{ mm}$$

$$u_p = 0.027 \times 2 \times (1.25\times10^5)^{0.2} = 0.56 \text{ mm}$$

Layer 3:
$\Delta F_3 = 0.3$

$$\Delta u_{el} = \frac{0.7(1 + 0.35).100}{150}. 0.3 = 0.189 \text{ mm}$$

$$u_p = 0.189 \times 2 \times (1.25\times10^5)^{0.3} = 12.8 \text{ mm}$$

Figure 3.28 Example of the Rut Depth Calculations

Appendix 3A

Theoretical Analysis of the Cracking Behavior of Three Layered Pavement Systems.

3.A.1 Introduction

This appendix describes the theoretical analysis which has been made on cracking of the layered flexible pavement systems. This analysis was thought to be necessary since in previously performed calculations three assumptions have been made, the validity of which should be verified. These assumptions were:

a. The maximum asphalt strain occurs at the bottom of the asphalt layer.
b. Only vertical forces are applied on the pavement.
c. There is a perfect adhesion between two adjacent layers, this means no slip of the layers occurs at the interface of two layers.

The validity of these assumptions and their influence on the earlier developed models and relations, will be discussed in this appendix.
Furthermore the uniqueness of the relation between the surface curvature index and the equivalent layer thickness will be discussed in this appendix. This is because it has been observed in some occasions that the previously developed relations yielded inconsistent results.

3.A.2 Location of the maximum tensile strain in the asphalt layer

The previously developed relations between the h_e or the SCI on one hand and the tensile strain in the asphalt layer on the other, are derived under the assumption that the maximum tensile strain in the asphaltic top layer of a three layered pavement system will occur at the bottom fibers of that top layer. Claessen |6| however has shown that the position of the maximum strain in the asphalt layer depends on the ratio E_2/E_1 and the thickness of the asphalt layer. Claessen et al. have stated that the maximum strain is not at the bottom of the layer if

$$\frac{E_2}{E_1} \cdot h_1 > 0.133 \text{ m} \qquad \text{eq. 3.A.1}$$

where E_2 = stiffness of the base |MPa|
E_1 = stiffness of the top layer |MPa|
h_1 = thickness of the top layer |m|

If $h_1 > 0.20$ m, the maximum strain will occur in the upper half of the top layer. If $h_1 \leq 0.20$ m, the maximum strain occurs in the lower half of the top layer. This would involve that the relations that have been presented in section 3.4.2.2 to estimate the magnitude of the maximum tensile strain at the bottom of the asphalt layer, need to be verified.
Furthermore all calculations were performed assuming that only vertical forces are acting on the pavement. In reality, radial inward shear forces occur under standing as well as under rolling wheels. These forces are normally neglected in the design of pavement structures since it is claimed that their influence is restricted to the upper part of the asphalt top layer. Wardle and Gerrard |24| have shown that this is indeed true but they also have shown that these shear forces, will lead to early surface cracking.
To estimate both the location of the maximum tensile strain in the asphaltic top layer and the effects of the inward shear forces, use was made of the CIRCLY cumputer program |5|, which is the only program known to the author, that is capable of calculating the influence of multiple, vertical and inward shear loads.

3.A.3 Loading Geometry

The CIRCLY program is capable of handling non uniform distributed loads. This option however was thought to be only of importance to the inward shear forces. The vertical forces were assumed to be uniformly distributed. The inward shear forces were modelled as indicated in figure 3.A.1.

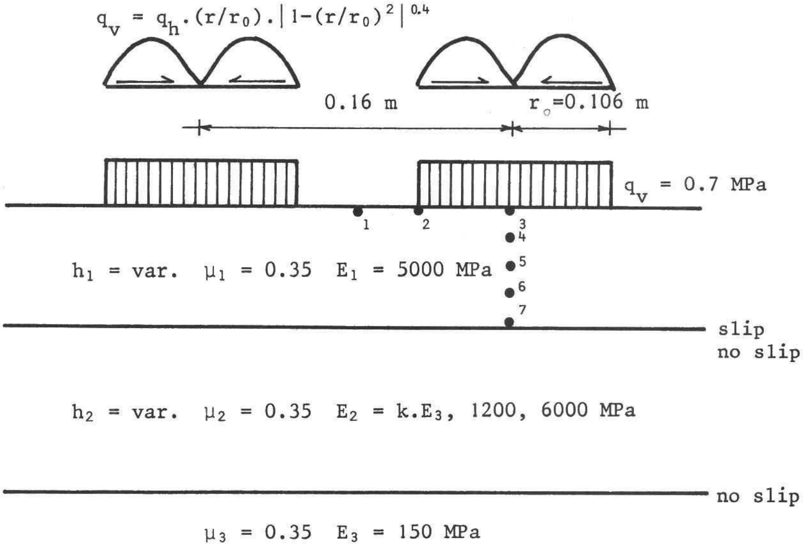

Figure 3.A.1 Characteristics of the evaluated Layered Systems

3.A.4 Pavement Geometry

The pavement geometry used in this part of the study is also shown in figure 3.A.1. The stiffness modulus of the asphalt top layer was set at 5000 MPa being a reasonable value for Dutch circumstances.
The stiffness modulus of the bound base layer was set at 1200 and 6000 MPa representing a moderate and very stiff base.
Also calculations were made on pavement systems with an unbound base. The stiffness of those unbound bases was calculated by means of the well known Shell relation:

$$E_2 = k\, E_3 \qquad \text{eq. 3.A.2}$$

where $k = 0.2\, h_2^{0.45}$ $(2 \leq k \leq 4)$
h_2 = thickness of the base |mm|
E_2 = stiffness of the base |MPa|
E_3 = stiffness of the subgrade |MPa|

The stiffness of the subgrade was set at 150 MPa being the average modulus determined from deflection measurements carried out on pavement sections in the province of Zuid Holland.
The thickness of the asphaltic top layer was set at 0.05, 0.10, 0.20, 0.30 and 0.40 m. Thick layers were used to represent overlay conditions.
The thickness of the base was set at 0.15, 0.30 and 0.60 m.

3.A.5 Calculation Results; Low Stiffness Bases

Table 3.A.1 summarizes the main results. From this it can be seen that in those cases where the asphalt layer is thick (> 0.15 m) the tensile strain in point 2 caused by the inward shear forces is the largest of all strain values considered.

Table 3.A.1 CIRCLY Results for Pavements with an Unbound Base

h_1 |m| / h_2 |m|	0.05	0.1	0.15	0.2	0.3	0.4
0.15	7	7	7	2,7	2	2
0.3	7	7	7	2	2	2
0.6	7	7	2,7	2	2	2

Note: The numbers indicate the positions in the pavement structure (fig.3.A.1)

Furthermore, it is remarkable to note that for all layer combinations studied, the tensile strain at point 2 is more or less constant. The mean strain value is $1.27 * 10^{-4}$ its standard deviation $1.75 * 10^{-5}$. Only for those cases where $h_1 = 0.05$ m the tensile strain at point 2 was $2 * 10^{-4}$.
It should be noted that the tensile strain in point 2 would cause cracking in the direction of travel (longitudinal cracking).
Considering the strains in the points 3 to 7 it should be noted that the maximum value occurred in point 7 for all layered systems.
Finally it is concluded that only for the h_1/h_2 ratio equal to 0.4/0.6 , the tensile strain at point 1 was higher than the tensile strain that occurred in points 3 to 7. It should be noted that this strain would cause cracking perpendicular to the direction of travel (transverse cracking).

From these calculations it can be concluded that the cracking as observed on traditional type flexible pavements which have rather thin asphaltic top layers ($\leq$ 0.15 m) can be classified as cracking which has grown from bottom to top. This kind of cracking indicates total failure of the pavement. On pavements with thick asphalt layers one will most probably observe longitudinal cracking which will grow from top to bottom. Later on an alligator type of cracking will be observed due to transverse cracks which will grow from bottom to top. One can consider the pavement to be failed if this latter type of cracking is observed.

3.A.6 Calculation Results; Stiff Bases

For all pavement systems having a stiff base (E_2 = 1200 or 6000 MPa) the tensile strain at point 2, caused by the inward shear forces, was the highest. For the systems having a base with E_2 = 1200 MPa, the mean value of the strain at point 2 was $1.41 * 10^{-4}$, while its standard deviation was $1.26 * 10^{-5}$. For the systems with a base stiffness of 6000 MPa this mean strain value is $1.49 * 10^{-4}$ and its standard deviation $1.79 * 10^{-5}$. These values are very close to the strain values calculated in point 2 for the low base stiffness constructions.
This has led to the conclusion that the strain at point 2 is hardly affected by the stiffness of the base or the layer thicknesses but is only dependent on the stiffness of the top layer. Furthermore it was concluded that for design pur-

poses the tensile strain at point 2 could be set at $1.5 * 10^{-4}$ for those cases where the stiffness of the asphalt top layer is equal to 5000 MPa.
It was also concluded that the tensile strain at point 1 was higher than the strain at point 3 to 7 for the h_1/h_2 combinations 0.3/0.6; 0.4/0.15; 0.4/0.3 and 0.4/0.6 if E_2 = 1200 MPa. This is also the case for all but three h_1/h_2 combinations if E_2 = 6000 MPa.
Considering the strain distribution over point 3 to 7 it could be concluded that for the systems with E_2 = 1200 MPa the maximum value was found at point 7 (except the h_1/h_2 = 0.4/0.6 combination).
For the layered systems with E_2 = 6000 MPa this maximum strain value was found at mid depth of the top layer or at $\frac{1}{4}$ h_1 below the surface.

From the calculation results it is concluded that most of the longitudinal cracking observed in the wheel paths of pavements with a stiff base can be considered as cracking which is growing from top to bottom. Most probably transverse cracking will also be observed on this pavement type. This latter type of cracking is most probably caused by fatigue cracking of the base or by tensile stresses due to shrinkage of the bound base (shrinkage is caused by environmental effects).

3.A.7 Results of Additional Calculations

In order to check whether the tensile strains at point 2 would change with a change in elastic modulus of the top layer, calculations were performed on a number of pavement systems with top layer stiffnesses of 1000 and 10000 MPa. For the systems having a top layer with an elastic modulus of 10000 PMa, the mean value of the strain at point 2 was $7.43 * 10^{-5}$, its standard deviation was $5.87 * 10^{-6}$. For the layered systems having a top layer with an elastic modulus of 1000 MPa, the mean value and standard deviation of the strain at point 2 were $8.12 * 10^{-4}$ and $5.39 * 10^{-5}$. Together with the strain values at point 2 determined for systems having a top layer elastic modulus of 5000 MPa. The following simple equation was derived.

$$\log \varepsilon_{t.e.} = 4.822 * 10^{-2} - 1.049 \log E_1 \quad (r = 0.999) \qquad \text{eq. 3.A.3}$$

where $\varepsilon_{t.e.}$ = tensile strain at the tire edges of a dual wheel load.
E_1 = elastic modulus of the top layer (MPa)

This equation can be used to assess the tensile strain at the pavement surface and to determine when and whether cracking which originates at the top of the pavement may occur.

3.A.8 Influence of Slip between the Layers

As mentioned before, all previous calculations were performed assuming perfect adhesion between all layers, this however will not always be the case. In a number of cases the adhesion between the layers is imperfect due to an irregular distribution or lack of tack coat, due to moisture, loose material , or dirt at the top of the layer to be overlaid.
It will be obvious that an imperfect adhesion will cause higher strains in the layers and will therefore result in an accelerated structural deterioration of the pavement. In order to study the effect of slip between the layers, calculations were performed on three layered pavement systems having top layer thicknesses of 0.1 , 0.2 and 0.3 m . The stiffness of the top layer was set

again at 5000 MPa. For the base and subgrade the same stiffness and thickness values were chosen as used in the calculations mentioned in the previous section.
Perfect adhesion was assumed between the subgrade and the base layer, no adhesion was assumed between the base and top layer. The effect of these assumptions on the surface curvature index and maximum horizontal strain is shown in table 3.A.2.

Table 3.A.2 Influence of full Adhesion or full Slip between Top Layer and Base on the Surface Curvature Index (SCI) and the Maximum Tensile Strain in the Asphaltic Top Layer

	$h_1\ \lvert m \rvert$	0.1		0.2		0.3	
$E_2\ \lvert MPa \rvert$	$h_2\ \lvert m \rvert$	$\frac{SCI_s}{SCI_a}$	$\frac{\varepsilon_s}{\varepsilon_a}$	$\frac{SCI_s}{SCI_a}$	$\frac{\varepsilon_s}{\varepsilon_a}$	$\frac{SCI_s}{SCI_a}$	$\frac{\varepsilon_s}{\varepsilon_a}$
300	0.15	1.22	1.31	1.16	1.25	1.09	1.2
400	0.30	1.25	1.36	1.19	1.33	1.13	1.3
500	0.60	1.21	1.37	1.18	1.38	1.14	1.39
1200	0.15	1.58	2.22	1.40	1.88	1.21	1.69
	0.30	1.45	2.07	1.39	2	1.25	1.88
	0.60	1.26	1.82	1.27	1.78	1.20	1.86
6000	0.15	1.90	29.3	1.78	5.72	1.48	3.56
	0.30	1.50	11.4	1.50	3.19	1.42	2.25
	0.60	1.31	5.05	1.24	1.92	1.19	1.33

SCI_s = Surface curvature index of there is no adhesion between top layer and base.
SCI_a = Surface curvature index if there is full adhesion between top layer and base.
ε_s = Maximum tensile strain in the asphalt layer if there is no adhesion between top layer and base.
ε_a = Maximum tensile strain in the asphalt layer if there is full adhesion between top layer and base.

This table shows a dramatic increase in maximum strain and surface curvature index if slip occurs between the top layer and the base. This is especially the case for the layered systems having a stiff base. In these cases the position of the maximum strain also changes from the upper half or middepth, to the bottom of the top layer. The tensile strain at point 2 (fig. 3.A.2), had a mean value of $1.4 \ast 10^{-4}$ and a standard deviation of $2.3 \ast 10^{-5}$. Knowing the strain values at point 2 for the layered systems having perfect adhesion between the layers, it can again be concluded that this surface strain is a constant for the given loading system and is only dependent on the stiffness of the top layer.

3.A.9 Relations between the Equivalent Layer Thickness and the Maximum Tensile Strain in the Asphalt Layer

From the results of the previous mentioned calculations, improved relations

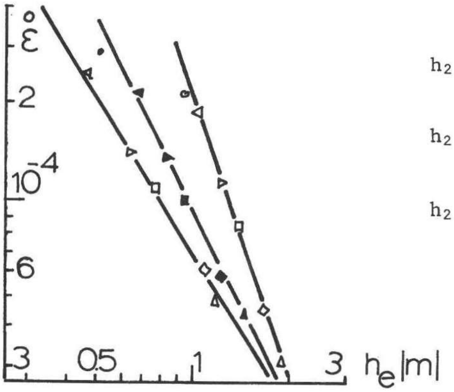

h_2 = 0.15 m: $\log \varepsilon = -4.183 - 1.581 \log h_e$
$r = -0.99$

h_2 = 0.3 m: $\log \varepsilon = -4.070 - 1.963 \log h_e$
$r = -0.99$

h_2 = 0.6 m: $\log \varepsilon = -3.674 - 2.884 \log h_e$
$r = -0.99$

$$\log \varepsilon = -4.381 + 1.158\, h_2 - (1.121 + 2.921\, h_2) \log h_e$$

$|h_e| = |m|$

Figure 3.A.2 *Relation between the Equivalent Layer Thickness (h_e) and the Maximum Tensile Strain in the Asphalt Layer (ε) for Pavements with an Unbound Base*

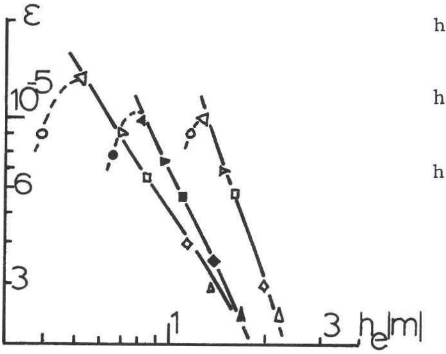

h_2 = 0.15 m: $\log \varepsilon = -4.294 - 1.572 \log h_e$
$r = -0.99$

h_2 = 0.3 m: $\log \varepsilon = -4.158 - 2.079 \log h_e$
$r = -0.99$

h_2 = 0.6 m: $\log \varepsilon = -3.617 - 2.998 \log h_e$
$r = -0.99$

$$\log \varepsilon = -4.565 + 1.547\, h_2 - (1.113 + 3.514\, h_2) \log h_e$$

$|h_e| = |m|$

Figure 3.A.3 *Relation between the Equivalent Layer Thickness (h_e) and the Maximum Tensile Strain in the Asphalt Layer (ε) for Pavements with a Moderate Stiff Bound Base (E_2 = 1200 MPa)*

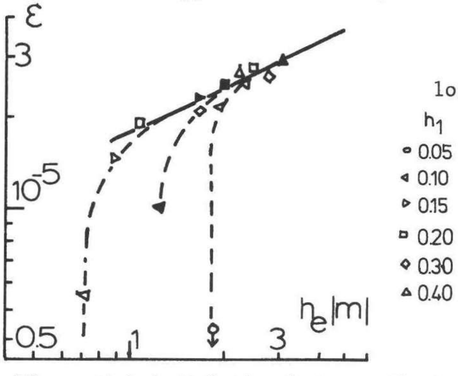

$\log \varepsilon = -4.779 + 0.458 \log h_e$ $r = 0.95$

$|h_e| = |m|$

Figure 3.A.4 *Relation between the Equivalent Layer Thickness (h_e) and the Maximum Tensile Strain in the Asphalt Layer (ε) for Pavements with a Stiff Bound Base (E_2 = 6000 MPa)*

between the h_e on one hand and the ε on the other were derived. They are shown in figures 3.A.2 to 3.A.4.
From figures 3.A.2 and 3.A.3, which give the results of the calculations on pavements having unbound and bound moderate stiff bases, it is concluded that in order to estimate the maximum tensile strain in the asphaltic top layer with a high degree of accuracy, the thickness of the base should be taken into account. Also the stiffness of the base is of importance but only to a limited extent. In cases of bound stiff bases (E_2 = 6000 MPa, fig. 3.A.4) the effect of the base thickness is absent. Furthermore it can be seen that the tensile strain will increase with increasing equivalent layer thickness.
In order to check whether the earlier developed relation between h_e and ε gave unreliable results, the old relation and the new one's were compared by plotting them into one graph (figure 3.A.5).

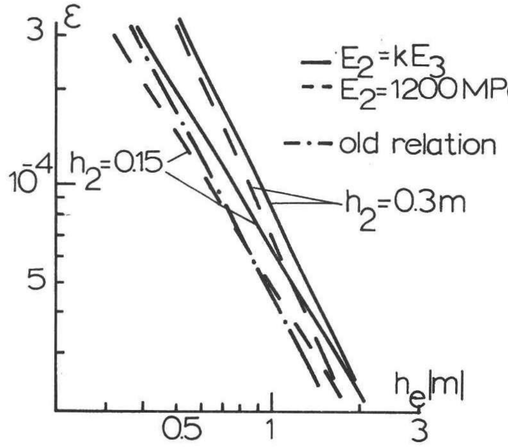

Figure 3.A.5 Comparison between the New Relation Equivalent Layer Thickness (h_e) vs Maximum Tensile Strain in the Asphalt Layer (ε), and the Previously developed Relation.

From figure 3.A.5 it can be concluded that by means of the new relations, higher strain levels are predicted. Furthermore it can be concluded that the old relation and the new relations, given for h_2 = 0.3 m, are almost parallel. For design purposes it seems reasonably to use the h_e-ε relation derived for unbound bases. This is because base thicknesses of 0.3 m are commonly used. Nevertheless it should be concluded that, unfortunately, the equivalent layer thickness is not the unique parameter to define the load carrying capacity of the pavement, as was suggested earlier.

3.A.10 Relations between the Surface Curvature Index and Maximum Tensile Strain in the Asphalt Layer.

Using the results of the calculations described in the previous sections, a new relation was derived between the surface curvature index on one hand and the maximum tensile strain in the asphalt layer on the other.
This relation is shwon in figure 3.A.6. In mathematical form this relation can be written as:

$$\log \varepsilon = -5.767 + 0.943 \log SCI \quad r^2 = 0.95, n = 52 \qquad \text{eq. 3.A.4}$$

where ε = maximum tensile strain in the asphalt layer due to a dual wheel loading of 50 kN
SCI = surface curvature index due to a dual wheel loading of 50 kN |µm|

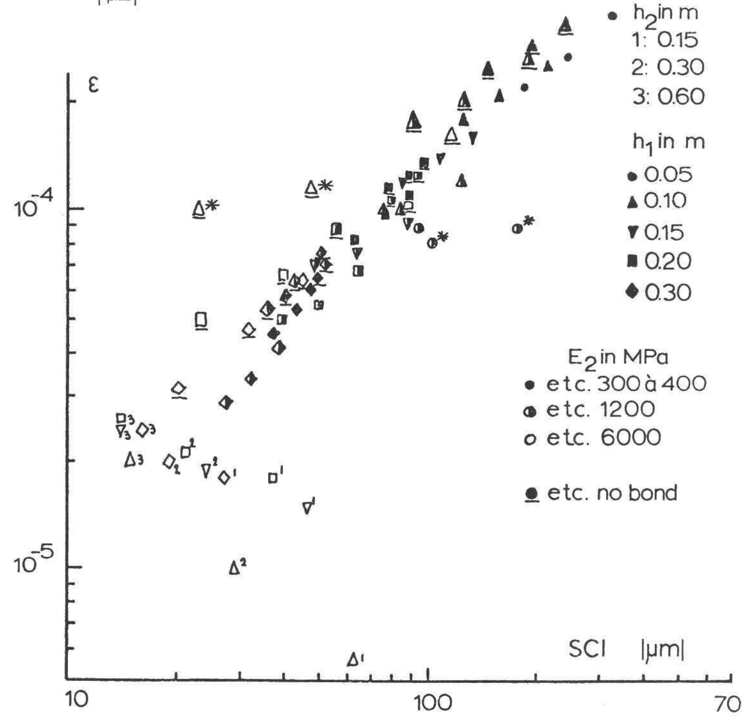

Figure 3.A.6 Relation between the Surface Curvature Index (SCI) and the Maximum Tensile Strain in the Asphalt Layer (ε) both due to a Dual Wheel Loading of 50 kN.

The main conclusion which can be drawn from figure 3.A.6 is that in general the surface curvature index is a good indicator for the maximum strain in the asphalt layer for pavement structures having a good adhesion between the layers as well as for pavement structures where this adhesion is absent. It should be noted however that at surface curvature index values of 80 µm and less, the strain values predicted by using the regression equation are too low for the pavements having a 0.1 m thick top layer and no adhesion between the top layer and the base. For these cases, the maximum asphalt strain tends to take a constant value of about 1.10^{-4}.

It should be noted that the points marked with an asterisk are not taken into account. These points represent structures which have a base stiffness of 1200 MPa. Here the tensile strain seems to be more or less constant taking a value of 9.10^{-5}.

Also the data points obtained from structures having a base layer stiffness of 6000 MPa and full adhesion between the layers were not taken into account. This is because for these types of construction the tensile strain decreases with increasing surface curvature index. Also the constructions with a 0.05 m thick top layer on a base with a stiffness of 6000 MPa are omitted since in these cases the asphalt layer was in compression. This opposed behavior can be explained by the fact that in these cases the stiff base is the main contributor in the load carrying capacity. Higher SCI values are now caused by the fact that the top layer stiffness is lower compared to the base stiffness. It should be noted that for these pavements with a stiff base, the maximum tensile strain is at most $2.5 * 10^{-5}$ which is in fact 6 times lower than the tensile strain due to the inward shear forces.

It might be argued that in case of a bound base, the tensile strain at the bottom of the base is more critical than the tensile strain in the asphalt layer especially if the bound base material has a lower fatigue resistance than the asphaltic material used in the top layer. Therefore also a relation was developed between the SCI and the base strain both due to a dual wheel loading of 50 kN |20|. This relation is:

$$\log \varepsilon_{base} = -5.858 + 0.966 \log SCI \quad r^2 = 0.97 \qquad \text{eq. 3.A.5}$$

where ε_{base} = tensile strain at the bottom of the base due to a dual wheel loading of 50 kN.
SCI = surface curvature index due to a dual wheel loadong of 50 kN |μm|

A comparison between the SCI vs $\varepsilon_{asphalt\ layer}$ relation developed here and the previously developed relation is given in figure 3.A.7

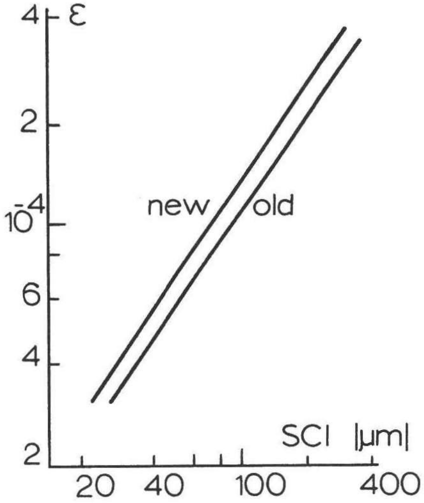

Figure 3.A.7 Comparison between the new SCI vs $\varepsilon_{asphalt}$ Relation and the Previously developed Relation.

As can be seen, both relations are parallel to each other but the relation derived here predicts strain values which are about 1.2 times higher than those which are obtained by using the old relation. The differences between both relations should be attributed to the effect of inward shear forces which were neglected in |20| and which were taken under consideration in this study. Figure 3.A.8 shows the new SCI vs asphalt strain relation together with the SCI vs base strain relation and the surface strain values as determined for an elastic modulus value of the top layer of 5000 MPa.

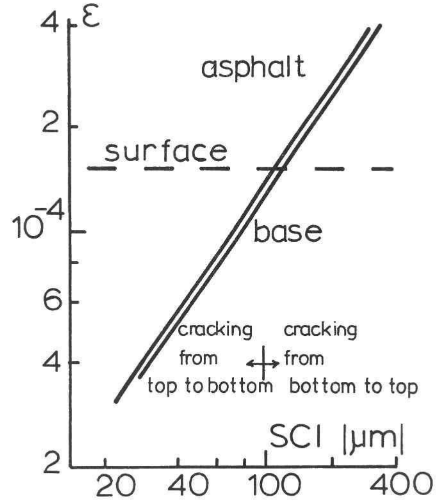

Figure 3.A.8 Relations between the Surface Curvature Index (SCI) and Maximum Tensile Strain in the Asphalt cq Base Layer (ε)

From figures 3.A.6 and 3.A.8 the following conclusions have been drawn

a. For pavements having SCI values of 100 μm and higher, cracking will grow from the bottom of the asphalt layer to the top.

b. For pavements having SCI values lower than 100 μm surface cracking may occur before fatigue cracking within the asphalt layer.

c. Whether fatigue cracking in the asphalt layer or the stabilized base will be predominant depends solely on the fatigue properties of the materials considered, since the tensile strain at the bottom of the base is almost equal to the maximum tensile strain in the asphalt layer.

d. Taking cores is considered to be an important aspect in pavement evaluation since this allows the determination of the adhesion between the layers.

One should be aware of the fact that these conclusions are only valid for the loading configuration considered.
The question also arises whether the conclusions are still valid if other subgrade moduli are considered.
A first indication that this question can be answered positively can already be obtained considering the previously determined relations between the SCI and the maximum tensile strain in the asphalt layer (figure 3.7). From this figure it can be concluded that the subgrade modulus has only a limited influence.
To get more evidence of this, it was checked whether the SCI due to a falling weight load geometry is affected by the subgrade modulus. Only a minor influence could be observed that could be described by

$$SCI_{E_3=100} = (-8.039 + 2.858 \log E_3) + (0.8397 + 0.0875 \log E_3) SCI_{E_3} \qquad \text{eq. 3.A.6}$$

where SCI_{E_3} = surface curvature index as measured |μm|
E_3 = subgrade modulus |MPa|
$SCI_{E_3=100}$ = surface curvature index of the pavement if the same structure was laid on a subgrade with E_3 = 100 MPa |μm|

From this equation it can easily be shown that, for practical purposes, the influence of the subgrade modulus on the SCI and so on the asphalt strain can be neglected.

3.A.11 Surface Curvature Index and Equivalent Layer Thickness

As mentioned before the surface curvature index and equivalent layer thickness were related to each other since it was thought that an equivalent thickness is a more meaningful parameter than a surface curvature index. This early developed relation has been shown in figure 3.6. Further studies however have indicated that the relation is not as unique as shown in figure 3.6 and therefore a more careful study on this relation was carried out. The results are shown in figures 3.A.9 to 3.A.11. The relations give rise to the following comments. In order to be able to assess the h_e from the SCI with a high degree of accuracy it is important to take into account the thickness of the base. The influence of the base thickness on the relation disappears if stiff bases are concerned. From the data shown in figure 3.A.11 it can be concluded that the equivalent layer thickness of pavements with a stiff base can better be estimated from the difference in deflection measured at the loading centre and at a distance of 1 m from the loading centre. We recall that usually the SCI is defined as the difference in deflection measured at the loading centre and at a distance of 0.5 m from the loading centre.
In order to check whether, and to what extent these improved relations differ from the previous developed relation, both the new and the old relations were plotted into one graph (fig. 3.A.12)

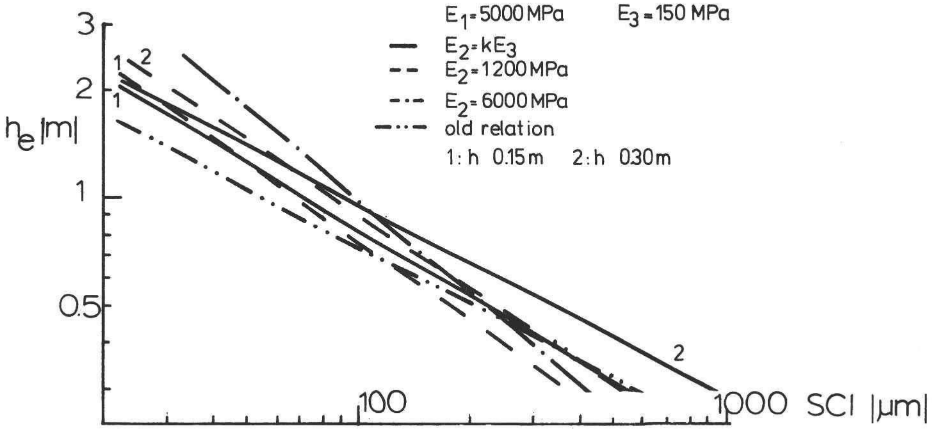

Figure 3.A.12 *Comparison between New Surface Curvature Index (SCI) vs Equivalent Layer Thickness (h_e) Relation and the Previously developed Relation.*

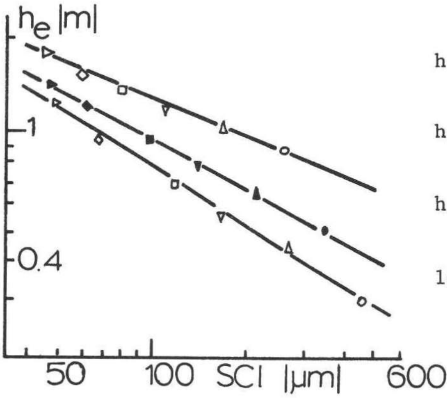

h_2= 0.15 m: $\log h_e = 1.142 - 0.613 \log SCI$
$r = -0.99$

h_2= 0.3 m : $\log h_e = 1.058 - 0.534 \log SCI$
$r = -0.99$

h_2= 0.6 m : $\log h_e = 0.945 - 0.408 \log SCI$
$r = -0.99$

$\log h_e = 1.199 - 0.429h_2-(0.676-0.450h_2) \log SCI$

$|h_e| = |m|$ $|SCI| = |\mu m|$

Figure 3.A.9 Relation between the Surface Curvature Index (SCI) and the Equivalent Layer Thickness (h_e) for Pavements with an Unbound Base.

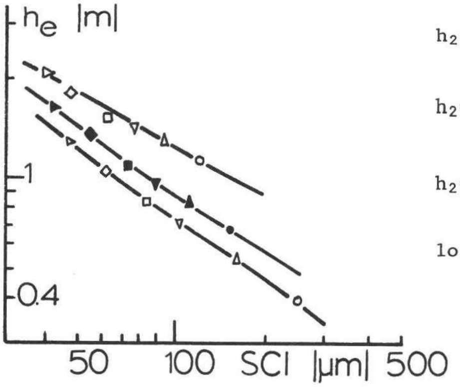

h_2= 0.15 m: $\log h_e = 1.324 - 0.716 \log SCI$
$r = -0.99$

h_2= 0.3 m : $\log h_e = 1.313 - 0.678 \log SCI$
$r = -0.99$

h_2= 0.6 m : $\log h_e = 1.155 - 0.518 \log SCI$
$r = -0.99$

$\log h_e = 1.403 - 0.397h_2-(0.796-0.453h_2) \log SCI$

$|h_e| = |m|$ $|SCI| = |\mu m|$

Figure 3.A.10 Relation between the Surface Curvature Index (SCI) and the Equivalent Layer Thickness (h_e) for Pavements with a Moderate Stiff Bound Base (E_2 = 1200 MPa)

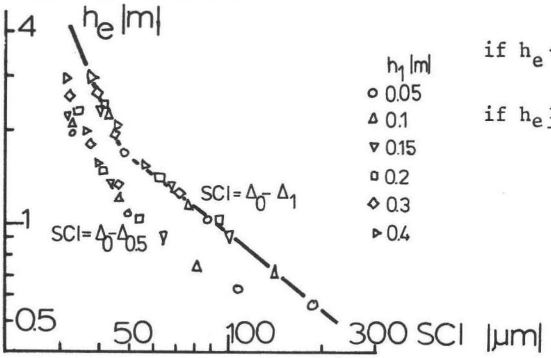

if $h_e < 2$: $\log h_e = 1.640-0.822 \log SCI$
$r = -0.99$

if $h_e \geq 2$: $\log h_e = 3.497-1.927 \log SCI$
$r = -0.93$

$|h_e| = |m|$
$|SCI| = |\mu m|$

Figure 3.A.11 Relation between the Surface Curvature Index (SCI) and the Equivalent Layer Thickness (h_e) for Pavements with a Stiff Bound Base (E_2 = 6000 MPa)

From figure 3.A.12 it can be concluded that the old relation was on the conservative side. This is caused by the fact that no inward shear forces were taken into account when developing the old relation.
Since the relations shown in figure 3.A.9 to 3.A.11 were derived for pavement systems having a stiffness of the top layer of 5000 MPa, it was also studied whether different stiffnesses of this layer might also influence the SCI vs h_e relation.
From the results of these calculations, shown in figure 3.A.13, it is concluded that there is indeed an influence of the stiffness of the top layer on the SCI vs h_e relation, but that this influence is only limited and can be neglected for practical purposes.

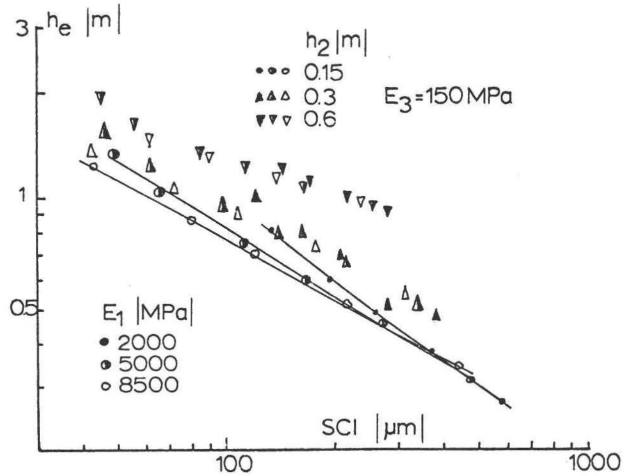

Figure 3.A.13 Comparison between the New Surface Curvature Index (SCI) vs Equivalent Layer Thickness (h_e) Relations and the Previously developed Relation.

Appendix 3B

Development of a Correction Method on the Equivalent Layer Thickness as determined by means of Deflection Measurements taken at Various Moments during the Year.

3.B.1 Temperature Corrections

Beuving and Molenaar |29| tried to correct the measured deflections for temperature influences using the deflection and temperature data as gathered. Only for pavements having a cold asphalt toplayer a linear relation between the measured air temperature and the measured surface curvature index could be derived. This relation however was not unique but was dependent on thickness of the asphaltic layer. Since only two layer thicknesses were considered, this dependency could not be studied further.

For all pavements having a hot mix asphaltic toplayer it was determined that only a linear relation between the air temperature and h_{es}, which is the equivalent layer thickness (h_e) of the construction translated to a reference subgrade having an elastic modulus of 100 MPa, existed.
This relation could be written as

$$h_{esT} = h_{es} + (\text{Temp} - 11) * 0.014 \qquad \text{eq. 3.B.1}$$

where $h_{es} = h_e \sqrt[3]{\frac{E_3}{100}}$ |m| eq. 3.B.2

E_3 = subgrade modulus |MPa|
h_e = equivalent layer thickness of the structure as determined from deflection measurements |m|
0.014 = increase of h_{es} at a temperature drop of 1°C
Temp = air temperature at the time of the deflection measurements |°C|

The reference temperature was set at 11°C since this is the weighted mean annual air temperature for Dutch circumstances |13|.
It should be noted that by comparing the h_{esT} values of different constructions with each other, the load carrying capacity of the layer above the subgrade is compared and not the load carrying capacity of the pavement structure!
So h_{esT} can be defined as the potential load carrying capacity.
It could be argued that the h_{es} is a rather artificial factor to which the temperature corrections are applied. For the following reasons this is thought not to be true. For pavement structures which have a base layer consisting of unbound materials, a raise in temperature not only means a softening of the asphaltic toplayer but also a stiffening of the base layer. Due to the lower stiffness of the asphalt layer at higher temperatures, which results in higher surface curvature indexes, the stress level in the base layer will increase. Since the elastic modulus of unbound granular materials is stress dependent, following equation 3.B.3, higher stress levels mean a higher elastic modulus.

$$E_2 = k_1 \, \theta^{k_2} \qquad \text{eq. 3.B.3}$$

where E_2 = elastic modulus of the granular base
k_1, k_2 = constants depending on the type of material, degree of compaction etc.
θ = first stress invariant

An increasing base modulus will of course reduce the surface curvature index. Therefore it is thought that the temperature correction approach based on the h_{es} is reasonable since this value takes into account both layer thicknesses.

Although the developed temperature correction technique is a simple one and is based on field observation, it is felt necessary to study the validity of equation 3.B.1 by means of a theoretical analysis. This is because the developed technique uses <u>air</u> temperatures instead of pavement temperatures as input.

This is considered to be a drawback since the pavement temperature might differ remarkably from the air temperature.
The desired theoretical validation of equation 3.B.1, can easily be obtained by checking to what extent the h_{es} is influenced by a change in stiffness of the asphaltic top layer.
We recall

$$h_e = 0.9\ h \sqrt[3]{\frac{E_1}{E_3}} + 0.9\ h_2 \sqrt[3]{\frac{E_2}{E_3}} \qquad \text{eq. 3.B.4}$$

and $h_{es} = h_e \sqrt[3]{\frac{E_3}{100}}$

It can easily be shown that if the elastic modulus of the base (E_2) remains constant, the influence of temperature on h_{es} can be calculated by

$$\frac{\Delta h_{es}}{\Delta T} = \frac{0.9\ h_1}{\sqrt[3]{100}} \left(\sqrt[3]{E_{1T_1}} - \sqrt[3]{E_{1T_2}}\right) \qquad \text{eq. 3.B.5}$$

where $\Delta h_{es}/\Delta Temp$ = change in h_{es} per change in temperature |m/°C|
h_1 = thickness of the bituminous top layer |m|
E_{1T_i} = elastic modulus of the bituminous layer at pavement temperature T_i |MPa|

Considering the change in bituminous mix stiffness as given in figure 3.B.1 |13| and by taking into account the difference between air and pavement temperature (figure 3.B.2 |13|), the change in h_{es} was determined for a pavement with a top layer consisting of a S-1-50 material and for a pavement with a top layer consisting of a S-2-100 material. The results are shown in table 3.B.1

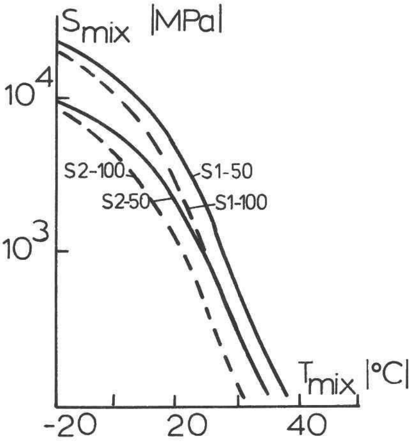

Figure 3.B.1 Mix Stiffness in relation to Mix Temperature

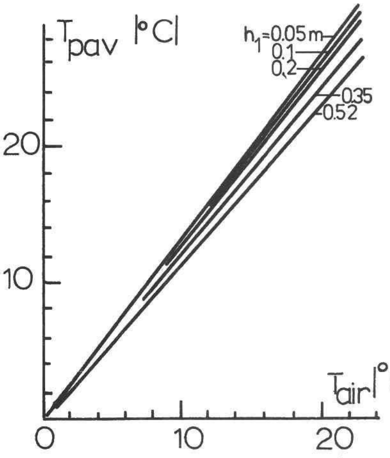

Figure 3.B.2 Pavement Temperature in relation to Air Temperature

As can be seen from table 3.B.1, the magnitude of the temperature corrections depends on
a. the thickness of the asphaltic layer
b. the type of bituminous mix
c. the temperature range considered.

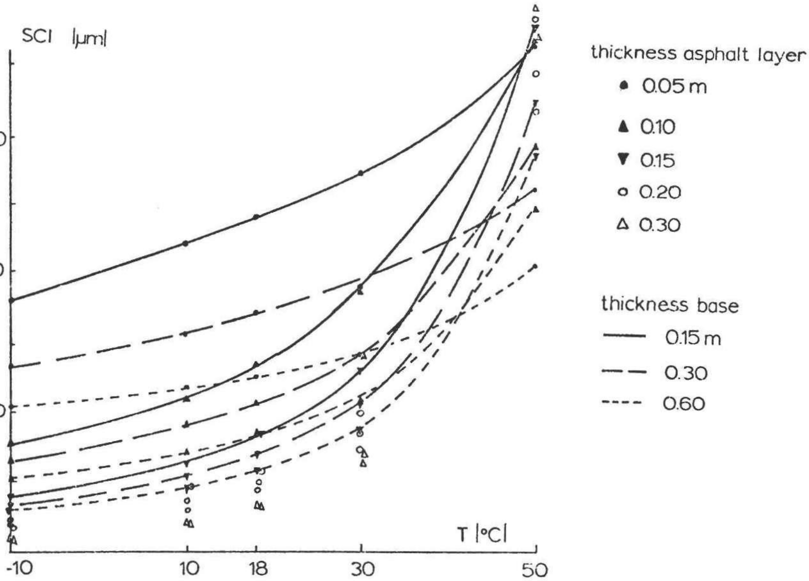

Figure 3.B.3 Influence of Temperature (Temp) on the Magnitude of the Surface Curvature Index (SCI)

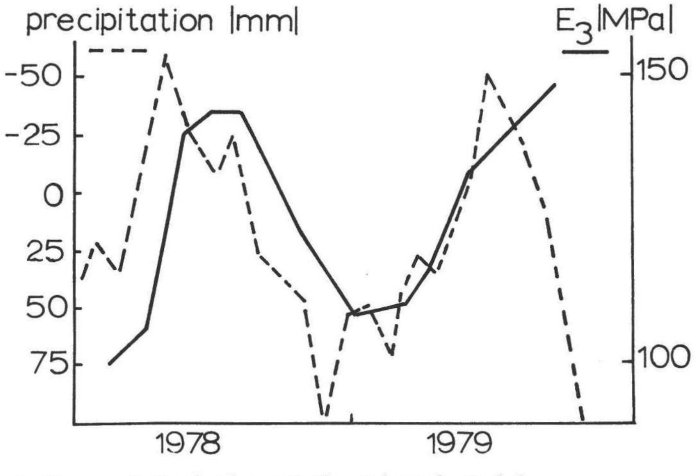

Figure 3.B.4 Seasonal Variation of the Subgrade Modulus

Another reason that necessitates to correct the equivalent layer thickness to a reference subgrade is, that the equivalent layer thickness itself strongly depends on the magnitude of the subgrade modulus and therefore a direct comparison of the bearing capacity of pavement structures based on a comparison of h_e is not possible. A given structure on a subgrade with a modulus of 150 MPa will last longer than the same structure on a subgrade with a modulus of 100 MPa. To overcome this problem the equivalent layer thickness is corrected in the following way

Table 3.B.1 Temperature Correction Factor in relation to the Thickness of the Asphalt Layer and the Type of Mix

h_1 |m|	$\Delta h_{es}/\Delta Temp$ |m/°C|		$\Delta h_{es}/\Delta Temp$ |m/°C|	
	T_1 = 0°C	T_2 = 11°C	T_1 = 11°C	T_2 = 21°C
	S-1-50	S-2-100	S-1-50	S-2-100
0.05	0.00496	0.00393	0.00619	0.00454
0.10	0.00973	0.0077	0.0126	0.00867
0.15	0.0148	0.0117	0.017	0.0119
0.20	0.0195	0.0154	0.0189	0.0147
0.30	0.0297	0.0235	0.0288	0.0224

From table 3.B.1 it can also be concluded that the developed empirical temperature correction factor ($\Delta h_{es}/\Delta Temp$ = 0.014; equation 3.B.1) seems to overestimate the temperature effects on pavements with thin asphalt layers while it seems to underestimate the temperature influences on pavements with thick asphalt layers.
Nevertheless the empirically derived temperature correction factor was considered to be accurate enough for practical purposes since

a. the differences between the empirically and theoretically developed factors are limited especially in the asphalt thickness range of 0.10 - 0.20 m
b. the theoretically developed correction factor does not take into account the influences of a variation in stress level on the stiffness of the base.

In order to check whether a simple temperature correction equation could be developed for the SCI, calculations on three layered systems were performed. In the calculations it was assumed that the mix stiffness of the top layer could be characterized by a S-1-50 mix |13|.
By taking a pavement temperature of 18°C as reference temperature, correction factors for SCI in relation to different types of construction could be derived. Examples are shown in figure 3.B.3.
From figure 3.B.3 it was concluded that no "simple" temperature correction equation could be developed for the SCI.

3.B.2 Corrections on Variations in the Subgrade Modulus

Beuving and Molenaar |29| have shown that the elastic modulus of the subgrade varies over the year in a sinusodial way. In fact the variation of the subgrade modulus follows with a time lag, the variation of the precipitation balance (figure 3.B.4). Van Gurp |30| has developed this further and showed that the amplitude of the variation of the elastic subgrade modulus varied between 9 and 40 MPa. The overall mean value was 25 MPa while the standard deviation was 9 MPa. The coefficient of variation of the subgrade modulus of the individual sections varied between 8% and 23%.
Furthermore it was concluded that the mean subgrade modulus was reached at the months April/May and October. This means that deflection measurements should preferably taken in these periods in order to avoid the necessity of correcting the deflection measurements for variations in the subgrade modulus since the magnitude of the variation is seldom known.

$$h_{ec} = h_{esT} \cdot (E_3/100)^{0.3} \qquad \text{eq. 3.B.7}$$

where h_{esT} = equivalent layer thickness as described above
E_3 = modulus of the subgrade under the construction considered |MPa|
h_{ec} = equivalent layer thickness if the structure was lying on a subgrade with E_3 = 100 MPa

3.B.3 Correction Procedure

Based on the foregoing the following correction procedure was developed.

a. Calculate the h_{es} for the pavement structure considered, using equation 3.B.2
b. Apply the temperature correction on h_{es} using equation 3.B.1
c. Apply the subgrade correction on h_{esT} using equation 3.B.7

Van Gurp and the author have developed a graphical procedure to perform this correction. This procedure is shown in figure 3.B.5

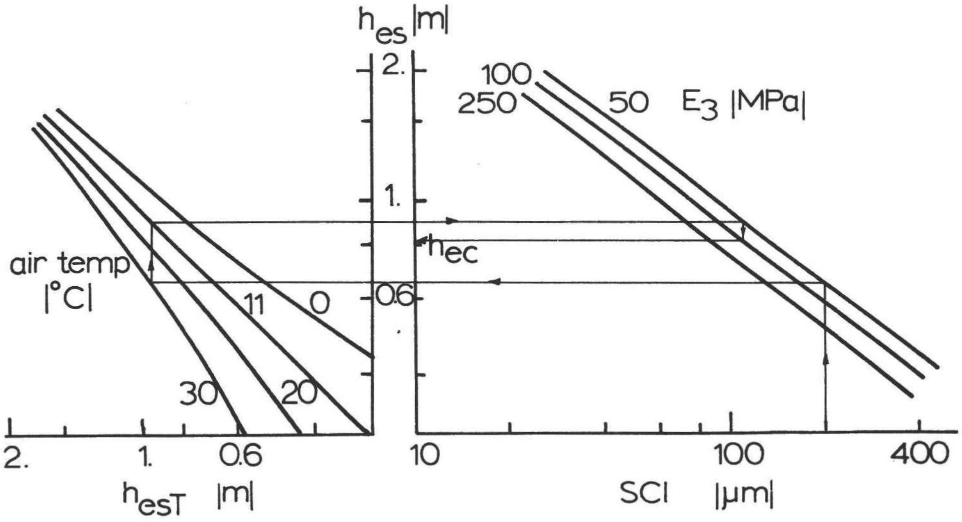

Figure 3.B.5 *Chart to determine the Corrected Equivalent Layer Thickness (h_{ec})*

Appendix 3C

Verification of the Equivalent Layer Thickness Deterioration Model by means of Deflection Measurements

3.C.1 Decrease of the Equivalent Layer Thickness h_{es} in Time

Using the results of falling weight deflection measurements, which were carried on the road sections mentioned in subsection 3.4.2.2.1, Beuving and Molenaar |29| showed that the decrease of the h_{es} in time was almost linear. Figure 3.C.1 gives an example of the decrease of the h_{es} in time of the S_{10} sections.

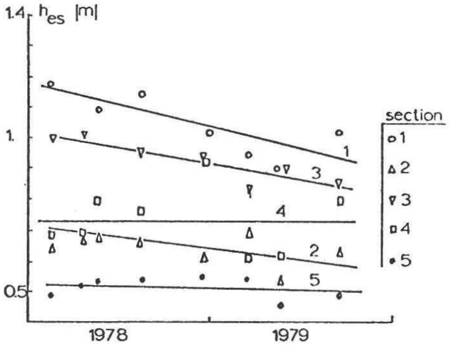

Figure 3.C.1a Decrease of h_{es} in Time as determined for the $S_{10}R$ Sections

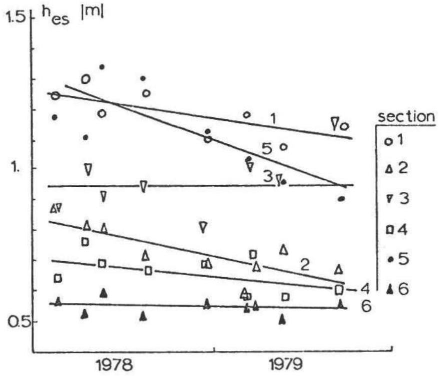

Figure 3.C.1b Decrease of h_{es} in Time as determined for the $S_{10}L$ Sections

Considering the results presented in figure 3.C.1, the following comments can be made

a. The more or less constant h_{es} value for sections 5R and 6L could be explained by the fact that the visual condition of these sections was already very bad at the time of the deflection measurements. The condition was in fact so bad that no further decrease of h_{es} could be expected. In other words, the threshold value for h_{es} was reached.

b. The variation of the h_{es} values over the year can be explained by the fact that no correction was applied to take in account the variation of the subgrade modulus over the year.

In order to get a better insight in the decrease of the h_{es} with respect to time use was made of the results of Benkelman beam measurements carried out earlier on the same road sections by the district engineers involved. Some results of this exercise are shown in figure 3.C.2. Again it can be noticed that the S_{10} 5R section had reached something like a threshold value. Also it can be observed that the shape of the deterioration curve is S-shaped.

3.C.2 Decrease of the Corrected Equivalent Layer Thickness h_{ec} in Time

After this early work of Beuving and Molenaar, van Gurp and the author used the h_{ec} to describe the structural deterioration of the pavements considered. They too found a more or less linear decrease of h_{ec} in time. Figure 3.C.3 shows the decrease h_{ec} for the same section as mentioned in figure 3.C.1. The next step was to describe the decrease of h_e with respect to the number of 100 kN equivalent single axles that have loaded the pavements. This information was obtained from a study carried out by Beuving |28| who has trans-

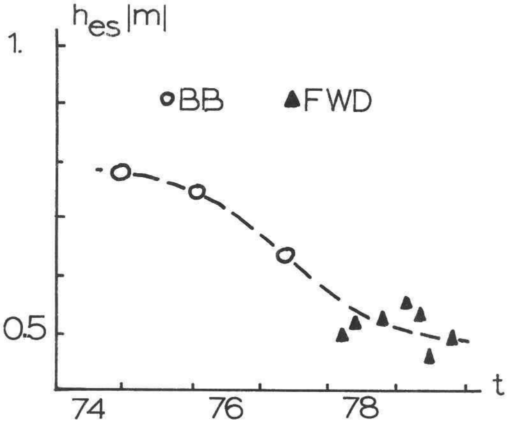

Figure 3.C.2 *Decrease of h_{es} as determined for the S_{10} 5R Section*

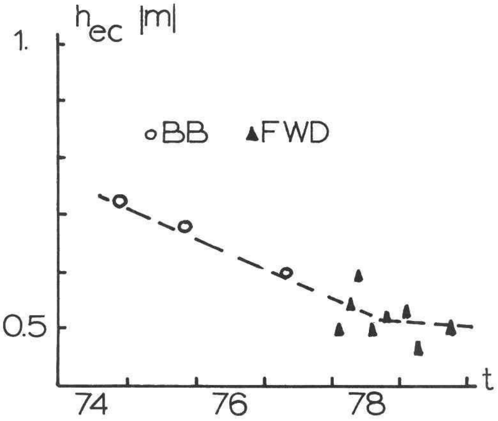

Figure 3.C.3 *Decrease of h_{ec} as determined for the S_{10} 5R Section*

lated traffic intensities obtained from the highway districts considered, into numbers of 100 kN equivalent single axle passages from the known percentage of truck traffic. Information on the types of trucks that have loaded the pavements and the relation between the truck silhouette and the load equivalency is given in figure 3.C.4. Figure 3.C.4 was derived from data taken from |31| and |32|.

The decrease of h_{ec} with respect to the applied number of load applications is shown in figure 3.C.5. Here again the same data are used as shown in figure 3.C.2.

Based on these results relations were derived of the shape

$$h_{ecn} = \frac{h_{eco}}{1 + e^{\beta \log(n/N)}} \qquad \text{eq. 3.C.1}$$

type	equiv. factor
	0.45
	0.95
	1.60
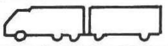	2.86
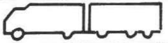	2.37
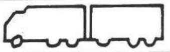	4.23
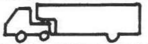	0.97
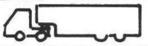	2.23
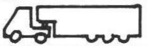	2.23
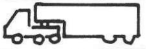	2.55
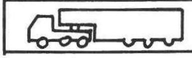	3.05

Figure 3.C.4 Relation between the Truck Silhouette and the Number of 100 kN Equivalent Single Axles per Truck

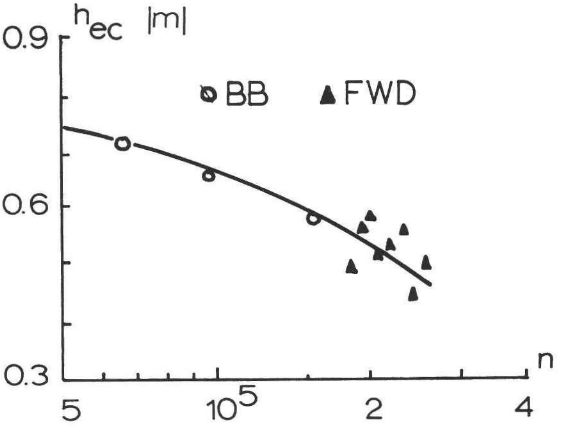

Figure 3.C.5 Decrease of h_{ec} with respect to n for the S_{10} 5R Section

where h_{ecn} = corrected equivalent layer thickness after n equivalent 100 kN single axle loads

h_{eco} = corrected equivalent layer thickness at time of construction (n = 0)

n = number of equivalent 100 kN single axle loads

N = allowable number of equivalent 100 kN single axle loads ($h_{ecn} = \frac{1}{2} h_{eco}$)

β = a constant

In section 3.4.2.2.1 it has been explained why equation 3.C.1 was used to describe the deterioration of the equivalent layer thickness.

3.C.2.1 Estimation of h_{eco}

In order to be able to calculate the two unknown parameters β and N from equation 3.C.1, h_{eco} needs to be known. Unfortunately no data were available from which reliable h_{eco} estimates could be obtained. Therefore values for h_{eco} had to be assessed in another way. In order to do so, the author decided to describe the decrease of h_{ecn} by means of equation 3.C.2

$$\ln(h_{ecn}) = b_0 - b_1\, n \qquad \text{eq. 3.C.2}$$

where $h_{eco} = e^{b_0}$
$b_0, b_1 =$ constants

This model was selected for the following reason.
As mentioned in section 3.4.2.2.1 the equivalent layer thickness deterioration model (eq. 3.C.1) closely matches the structural deterioration model which has been described in section 3.4.2.1. This latter model describes the decrease of the probability of survival P with respect to the number of load repetitions n for different values of h_e.
Due to the agreement between the "P model" and the "h_e model". The deterioration of h_e with respect to n can be calculated from the P model by

$$h_{ecn} = P_n \times h_{eco} \qquad \text{eq. 3.C.3}$$

where h_{ecn} = corrected equivalent layer thickness after application of n load repetitions
P_n = probability of survival after n load repetitions
h_{eco} = corrected equivalent layer thickness at the time of construction.

So given the decrease of P with respect to n for a given h_{eco} (figure 3.C.6), the decrease of h_{ec} with respect to n can be determined (figure 3.C.7).

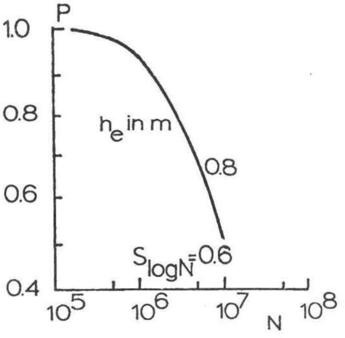

Figure 3.C.6 Decrease of the Probability of Survival (P) with respect to the Number of Load Applications (log n) for a given Equivalent Layer Thickness (h_e)

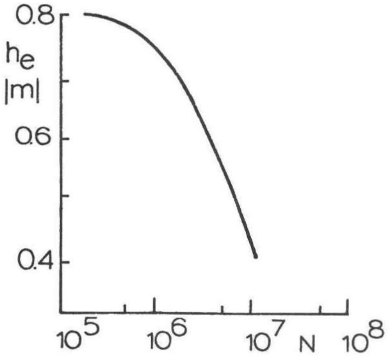

Figure 3.C.7 Decrease of the Equivalent Layer Thickness (h_e) with respect to the Number of Load Applications (log n)

If the decrease of h_e is plotted with respect to n instead of log n, figure 3.C.7 transforms into figure 3.C.8. The shape of the Equivalent layer thickness deterioration curve as shown in figure 3.C.8 can be represented with reasonable accuracy by means of equation 3.C.2.

Resuming the foregoing, it can be stated that equation 3.C.2 is <u>only</u> used to assess h_{eco} values. The deterioration of h_{ecn} is described with the more general model represented by equation 3.C.1

It should be noted that equation 3.C.2 was only used to fit the data obtained on road sections with hot mix asphalt concrete layers. It was not used to fit the data obtained on road sections with cold asphalt layers, since on those sections no decrease of h_{ec} could be observed (the h_{ec} values varied between 0.7 and 0.8 m).

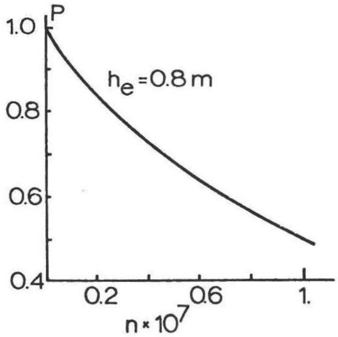

Figure 3.C.8 *Deterioration of the Equivalent Layer Thickness (h_e) with respect to the Number of Load Applications (n)*

The results of the analysis described here are given in table 3.C.1. They give rise to the following comments.
First of all one will notice that the measurements are taken over limited time period. At best data points are available over a six year period (S_{10}). Fortunately the S_7 sections are part of a very heavily trafficked road which means that, although the measurements are carried out over a rather short period, a considerable amount of traffic has passed the pavement section (the average daily traffic is about 9000 vehicles in one direction). The same applies also to the S_{22} B road sections where the traffic intensity per lane is about 7000 vehicles per day.
The importance of having more widely spaced data is best shown by the results of the S_{42} sections. By adding one data point (S_{42} R section) the values for r^2 drop dramatically.

Considering the S_1 sections it can be noted that no decrease of h_{ec} in time could be observed for the 1L section, in fact a small increase of h_{ec} was noted. No clear explanation for this could be found. For these reasons no results of the 1L sections are given in table 5. Furthermore a difference in h_{eco} is noticed between the L and R sections. This might be caused by the fact that both lanes don't carry the same amount of traffic what was assumed in the analyses.
This statement is more or less confirmed by the difference in deterioration rate b_1 derived for the L and R sections.

In order to be able to check which h_{eco} is most suitable for the S_1 section, this value was calculated from the known layer thicknesses and assumed values for the elastic modulus of the asphaltic top layer and sand cement stabilized base.
It was concluded that h_{eco} must be somewhere between 1.3 and 1.4 m. From this it was concluded that the amount of traffic carried by the L sections has been underestimated.

The results of the S_7 sections are considered to be reasonably consistent. However a difference in h_{eco} as noticed on the S_1 section is observed here too. The same explanation as given for the S_1 sections can be given here.

The h_{eco} values as determined for the S_{10} sections show a marked difference between each of them. This is due to the fact that each section has a different type of base material. This is shown in table 3.C.2.

Table 3.C.1 *Results of the Regression Analysis* $ln(h_{ecn}) = b_0 - b_1 n$

Road Number	Section Number	b_0	b_1	n	r^2	h_{eco}|m|	Measuring date's 7808 = year 1978, month august
S_1	2L	0.605	1.745 E-6	6	0.87	1.83	7803, 7805, 7808, 7812 (7903, 7903), 7905
	3L	0.504	1.60 E-6	7	0.84	1.66	7504*, 7803, 7805, 7808, 7812 (7903, 7903), 7905
	1R	0.38	5.261 E-7	7	0.58	1.46	as 3L
	2R	0.317	3.46 E-7	7	0.47	1.37	as 3L
	3R	0.352	7.013 E-7	5	0.15	1.42	as 3L except 7504 and 7803
S_7	1L	0.264	1.666 E-7	5	0.86	1.30	7803, 7804, 7808, 7812, 7805
	2L	0.43	3.08 E-7	5	0.91	1.54	as 1L
	3L	0.216	1.163 E-7	5	0.82	1.24	as 1L
	1R	0.489	3.403 E-7	5	0.99	1.63	as 1L
	2R	0.362	2.039 E-7	5	0.88	1.72	as 1L
	3R	0.485	3.748 E-7	5	0.95	1.62	as 1L
S_{10}	1L	0.435	1.212 E-6	8	0.32	1.54	7802, 7804, 7805, 7808, 7812, 7903, 7905, 7909
	2L	0.277	2.346 E-6	8	0.38	1.32	as 1L
	4L	0.0263	1.874 E-6	8	0.64	1.02	as 1L
	5L	0.926	3.376 E-6	7	0.72	2.52	7802, 7804, 7805, 7808, 7812, 7905, 7909
	6L	-0.427	8.241 E-7	9	0.079	0.65	as 1L
	1R	0.606	2.223 E-6	11	0.89	1.83	7411*, 7511*, 7704*, 7802, 7804, 7805, 7808, 7812, 7903, 7905, 7909
	2R	0.561	4.419 E-6	10	0.71	1.75	as 1R except 7411
	3R	0.723	3.278 E-6	11	0.97	2.06	as 1R
	4R	0.503	3.245 E-6	10	0.89	1.65	as 1R except 7511
	5R	-0.224	1.981 E-6	11	0.73	0.8	as 1R

Note: * means Benkelman beam measurement, others are falling weight measurements.

Table 3.C.1 *continued*

Road Number	Section Number	b_0	b_1	n	r^2	$h_{eco}\lvert m\rvert$	Measuring date's
S_{22} B	1L	0.463	2.28 E-7	9	0.71	1.59	7512*, 7710*, 7803, 7804, 7805, 7808, 7812, 7907, 8005
	2L	0.495	2.577 E-7	8	0.74	1.64	as 1L except 7710
	5L	0.407	1.769 E-7	8	0.47	1.5	as 2L
	1R	0.561	2.48 E-7	8	0.37	1.75	as 1L except 7512*
	2R	0.402	0.122 E-8	9	0.39	1.49	as 1L
	5R	0.578	3.33 E-7	7	0.96	1.78	as 1L except 7512*, 7710*
S_{42}	1L	0.495	2.827 E-6	3	0.93	1.64	7803, 7806, 7809
	3L	0.568	3.227 E-6	3	0.8	1.77	as 1L
	4L	0.234	1.239 E-6	3	1	1.26	as 1L
	5L	0.623	3.367 E-6	3	0.99	1.87	as 1L
	1R	0.112	5.129 E-7	4	0.26	1.12	7803, 7806, 7809, 7905
	2R	0.129	3.283 E-7	4	0.027	1.14	as 2R

Table 3.C.3 *Values of β as determined for the different Road Sections*

Road Number	Section Number	r^2	β	N
S_1	2L	0.54	2.72	3.98 E 5
	3L	0.90	3.41	4.31 E 5
	1R	0.81	5.7	1.35 E 6
	2R	0.84	2.43	2.01 E 6
	3R	0.42	3.3	9.9 E 5
S_7	1L	0.82	2.9	4.17 E 6
	2L	0.88	3.1	2.24 E 6
	3L	0.73	2.43	5.97 E 6
	1R	0.98	2.64	2.04 E 6
	2R	0.60	1.84	2.52 E 6
	3R	0.94	2.64	1.86 E 6
S_{10}	1L	0.32	9.5	5.75 E 5
	2L	0.44	3.1	2.95 E 5
	4L	0.66	4.4	3.23 E 5
	5L	0.75	3.41	2.06 E 5
	1R	0.91	3.1	3.13 E 5
	2R	0.80	4.0	1.57 E 5
	3R	0.99	3.0	2.12 E 5
	4R	0.96	3.4	2.14 E 5
	5R	0.87	3.3	3.49 E 5
S_{22} B	1L	0.45	2.89	3.04 E 6
	2L	0.23	1.29	2.69 E 6
	5L	0.81	1.32	3.93 E 6
	1R	0.62	0.88	2.8 E 6
	2R	0.05	0.94	7.63 E 6
	5R	0.95	2.8	2.09 E 6
S_{42}	1L	0.43	2.69	2.45 E 5
	3L	0.79	2.69	2.14 E 5
	4L	1.0	2.55	5.62 E 5
	5L	0.99	2.82	2.05 E 5
	1R	0.41	4.3	1.35 E 6

Note: N is the number of load applications to $h_{ecn} = 0.5\ h_{eco}$

Table 3.C.2 Base Materials used in the S_{10} Road Sections and h_{eco} Values estimated from Construction Data

Section	Type of Material	Estimated h_{eco} |m| from Construction Data	Corresponds to Sections	
A	Blast Furnance Slag (Thyssen Group, Germany)	1.44	1L	1R
B	Blast Furnance Slag (IJmuiden, Holland)	1.01	2L	2R
C	Blast Furnance Slag (3 Components Slag, Mannesmann, Germany)	1.86 - 1.59	3L,4L,5L	3R,4R
D	Red Burnt Colliery Shale	0.79	6L	5R
E	Lava	0.87		

Since a lot of plate bearing tests, Benkelman beam deflection tests, and measurements with a heavy vibrator where taken at the time of construction, and some time after construction was completed, it was possible by using these data, to derive h_{eco} values for the different sections. These values are given too in table 3.C.2.
By comparing the h_{eco} values fiven for the L and R sections it is concluded that the R sections have carried more traffic than the L sections.
No results for the 3L sections are given since no decrease of h_{ec} could be determined. Again no clear explanation for this phenomenon could be found.
The remarkable low r^2 as determined for the 6L section, which is in fact the same type of construction as the 5R section, can be explained by the fact that this section was already completely deteriorated at the time of the first measurements.

Also for S_{22} B sections a difference in h_{eco} can be seen for the L and R sections. Here no explanation can be found with the argument the amount of traffic carried by the L and R sections is not equal, since the R sections are thicker than the L sections. The data of the 3L, 4L, 3R and 4R sections have not been given since here again no decrease in h_{ec} could be determined.

3.C.2.2 Calculation of Bèta and its Relation to the Type of Construction

The caclulated values of h_{eco} which are given in table 3.C.2, were used to calculate values for β as given in equation 3.C.1. Also the pavement life N has been calculated. It is defined here as the number of load applications at which the ratio h_{ecn}/h_{eco} has decreased to 0.5. The results of this analysis are given in table 3.C.3.
Table 3.C.4 gives the mean value of β and its standard deviation for the road sections considered.

In general it can be concluded that the exponential model (equation 3.C.1) described the observed behavior reasonably well. This means that it is not necessary to reject the proposed equation to describe the deterioration of the equivalent layer thickness; this equation is:

$$\frac{h_{ecn}}{h_{eco}} = \frac{1}{1 + e^{\beta \log(n/N)}} \qquad \text{eq. 3.C.4}$$

Table 3.C.4 *Mean Values and Standard Deviations of β as determined for the Road Sections considered*

Road Number	β Mean Value	β Standard Deviation
1. S_1	3.51	1.29
2. S_7	2.59	0.44
3. S_{10} *	4.24	2.18
4. S_{10} **	3.49	0.52
5. S_{22} B***	1.84	0.94
6. S_{42} ****	2.69	0.11
Overall (1+2+4+5+6)	2.82	0.70

*	only blast furnance slag sections
**	all blast furnance slag sections but 1L
***	all sections but 2R
****	only L sections

Note: No overlay was applied on the S_1 and S_{10} road sections.
The other pavement sections had received one or more overlays.

Furthermore it was concluded that β might be dependent on the type of construction. From table 3.C.4 it can be observed that on the pavement sections which had not yet received an overlay, higher β values were obtained than on the pavements which had been overlaid before (note the difference between the β values for the S_1 and S_{10} sections on one hand and the β values for the other sections on the other).
This conclusion was underscored by the results of the analysis of variance carried out to determine whether significant differences existed between the β values as obtained for the different road constructions.
The results of this analysis of variance are given in table 3.C.5.

Table 3.C.5 *Results of the Analysis of Variance carried out on the β values of the Road Sections considered*

Significant Difference Between		No Significant Difference Between
S_1 - S_7	S_7 - S_{22}	S_1 - S_{10}
S_1 - S_{22}	S_{10} - S_{22}	S_7 - S_{42}
S_1 - S_{42}	S_{10} - S_{42}	
S_7 - S_{10}	S_{22} - S_{42}	

confidence level: 95%

The fact that β decreases if overlays are applied can be explained as follows. It has been mentioned in the previous section that the theoretically derived "P model" and the "h_e model" are exchangable. This also means that $S_{\log N}$ and β, which are describing the shape of these models, are exchangable.
It has been shown in section 3.4.2.1 that $S_{\log N}$ is influenced to a rather large extent by the variances of the thicknesses and elastic moduli of the various layers.
We recall

$$S^2_{\log N} = a_1{}^2 b_1{}^2 S^2_{\log h_e} \qquad \text{eq. 3.C.5}$$

where $$S^2_{he} = \sum_{i=1}^{L-1} (\frac{\delta f}{\delta h_i})^2 S^2_{h_i} + \sum_{i=1}^{L} (\frac{\delta f}{\delta E_i})^2 S^2_{E_i}$$

where $$f = 0.9 \sum_{i=1}^{L-1} h_i \sqrt[3]{\frac{E_i}{E_s}}$$

h_i = thickness of layer i
E_i = elastic modulus of layer i
E_s = elastic modulus of the subgrade
a_1, b_1 = constants
L = number of layers

It can easily be shown that by adding one layer to the system, $S_{\log N}$ will increase due to the variation in material properties and thickness of this layer. From figure 3.16 it can be observed that an increasing $S_{\log N}$ means a decreasing β. So if an overlay is applied β will tend to decrease.

Appendix 3D

Calculation of the Variance of the Logarithm of the Equivalent Layer Thickness.

Calculation of the Variance of the Logarithm of the Equivalent Layer Thickness

As has been shown in section 3.4.2.1 the value of $S^2_{\log h_e}$ determines to a larger extent the value of $S^2_{\log N}$.
In this appendix the derivation of $S^2_{\log h_e}$ will be given and it will be shown which parameters are of main importance. In the analysis it is assumed that the pavement can be represented as a three layered system.

The equivalent layer thickness of a three layer system is calculated with

$$h_e = 0.9\, h_1 \sqrt[3]{\frac{E_1}{E_3}} + 0.9\, h_2 \sqrt[3]{\frac{E_2}{E_3}} \qquad \text{eq. 3.D.1}$$

By taking the logarithm, equation 3.D.1 transforms to

$$\log(h_e) = \log(0.9(h_1 \sqrt[3]{\frac{E_1}{E_3}} + h_2 \sqrt[3]{\frac{E_2}{E_3}})) \qquad \text{eq. 3.D.2}$$

By following the approach as indicated in equation 3.6, $S_{\log h_e}$ can be calculated as follows

$$\begin{aligned} S^2_{\log h_e} = {} & (\frac{1}{\ln 10})^2 \{ (\frac{\sqrt[3]{E_1/E_3}}{h_1 \sqrt[3]{E_1/E_3} + h_2 \sqrt[3]{E_2/E_3}})^2 S^2_{h_1} + (\frac{\sqrt[3]{E_2/E_3}}{h_1 \sqrt[3]{E_1/E_3} + h_2 \sqrt[3]{E_2/E_3}})^2 S^2_{h_2} \\ & + (\frac{1/3\, h_1/\sqrt[3]{E_1^2 E_3}}{h_1 \sqrt[3]{E_1/E_3} + h_2 \sqrt[3]{E_2/E_3}})^2 S^2_{E_1} + (\frac{1/3\, h_2/\sqrt[3]{E_2^2 E_3}}{h_1 \sqrt[3]{E_1/E_3} + h_2 \sqrt[3]{E_2/E_3}})^2 S^2_{E_2} \\ & + (\frac{-1/3\, h_1 \sqrt[3]{E_1/E_3^4} - 1/3\, h_2 \sqrt[3]{E_2/E_3^4}}{h_1 \sqrt[3]{E_1/E_3} + h_2 \sqrt[3]{E_2/E_3}})^2 S^2_{E_3} \} \qquad \text{eq. 3.D.3} \end{aligned}$$

Reorganizing equation 3.D.3, results in

$$\begin{aligned} S^2_{\log h_e} = {} & 0.1886\ \{ (\frac{0.9 \sqrt[3]{E_1/E_3}}{h_e})^2 S^2_{h_1} + (\frac{0.9 \sqrt[3]{E_2/E_3}}{h_e})^2 S^2_{h_2} \\ & + (\frac{0.3\, h_1}{h_e \sqrt[3]{E_1^2 E_3}})^2 S^2_{E_1} + (\frac{0.3\, h_2}{h_e \sqrt[3]{E_2^2 E_3}})^2 S^2_{E_2} \\ & + (-\frac{1}{3E_3})^2 S^2_{E_3} \} \qquad \text{eq. 3.D.4} \end{aligned}$$

Van Gurp |14| has calculated values of $S_{\log h_e}$ for 70 three layer systems. These systems are shown in table 3.D.1. In his analysis, van Gurp did not take into account the influence of the variance of E_3. Furthermore he assumed constant values for the coefficient of variation of h_1, E_1, h_2 and E_2. These values are listed in table 3.D.2.
From his calculation results, van Gurp concluded that $S^2_{\log h_e}$ did not show a large amount of variation. In fact he concluded that for a given value of E_3, constant values for $S^2_{\log h_e}$ could be discerned. These are given in table 3.D.3.

Table 3.D.1 *Constructions for which* $S_{log\ h_e}$ *was calculated* |14|

		h_2	150			300			600		
E_3	E_2	h_1 / E_1	50	100	200	50	100	200	50	100	200
150	6000	10000		x							
		5000					x				x
		1000									
	1200	10000	x								
		5000		x		x					
		1000					x				
	300	10000	x							x	
		5000	x				x				
		1000				x			x		
100	6000	10000							x		
		5000			x						
		1000									
	1200	10000		x				x			
		5000							x		
		1000			x						x
	300	10000			x	x					
		5000									
		1000		x	x	x			x		
50	6000	10000				x				x	
		5000									
		1000									x
	1200	10000		x							
		5000						x		x	
		1000					x				
	300	10000	x								x
		5000	x					x			
		1000				x					
50	180	10000							x		
		5000								x	x
		1000							x		x
	130	10000									
		5000				x	x				
		1000					x	x			
	100	10000		x							
		5000	x		x						
		1000	x	x							
20	72	16496							x	x	
		11053								x	x
		3675							x		x
	52	16496				x		x			
		11053				x	x				
		3675					x	x			
	40	16496		x	x						
		11053	x		x						
		3675	x	x							

Note: |E| = |MPa| |h| = |mm|

Table 3.D.2 Coefficients of Variation as used in van Gurp's Analysis |14|

Parameter	Coefficient of Variation
h_1	0.1
E_1	0.15
h_2	0.1
E_2	0.2

Table 3.D.3 Values of $S^2{log}\ h_e$ as calculated by van Gurp |14|

E_3 $\|MN/m^2\|$	$S^2\log h_e$
150	0.0015
100	0.0017
50	0.0015
20	0.0016

From equation 3.D.4, it can be observed that a value of

$$0.02096 * \frac{S^2_{E_3}}{E_3{}^2}$$

should be added to the values given in table 3.D.2 in order to take into account the variability of the subgrade on the variance of log h_e.
Table 3.D.4 gives an overview of the values which should be added to the values given in table 3.D.3 in relation to different values of the variance of E_3.

Table 3.D.4 Values of $S_{log\ h_e}$ which should be added to the Values given in Table 3.D.2, if the Influence of the Variation of the Subgrade Modulus (E_3) is taken into account.

Coefficient of Variation of E_3	Influence on $S^2\log h_e$
0.1	0.0002
0.2	0.0008
0.3	0.0019
0.4	0.0034
0.5	0.0052

Since the values given in table 3.D.4 should be added to the values given in table 3.D.3, it can be concluded that the variation in the subgrade modulus has a large influence on the value of $S^2\log h_e$. Because it has been observed that the coefficient of variation of E_3 is normally about 0.3, a value of 0.0035 can be used for practical purposes for $S^2\log h_e$.

References

|1| HUDSON, W.R.; FINN, F.N.; McCULLOUGH, B.F.; NAIR, K.; VALLERGA, B.A.
Systems Approach to Pavement Design: Systems Formulation, Performance Definition and Material Characterization
Final Report NCHRP Project 1 - 10
Washington D.C. - 1968

|2| ______________________
Sessions I, II, III, IV
"Proceedings 4th Int. Conf. Structural Design of Asphalt Pavements"
Ann Arbor - 1977

|3| DE JONG, D.L.; PEUTZ, M.G.F.; KORSWAGEN, A.R.
Computer Program BISAR
External Report AMSR.0006.73
Royal/Shell Laboratory, Amsterdam - 1973

|4| KENIS, W.J.
Predictive Design Procedures, Vesys Users Manual
Report FHWA-RD-77-154, Federal Highway Administration
Washington D.C. - 1978

|5| WARDLE, L.J.
Program CIRCLY, a Computer Program for the Analysis of Multiple Complex Circular Loads on layered Anisotropic Media
CSIRO, Australia - 1977

|6| CLAESSEN, A.I.M.; EDWARDS, J.M.; SOMMER, P.; UGE, P.
Asphalt Pavement Design - the Shell Method
"Proceedings 4th Int. Conf. Structural Design of Asphalt Pavements"
Ann Arbor - 1977

|7| DAUZATS, M.; LINDER, R.
A Method for the Evaluation of the Structural Condition of Pavements with Thick Bituminous Road Bases
"Proceedings 5th Int. Conf. Structural Design of Asphalt Pavements"
Delft - 1982

|8| MOAVENZADEH, F.; BRADEMEYER, B.
A Stochastic Model for Pavement Performance and Management
"Proceedings 4th Int. Conf. Structural Design of Asphalt Pavements"
Ann Arbor - 1977

|9| MOLENAAR, A.A.A.
A Theoretical Study on the Assessment of the Structural Condition of Pavements using Deflection Measurements (in Dutch)
Memorandum WB-A; Dep. of Civil Engineering; Chair of Highway Engineering
Delft University of Technology - 1976

|10| ZIJLSTRA, M.
Relations between Deflection Parameters, the Pavement Life, and the Stiffness of the Constitutive Layers; the Influence of the Magnitude of the Stress Levels in the Bituminous Layer on the Development of Permanent Deformation (in Dutch)
Memorandum WB-F; Dep. of Civil Engineering; Chair of Highway Engineering
Delft University of Technology - 1977

|11| MOLENAAR, A.A.A.
A Theoretical Study on the Assessment of the Structural Condition of Pavements using Deflection Measurements (in Dutch)
Report WB-9 (7-77-6-115-1); Dep. of Civil Engineering; Lab. for Road and Railroad Research; Delft University of Technology - 1977

|12| VAN DIJK, W.; VISSER, W.
The Energy Approach to Fatigue for Pavement Design
"Proceedings Association of Asphalt Paving Technologists", Vol. 46 - 1977

|13| SHELL INTERNATIONAL PETROLEUM COMPANY LTD
Shell Pavement Design Manual
London - 1978

|14| VAN GURP, Ch.A.P.M.
Optimization of the Thickness Design of Asphalt Pavements and Overlays (in Dutch)
Memorandum WB-K; Dep. of Civil Engineering; Chair for Highway Engineering
Delft University of Technology - 1979

|15| MOLENAAR, A.A.A.; VAN GURP, Ch.A.P.M.
Optimization of Overlay Designs based on limiting the Asphalt and Subgrade Strain
"Proceedings Int. Symp. on Pavement Evaluation and Overlay Design"
Rio de Janeiro - 1979

|16| MOLENAAR, A.A.A.; VAN GURP, Ch.A.P.M.
Optimization of the Thickness Design of Asphalt Concrete Overlays (in Dutch)
"Wegen", Vol. 54 no. 6 - 1980

|17| MOLENAAR, A.A.A.; VAN GURP, Ch.A.P.M.
Optimization of the Thickness of Asphalt Concrete
"Proceedings 10th Australian Road Research Board Conference" Vol. 10(2)
Sidney - 1980

|18| MOLENAAR, A.A.A.; VAN GURP, Ch.A.P.M.
Verification of a Model for the Prediction of the Structural Deterioration of Pavements (in Dutch)
"Wegen", Vol. 55 no. 8 - 1981

|19| MOLENAAR, A.A.A.; VAN GURP, Ch.A.P.M.
Structural Performance Model and Overlay Design Method for Asphalt Concrete Overlays
61th Annual Meeting Transportation Research Board
Washington D.C. - 1982

|20| MOLENAAR, A.A.A.; VAN GURP, Ch.A.P.M.
A Pavement Management System for Provincial Roads in the Netherlands
"Proceedings 5th Int. Conf. Structural Design of Asphalt Pavements"
Delft - 1982

|21| ODEMARK, N.
Investigations on the Elastic Properties of Soils and the Design of Pavements according to the Theory of Elasticity
Statens Vaeginstitut, Stockholm - 1949

|22| MOLENAAR, A.A.A.; VAN DER VELDEN, G.
Tables for the Calculation of Elastic Moduli Value from Deflection Measurements (in Dutch)
Report WB-10 (7-77-5-115-2); Dep. of Civil Engineering; Lab. for Road and Railroad Research; Delft University of Technology - 1977

|23| YANDELL, W.O.; LYTTON, R.L.
Residual Stresses due to Travelling Loads and Reflection Cracking
RR 207-6; Texas Transportation Institute
Texas A&M University - 1979

|24| WARDLE, L.J.; GERRARD, C.M.
Rational Design of Surface Pavement Layers
"Australian Road Research", Vol. 10 no. 2 - 1980

|25| HAUGEN, E.B.
Probabilistic Approaches to Design
John Wiley & Son Inc., New York - 1968

|26| DARTER, M.I.; HUDSON, W.R.
Probabilistic Concepts applied to Flexible Pavement System Design
RR 123-18; Center for Highway Research
University of Texas at Austin - 1974

|27| WESTERGAARD, H.M.
Stresses in Concrete Pavements computed by Theoretical Analysis
"Public Roads", Vol. 7 no.2 - 1926

|28| BEUVING, E.
Calculation of the Traffic Intensities and Number of Equivalent 100 kN Single Axles on 9 Roads of the Province of Zuid Holland (in Dutch)
Report WB-15 (7-80-115-8); Dep. of Civil Engineering; Lab. for Road and Railroad Research; Delft University of Technology - 1980

|29| BEUVING, E.; MOLENAAR, A.A.A.
Deflection Measurements for the Determination of the Structural Deterioration of Pavements (in Dutch)
Report WB-25 (7-80-115-20); Dep. of Civil Engineering; Lab. for Road and Railroad Research; Delft University of Technology - 1980

|30| VAN GURP, Ch.A.P.M.
Adjustment of Subgrade Modulus and Equivalent Layer Thickness for Climatic Influences
Report 7-82-115-32; Dep. of Civil Engineering; Lab. for Road and Railroad Research; Delft University of Technology - 1982

|31| DUIVENVOORDEN, J.J.; DIJKINK, J.H.; VAN DER LOO, J.M.M.; PIJNENBURG, J.A.M.
Study on the Axle Load Distribution of Different Types of Trucks having different Axle Configurations (in Dutch)
Internal Report; Dep. of Civil Engineering; Chair of Highway Engineering
Delft University of Technology - 1975

|32| WORKING GROUP O_3, STUDY CENTRE FOR ROAD CONSTRUCTION
Axle Load Patterns on Roads (in Dutch)
"Wegen", Vol. 55 no. 2 - 1981

|33| DORMON, G.M.; METCALF, C.T.
Design Curves for Flexible Pavements based on Layered System.Theory
"Highway Research Record" no. 71, Washington D.C. - 1963

|34| BARKER, W.R.; BRABSTON, W.N.; CHOU, Y.T.
A General System for the Structural Design of Flexible Pavements
"Proceedings 4th Int. Conf. Structural Design of Asphalt Pavements"
Ann Arbor - 1977

|35| VEVERKA, V.
Evaluation of Rutdepth in Flexible Pavements (in French and Dutch)
"La Technique Routiere", Vol. 24 no. 3 - 1979

|36| DESCORNET, G.H.D.
Repeated Compression Tests on Granular Materials
"Proceedings 9th Int. Conf. on Soil Mechanics and Foundation Engineering"
Tokyo - 1977

|37| FRANCKEN, L.
Permanent Deformation Law of Bituminous Road Mixes in Repeated
Triaxial Compression
"Proceedings 4th Int. Conf. Structural Design of Asphalt Pavements"
Ann Arbor - 1977

|38| REICHERT, J.
Influence of Repeated Loading on the Deformation of Pavement Layers
"Proceedings 5th Int. Conf. on Soil Mechanics and Foundation Engineering"
Paris - 1961

|39| VERSTRAETEN, J.; VEVERKA, V.; FRANCKEN, L.
Rational and Practical Designs of Asphalt Pavements to avoid
Cracking and Rutting
"Proceedings 5th Int. Conf. Structural Design of Asphalt Pavements"
Delft - 1982

|40| AHLVIN, R.G.; ULERY, H.H.
Tabulated Values for determining the Complete Pattern of Stresses, Strains
and Deflections beneath a Uniform Circular Loading on a Homogeneous
Half Space
"Highway Research Board Bulletin" no. 342, Washington D.C. - 1962

Chapter 4

VISUAL CONDITION SURVEYS
AND
PLANNING OF MAINTENANCE

TABLE OF CONTENTS

4.1 Introduction

The easiest way to determine whether the pavement performs as designed, is to observe the deterioration of the pavement condition by means of periodical visual condition surveys.

The results of

a. to predict future condition
b. to determine when predefined minimum acceptance levels are reached
c. to establish maintenance urgencies and needs
d. to plan maintenance and rehabilitation activities
e. to adjust designs and/or design methods

It should be noted that the above-mentioned goals of the visual condition surveys can only be met if the results of the surveys themselves are uniform and reliable. This means that the condition surveys should be carried out according to well defined guidelines.
This involves that visual condition surveys should only be conducted according to user's guides with detailed definitions of distress types, and their degree and extent classes.

The main goal of visual condition surveys is the planning of maintenance and rehabilitation. A number of steps can be recognized in reading this major goal, they are

a. the development of a visual conditon survey method
b. the modelling of the observed pavement deterioration
c. the development of thresholds or minimum acceptance levels
d. the development of guidelines for a maintenance planning technique

Each step will be described in the subsequent sections.
Finally the procedure of estimating the remaining life and scheduling of maintenance works will be illustrated by means of an example.

4.2 Visual Condition Survey Method

Up till now a large number of visual condition survey methods has been developed. Hellings and Wienbelt |1| evaluated five of these methods |2, 3, 4, 5, 6| on their applicability for the Netherlands. They concluded that the condition survey method developed at the Texas A & M University could be used very well in Dutch circumstances and that it needed only minor adjustments to meet Dutch requirements. The revised method is described and documented in |7|. A short description of the method will be given hereafter.

The visual condition surveys are conducted using the inspection sheet which is shown in figure 4.1. As can be seen from this figure almost all damage types considered can be classified into a quantity and severity class. Each combination of quantity and severity class is translated into a number of deduct points. The deduct point table is given in table 4.1.
This deduct point table is used in the following way to describe the pavement condition.

a. First of all an overall pavement rating score PRS is calculated from the total amount of deduct points ΣDP using
   $RPS = 100 - \Sigma DP$
b. Secondly four deduct points subtotals are calculated. These four

Delft University of Technology, Department of Civil Engineering, Lab. for Road and Railroad Research

General			Surface Texture						Cracking				Deformations		Verge
Date: Road Number:			Raveling	Flushing	Patching	number of Core Holes	Potholes	number of Failures	Transverse Cracking	Longitudinal Cracking	Alligator Cracking	Crack Sealing 1 yes 2 partial 3 no	Rutting	Corrugations	0 not present 1-2 good 3-4 fair 5-6 poor
			% area (1) 1-15 (2) 16-30 (3) >30	% area (1) 1-15 (2) 16-30 (3) >30	% area (1) 1-15 (2) 16-30 (3) >30		m^2 (1) 0.01-1 (2) 1-2 (3) >2		number per 100 m (1) 1-7 (2) 8-15 (3) >15	m per m^1 (1) 0.1-1 (2) 1-2 (3) >2	% area (1) 1-5 (2) 6-25 (3) >25		% area (1) 1-15 (2) 16-30 (3) >30	% area (1) 1-15 (2) 16-30 (3) >30	
	from km to km	Lane	slight moderate severe	slight moderate severe	good fair poor				slight moderate severe	slight moderate severe	slight moderate severe		slight moderate severe	slight moderate severe	Pavement Edge Condition Shoulder Shoulder Edge Condition Verge
1															
2															
3															
4															
5															
6															
7															
8															
9															
10															
11															
12															
13															
14															

Figure 4.1 *Delft University Inspection Sheet*

Table 4.1 Deduct Point Table

Distress type	Degree	Extent or Amount		
		(1)	(2)	(3)
Raveling	Slight	5	8	10
	Moderate	10	12	15
	Severe	15	18	20
Flushing	Slight	5	8	10
	Moderate	10	12	15
	Severe	15	18	20
Patching	Good	0	2	5
	Fair	5	7	10
	Poor	7	15	20
Unfilled Cores	1)	5	8	12
Potholes		7	12	18
Failures	2)	20	30	40
Transverse Cracking (sealed)	Slight	2	5	8
	Moderate	5	8	10
	Severe	8	10	15
(partially sealed)	Slight	3	7	10
	Moderate	7	10	15
	Severe	10	15	20
(not sealed)	Slight	3	7	12
	Moderate	7	12	15
	Severe	12	15	20
Longitudinal Cracking (sealed)	Slight	2	5	8
	Moderate	5	8	10
	Severe	8	10	15
(partially sealed)	Slight	3	7	12
	Moderate	7	12	15
	Severe	12	15	20
(not sealed)	Slight	5	10	15
	Moderate	10	15	20
	Severe	15	20	25
Alligator Cracking	Slight	5	10	15
	Moderate	10	15	20
	Severe	15	20	25
Rutting	Slight	0	2	5
	Moderate	5	7	10
	Severe	10	12	15
Corrugations	Slight	5	8	10
	Moderate	10	12	15
	Severe	15	18	20

1) (1) = 1-3 (2) = 4-6 (3) = >6
2) (1) = 1 (2) = 2 (3) = >2

DETAILED VISUAL CONDITION SURVEY CONDUCTED
ON THE TRUNK ROAD NETWORK OF DISTRICT AB
FEBRUARY-MARCH 1982

NOTATION FORM

ROAD CODE	GENERAL			SURFACE						CRACKING				DEFORM.		SHOULDER						DEDUCT POINTS		CLASS			DATE OF		
																PAVED				UNP									
	SECTION NUMBER	FROM- TO	LANE	RAVELING	FLUSHING	PATCHING	UNFILLED CORES	POTHOLES	FAILURES	TRANSVERSE CRACKING	LONGITUDINAL CRACKING	ALLIGATOR CRACKING	CRACK SEALING	RUTTING	CORRUGATIONS	ROADSIDE	SHOULDER	SHOULDERSIDE	VERGE	ROADSIDE	SHOULDER	ROADWAY	SHOULDER	ROAD	CONSTRUCTION	TRAFFIC	CONSTRUCTION	REHABILITANCE	SURVEY
				LMS	LMS	GMP				LMS	LMS	LMS		LMS	LMS														
AB S 22	1	0.40- 0.50	L	1	1					1	1	1	2	1						4	2	25	30	1	5	4	0	7803	8202
AB S 22	2	0.60- 0.70	L	1	1					1	1		2	2						4	2	26	30	1	5	4	0	7803	8202
AB S 22	3	0.90- 1.00	L	1	2					1	1	1	2	2						3	2	30	25	1	5	4	0	7803	8202
AB S 22	4	1.00- 1.10	L	1	1					1	1		2	2						4	3	22	35	1	5	4	0	7803	8202
AB S 22	5	1.89- 1.90	L	2							1		3							4	2	13	30	1	5	4	0	7803	8202
AB S 22	6	0.20- 0.30	R	1	1					1	1		3	2						3	3	20	30	1	5	4	0	7803	8202
AB S 22	7	0.30- 0.40	R	1	2					1	1		3	2						3	3	23	30	1	5	4	0	7803	8202
AB S 22	8	0.40- 0.50	R	1	2					2	1		3	1						3	3	35	30	1	5	4	0	7803	8202
AB S 22	9	0.90- 1.00	R	1	2			1		1	1	1	2	1						3	3	40	30	1	5	4	0	7803	8202
AB S 22	10	1.80- 1.90	R	1	1						1	2	3							4	3	25	35	1	5	4	0	7803	8202
AB S 15	11	4.40- 4.50	L	2	1	1				1	1	1	2	1		2	2	3	3			34	25	1	5	3	7205	0	8202
AB S 15	12	5.10- 5.20	L	2	1					1	1	1	3			2	3	4	3			26	30	1	5	3	7205	0	8202
AB S 15	13	5.30- 5.40	L	1	1					1	1		2			2	2	3	3			20	25	1	5	3	7205	0	8202
AB S 15	14	4.40- 4.50	R	2	1	1				1		2	3			2	3	4	4			40	32	1	5	3	7205	0	8202
AB S 15	15	4.50- 4.60	R	1	1					1	1	2	2			3	3	4	4			26	35	1	5	3	7205	0	8202
AB S 15	16	4.70- 4.80	R	1	1					1	1	1	2			3	4	3	3			21	32	1	5	3	7205	0	8202
AB S 15	17	5.50- 5.60	R	1	1	1				1			3			4	4	3	4			18	37	1	5	3	7205	0	8202

NOTE: Figures 4.2, 4.3, and 4.4 are typewriter copies of the original computer printout

Figure 4.2 Printout of the Data introduced into the Computer Program subtotals are:

1. number of deduct points due to raveling
2. number of deduct points due to failures, potholes, bad repairs and unfilled coreholes
3. number of deduct points due to transverse, longitudinal and alligator cracking
4. number of deduct points due to rutting and corrugations.
   These four subtotals are introduced since it enables the highway engineer to determine which type of distress is predominant. This is thought to be of importance since the type of defect together with its severity and extent will determine the type of maintenance or rehabilitation works.

Since the inspections will result in a mass of data, computerprograms to process the data have been written by Duivenvoorden |8| and Van Gurp |9|. Typical examples of the printout are given in figures 4.2. to 4.4.

Figure 4.2 shows the printout of the data as introduced into the computer program. Figure 4.3 shows the amount of deduct points assigned to the forementioned four subtotals. In this figure also the deduct points due to raveling and longitudinal plus alligator cracking are given. These are, as will be described later on, used in the remaining life calculations. Figure 4.4 shows the graphical representation of the total number of deduct points.

The visual condition survey method is, as will be indicated later on, succesfully used on a large number of road sections since 1976. The survey results are used in the modelling of the observed pavement deterioration as will be described in the next section.

4.3 Modelling of the Observed Pavement Deterioration

As has been mentioned, visual condition surveys have been conducted on road sections that are a part of the provincial road network of the province of Zuid Holland. Information on the location of the sections, their construction, subsoil and traffic intensities has been given in chapter 2.

Typical examples of the deterioration, expressed by the total number of deduct points, of the 100 m long survey sections within a specific road section are given in figure 4.5.

The exponentional increase in distress, as depicted in figure 4.5, was observed on all road sections.
Development of a deterioration model based on the data obtained on the individual 100 m survey sections,was not considered to be appropriate. Therefore the survey sections were merged into larger subsections. The author decided that decisions on the magnitude (length) of these subsections should be based on the load carrying capacity of the pavement. Within a subsection, this load carrying capacity had to be more or less constant. In order to create such subsections, deflection measurements were carried out on the pavement considered.

The condition of each subsection was characterized by the mean value of the PRS values of the 100 m survey sections. Application of this technique on the data given in figure 4.5, yields to deterioration curves as shown in figure 4.6.

```
TABLE WITH THE TOTAL NUMBER OF DEDUCT POINTS FOR THE ROADWAY
AND THE SUBTOTALS OF THE DEDUCT POINTS


SUBTOTAL 1 IS SUM OF DEDUCT POINTS FOR : RAVELING
                                         FLUSHING

SUBTOTAL 2 IS SUM OF DEDUCT POINTS FOR : PATCHING
                                         UNFILLED CORES
                                         POTHOLES
                                         FAILURES

SUBTOTAL 3 IS SUM OF DEDUCT POINTS FOR : TRANSVERSE CRACKING
                                         LONGITUDINAL CRACKING
                                         ALLIGATOR CRACKING

SUBTOTAL 4 IS SUM OF DEDUCT POINTS FOR : RUTTING
                                         CORRUGATIONS

SUBTOTAL 5 IS SUM OF DEDUCT POINTS FOR : RAVELING

SUBTOTAL 6 IS SUM OF DEDUCT POINTS FOR : LONGITUDINAL CRACKING
                                         ALLIGATOR CRACKING


                                    TOTAL    SUB    SUB     SUB     SUB  SUB    SUB
 NR DIST ROAD   LANE  FROM- TO     DEDUCT  TOTAL  TOTAL   TOTAL   TOTAL TOTAL  TOTAL
                                   POINTS    1      2       3       4     5      6

  1  AB  S 22    L    0.40- 0.50     25     10      0      15       0     5      8
  2  AB  S 22    L    0.60- 0.70     26     10      0      14       2     5      7
  3  AB  S 22    L    0.90- 1.00     30     13      0      15       2     5     12
  4  AB  S 22    L    1.00- 1.10     22     10      0      10       2     5      7
  5  AB  S 22    L    1.80- 1.90     13      8      0       5       0     8      5
  6  AB  S 22    R    0.20- 0.30     20     10      0       8       2     5      5
  7  AB  S 22    R    0.30- 0.40     23     13      0       8       2     5      5
  8  AB  S 22    R    0.40- 0.50     35     13      0      12      10     5      5
  9  AB  S 22    R    0.90- 1.00     40     13      7      15       5     5     12
 10  AB  S 22    R    1.80- 1.90     25     10      0      15       0     5     15
 -----------------------------------------------------------------------------------
 11  AB  S 15    L    4.40- 4.50     34     13      5      11       5     8      8
 12  AB  S 15    L    5.10- 5.20     26     13      0      13       0     8     10
 13  AB  S 15    L    5.30- 5.40     20     10      0      10       0     5      7
 14  AB  S 15    R    4.40- 4.50     40     18      5      17       0     8     10
 15  AB  S 15    R    4.50- 4.60     26     10      0      16       0     5     13
 16  AB  S 15    R    4.70- 4.80     21     10      0      11       0     5      8
 17  AB  S 15    R    5.50- 5.60     18     15      0       3       0     5      0
 -----------------------------------------------------------------------------------
 18  AB  S 22    L    3.70- 3.80     54     30     12      12       0    15      5
 19  AB  S 22    L    4.50- 4.60     49     27     17       5       0    15      5
 20  AB  S 22    L    4.60- 4.70     47     27     10      10       0    15     10
 21  AB  S 22    R    3.60- 3.70     30     20      7       3       0     5      0
 22  AB  S 22    R    3.70- 3.80     42     20      0      22       0     5     15
 23  AB  S 22    R    4.00- 4.10     17     17      0       0       0     5      0
 -----------------------------------------------------------------------------------
 24  AB  S 22A   L    2.90- 3.00     30     18      0       5       7     8      5
 25  AB  S 22A   L    3.00- 3.10     20     10      0      10       0     5     10
 26  AB  S 22A   L    3.20- 3.30     36     18      5      13       0    10     13
 27  AB  S 22A   L    3.30- 3.40     50     13     12      20       5     5     20
 28  AB  S 22A   R    2.90- 3.00     28     18      0       5       5     8      5
 29  AB  S 22A   R    3.00- 3.10     18     13      0       5       0     8      5
 30  AB  S 22A   R    3.20- 3.30     50     16      7      22       5     8     22
 31  AB  S 22A   R    3.30- 3.40     23     13      0      10       0     5     10
 -----------------------------------------------------------------------------------
 32  AB  S  7    L    6.30- 6.40     10      5      0       5       0     0      5
 33  AB  S  7    L    6.80- 6.90     19     10      0       9       0     5      7
 34  AB  S  7    L    6.90- 7.00     16     13      0       3       0     5      0
 35  AB  S  7    R    6.30- 6.40     25     10      0      15       0     5     15
 36  AB  S  7    R    6.80- 6.90     60      8     27      20       5     8     20
 37  AB  S  7    R    6.90- 7.00     15      5      7       3       0     0      0
 -----------------------------------------------------------------------------------
```

Figure 4.3 *Deduct Points as assigned to the Subtotals*

```
GRAPH WITH THE TOTAL NUMBER OF DEDUCT POINTS FOR THE ROADWAY

WARNING LEVEL SET TO 40 DEDUCT POINTS

                                   1         2         3         4         5         6         7         8         9         1
NR ROAD  LANE  FROM- TO   |1234567890123456789012345678901234567890123456789012345678901234567890123456789012345678901234567890
                          |                                                                                                   0

 1 S 22    L  0.40- 0.50  |xxxxxxxxxxxxxxxxxxxxxxxxx              :
 2 S 22    L  0.60- 0.70  |xxxxxxxxxxxxxxxxxxxxxxxxxx             :
 3 S 22    L  0.90- 1.00  |xxxxxxxxxxxxxxxxxxxxxxxxxxxxxx         :
 4 S 22    L  1.00- 1.10  |xxxxxxxxxxxxxxxxxxxxxx                 :
 5 S 22    L  1.80- 1.90  |xxxxxxxxxxxxx                          :
 6 S 22    R  0.20- 0.30  |xxxxxxxxxxxxxxxxxxxx                   :
 7 S 22    R  0.30- 0.40  |xxxxxxxxxxxxxxxxxxxxxxx                :
 8 S 22    R  0.40- 0.50  |xxxxxxxxxxxxxxxxxxxxxxxxxxxxxxxxxxx    :
 9 S 22    R  0.90- 1.00  |xxxxxxxxxxxxxxxxxxxxxxxxxxxxxxxxxxxxxxxx
10 S 22    R  1.80- 1.90  |xxxxxxxxxxxxxxxxxxxxxxxxx              :
11 S 15    L  4.40- 4.50  |xxxxxxxxxxxxxxxxxxxxxxxxxxxxxxxxxx     :
12 S 15    L  5.10- 5.20  |xxxxxxxxxxxxxxxxxxxxxxxxxx             :
13 S 15    L  5.30- 5.40  |xxxxxxxxxxxxxxxxxxxx                   :
14 S 15    R  4.40- 4.50  |xxxxxxxxxxxxxxxxxxxxxxxxxxxxxxxxxxxxxxxx
15 S 15    R  4.50- 4.60  |xxxxxxxxxxxxxxxxxxxxxxxxxx             :
16 S 15    R  4.70- 4.80  |xxxxxxxxxxxxxxxxxxxxx                  :
17 S 15    R  5.50- 5.60  |xxxxxxxxxxxxxxxxxx                     :
18 S 22    L  3.70- 3.80  |xxxxxxxxxxxxxxxxxxxxxxxxxxxxxxxxxxxxxxxxxxxxxxxxxxxxxx
19 S 22    L  4.50- 4.60  |xxxxxxxxxxxxxxxxxxxxxxxxxxxxxxxxxxxxxxxxxxxxxxxxx
20 S 22    L  4.60- 4.70  |xxxxxxxxxxxxxxxxxxxxxxxxxxxxxxxxxxxxxxxxxxxxxxx
21 S 22    R  3.60- 3.70  |xxxxxxxxxxxxxxxxxxxxxxxxxxxxxx         :
22 S 22    R  3.70- 3.80  |xxxxxxxxxxxxxxxxxxxxxxxxxxxxxxxxxxxxxxxxxx
23 S 22    R  4.00- 4.10  |xxxxxxxxxxxxxxxxx                      :
24 S 22A   L  2.90- 3.00  |xxxxxxxxxxxxxxxxxxxxxxxxxxxxxx         :
25 S 22A   L  3.00- 3.10  |xxxxxxxxxxxxxxxxxxxx                   :
26 S 22A   L  3.20- 3.30  |xxxxxxxxxxxxxxxxxxxxxxxxxxxxxxxxxxxx   :
27 S 22A   L  3.30- 3.40  |xxxxxxxxxxxxxxxxxxxxxxxxxxxxxxxxxxxxxxxxxxxxxxxxxx
28 S 22A   R  2.90- 3.00  |xxxxxxxxxxxxxxxxxxxxxxxxxxxx           :
29 S 22A   R  3.00- 3.10  |xxxxxxxxxxxxxxxxxx                     :
30 S 22A   R  3.20- 3.30  |xxxxxxxxxxxxxxxxxxxxxxxxxxxxxxxxxxxxxxxxxxxxxxxxxx
31 S 22A   R  3.30- 3.40  |xxxxxxxxxxxxxxxxxxxxxxx                :
32 S  7    L  6.30- 6.40  |xxxxxxxxxx                             :
33 S  7    L  6.80- 6.90  |xxxxxxxxxxxxxxxxxxx                    :
34 S  7    L  6.90- 7.00  |xxxxxxxxxxxxxxxx                       :
35 S  7    R  6.30- 6.40  |xxxxxxxxxxxxxxxxxxxxxxxxx              :
36 S  7    R  6.80- 6.90  |xxxxxxxxxxxxxxxxxxxxxxxxxxxxxxxxxxxxxxxxxxxxxxxxxxxxxxxxxxxx
37 S  7    R  6.90- 7.00  |xxxxxxxxxxxxxxx                        :
38 S 30    L  1.00- 1.10  |xxxxxxxxxxxxx                          :
39 S 30    L  2.10- 2.20  |xxxxxxxxxxxxxxxxxxxxxxxx               :
40 S 30    L  2.20- 2.30  |xxxxxxxxxxxxxxx                        :
41 S 30    R  1.00- 1.10  |xxxxxxxxxxxxxxxx                       :
42 S 30    R  2.10- 2.20  |xxxxxxxxxxxxxxxxxxxxxxxxxxxxx          :
43 S 30    R  2.20- 2.30  |xxxxxxxxxxxxxxxxxxxxxx                 :
```

Figure 4.4 Graphical Representation of the Total Number of Deduct Points

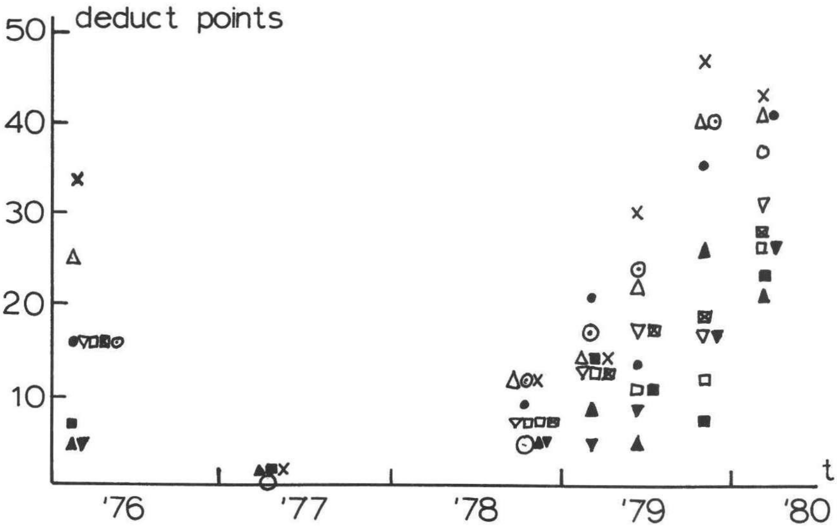

Figure 4.5 *Increase of the Total Number of Deduct Points on ten 100 m sections of the S36*

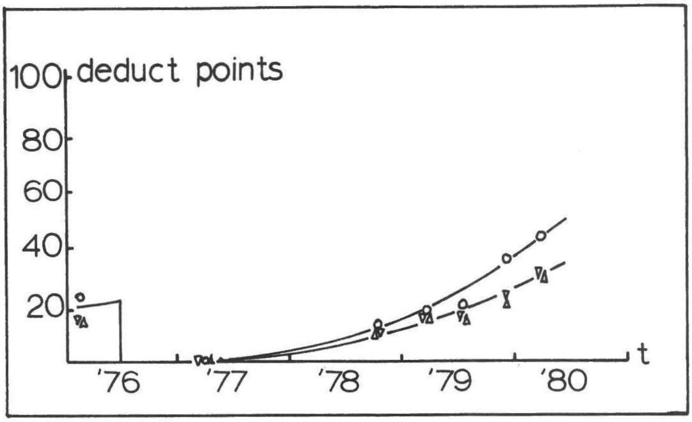

Figure 4.6 *Increase of the Total Mean Number of Deduct Points as observed on three Subsections of the S36*

It should be noted that simular curves were derived for raveling and longitudinal plus alligator cracking. No such curves could be derived for bleeding, rutting and transverse cracking. The inability to derive deterioration curves for bleeding and transverse cracking might be explained by the fact, that these defects are mainly caused by climatic effects and only to a limited extent by

repeated traffic loading.
The reason why no rutting deterioration curves could be derived is twofold:

<u>a.</u> in general a very little amount of rutting was observed

<u>b.</u> too few data were available since only a few measurements could be taken due to restricted availability of manpower and equipment that was required to meet all savety requirements

In order to be able to describe in a uniform way the deterioration of the pavement condition in terms of raveling, longitudinal plus alligator cracking, and total number of deduct points, a value P_v called the visual condition index was introduced |10,11|.
P_v is called by

$$P_v = 1 - \frac{DP}{DP_{max}} \qquad \text{eq. 4.1}$$

where DP = number of deduct points due to the present distress

DP_{max} = maximum number of deduct points for the distress type considered.

From table 4.1 it can be seen that $DP_{max} = 20$ in case of raveling and that $DP_{max} = 50$ in case of longitudinal and alligator cracking. For the overall condition DP_{max} is set at 100. So if e.g. a given section gets 15 deduct points due to raveling, 25 due to longitudinal and alligator cracking and 50 due to the overall condition, then

$$P_{raveling} = 1 - \frac{15}{20} = 0.25$$

$$P_{cracking} = 1 - \frac{25}{50} = 0.5$$

$$P_{overall\ condition} = 1 - \frac{50}{100} = 0.5$$

Figure 4.7 shows what the results of these calculations are, using the data given in figure 4.6.
The same type of curves were derived for $P_{raveling}$ and $P_{cracking}$.

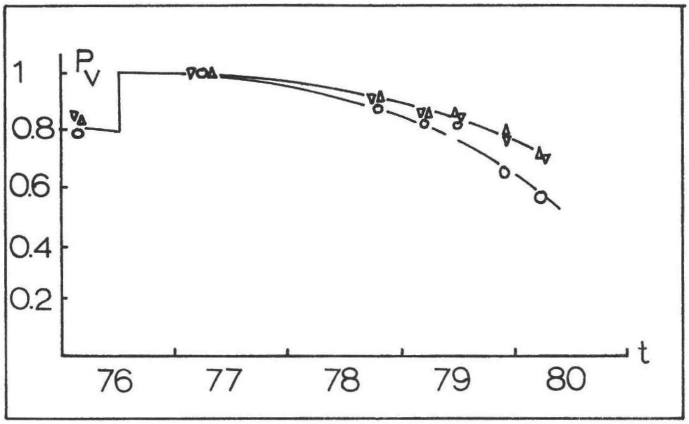

<u>Figure 4.7</u> Decrease of P_v as determined for Three Subsections of the S36.

The decrease of P_V with time as shown in figure 4.7 was described with the equation:

$$1 - P_v = e^{\alpha(\frac{t}{T}-1)} \qquad \text{eq. 4.2}$$

in which P_v = as defined above

α = a constant depending on the type of construction

t = number of years between time of inspection and construction or last rehabilitation activity

T = pavement life; the pavement life is reached if P = 0

Figure 4.8 is a graphical representation of equation 4.2.

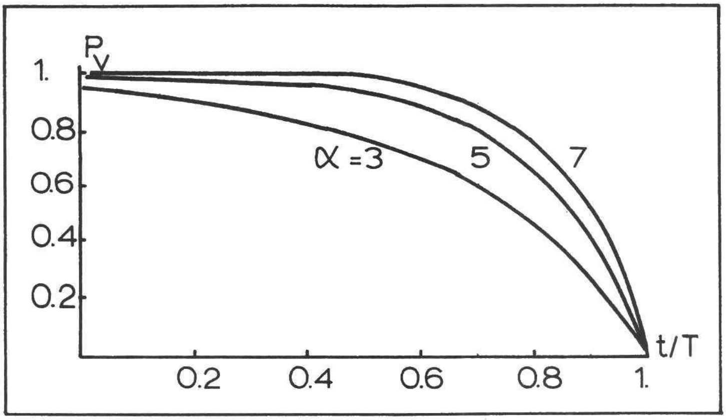

Figure 4.8 *Performance Model to describe the Visual Deterioration of Pavement Deterioration*

4.4 Application of the Deterioration Model on the Road Sections considered

Equation 4.2 has been used to describe the observed deterioration of the road sections considered.

The two unknown parameters in equation 4.2. being α and T, can be solved by means of simple linear regression. Table 4.2 summarizes the results of the calculations performed. From this table it can be seen that most alpha values range from 4 to 5.5. Only the sections of the S_1, S_{10} and $S_{22}H$ show different α values. A possible explanation of this different behavior in relation to the type of construction will be given hereafter.

S_1 Sections

The reason why the sections S_1 show a different behavior arises from its construction type. This construction is a rather stiff construction due to the cement stabilized base with an elastic modulus of about 6000 MPa. It is a well known fact that the distress development of stiff pavements is more or less brittle which means that the α values for cracking and also for the total number of deduct points will be rather high.

The question however is why also the α value for raveling is that high at the S_1 since it might be argued that raveling is a construction independent distress type. Up till now no satisfactory explanation could be found for the high $\alpha_{raveling}$ values. It might however be stipulated that differences in $\alpha_{raveling}$ values between stiff and flexible constructions might be due to differences in deformation on micro-scale and differences in kneading action of traffic.

S_{10} Sections

Also the variation in α values as determined for the S_{10} sections can be explained by taking into account the stiffness of the base layers. Figure 4.9 shows the variation in time of the base modulus of the $S_{10}R$ sections.
Sections 1 and 3 are the sections having a rather stiff base of blast furnance slag which exhibits a considerable amount of cementation.
From table 4.2 it can be seen that those two sections have rather high values for $\alpha_{cracking}$ and α_{total}. Once again it can be stated that this is reasonable since we are dealing with stiff bases. Just like for all S_1 sections no satisfactory explanation could be given for the high $\alpha_{raveling}$ values observed on those two sections.
The same behavior is observed at the $S_{10}L$ sections. Here section 1 and 5 show high alpha values which correspond to stiff base layers (fig. 4.10).
By considering table 4.2 together with figures 4.9 and 4.10 it can be seen that the sections with rather low base moduli (sections 2R, 4R, 5R, 2L, 6L) also show low values for alpha.

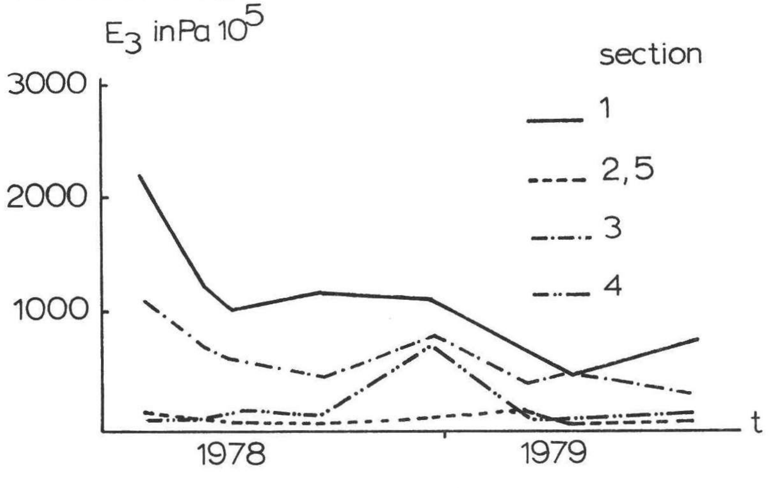

Figure 4.9 Deterioration of the Base of the $S_{10}R$ sections

Having made plausible that constructions with a stiff cemented base do have high α values, some comments should be made on the α values as derived for the S_{42} sections. Although these sections do have a blast furnance clay base too, they do not seem to have the same high α values. This might be contributed to the fact that hardly any distress was encountered on these sections which makes the α predictions rather unreliable (see low r^2 values for the cracking model in table 4.2). For this reason the S_{42} sections are not used in the evaluation proces on the dependency of α on the type of construction (see section 4.5).

Table 4.2 *Values of α due to Raveling, Cracking and Overall Condition*

Road Number	Section Number	α Raveling	T Raveling	r^2	α Cracking	T Cracking	r^2	α Total	T Total	r^2	Yearly traffic growth
S_1	1L	8.6	8.4	0.89	7.3	11.7	0.69	7.6	9.8	0.99	
	2L	8.7	8.3	0.9	7.4	12.6	0.63	7	9.5	0.96	
	3L	8.7	8.3	0.9	7.3	12.	0.78	7	10.1	0.96	5.5%
	1R	8.7	8.3	0.9	7.9	11.	0.72	7.7	9.7	0.98	
	2R	8.8	8.2	0.91	8	11.2	0.72	7.1	9.8	0.97	
	3R	8.9	8.2	0.91	7.9	10.6	0.74	7.7	9.3	0.99	
S_{10}	1L	8	7.	0.83	8.1	7.6	0.92	8.4	7.2	0.93	
	2L	10.6	7.2	0.9	3.8	8.1	0.82	5.6	7.5	0.89	
	3L	8.5	7.2	0.94	5	7.7	0.91	6.3	7.5	0.96	
	4L	4.2	7.4	0.96	4	7.7	0.9	3.8	7.9	0.75	
	5L	10.9	7.1	0.88	10	7.6	0.91	10.9	7.1	0.91	
	6L	3.5	8.4	0.72	3.1	9.1	0.51			0.59	8%
	1R	8.7	7.	0.94	8.8	7.5	0.99	9	7.3	0.99	
	2R	7.7	7.3	0.79	2.1	12	0.35	3.5	8.9	0.82	
	3R	10.4	7.3	0.9	5.9	7.4	0.91	7.7	7.3	0.94	
	4R	7.9	7.2	0.82	2.5	8.	0.88	3.8	7.6	0.95	
	5R	4.6	7.6	0.93	4	8.5	0.69	4.8	7.8	0.81	
$S_{22}B$	1L	5.8	4.8	0.89	5.1	19.2	0.21	5.5	5.9	0.89	
	2L	5.8	4.7	0.89	5.1	17.9	0.28	5.5	5.9	0.88	
	3L	5.9	4.6	0.9	4.8	9.1	0.29	5.5	5.3	0.82	
	4L	4.6	4.4	0.91	5.7	5.3	0.91	5.2	5.	0.97	
	5L	5.9	4.4	0.9	5.6	6.1	0.84	5.6	5.1	0.86	6%
	1R	5.7	5.3	0.91	5.7	9.4	0.38	5.7	5.9	0.95	
	2R	5.9	4.8	0.9	5.5	5.8	0.87	5.6	5.2	0.9	
	3R	5.8	4.7	0.91	5.4	5.8	0.83	5.3	5.2	0.91	
	4R	5.8	4.9	0.91	5.6	7.2	0.88	5.3	5.7	0.97	
	5R	5.8	4.8	0.91	5.9	7.4	0.54	5.4	5.4	0.98	
	6R	5.8	4.7	0.9	5.4	7.6	0.52	5.3	5.6	0.95	

Table 4.2 Continued

Road Number	Section Number	α Raveling	T Raveling	r^2	α Cracking	T Cracking	r^2	α Total	T Total	r^2	Yearly traffic growth
$S_{22}H$	1L	4.6	4.4	0.76	-	-	-	2.7	7.4	0.78	
	2L	4.6	4.4	0.74	5.8	8.1	0.73	4.6	6.2	0.72	6%
	1R	4.6	4.4	0.76	2.3	11.2	0.18	2.5	8.3	0.58	
	2R	4.6	4.4	0.74	2.2	8.6	0.76	2.7	6.8	0.76	
S_{29}	1L	5.8	4.9	0.89	-	-	-	4	8.1	0.94	
	2L	5.8	4.9	0.9	4.9	34.	0.25	4	7	0.9	
	3L	5.8	4.9	0.9	-	-	-	4	7.7	0.93	6.7%
	1R	5.8	4.9	0.9	-	-	-	3.9	8.4	0.91	
	2R	5.8	4.8	0.88	-	-	-	3.9	7.6	0.86	
	3R	5.8	4.8	0.88	5.6	9.4	0.51	5.4	6.6	0.76	
	4R	5.8	4.8	0.88	5.6	9.4	0.52	4.2	6.7	0.93	
S_{36}	1L	5.1	3.9	0.83	4.8	4.8	0.76	5.5	4.4	0.97	
	2L	5.3	3.8	0.88	4.3	4.3	0.89	5.6	4.3	1.0	
	3L	5.3	3.7	0.89	4.1	4.1	0.91	5.3	4.	0.9	2.7%
	1R	5.1	4.	0.82	4.3	4.3	0.78	5.5	4.2	0.98	
	2R	4.9	3.9	0.76	4.8	4.8	0.77	5.5	4.6	0.98	
	3R	5.1	3.8	0.82	4.8	4.8	0.9	5.4	4.5	0.98	
S_{42}	1L	5.8	4.9	0.73	5.7	9.4	0.54	5.7	6.5	0.82	
	2L	5.8	4.9	0.73	-	-	-	5.6	7	0.82	
	3L	5.9	4.9	0.86	-	-	-	5.6	6.9	0.82	
	4L	5.9	4.8	0.86	4.9	25.9	0.13	5.7	6.7	0.81	5.7%
	5L	5.9	4.8	0.86	5.6	9.	0.38	5.8	6.	0.81	
	1R	5.8	4.9	0.73	5.1	16.	0.3	5.7	6.6	0.86	
	2R	5.9	4.9	0.87	-	-	-	5.7	6.8	0.83	

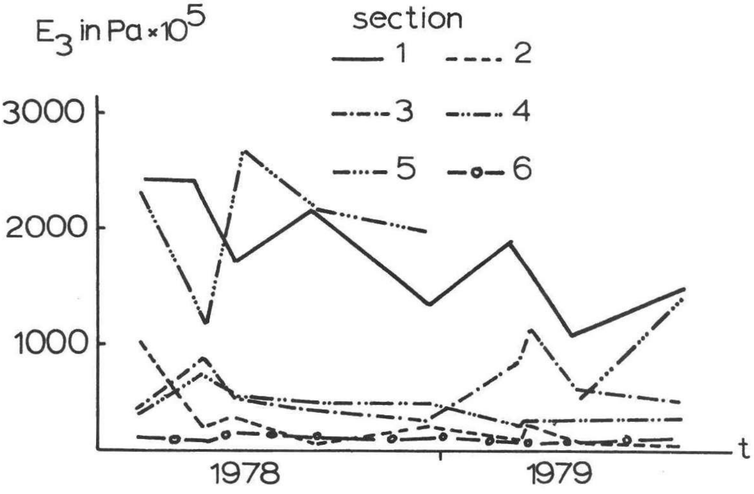

Figure 4.10 *Deterioration of the Base of the $S_{10}L$ Sections*

$S_{22}H$ Sections:

The reason for the different damage development of the $S_{22}H$ sections is caused by the fact that on that road very often minor maintenance activities are applied to restore the damage which is due to a gradual increasing slope failure of the dike on which the pavement is constructed. Due to these maintenance activities the damage development shows a rather irregular pattern (fig. 4.11).

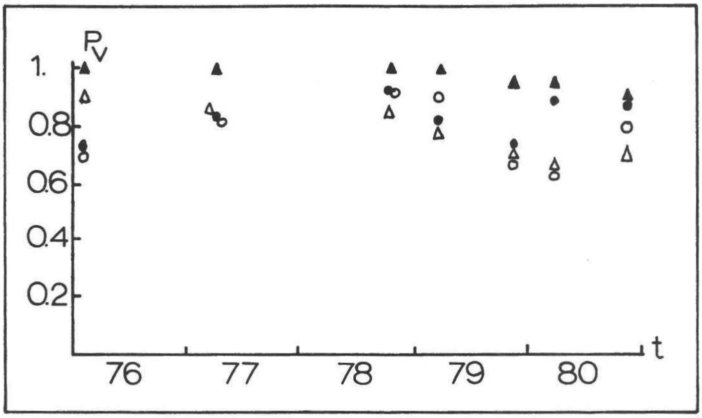

Figure 4.11 *Irregular Pattern of the Deterioration of the $S_{22}H$ Sections*

Bibliotheek TU Delft
Afdeling Leverantie
Prometheusplein 1
2600 MG Delft
Informatie of verlengen: 015 278 56 78
Information or extending loan period: + 31 (0) 15 278 56 78

LOOPBON VOOR DOCUMENTAANVRAGEN
COLLECTION TICKET FOR DOCUMENT REQUESTS

11 NOV 2004

Aangevraagd op/ requested on: 14/10/2004 Tijd/ time: 12:19

Uiterlijk terugbezorgen op (stempel datum)/ return expiring date (stamp):

Documentgegevens (auteur, titel)/ document data (author, title):

Molenaar, Andreas Aadrianus Anthonius : Structural performance and design of flexible road constructions and asphalt concrete overlays S.l. : s.n., 1983 (#000282180)

Item: 818984 > 17313401 < Central~Library closed stacks loan
===========

Requested for : ID 99427 Status 03 Type CO

Rasmussen, S.
Fac. Civiele Techniek
Stevinweg 1/CT1 K1.04
2628 CN DELFT RAS baknr.
10

Opmerkingen/remarks:

Afhaallokatie/ Pickup Location: Central loan/return desk
======================

Uw aanvraag wordt niet gehonoreerd in verband met/ your request cannot be supplied for the following reason:

() Afwezig/ not available
() Openstaande boete/ outstanding fine
() U heeft teveel boeken/ you have too many books
() Alleen ter inzage/ only for perusal in the library
() Overig namelijk/ other namely:

===

Rasmussen, S.

14/10/2004

74
155

4.5 Dependency of Alpha on the Type of Construction

Although only a limited amount of road sections was taken under consideration in this study, it is thought that a dependency of alpha on the type of construction has been shown.
Summarizing the results of table 4.2 in conjunction with the explanation which has been given of the behavior of the S_1 and S_{10} sections it can be concluded that alpha will increase with increasing stiffness of the structure. Normally alpha will range from 4 to 5, while for structures with stiff stabilized base layers alpha will be 7 or higher. On the other hand for constructions which have relatively thin asphaltic top layers and low stiffness bases, the alpha values will vary around 3.
In more fundamental terms it can be stated that the magnitude of alpha is dependent on the magnitude of the strain levels in the (semi) bound layers of the pavement structure. Low strain values will result in high alpha values, while a high strain level will result in low alpha values.
In this sense the alpha values should be related with the surface curvature index since, as shown before, this value is a good indication of the strain level in the pavement structure. This will be discussed in a later section.
Prior knowledge of the alpha value is important for the planning of maintenance since the pavement life T can be calculated knowing P, t and α (equation 4.2). Therefore it is recommended to use the alpha values given in table 4.3 for pavement life estimations if none or only a limited number of condition surveys has been conducted in the past.

Table 4.3 Values of α in relation to the Construction Type

Type of Distress	RAV	CRK	ALL
Construction Type			
. asphalt layers on cement bound base	5	7.6	7.4
. asphalt layers on base of blast furnace slag showing cementation	5	5-8.5	6-8.7
. asphalt layers on unbound base	5	3-3.5	4.3
. bituminous construction	5	5.5	5.5

RAV = raveling
CRK = longitudinal and alligator cracking
ALL = overal pavement condition

It should be noted that in spite of the large variation which has been observed in the α_{RAV} values, this value was arbitrarely set at 5 for all construction types. This is done to overcome unrealistic remaining life predictions based on raveling.

4.6 Visual Deterioration in Relation to the Number of Load Applications

The presented models are based on a time scale. It might be argued that for instance load associated cracking should be related to the numer of load

Table 4.4 Cumulative Number of Load Repetitions in relation to Traffic Growth Rate

Year	4%	Σ	6%	Σ	8%	Σ	10%	Σ
1	1.04	1.04	1.06	1.06	1.08	1.08	1.1	1.1
2	1.08	2.12	1.12	2.18	1.17	2.25	1.21	2.31
3	1.12	3.24	1.19	3.37	1.26	3.51	1.33	3.64
4	1.17	4.41	1.26	4.63	1.36	4.87	1.46	5.1
5	1.22	5.63	1.34	5.97	1.47	6.34	1.61	6.71
6	1.27	6.9	1.42	7.39	1.59	7.93	1.77	8.48
7	1.32	8.22	1.50	8.89	1.71	9.64	1.95	10.43
8	1.37	9.59	1.59	10.48	1.85	11.49	2.14	12.57
9	1.42	11.01	1.69	12.17	2.	13.49	2.36	14.93
10	1.48	12.49	1.79	13.96	2.16	15.65	2.59	17.52
11	1.54	14.03	1.90	15.86	2.33	17.98	2.85	20.37
12	1.60	15.63	2.01	17.87	2.52	20.5	3.14	23.51
13	1.67	17.30	2.13	20.	2.72	23.22	3.45	26.96
14	1.73	19.30	2.26	22.26	2.94	26.16	3.8	30.76
15	1.80	20.83	2.4	24.66	3.17	29.33	4.18	34.94
16	1.87	22.70	2.54	27.2	3.43	32.76	4.59	39.53
17	1.95	24.65	2.69	29.89	3.7	36.46	5.05	44.58
18	2.03	26.68	2.85	32.74	4	40.46	5.56	50.16
19	2.11	28.79	3.03	35.77	4.32	44.78	6.12	56.28
20	2.19	30.98	3.21	38.98	4.66	49.44	6.73	63.01

repetitions in stead of the time period the construction is subjected to traffic. This is especially true if the amount of traffic and especially the traffic growth is not the same on each road. In the presented model, differences in amount of traffic of the road sections considered are overcome by using a time ratio t/T. It should be checked to what extent the differences in traffic growth do influence the shape of the model.
In order to do so, the t/T scale of the horizontal axis of figure 4.8 was transformed into a n/N scale where n stands for the applied number of load applications and N for the number of load applications to $P_V = 0$.
Table 4.4 was used for these transformation purposes. One and another has resulted in figure 4.12 where the decrease of the visual condition is given with respect to t/T and n/N. This latter factor is given for different traffic growth rates and for different values of the pavement life.

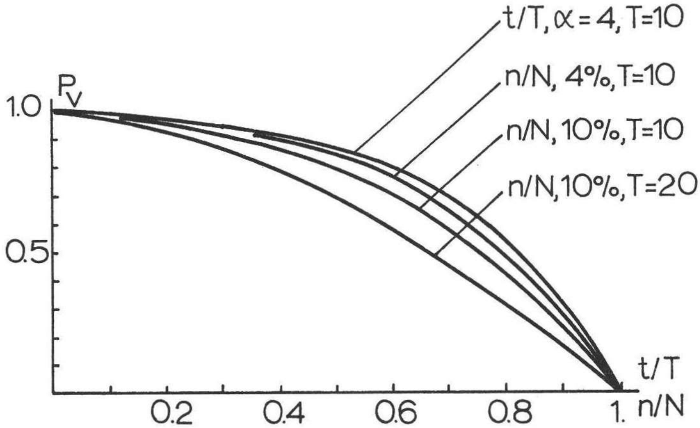

Figure 4.12 *Visual Deterioration Performance Model related to different Traffic Growth Rates and Pavement Lifes*

An example will be given to describe the proposed procedure.
a. Assume the pavement life is 20 years
b. For an annual traffic growth rate of 10%, the ratio of applied number of load applications to allowable number of load applications equals 2.31/63.01 if t/T = 0.1 = 2 years (see also table 4.4 underscored values).
c. Assume the pavement life is 10 years
d. For an annual traffic growth rate of 10%, the ratio of applied number of load applications to allowable number of load applications equals 5.1/17.52 if t/T = 0.4 = 4 years.

As can be concluded form figure 4.12, the shape of the deterioration curve as characterized by alpha, is affected if n/N is used instead of t/T. Especially for the higher traffic growth rates and longer pavement life values (about 20 years), a considerable difference between the t/T and n/N performance curves can be observed. Fortunately the traffic growth rates of all pavement sections considered were about the same and the pavements lifes were usually less than 10 years. From this it is concluded that the straight forward comparison of α values as given in table 4.2 is acceptable.

4.7 Acceptance Levels based on Visual Condition Surveys

It will be recognized that $P_V = 0$ conditions coïncides with a considerable amount of distress. For reasons of e.g. safety and maintenance budget minimization, such an amount of distress may not be acceptable. Therefore it is considered necessary to establish minimum acceptance levels for P_V.

From discussions with highway authorities which are familiar with the used inspection method, and from observed maintenance practice, it became obvious that a need was felt to start maintenance activities on a road section, when P_V had been dropped to 0.6. The severe winter of 1978/1979 (information on this winter has been given in chapter 2) has confirmed this action level |12|. Condition surveys conducted on a number of sections just before and after the winter showed that no spontaneous increase in distress could be observed if $P_{V\ ALL}$ was 0.8 or higher, but that a remarkable decrease in $P_{V\ ALL}$ was observed if this factor had reached a value of 0.6 before the winter started. This has led to the conclusion that $P_V = 0.6$ is a reasonable minimum acceptance level for $P_{V\ ALL}$. From the same observations it was concluded that a reasonable minimum acceptance level for $P_{V\ CRK}$ was about 0.7.

The minimum acceptance level for raveling is set at 0.25. This low level can be accepted since raveling is not considered to be a structural type of distress, and since the maintenance activities to restore the quality of the pavement surface at a condition level of $P_{V\ RAV} = 0.4$, will be almost the same as those executed at $P_{V\ RAV} = 0$.

4.8 Guidelines for a Maintenance Planning Technique

It needs no argumentation that it is desireable to plan the maintenance budget in such a way that the yearly needed maintenance budget is kept at a fairly constant level. Therefore it might not be wise to perform maintenance works at the moment that the condition index drops below the minimum acceptance level. It is in fact better to define a maintenance urgency range by setting a warning level as well as an ultimate minimum acceptance level for the condition index. The numerical values of these two levels are given in table 4.5.

Table 4.5 *Warning and Acceptance Levels for Raveling, Cracking and the Overall Condition*

Damage Type	Level		
	Warning	Minimum Acceptance	Ultimate Minimum Acceptance
RAV	0.4	0.25	0.
CRK	0.8	0.7	0.6
ALL	0.7	0.6	0.5

RAV = raveling
CRK = longitudinal + alligator cracking
ALL = overall condition

By using both the minimum acceptance levels and the maintenance urgency range, maintenance activities can be planned in such a way that the yearly needed maintenance budget can be kept at a constant level as well as possible. This will be illustrated by means of an example.

Figure 4.13 shows for a number of road sections the time period which lies between passing the warning level and passing the ultimate urgency level. Also the moment at which the minimum acceptance level is reached is indicated. If maintenance is planned based on the minimum acceptance level a distribution of maintenance works as indicated in row 1 in fig 4.13 is obtained. If the urgency range is taken into account, a leveling of maintenance works over the analysis period can be obtained, as is indicated in row 2 of fig. 4.13.
It should be noted that in this example the leveling is obtained by accelerating the date of maintenance, compared with the method where only the minimum acceptance level is the decisive criterion.
Finally it should be noted that a computer program has been developed by Van Gurp |13, 14| which incorporates the techniques which are described in this chapter. This program has shown to be a powerful tool in the planning of maintenance if used on a full scale base |15|.

4.9 Summary

This chapter has described the visual condition survey technique as used by the laboratory for Road and Railroad Research of the Delft University. Furthermore attention has been paid to the development of a performance model based on these surveys which can be used for the prediction of future deterioration. Furthermore the development of minimum acceptance levels for the visual condition has been described.
It should be noted that use of both the guidelines for the selection of α values and the minimum acceptance levels is restricted to the types of pavement construction considered in this study, and to environmental conditions that are comparable with Dutch conditions.
In the last section of this chapter guidelines are given for a maintenance planning technique. These guidelines are based on the developed methods and techniques.

4.10 Example

The visual condition survey method as well as the interpretation technique and performance models has been used to evaluate the condition of 130 km of the secundary road network system of the province of Zuid-Holland |15|.
According to the provincial highway authorities these road sections had to be maintained within a four year period. Figure 4.14 shows the location of the road sections within the province.
To reduce the amount of surveys, only 50% of each section was inspected. The location of the inspection sections within the road sections considered was selected by means of a random procedure. The inspection sections were 100 m in length. Figures 4.15 and 4.16 give a general view of the condition of the surveyed sections. To assess the remaining life of these sections, the computer program PLAIN was used |13, 14|. As already mentioned in section 4.3, the 100 m survey sections were merged into larger sections. The condition of these latter sections was characterized by the mean and standard deviation of

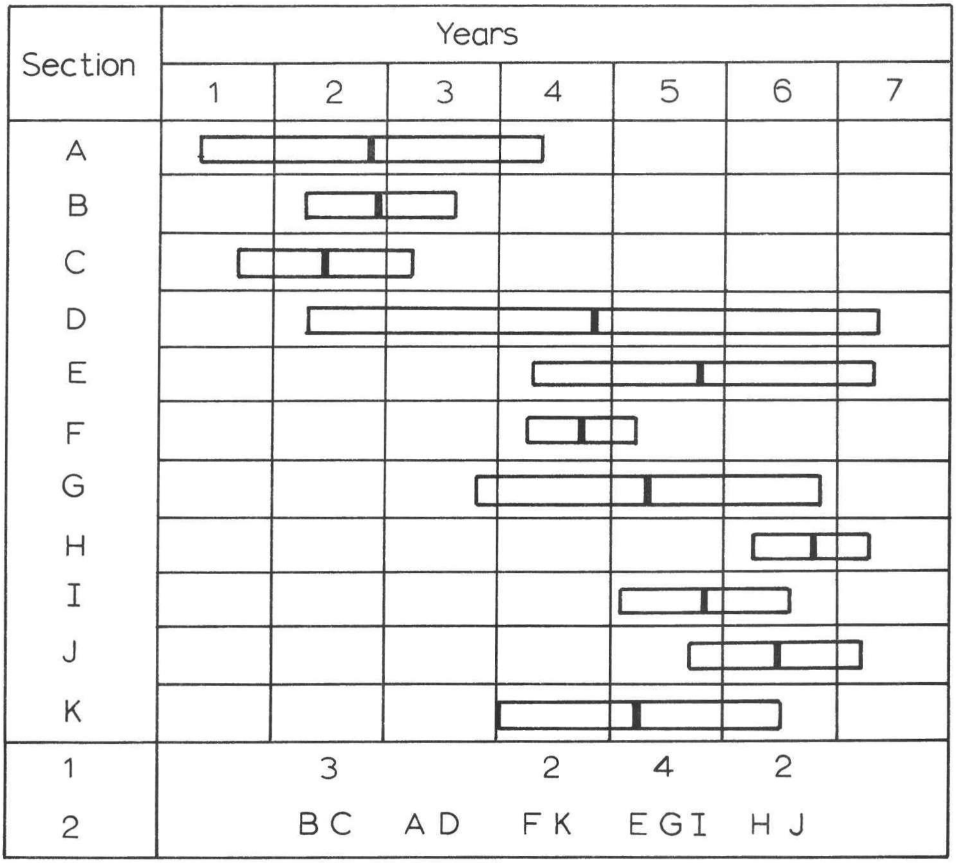

Row 1: Number of sections that need to be maintained due to reaching the minimum acceptance level

Row 2: Leveling of maintenance activities by taking into account the warning level and ultimate minimum acceptance level

Figure 4.13 *Planning of Maintenance Activities*

Figure 4.14 Location of the Road Sections

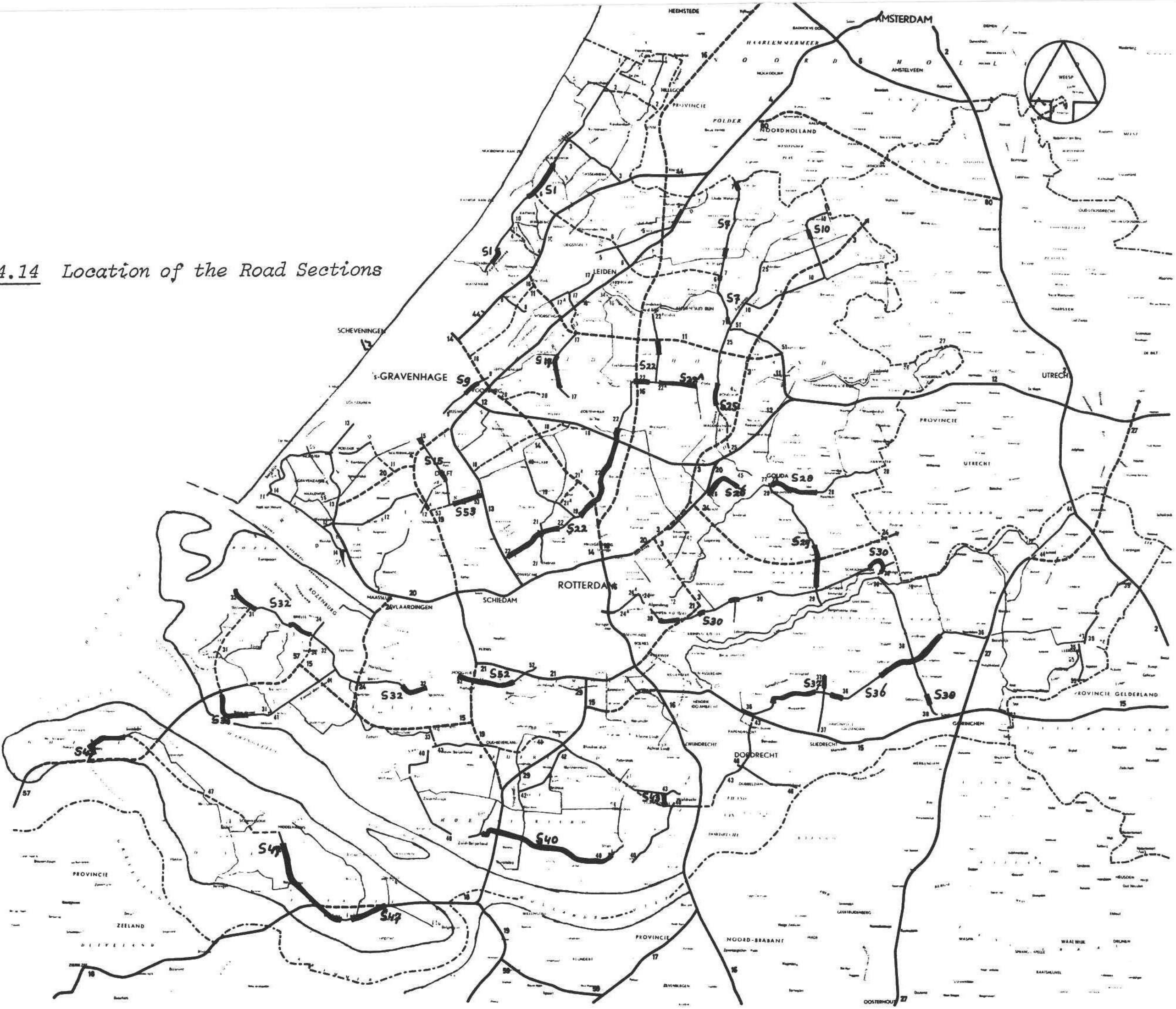

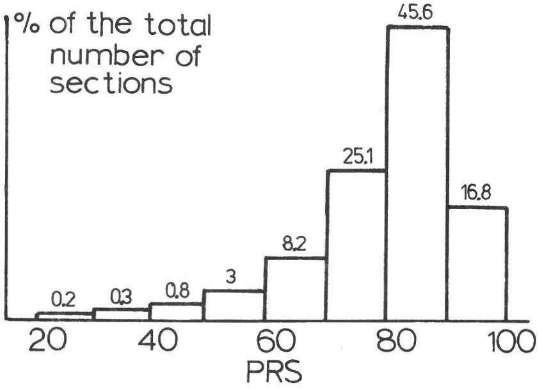

Figure 4.15 Distribution of the PRS Values as determined for all Surveyed Sections

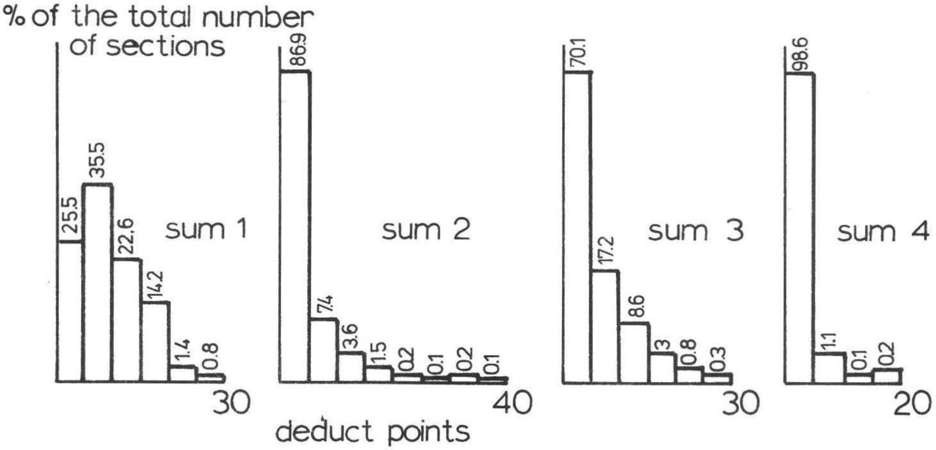

Figure 4.16 Distribution of the Deduct Points within the Four Sub Totals for all Surveyed Sections

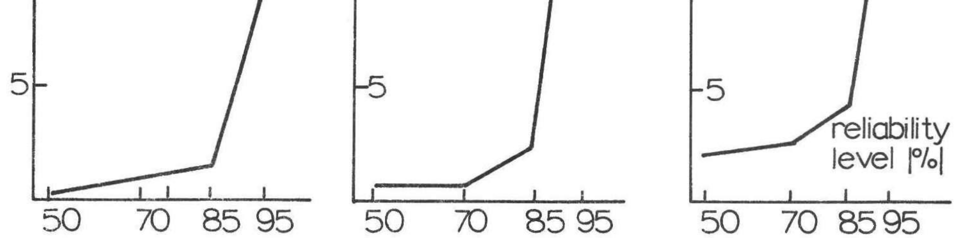

Figure 4.17 Relationship between the Amount of Maintenance needed in the First Year and the Reliability Level of the Input Deduct Point Level

its individual survey section ratings.
Several combinations of this mean and standard deviation of the deduct points were entered in the computer program PLAIN to determine the most desireable reliability level (see table 4.6).
For each reliability level the total pavement area that should be maintained in the first year of the analysis was determined (see fig. 4.17). For the analysis the minimum acceptance levels as given in table 4.7 were used.
It should be noted that raveling was not taken into account in the determination of the maintenance priorities.

Table 4.6 Reliability levels and Associated Deduct Point Levels used in the Analysis

Reliability level |%|	Imput Deduct Point Level
50	$\bar{x}$
70	$\bar{x} + 0.52\sigma$
85	$\bar{x} + 1.04\sigma$
95	$\bar{x} + 1.65\sigma$

Note: $\bar{x}$ = mean value
σ = standard deviation

Table 4.7 Minimum Acceptance Levels used in the Analysis

	Minimum Acceptance Level	Ultimate Minimum Acceptance Level
Cracking	0.7	0.6
Overall Condition	0.6	0.5

From figure 4.17 it was concluded that up to a reliability level of 85% the total pavement area that needed maintenance hardly increased, while at reliability levels higher than 85% a sharp increase of that area occurred. This meant that by a small increase of the maintenance budget, compared with the budget needed for a reliability level of 50%, a reliability level as high as 85% could be obtained. Therefore this level was selected for the remaining part of the analysis.

The next step was,the analysis of the condition phase 2 for cracking together with condition phase 2 for the overall condition. Condition phase 2 is defined as the time period that the visual conditon index needs, to drop from the minimum acceptance level to the ultimate minimum acceptance level.
An abstract of the PLAIN calculation is displayed in figure 4.18. The data in this figure were used in the determination of the maintenance priorities. For this,the same procedure as indicated in figure 4.13 was used.

Then a plot was made of the cumulative pavement area which needed to be maintained over the years. By assuming a "mean maintenance activity" which consisted of a 50 mm thick overlay, the needed maintenance budget over the years could be determined. Also the mean annual maintenance budget could be calculated in this way.
Figure 4.19 shows some results.

Finally it was checked whether there were still pavement sections which needed maintenance due to excessive raveling. It was found that all sections which exhibited excessive raveling needed already maintenance due to an unacceptable overall condition or due to an unacceptable amount of cracking.

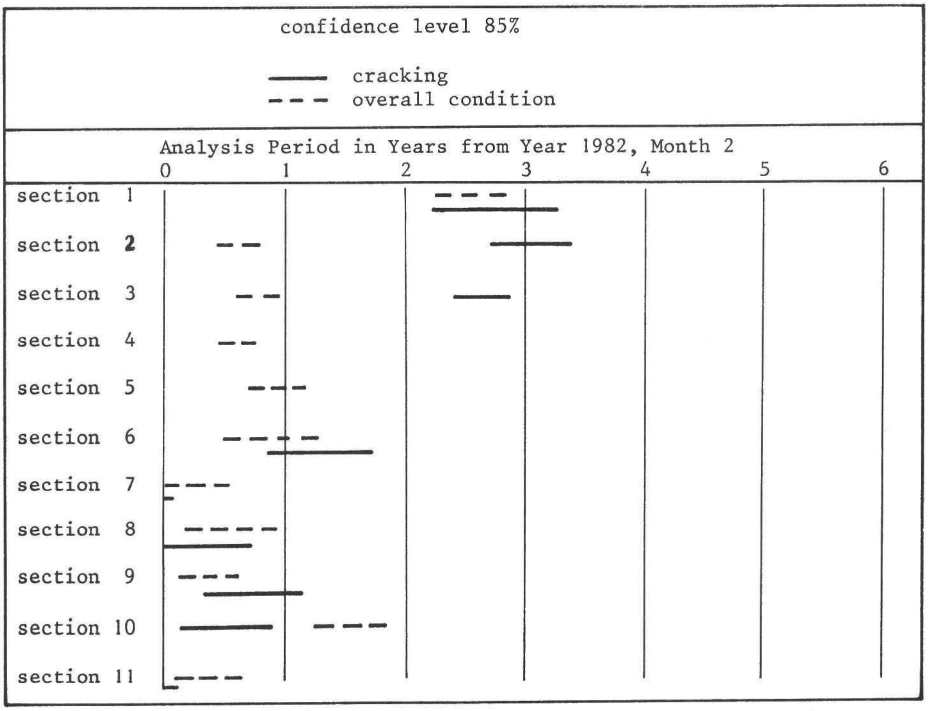

Figure 4.18 *Condition Phase 2 of Cracking and Overall Condition*

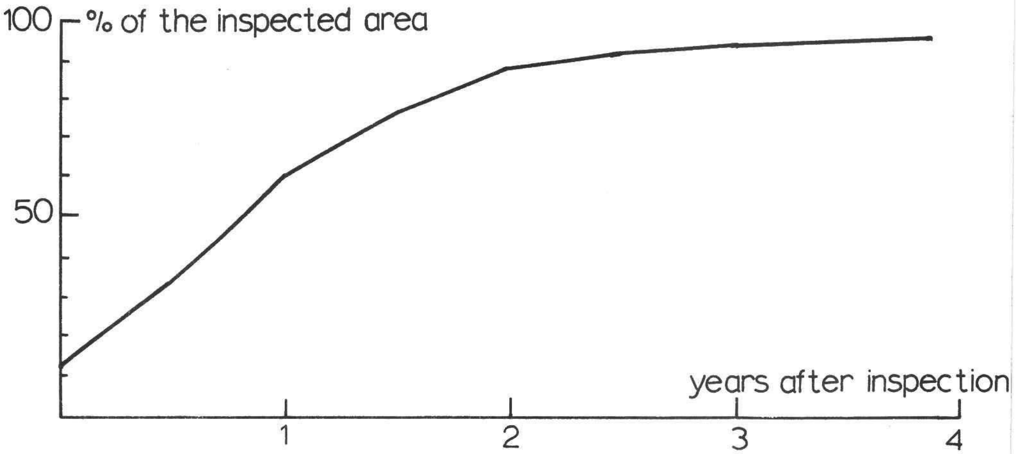

Figure 4.19 *Cumulative Pavement Area to be Maintained in Time*

References

|1| HELLINGS, J.J.; WIENBELT, W.
Comparison of a Number of Visual Condition Survey Systems and Elaboration and Use of the Chosen Texas System (in Dutch)
Report WB-2; Department of Civil Engineering; Chair of Highway Engineering
Delft University of Technology - 1976

|2| CHONG, G.J.; PHANG, W.A.; WRONG, G.A.
Manual for Condition Rating of Flexible Pavement Distress Manifestations
Ministry of Transportation and Communications
Ontario/Downsview - 1975

|3| EPPS, J.A.; MEYER, A.H.; LARRIMORE, I.E.; JONES, H.L.
Roadway Maintenance Evaluation, User's Manual
RR 151-2; Texas Transportation Institute
Texas A&M University - 1974

|4| KERSTEN, M.S.; SKOK, E.L.
Surface Condition Rating System for Bituminous Pavements
Civil and Mineral Engineering Department; University of Minnesota
Minneapolis - 1973

|5| PETERS, C.H.; WINGATE, P.J.F.
The CHART System of assessing Structural Maintenance Needs of Highways
Supplementary Report 153 UC; Transport and Road Research Laboratory
Crowthorne - 1975

|6| SEBASTYAN, G.Y.
Airfield Pavement Evaluation Procedures
"Journal of the Aero Space Transport Division";
Proceedings of the American Society of Civil Engineers; Vol 91,No AT 2 - 1965

|7| MOLENAAR, A.A.A.; HELLINGS, J.J.; HUMER, R.P.; WIENBELT, W.; ZIJLSTRA, M.
Manual and Catalogue of Defects for the Visual Condition Surveys on Roads (in Dutch)
Report WB-3; Department of Civil Engineering; Chair of Highway Engineering
Delft University of Technology - 1977

|8| DUIVENVOORDEN, J.J.
Computer Program WBP1, Road Rating Program 1 (in Dutch)
Report WB-5; Department of Civil Engineering; Chair of Highway Engineering
Delft University of Technology - 1977

|9| VAN GURP, Ch. A.P.M.
Pavement Rating Programs for Visual Condition Surveys and Ride Index Measurements
Report 7-82-115-31; Department of Civil Engineering; Lab. for Road and Railroad Research; Delft University of Technology - 1982

|10| MOLENAAR, A.A.A.
Visual Condition Surveys, a Tool in the Planning of Maintenance of Road Pavements (in Dutch)
"Wegen", Vol. 55, No. 7 - 1981

|11| MOLENAAR, A.A.A.
Visual Condition Surveys, a key Tool in the Planning of Maintenance
Paper prepared for the "Seminar on Maintenance and Drainage Aspects"
Indian Roads Congress; Bangalore - 1982

|12| MOLENAAR, A.A.A.
Measurements on Frost Damage on Provincial Roads in Zuid Holland (in Dutch)
Publication N, "The Winter of 1978 - 1979"
Study Centre for Road Construction; Arnhem - 1980

|13| VAN GURP, Ch. A.P.M.
Pavement Life Assessment by Visual Inspections, Vol. 1: Performance Models and User's Guide
Report 7-82-115-29; Department of Civil Engineering; Lab. for Road and Railroad Research; Delft University of Technology - 1982

|14| VAN GURP, Ch.A.P.M.
Pavement Life Assessment by Visual Inspections, Vol. 2: Description of the Computer Program
Report 7-82-115-30; Department of Civil Engineering; Lab. for Road and Railroad Research; Delft University of Technology - 1982

|15| VALK, H.; VAN VELZEN, F.J.M.; MOLENAAR, A.A.A.; VAN GURP, Ch.A.P.M.
The Delft University Pavement Management System tested in Practice (in Dutch)
Report 7-82-115-33; Department of Civil Engineering; Lab. for Road and Railroad Research; Delft University of Technology - 1982

Chapter 5

DEFLECTION TESTING AND ANALYSIS
ASSESSMENT OF REMAINING STRUCTURAL LIFE
AND FUTURE PERMANENT DEFORMATION

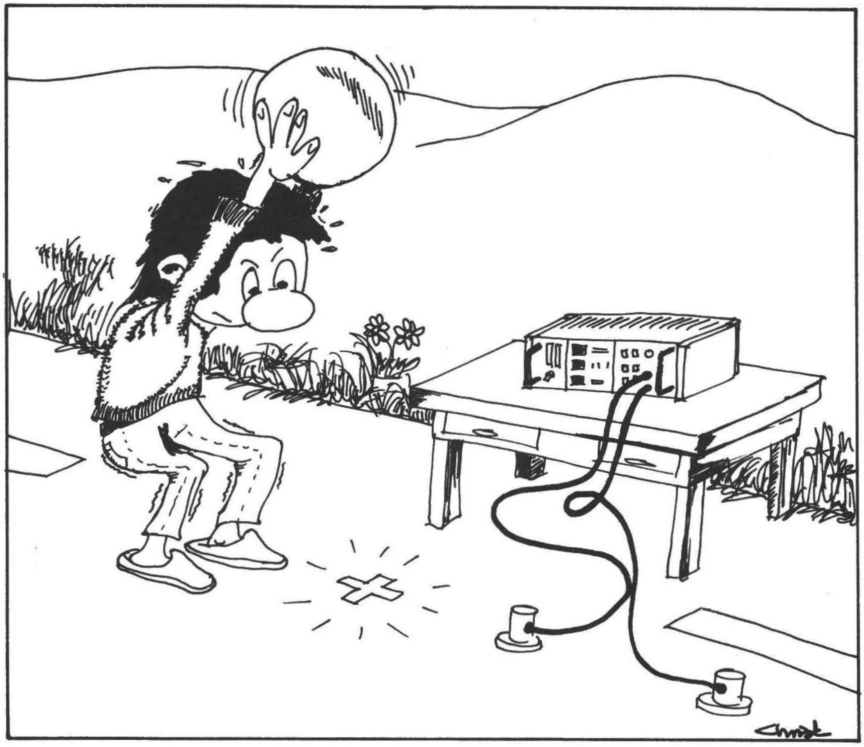

TABLE OF CONTENTS

5.1 Introduction

As has been mentioned in chapter 4, visual condition surveys are a simple and economical way of monitoring the pavement condition in terms of surface distress (raveling, bleeding, potholes), cracking and permanent deformation (rutting). Nevertheless diagnostic surveys on the structural pavement condition , which is related to the cracking conditions, should be undertaken to determine more precisely the extent of the structural deterioration and to determine the length of the time period to pavement failure. Also a diagnostic survey on the rutting conditions should be performed in order to determine which part of the structure is the origin of the rutting and to estimate how the future rutting developments might be.
In order to be able to make such an evaluation, knowledge is needed on the deformation, cracking and fracture characteristics of the materials used in the different pavement layers,as well as on the stress and strain conditions in the pavement due to traffic loads. This knowledge can be obtained by measuring the respons of the pavement structure to a given realistic load and by measuring the respons of the individual materials to loading conditions which are representative for the in situ conditions. In other words: this knowledge can be obtained by means of deflection measurements and testing of cores taken from the pavement structure.
Deflection measurements are, in first place, tests to evaluate the respons of the pavement structure to a realistic load. Secondly the stress, strain and deformation conditions in the pavement can be assessed by means of these tests; this has been indicated in chapter 3. Finally it is possible to assess the deformation characteristics of the individual pavement layers.
The assessment of cracking fracture deformation characteristics of the individual pavement materials is the main objective of core testing. If the deformation characteristics are determined, the stress and strain conditions as well as the respons of the pavement structure due to a given load can be calculated.

Considering the time and costs involved with deflection and core testing, the following statements can be made.
Deflection measurements are not time consuming and can be performed at relatively low costs, while core testing is time consuming and relatively costly. For reasons of time and costs and for the type of information which is obtained, deflection measurements are normally preferred for the routine evaluation of the structural condition of a pavement network.
This chapter deals with the analysis of deflection measurement results and especially with the assessment of the structural pavement condition as well as the assessment of the remaining life of the pavement structure. Furthermore guidelines will be given on where and when deflection measurements should be taken. Also a method will be presented which enables the assessment of the structural condition by means of deflection measurements if this is not possible by means of deflection measurements.

First of all however attention is paid to the statistical treatment of deflection data. This treatment is needed to reduce the large amount of data, which is a result of deflection surveys, to workable properties.

5.2 Statistical Treatment of Deflection Data

Deflection surveys normally result in a large amount of data. It is not possi-

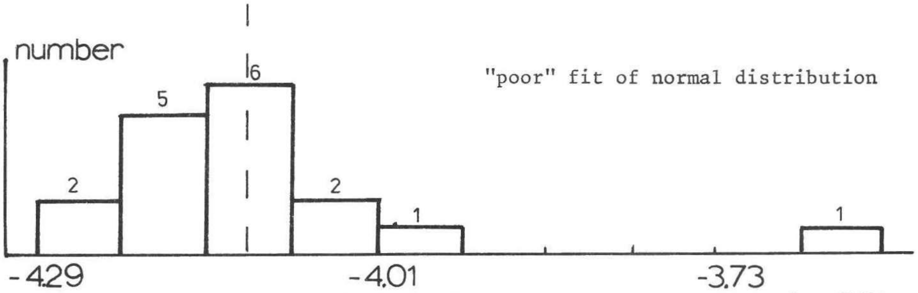

distribution of log SCI on the S km 6.3 - km 6.8

$\overline{\text{log SCI}}$ = -4.11 skewness = 2.32 kurtosis = 5.3

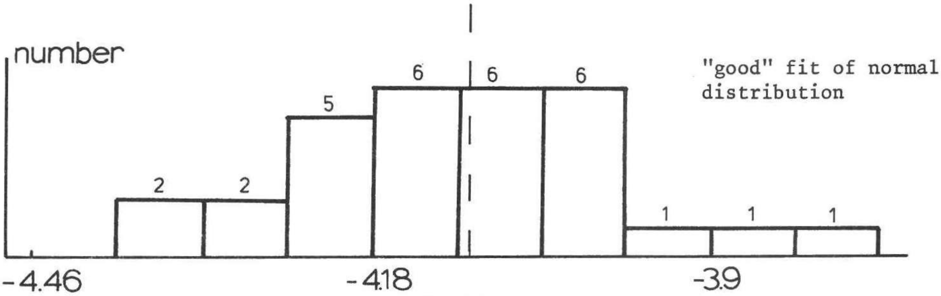

distribution of log SCI on the S km 30.9 - km 31.9

$\overline{\text{log SCI}}$ = -4.1 skewness = 0.25 kurtosis = -0.04

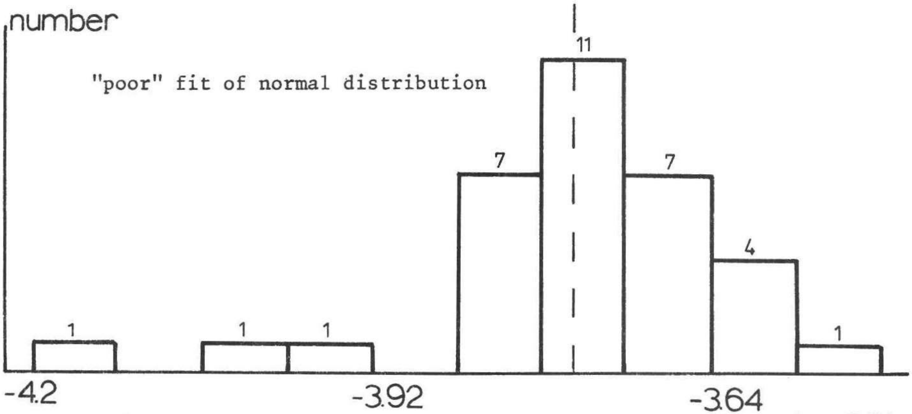

distribution of log SCI on the S km 16.8 - km 18

$\overline{\text{log SCI}}$ = -3.75 skewness = -1.56 kurtosis = 3.65

Figure 5.1 Examples of log SCI distributions

ble and not necessary to make an in depth evaluation of the data of all individual tests. A considerable reduction of data can be obtained by combining individual tests into sample populations. Such a population covers usually a complete road section, although sometimes smaller subsections can be more desirable.
Statistical tests are run for each population to check and measure:

a. the central tendency of the deflection data
b. the dispersion or scatter around the mean
c. the degree of fitting of the data in a normal distribution.

Re a. Measure of central tendency is provided by the mean and the median. In a normal distribution mean equals median.

Re b. Dispersion is measured by the standard deviation and the range. The range is the difference between the largest and smallest deflection value.

Re c. Checking whether the population data fit the normal distribution requirements is done by skewness and kurtosis |1|. Skewness is the degree of asymmetry. Kurtosis is the degree of peakedness.

Skewness and Kurtosis are defined as

$$\text{Skewness} = \frac{\Sigma(x_i-\bar{x})}{(n-1)\sigma^3} \qquad \text{eq. 5.1}$$

$$\text{Kurtosis} = \frac{\Sigma(x_i-\bar{x})^4}{(n-1)\sigma^4} - 3 \qquad \text{eq. 5.2}$$

$\bar{x}$ = mean of all observations
x = individual observation
n = number of observations

Both skewness and kurtosis will be equal to zero in case of a normal distribution. Figure 5.1 gives several examples of distributions exhibiting some degree of skewness and peakedness.

It is very important to have an indication whether the deflection data population can be described by a normal distribution since, as has been described in the previous chapters, the distribution of e.g. the equivalent layer thickness or surface curvature index was taken as being normal or log-normal. It is obvious that this assumption should be verified and validated.

If the population of deflections is e.g. skewed to the right, this dispersion of the normal distribution can be caused by some deflections indicating a weak spot. These data may then be deleted from the population or put into another subpopulation, because this spot needs a special maintenance action, different from the average action suited for the rest of the population or road section. Since very often on a given road sections, the deflections measured on one part of the section are significant higher or lower than those measured on another part, it is desirable to cut the main section into subsections, each with a significant different load carrying capacity. In order to be able to discern these subsections, plots of the cumulative sums of the deviations of the mean of the deflections or calculated equivalent layer thicknesses should be made |2|.
The cumulative sum is calculated in the following way

$$\begin{aligned} S_1 &= x_1 - \bar{x} \\ S_2 &= x_2 - \bar{x} + S_1 \qquad \text{eq. 5.3} \\ S_i &= x_i - \bar{x} + S_{i-1} \end{aligned}$$

where x_i = deflection measured in point i
$\bar{x}$ = mean deflection
S_i = cumulative sum of the deviations of the mean deflection at point i

By means of the cumulative sums it can easily be determined to what extent the deflections measured on a certain part of the road section are different from the mean deflection. The parts discriminated in this way can then be treated seperately in an overlay design procedure.

The statistical treatments described here will be illustrated by means of an example which will be given at the end of this chapter.

5.3 Assessment of the Structural Condition Index and the Shape of the Deterioration Function by means of Deflection Measurements

As has been shown in chapter 3, the structural condition of the pavement can be characterized by means of the structural condition index P which is defined as

$$P = \frac{h_{ecn}}{h_{eco}} \qquad \text{eq. 5.4}$$

where h_{ecn} = corrected equivalent layer thickness after n load applications
h_{eco} = corrected equivalent layer thickness just after construction.

In order to be able to calculate P, one needs to know h_{eco}! This stresses the importance of taking deflection measurements after construction of a pavement section has completed. Unfortunately these measurements will seldom be available. In those conditions it is recommended to take deflection measurements between the wheelpaths to obtain "candidate" h_{eco} values. The h_{eco} values obtained in this way should be qualified as candidate values since the area between the wheelpaths will always be subjected to some load applications.
In general three important aspects should be taken into account in the selection of locations where h_{eco} measurements will be taken. They are

a. the location should not be subjected to traffic loads
b. the location should be representative for the loaded structure
c. the location should not exhibit signs of other structural distress, e.g. thermal cracking, joints etc.

It has been shown in chapter 3 that the amount of future deterioration depends on the expected number of load applications, the structural condition index P and the shape of the deterioration function characterized by $S_{\log N}$. Values for this latter factor should be determined by means of deflection measurements too.
As has been shown in section 3.4.2.1, that $S_{\log N}$ can be calculated by means of

$$S^2_{\log N} = a_1{}^2 b_1{}^2 S^2_{\log h_e} + S^2_{l.o.f.}(\log N - \log \varepsilon) \qquad \text{eq. 5.5}$$

where a_1 = slope of the fatigue relation
b_1 = slope of the log h_e vs log ε relation (= 2)
$S^2_{l.o.f.}$ = lack of fit of the equation used to describe the fatigue relation (= 0.16)

The reader is referred to section 3.4.1.1 for the calculation of h_e from the surface curvature index (SCI) that results from deflection measurements.

The question could now arise whether or not $S^2{}_{\log N}$ cannot be calculated directly from the SCI values. From the derivations given in chapter 3 it can be concluded that, theoretically, this possibility exists. However it has been shown in section 3.4.2.2.2 that considerable corrections on the measured SCI values should be applied due to the variation in temperature and subgrade stiffness. These correction factors have been developed for the h_{ec} values but not for the SCI.
Nevertheless a first crude indication on the magnitude of P and $S_{\log N}$ can be obtained directly from the SCI by taking:

$$P = (SCI_0/SCI_n)^{d_1} \qquad \text{eq. 5.6}$$

and $$S^2{}_{\log N} = a_1{}^2 c_1{}^2 S^2{}_{\log SCI} + S^2{}_{l.o.f.(\log N - \log \varepsilon)} \qquad \text{eq. 5.7}$$

where SCI_0 = SCI at the time of construction
SCI_n = SCI after n load applications
d_1 = absolute value of the slope of the SCI vs h_e relation (a reasonable value is 0.53)
c_1 = slope of the log SCI vs log relation (= 0.943)
all other variables have been defined before.

Although the procedure to calculate P seems very simple, one should be aware of the fact that in a number of cases the ratios h_{ecn}/h_{eco} and SCI_0/SCI_n might be larger than one. Table 5.1 gives some results of deflection measurements taken on 26 different pavement sections.
On 7 sections the h_{ec} ratio was larger than 1, and on also 7 sections the same appeared to be the case with the SCI ratio.
Even in two cases the maximum deflections measured between the wheelpaths were larger than those measured in the wheelpaths.
This unexpected behavior might be caused by one, or a combination of the following reasons
a. post compaction of the granular base due to traffic loads; this will cause a stiffening of the base and a decrease of the SCI measured in the wheelpaths, which results in an increase of the SCI ratio;
b. extension of cracking from the wheelpaths to the area between the wheelpaths; this will cause an increase of the SCI measured between the wheelpaths and so an increase of the SCI ratio.

The justness of these reasons and their impact on the applicability of deflection measurements to assess the structural condition of the pavement will be discussed in the next section.

5.4 Relation between Structural and Visual Condition ; Assessment of the Structural Condition Index by means of Visual Condition Surveys

In the determination of a relation between the structural and visual pavement condition, special emphasis has to be placed on solving the problem which structural condition coincides with a visual condition described by $P_v = 0$. In order to solve this problem a limited number of finite element calculations were made on cracked and uncracked pavements. The loading conditions and the pavement systems studied are shown in figure 5.2.

Table 5.1 Structural Condition Index as determined on several Road Sections

Road Section			$P = \frac{h_{ec}\text{ wheelpath}}{h_{ec}\text{ between wheelpaths}}$	$P = (\frac{\text{SCI between wheelpaths}}{\text{SCI wheelpath}})^{0.53}$
S_7	4.6 - 5.0	L	1.03 (1)	1.09
		R	0.99	1.01
	6.3 - 6.9	L	1.07 (2)	1.14
		R	1.04 (3)	1.05
	11.8 - 12.2	L	0.94	0.84
		R	1.03 (4)	1.10
S_{15}	1.6 - 2	L	0.88	0.81
		R	0.91	0.89
	4.4 - 5.9	L	0.76	0.45
		R	0.74	0.43
S_{22}	0.9 - 2	L	0.88	0.84
		R	0.80	0.73
	3.4 - 5.2	L	0.93	0.85
		R	0.90	0.80
	23.4 - 24.4	L	0.95	0.86
S_{22}A	3.1 - 3.5	R	1.03 (5)	1.03
S_{29}	9.0 - 10.0	L	0.88	0.90
S_{30}	6.2 - 7.2	L	1.15 (6)	1.33
		R	0.86	0.83
S_{36}	16.8 - 18.0	L	0.93	0.83
		R	0.89	0.86
S_{40}	3.9 - 4.8	L	0.91	0.88
		R	0.86	0.82
S_{47}	30.9 - 31.9	L	0.98	0.86
		R	1.02 (7)	0.95

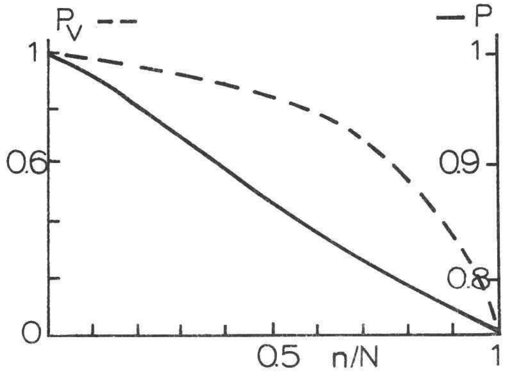

Figure 5.3a Relation between Structural (P) and Visual Condition (P_v) if the Surface Curvature Index (SCI) is larger than 200 μm

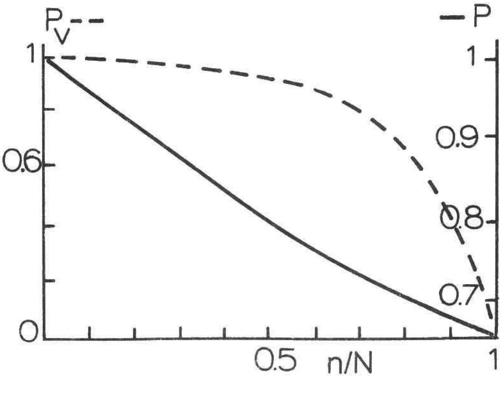

Figure 5.3b Relation between Structural (P) and Visual Condition (P_v) if the Surface Curvature Index is smaller than 140 μm

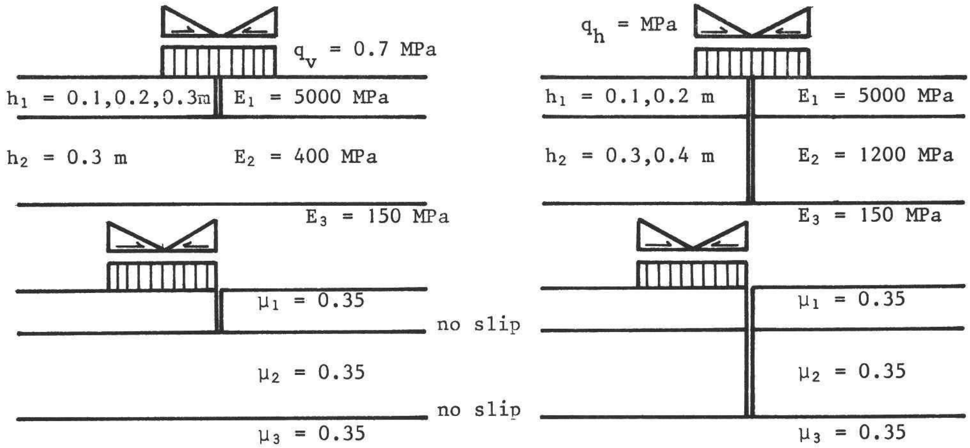

Figure 5.2 Cracked Layered Systems analysed to determine $P_{failure}$

Especially these conditions (cracked bound layers, no load transfer across the crack) were analysed since they were defined as structural failure conditions (appendix 3C).

With regard to the agreement with the visual condition, the following statement can be made.

It has been described in chapter 4 that the visual condition index (P_v) related to cracking equals zero if about 50% of the pavement surface shows severe cracking. In those conditions little or no load transfer will take place across the crack. From this, the author concluded that the conditions described in figure 5.2 represent $P_v = 0$ conditions.

From the calculation results it was concluded that the h_{en}/h_{eo} ratio which characterizes the failure stage of the pavement, is dependent on the type of construction, but also on the position of the load to the location of the crack.

If we assume that in most cases deflection measurements will be taken in such a way that the loading wheel or loading plate covers the crack, then the following practical guidelines can be given for the determination of the h_{en}/h_{eo} ratio which characterizes the failure condition.

$$\left.\begin{array}{l} \text{if SCI} \geq 200\ \mu\text{m}\ P_{failure} = h_{en}/h_{eo} = 0.75 \\ \text{if SCI} \leq 140\ \mu\text{m}\ P_{failure} = h_{en}/h_{eo} = 0.65 \end{array}\right\} \quad \text{eq. 5.8}$$

For intermediate SCI values, $P_{failure}$ can be determined by means of linear interpolation.

Having defined the relation between the visual and structural condition, figure 5.3 was derived. In this figure the visual condition performance model and the structural performance model are related to each other.

Figure 5.3 enables the estimation of the structural condition index (P) from a known value of the visual condition index (P_v). *This procedure is also indicated in figure 5.3.*

It is believed by the author that the above described procedure enables the pavement engineer to make reasonable estimates on the magnitude of P from the observed visual distress, if P cannot be determined by means of deflection measurements.

Table 5.2 Decision Criteria used in the determination of the Sections where Deflection Measurements should be taken

Road	Section |km|	Criterion 1	2	3	4	5	6	
S_7	4.6 - 5.0		x	x		x	x	(1)
S_7	6.3 - 7.3			x				(2)(3)
S_7 L	11.82 - 12.27			x			x	
S_7 R	11.82 - 12.27		x	x		x	x	(4)
S_{15} L/M	1.65 - 2.0		x	x		x	x	
S_{15} R	1.65 - 2.0		x	x				
S_{15} R	4.4 - 6.0			x				
S_{22}	0.0 - 2.6			x		x	x	
S_{22} S	3.2 - 3.5		x	x				
S_{22} L/M	3.5 - 5.25			x		x	x	
S_{22}	22.31 - 24.35					x	x	
S_{22} A	2.95 - 3.45		x	x		x	x	(5)
S_{28}	0.05 - 0.45				x			
S_{29}	8.9 - 10.0		x	x				
S_{30}	3.2 - 5.4			x			x	
S_{30}	5.8 - 7.5					x		(6)
S_{32} L	1.65 - 2.95			x				
S_{32} R	1.65 - 2.95			x				
S_{36}	16.0 - 18.7			x				
S_{40}	2.8 - 5.1		x	x				
S_{47}	20.5 - 24.3	x						
S_{47}	30.1 - 31.85					x	x	(7)
S_{52} R	2. - 2.8		x	x				
S_{52} L	3.5 - 4.8			x				
S_{52} R	4.8 - 6.55			x				

Note: Criterion 1: P_v (CRK) ≤ 0.8 rigid base
Criterion 2: P_v (CRK) ≤ 0.7
Criterion 3: P_v (ALL) ≤ 0.7 and P_v (CRK) ≤ 0.8
Criterion 4: $t < 3$ years and P_v (CRK) ≤ 0.8
Criterion 5: $t \geq 3$ years and $(T-t)_{CRK} \leq 2$ years
Criterion 6: $t \geq 3$ years and $(T-t)_{ALL} \leq 2$ years and P_v (CRK) ≤ 0.8

t = time since last maintenance activity
Due to time limitations deflection measurements could not be performed on each section.

Reliability level is 85%

5.5 Guidelines for the Applicability of Deflection Measurements to determine the Structural Condition Index

As has been shown in section 5.3, conditions may occur where the structural condition index, determined with deflection measurements, takes values larger than one. In order to derive guidelines for the determination of the applicability of deflection measurements to determine the structural condition index, the data given in table 5.1 were analysed together with the results of the visual condition surveys that were carried out too.
Table 5.2 shows the criteria on which it was decided to perform deflection measurements. A first observation of table 5.1 together with table 5.2 shows that especially on sections where P_V (CRK) is low (less than 0.7; criterion 2) and the remaining life based on cracking, as determined by means of the visual condition surveys, is low (less than 2 years; criterion 5), the structural index is larger than one. This is illustrated in figure 5.4.

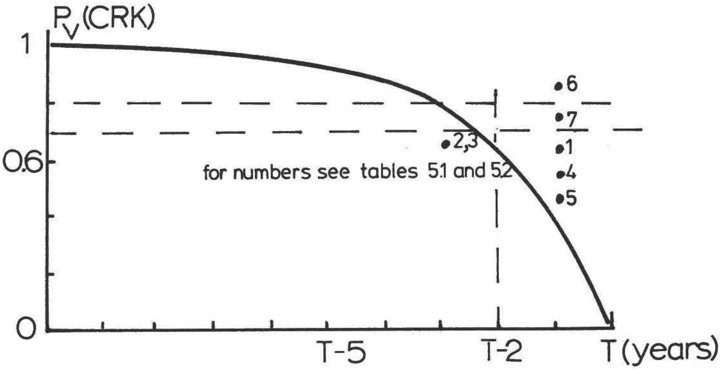

Figure 5.4 *Visual Condition related to inaccurate Structural Condition Index Values determined by means of Deflection Measurements*

In figure 5.4 also the S_{30} and S_{47} sections where the structural condition index was larger than one, are depicted. For these sections the remaining life is short (less than 2 years) while the visual condition is still acceptable (S_{30}: P_V(ALL)= 0.77; S_{47}: P_V(ALL)= 0.81).
It has been shown in section 5.4 that a low visual condition index and/or a short remaining life, as determined by means of visual condition surveys, must result in a low structural condition index. In these conditions it is very likely that wheelpath cracking has extended to the area between the wheelpaths. As has been stipulated in section 5.3, this can result in structural condition index values as determined by means of deflection measurements of larger than one.

From this the author concluded that especially *in those cases where the remaining life, determined by means of visual condition surveys, is less than 2 years and the visual condition is rather bad (P_v(CRK) and/or P_v(All) is less than 0.7), deflection measurements might not give a proper indication of the structural condition index.*
In those circumstances it is recommended to assess this index by means of visual condition surveys. It should be noted that this problem is overcome if the h_{eco} values can be determined from deflection measurements that are taken immediately after construction has been completed!

5.6 Assessment of the Remaining Structural Life

In section 5.3 it has been shown how the structural condition index (P), and the shape of the curve describing the structural deterioration ($S_{\log N}$), can be determined by means of deflection measurements. In section 5.4 it has been shown how the structural condition index can be determined by means of visual condition surveys if this is not possible by means of deflection measurements. Having determined P and $S_{\log N}$, the remaining life can easily be assessed by means of the procedure indicated in figure 5.5

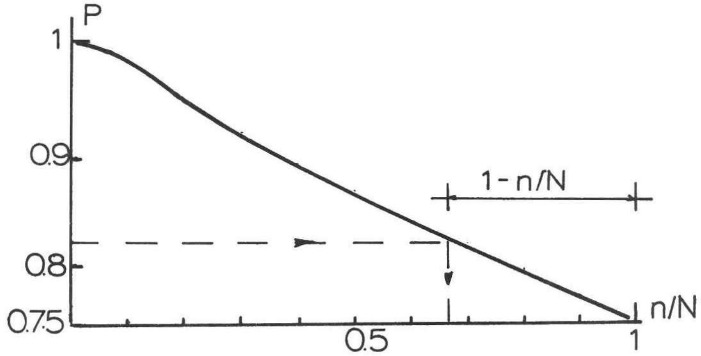

Figure 5.5 Procedure to Assess the Remaining Life

It will be obvious that the remaining life of pavements equals 1-n/N. This ratio can be translated into a number of years in the following way.

t_0	t_1	t_2
time of construction	time of measurements	end of pavement life

Amount of traffic in year t_1 : I
Traffic growth period $t_0 - t_1$: i_1
Traffic growth period $t_1 - t_2$: i_2

Total amount of traffic in period $t_0 - t_1$: C_1

$$C_1 = I.\ \frac{-1 + (1+i_1)^{t_1+1-t_0}}{i_1(1+i_1)^{t_1+1-t_0}} \qquad \text{eq. 5.9}$$

Total amount of traffic in period $t_1 - t_2$: C_2

$$C_2 = I.\ (1+i_2).\ \frac{-1 + (1+i_2)^{t_2-t_1}}{i_2} \qquad \text{eq. 5.10}$$

Ratio 1 - n/N determined by means of measurements: X

The remaining life of the pavement expressed in a number of years can now be calculated from

$$\frac{C_1}{C_1 + C_2} = X \qquad \text{eq. 5.11}$$

It should be noted that this approach to the calculation of the remaining life, can only be used if neither a sharp increase of the mean truck axle load, nor a substantial change in the population of trucks and the percentage of truck traffic has taken place.

5.7 Estimation of Future Permanent Deformation

In the previous sections only attention has been paid to the assessment of the structural condition and remaining life by means of deflection measurements. It will be obvious that the assessment of future rutting development is of importance too. This section deals with the assessment of future permanent deformation by means of deflection measurements. Two approaches will be described

a. An approach which is based on simple relations that exist between the elastic deformation on one hand and the permanent deformation or rutting on the other.

b. An approach that is based on theoretical considerations concerning the permanent deformation behavior of pavement materials.

5.7.1 Estimation of the Elastic and Permanent Deformation of Pavement Layers from Deflection Measurements

In chapter 3 the permanent deformation model, developed at the Belgian Road Research Centre |3|, was described. Here we recall the basic equation which is

$$u_p = b_0 u_e n^{b_1} \qquad \text{eq. 5.12}$$

where u_p = permanent deformation |m|
u_e = elastic deformation |m|
n = number of load repetitions
b_0, b_1 = constants

In this section it will be shown how, for pavements with an unbound base, u_e can be determined directly from the surface curvature index determined by means of deflection measurements.

From extensive BISAR calculations on three layer pavement systems with an unbound base, it became obvious that the elastic deformation of the different pavement layers due to a dual wheel loading, could be estimated rather simply. The calculated surface curvature index was correlated by the author to the vertical elastic deformation at the interface of top layer and base layer and to the vertical elastic deformation at the interface of base layer and subgrade. Table 5.3 shows the results of the regression analysis which was carried out to obtain the desired relations.
As can be seen from table 5.3 no construction details are needed to make a reliable estimate of the elastic deformation at the interface between top and base layer. This is not the case for the estimation of the elastic deformation at the interface between base layer and subgrade, here the thickness of the base layer, needs to be known. It is recognized that this magnitude may be hard to obtain especially if rather old constructions are considered. However it is believed that still a reliable estimate of the elastic subgrade deformation can be made, by using averages for the coefficients given in table 5.4.

The estimation of the permanent deformation of the pavement from deflection measurements can be done in the following way.
From e.g. falling weight deflection measurements, the surface curvature index

Table 5.3 *Coefficients of the Regression Equation Surface Curvature Index (SCI) vs Elastic Deformation (u_e)*

E_3 |MPa|	Interface top layer/base layer b_0	b_1	r^2	n	Thickness base layer |m|	Interface base layer/subgrade b_0	b_1	r^2	n
20	2.064	0.422	0.97	18	0.15	2.139	0.389	1	6
					0.3	2.196	0.343	1	6
					0.6	2.355	0.232	1	6
50	1.66	0.494	0.94	72	0.15	1.853	0.408	0.79	24
					0.3	1.916	0.346	0.90	24
					0.6	1.834	0.319	0.97	24
100	1.47	0.517	0.94	54	0.15	1.69	0.403	0.97	18
					0.3	1.722	0.354	0.94	18
					0.6	1.661	0.309	0.90	18
150	1.329	0.545	0.95	54	0.15	1.571	0.41	0.96	18
					0.3	1.639	0.337	0.91	18
					0.6	1.542	0.304	0.95	18
250	1.289	0.491	0.83	24	0.2	1.485	0.335	0.77	13
					0.4	1.421	0.334	0.76	11
350	1.224	0.483	0.79	23	0.2	1.38	0.344	0.77	13
					0.4	1.39	0.286	0.63	10

Note: $\log u_e = b_0 + b_1 \log SCI$ $|u_e, SCI| = |\mu m|$

of the pavement and the subgrade modulus can be obtained. The falling weight SCI is translated to a dual wheel SCI using

$$\left.\begin{aligned}\log SCI_{dw} &= -0.991 + 1.455 \log SCI_{FWD} \quad \text{if} \quad SCI_{FWD} < 100 \\ \log SCI_{dw} &= 0.0125 + 0.939 \log SCI_{FWD} \quad \text{if} \quad SCI_{FWD} \geq 100\end{aligned}\right\} \quad \text{eq. } 5.13$$

$|SCI| = |\mu m|$

A graphical representation of equation 5.13 is given in figure 5.6
In order to be able to determine the elastic deformation of the top layer, the elastic deformation at the pavement surface needs also to be known. This deformation due to a dual wheel loading can be estimated from the falling weight maximum deflection by means of equation 5.14

$$\log u_{e\ surface} = 0.09 + 0.948 \log \Delta_{0FWD} \qquad \text{eq. } 5.14$$

Δ_{0FWD} = maximum deflection due to the falling weight load $|\mu m|$
$|u_{e\ surface}| = |\mu m|$

Having now relations to determine the elastic deformation at the individual interfaces, the elastic deformation of each layer can be calculated by subtracting the deformation at the lower interface from the deformation at the upper interface. The permanent deformation of each layer can then be calculated by means of equation 5.12. Typical values for b_0 and b_1 are given in table 5.4 |4|.

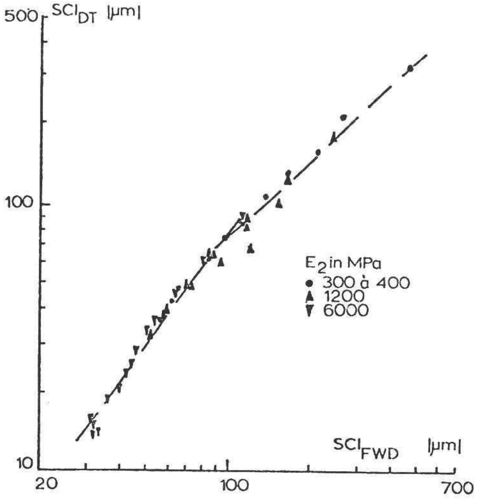

Figure 5.6 *Relation between the Surface Curvature Index due to a Falling Weight Load (P = 50 kN), (SCI_{FWD}) and the Surface Curvature Index due to a Dual Wheel Load (P = 50 kN), (SCI_{DT})*

Table 5.4 *Values for b_0 and b_1 to be used in the calculation of the Permanent Deformation*

Materials	$u_p = u_e * b_0 n^{b_1}$	Modulus |MPa|
Bituminous layers	$u_p = u_e * 4.49\ n^{0.25}$	5 000 (summer)
Stone base	$u_p = u_e * 2\ n^{0.3}$ if $h < 0.12$ m $u_p = u_e * 2\ n^{0.2}$ if $h > 0.12$	500
Lean concrete base		15 000
Granular subbase	$u_p = u_e * 2\ n^{0.3}$	200
Subgrade	$u_p = u_e\ (1 + 0.7 \log n)$	5, 10, 20, 40

In many cases, the amount of rutting calculated in this way will not be equal to the amount of rutting which is really observed. This might be due to the fact that the number of load repetitions applied to the pavement is not exactly known. Also the used permanent deformation models might not be appropriate for the pavement section considered (the selected b_0 and/or b_1 value might not be the right one).

In order to overcome this inequality it is proposed by the author to correct the calculated rutdepths with a factor in order to match it with the observed rut depth. This correction factor should also be used in the prediction of future permanent deformation behavior.

In formula this procedure can be written as

$$u_p = (u_{e1} * b_0 n^{b_1})CF \qquad \text{eq. 5.15}$$

where CF = correction factor
all other variables are as defined before

By means of the above described procedure, one obtains reasonable accurate and reliable rut depth estimates. Nevertheless the presented procedure is thought to be insufficient for an in depth evaluation of the rutting behavior of pavements. Therefore a need was felt for a method which enables a more proper evaluation and prediction of the rut depth development. Such a method is hypothesized in the next section.

5.7.2 Assessment of the Permanent Deformation Behavior of Pavements by means of Repeated Load Deflection Testing

Before it will be shown how the permanent deformation behavior of pavements can be assessed by means of repeated load deflection testing, first of all a generalized permanent deformation model will be described. After that it will be shown how by means of repeated load deflection testing the parameters of this generalized model can be quantified.

In general the permanent deformation of pavement materials is described by means of equation 5.16.

$$\log \varepsilon_p = b_0 + b_1 \log n \qquad \text{eq. 5.16}$$

or

$$\varepsilon_p = b_0 n^{b_1}$$

where ε_p = permanent strain
n = number of load repetitions
b_0 = intercept value
b_1 = slope value

It should be noted that equation 5.16 is a simplification of the real deformation behavior. It has been shown |5, 6| that pavement performance as well as the permanent deformation behavior can be described more generally by means of

$$\varepsilon_p = \varepsilon_0 e^{-(\frac{\phi}{n})^\gamma} \qquad \text{eq. 5.17}$$

where ε_0 = the permanent strain which will be reached ultimately
ϕ,γ = constants

Both equation 5.16 and 5.17 are shown in figure 5.7.

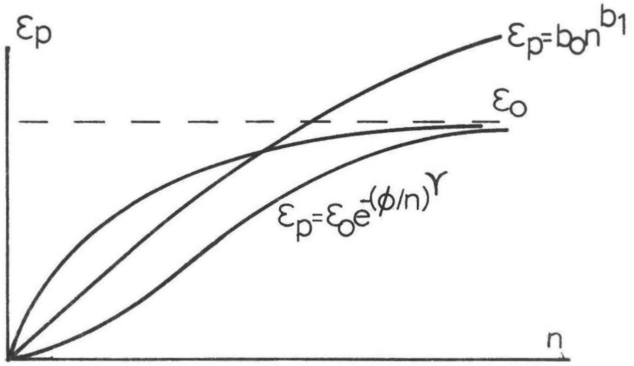

Figure 5.7 Schematical Representation of two Permanent Deformation Models.

Equation 5.17 can be rewritten to

$$u_p = u_0 e^{-(\frac{\phi}{n})^{\gamma}} \qquad \text{eq. 5.18}$$

where u_p = permanent deformation
u_0 = permanent deformation which will be reached ultimately

By taking the derivative of u_p to n we obtain

$$\frac{\partial u_p}{\partial_n} = u_0 e^{-(\frac{\phi}{n})^{\gamma}} \gamma (\frac{\phi}{n})^{\gamma} \cdot \frac{1}{n} \qquad \text{eq. 5.19}$$

which can be written as

$$\frac{\partial u_p}{\partial_n} = \frac{u_p{}^{\gamma}}{n} (\frac{\phi}{n})^{\gamma} \qquad \text{eq. 5.20}$$

Reorganizing equation 5.20 results in

$$(\frac{\frac{\partial u_p}{u_p}}{\frac{\partial n}{n}}) = \frac{\partial(\log u_p)}{\partial(\log n)} = \gamma(\frac{\phi}{n})^{\gamma} = (\gamma\phi^{\gamma})(n)^{-\gamma} \qquad \text{eq. 5.21}$$

Figure 5.8 is a graphical representation of equation 5.21

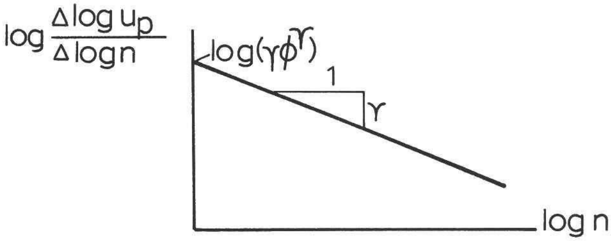

Figure 5.8 Schematical Representation of Equation 5.21

This equation can be used together with repeated load deflection testing for the assessment of the permanent deformation behavior of pavements.

During this study it was not possible to evaluate in this way the permanent deformation behavior of asphalt pavements. Nevertheless it is believed that the presented method is a powerfull technique in the assessment of future permanent deformation.

5.8 Summary

In this chapter it has been described how the structural condition of the pavement, which is related to the cracking conditions, and the remaining structural life can be assessed by means of deflection measurements.
It has been shown how the visual condition index and structural condition index are related to each other and how the remaining structural life can be assessed by means of visual condition surveys if deflection measurements result in unreliable condition index values.
Guidelines have been given that can be used to recognize conditions where de-

flection measurements may yield unreliable equivalent layer thickness ratios. In this regard, the importance of taking deflection measurements immediately after construction has been completed, is stressed.

Also a method has been presented by which future permanent deformation can be estimated by means of deflection measurements.
Finally a technique was postulated which enables the assessment of an in situ permanent deformation model using repeated load deflection tests.

5.9 Examples

In this section two examples will be given which are covering parts of the models described in this chapter. The first example will deal with the assessment of the remaining life of a pavement section from measured deflections. This example will also illustrate the results of the statistical treatments as described in section 5.2.
The second example will show how the described permanent deformation models can be used in the assessment of future rut depth.

5.9.1 Remaining Life Estimation

Figure 5.9 shows the results of deflection measurements taken on the outer wheel path of the right hand side lane of a given provincial road. Figure 5.10 gives the mean values, standard deviation of both the measured deflections as well as the equivalent layer thicknesses, strain values etc. which are calculated from the measured deflections.
Also the values for the median, skewness and kurtosis as calculated for the variables considered, are given in figure 5.10. Finally figure 5.10 gives the value for $S_{\log N}$ which is 1.253
Figure 5.11 shows the values of h_{ec} along the pavement section as calculated from deflection measurements. Figure 5.12 shows the values of the cumulative sums of the deviations of the mean of h_{ec} along the pavement section.
From this figure it can be concluded that from km 4.42 to km 4.93 the h_{ec} values are about equal to the mean value of h_{ec} as calculated for the entire section.
From km 4.93 to km 5.15 the h_{ec} values are lower than the mean value and from km 5.15 to km 5.55 the h_{ec} values are higher than the mean value.
Since the differences are still rather small, it is decided that no further subdivision is necessary.
Figure 5.13 shows the mean values of the most important variables as determined from the measurements taken between the wheelpaths of the right hand side lane.
From the results given in figure 5.10 and 5.13 the structural condition index (P) is calculated from:

$$P = 0.977/1.94 = 0.5 \qquad \text{eq. 5.22}$$

Since the SCI is larger than 200 µm, $P_{failure}$ is set at 0.75 (equation 5.8). So it is concluded that the pavement has failed which means that it has reached the condition in which the bound layers are cracked from bottom to top and no load transfer across the crack takes place.
The remaining structural life is considered to be zero and immediate maintenance action is recommended.

DEFLECTION MEASUREMENTS - PROVINCIAL ROAD - OUTER WHEELPATH - JUNE 9, 1982

TABLE WITH INPUT DATA

POSITION	TEMPERATURE		FORCE	GEO 1 0.0 M	GEO 2 0.30M	GEO 3 0.50M	GEO 4 1.00M	GEO 5 1.50M	GEO 6 2.00M
	AIR	PAV.							
4.420 RB	20.0	25.0	55.3	359.	259.	198.	138.	71.	59.
4.470 RB	20.0	25.0	54.1	315.	186.	161.	107.	73.	53.
4.490 RB	20.0	25.0	52.6	239.	204.	176.	113.	77.	57.
4.510 RB	20.0	25.0	53.2	338.	185.	150.	92.	66.	52.
4.540 RB	20.0	25.0	54.4	258.	210.	176.	107.	72.	53.
4.560 RB	20.0	25.0	53.8	235.	206.	180.	120.	78.	57.
4.610 RB	20.0	25.0	52.2	695.	213.	175.	101.	60.	42.
4.640 RB	20.0	25.0	52.5	339.	224.	189.	125.	68.	52.
4.670 RB	20.0	25.0	52.6	406.	295.	248.	139.	86.	63.
4.730 RB	20.0	25.0	54.8	365.	208.	179.	116.	82.	60.
4.750 RB	20.0	25.0	53.8	625.	268.	218.	129.	85.	64.
4.770 RB	20.0	25.0	54.2	600.	256.	212.	125.	79.	56.
4.830 RB	20.0	25.0	54.2	327.	239.	206.	136.	84.	59.
4.860 RB	20.0	25.0	54.0	253.	208.	173.	106.	72.	59.
4.880 RB	20.0	25.0	53.7	455.	169.	159.	101.	62.	45.
4.930 RB	20.0	25.0	54.9	333.	204.	177.	116.	73.	52.
4.960 RB	20.0	25.0	54.3	635.	217.	208.	115.	71.	57.
4.980 RB	20.0	25.0	54.4	404.	284.	241.	133.	75.	56.
5.020 RB	20.0	25.0	54.5	400.	250.	211.	121.	89.	53.
5.060 RB	20.0	25.0	54.1	267.	229.	197.	120.	72.	57.
5.080 RB	20.0	25.0	54.4	262.	214.	186.	118.	74.	55.
5.130 RB	20.0	25.0	54.2	312.	230.	186.	119.	71.	54.
5.150 RB	20.0	25.0	54.9	262.	167.	148.	102.	66.	45.
5.180 RB	20.0	25.0	55.4	879.	129.	114.	77.	53.	44.
5.220 RB	20.0	25.0	55.4	583.	136.	120.	86.	62.	47.
5.250 RB	20.0	25.0	54.8	395.	243.	179.	111.	68.	43.
5.280 RB	20.0	25.0	55.3	365.	169.	145.	97.	65.	44.
5.310 RB	20.0	25.0	52.9	485.	143.	125.	87.	61.	44.
5.350 RB	20.0	25.0	54.9	725.	153.	130.	90.	63.	46.
5.390 RB	20.0	25.0	55.2	525.	157.	137.	93.	63.	45.
5.430 RB	20.0	25.0	54.7	400.	156.	133.	93.	65.	46.
5.550 RB	20.0	25.0	51.9	296.	164.	150.	107.	67.	50.
5.580 RB	20.0	25.0	52.0	365.	165.	143.	100.	68.	47.
5.620 RB	20.0	25.0	53.4	216.	182.	148.	92.	62.	44.
5.650 RB	20.0	25.0	54.2	215.	188.	155.	98.	65.	44.
5.680 RB	20.0	25.0	54.5	214.	183.	145.	100.	68.	46.
5.730 RB	20.0	25.0	54.6	250.	197.	165.	108.	70.	44.
5.760 RB	20.0	25.0	54.4	385.	167.	140.	89.	57.	43.
5.790 RB	20.0	25.0	54.2	200.	148.	131.	92.	66.	49.
5.820 RB	20.0	25.0	54.2	335.	159.	143.	102.	71.	43.
5.850 RB	20.0	25.0	52.5	254.	156.	136.	91.	63.	48.
5.880 RB	20.0	25.0	54.4	224.	200.	253.	96.	65.	49.

NOTE: Figures 5.9 to 5.13 are typewriter copies of the original computer printout

Figure 5.9a Results of a Deflection Survey

TABLE WITH DATA DERIVED FROM THE DEFLECTION DATA

POSITION	SUBGRADE MODULUS	SURFACE CURVATURE INDEX					EQUIVALENT LAYER THICKNESS			TENSILE ASPHALT STRAIN	COMPRESS. SUBGRADE STRAIN	ELASTIC SURFACE DEFORM.
		FALLING WEIGHT			DUAL WHEEL							
		MEAS.	50 KN	LOG	50 KN	LOG	HES	HEST	HEC			
4.420 RB	133.6	161.	146.	2.1631	111.	2.0436	0.727	0.853	0.930	0.874E-04	0.254E-03	296.
4.470 RB	145.6	154.	142.	2.1533	108.	2.0344	0.711	0.837	0.937	0.839E-04	0.251E-03	267.
4.490 RB	131.5	63.	60.	1.7773	39.	1.5950	1.242	1.368	1.486	0.235E-04	0.116E-03	211.
4.510 RB	146.0	188.	177.	2.2472	133.	2.1226	0.640	0.766	0.858	0.109E-03	0.290E-03	290.
4.540 RB	146.4	82.	75.	1.8772	55.	1.7403	1.005	1.131	1.268	0.346E-04	0.151E-03	220.
4.560 RB	134.6	55.	51.	1.7085	31.	1.4949	1.387	1.513	1.654	0.173E-04	0.969E-04	203.
4.610 RB	177.6	520.	498.	2.6973	351.	2.5453	0.356	0.482	0.573	0.405E-03	0.570E-03	584.
4.640 RB	144.0	150.	143.	2.1549	109.	2.0360	0.713	0.839	0.936	0.844E-04	0.251E-03	294.
4.670 RB	118.9	158.	150.	2.1766	114.	2.0564	0.745	0.871	0.917	0.924E-04	0.260E-03	348.
4.730 RB	130.2	186.	170.	2.2297	128.	2.1062	0.681	0.807	0.873	0.105E-03	0.282E-03	303.
4.750 RB	119.7	407.	378.	2.5778	271.	2.4330	0.476	0.602	0.635	0.272E-03	0.480E-03	513.
4.770 RB	138.0	388.	358.	2.5538	257.	2.4105	0.465	0.591	0.651	0.258E-03	0.461E-03	490.
4.830 RB	130.9	121.	112.	2.0478	86.	1.9353	0.832	0.958	1.039	0.639E-04	0.211E-03	276.
4.860 RB	130.5	80.	74.	1.8697	54.	1.7294	1.063	1.189	1.288	0.350E-04	0.147E-03	217.
4.880 RB	170.5	296.	276.	2.4403	201.	2.3039	0.483	0.609	0.715	0.189E-03	0.394E-03	381.
4.930 RB	150.7	156.	142.	2.1525	108	2.0337	0.702	0.828	0.936	0.832E-04	0.251E-03	277.
4.960 RB	135.8	427.	393.	2.5946	281.	2.4488	0.447	0.573	0.628	0.289E-03	0.489E-03	516.
4.980 RB	138.5	163.	150.	2.1756	114.	2.0553	0.707	0.833	0.919	0.900E-04	0.259E-03	336.
5.020 RB	146.7	189.	173.	2.2390	130.	2.1150	0.644	0.770	0.864	0.107E-03	0.287E-03	332.
5.060 RB	135.3	70.	65.	1.8109	44.	1.6438	1.161	1.287	1.409	0.268E-04	0.127E-03	228.
5.080 RB	141.1	76.	70.	1.8442	49.	1.6923	1.079	1.205	1.336	0.304E-04	0.138E-03	223.
5.130 RB	143.2	126.	116.	2.0653	90.	1.9519	0.789	0.915	1.019	0.657E-04	0.218E-03	264.
5.150 RB	174.3	114.	104.	2.0163	81	1.9058	0.766	0.892	1.054	0.544E-04	0.206E-03	221.
5.180 RB	180.0	765.	690.	2.8391	477.	2.6784	0.302	0.428	0.511	0.618E-03	0.691E-03	690.
5.220 RB	168.4	463.	418.	2.6210	298.	2.4737	0.398	0.524	0.612	0.321E-03	0.511E-03	467.
5.250 RB	182.2	216.	197.	2.2946	147.	2.1672	0.551	0.677	0.810	0.123E-03	0.320E-03	326.
5.280 RB	179.7	220.	199.	2.2987	148.	2.1709	0.552	0.678	0.808	0.125E-03	0.321E-03	300.
5.310 RB	171.8	360.	340.	2.5318	245.	2.3899	0.435	0.561	0.660	0.248E-03	0.450E-03	410.
5.350 RB	170.5	595.	542.	2.7339	380.	2.5796	0.349	0.475	0.557	0.447E-03	0.598E-03	580.
5.390 RB	175.3	388.	351.	2.5459	253.	2.4031	0.424	0.550	0.651	0.258E-03	0.461E-03	425.
5.430 RB	169.9	267.	244.	2.3875	180.	2.2544	0.513	0.639	0.750	0.162E-03	0.364E-03	331.
5.550 RB	148.1	146.	141.	2.1482	107.	2.0296	0.710	0.836	0.941	0.824E-04	0.249E-03	261.
5.580 RB	158.0	222.	213.	2.3293	158.	2.1997	0.566	0.692	0.793	0.137E-03	0.331E-03	318.
5.620 RB	173.4	68.	64.	1.8039	43.	1.6337	1.060	1.186	1.399	0.232E-04	0.128E-03	189.
5.650 RB	176.0	60.	55.	1.7431	35.	1.5452	1.169	1.295	1.534	0.175E-04	0.110E-03	185.
5.680 RB	169.3	69.	63.	1.8014	43.	1.6301	1.076	1.202	1.408	0.232E-04	0.127E-03	184.
5.730 RB	177.4	85.	78.	1.8912	58.	1.7607	0.902	1.028	1.221	0.343E-04	0.161E-03	212.
5.760 RB	180.9	245.	225.	2.3525	167.	2.2215	0.518	0.644	0.769	0.146E-03	0.348E-03	321.
5.790 RB	157.9	69.	64.	1.8038	43.	1.6336	1.105	1.231	1.412	0.242E-04	0.126E-03	173.
5.820 RB	180.2	192.	177.	2.2483	133.	2.1236	0.583	0.709	0.846	0.107E-03	0.297E-03	282.
5.850 RB	156.1	118.	112.	2.0507	87.	1.9381	0.775	0.901	1.029	0.618E-04	0.214E-03	224.
5.880 RB	158.5	71.	65.	1.8146	45.	1.6493	1.083	1.209	1.388	0.254E-04	0.130E-03	192.

HOT MIX ASPHALT TEMPERATURE ADJUSTMENT HAS BEEN APPLIED

Figure 5.9b *Results of a Deflection Survey*

TABLE WITH STATISTICAL PARAMETERS

VARIABLE	NO. OF DATA	MEAN	MEDIAN	STANDARD DEVIATION	SKEWNESS	KURTOSIS	MINIMUM	MAXIMUM
LOADING FORCE	42	0.540 E+02	0.542 E+02	0.954 E+00	-0.751	-0.371	0.519 E+02	0.554 E+02
DEFLECTION GEOPHONE 1	42	0.381 E+03	0.339 E+03	0.159 E+03	1.253	1.002	0.200 E+03	0.879 E+03
DEFLECTION GEOPHONE 2	42	0.198 E+03	0.199 E+03	0.410 E+02	0.451	-0.549	0.129 E+03	0.295 E+03
DEFLECTION GEOPHONE 3	42	0.168 E+03	0.163 E+03	0.323 E+02	0.543	-0.364	0.114 E+03	0.248 E+03
DEFLECTION GEOPHONE 4	42	0.107 E+03	0.107 E+03	0.155 E+02	0.326	-0.768	0.770 E+02	0.139 E+03
DEFLECTION GEOPHONE 5	42	0.697 E+02	0.680 E+02	0.796 E+01	0.519	-0.071	0.530 E+02	0.890 E+02
DEFLECTION GEOPHONE 6	42	0.506 E+02	0.495 E+02	0.627 E+01	0.370	-1.128	0.420 E+02	0.640 E+02
SUBGRADE MODULUS	42	0.155 E+03	0.153 E+03	0.192 E+02	-0.091	-1.375	0.119 E+03	0.182 E+03
SCI FALLING WEIGHT	42	0.213 E+03	0.160 E+03	0.163 E+03	1.466	1.775	0.550 E+02	0.765 E+03
SCI FALLING WEIGHT (F=50KN)	42	0.197 E+03	0.148 E+03	0.149 E+03	1.422	1.552	0.511 E+02	0.690 E+03
LOG(SCI) FALLING WEIGHT (F=50KN)	42	0.219 E+01	0.217 E+01	0.307 E+00	0.240	-0.949	0.171 E+01	0.284 E+01
SCI DUAL WHEEL (F=50KN)	42	0.143 E+03	0.112 E+03	0.105 E+03	1.278	1.146	0.313 E+02	0.477 E+03
LOG(SCI) DUAL WHEEL (F=50KN)	42	0.205 E+01	0.205 E+01	0.315 E+00	0.041	-0.970	0.149 E+01	0.268 E+01
EQUIVALENT LAYER THICKNESS HES	42	0.736 E+00	0.709 E+00	0.279 E+00	0.476	-0.803	0.302 E+00	0.139 E+01
EQUIVALENT LAYER THICKNESS HEST	42	0.862 E+00	0.835 E+00	0.279 E+00	0.476	-0.803	0.428 E+00	0.151 E+01
EQUIVALENT LAYER THICKNESS HEC	42	0.977 E+00	0.924 E+00	0.308 E+00	0.490	-0.902	0.511 E+00	0.165 E+01
TENSILE ASPHALT STRAIN	42	0.133 E-03	0.887 E-04	0.132 E-03	1.780	3.089	0.173 E-04	0.618 E-03
COMPRESSIVE SUBGRADE STRAIN	42	0.289 E-03	0.256 E-03	0.149 E-03	0.790	-0.140	0.969 E-04	0.691 E-03
ELASTIC SURFACE DEFORMATION	42	0.318 E+03	0.292 E+03	0.124 E+03	1.181	0.728	0.173 E+03	0.690 E+03
STRUCT.CONDITION INDEX (HEC)	42	0.547 E+00	0.496 E+00	0.235 E+00	0.442	-0.936	0.153 E+00	0.105 E+01
STRUCT.CONDITION INDEX (SCI)	42	0.457 E+00	0.407 E+00	0.221 E+00	0.443	-1.018	0.991 E-01	0.941 E+00

STANDARD DEVIATION OF THE LOGARITHM OF THE NO. OF 100KN SINGLE AXLE LOADS	1.253

Figure 5.10 Results of the Statistical Treatments applied on the Data given in figure 5.11

```
          EQUIVALENT LAYER THICKNESS  HEC

POSITION             0.5110 E+00     0.7396 E+00     0.9683 E+00     0.1197 E+01     0.1426 E+01     0.1654 E+01
                          |---+---|---+---|---+---|---+---|---+---|---+---|---+---|---+---|---+---|---+---|
  4.420 RB    0.9299 E+00 xxxxxxxxxxxxxxxxxxxxxxxxxxxxxx
  4.470 RB    0.9369 E+00 xxxxxxxxxxxxxxxxxxxxxxxxxxxxxx
  4.490 RB    0.1486 E+01 xxxxxxxxxxxxxxxxxxxxxxxxxxxxxxxxxxxxxxxxxxxxxxxxxxxxxxxxxxxxxxxxxxxxx
  4.510 RB    0.8580 E+00 xxxxxxxxxxxxxxxxxxxxxxxxx
  4.540 RB    0.1268 E+01 xxxxxxxxxxxxxxxxxxxxxxxxxxxxxxxxxxxxxxxxxxxxxxxxxxxxx
  4.560 RB    0.1654 E+01 xxxxxxxxxxxxxxxxxxxxxxxxxxxxxxxxxxxxxxxxxxxxxxxxxxxxxxxxxxxxxxxxxxxxxxxxxxxxxxxxx
  4.610 RB    0.5730 E+00 xxxxx
  4.640 RB    0.9358 E+00 xxxxxxxxxxxxxxxxxxxxxxxxxxxxxx
  4.670 RB    0.9170 E+00 xxxxxxxxxxxxxxxxxxxxxxxxxxxxx
  4.730 RB    0.8734 E+00 xxxxxxxxxxxxxxxxxxxxxxxxxx
  4.750 RB    0.6351 E+00 xxxxxxxxx
  4.770 RB    0.6510 E+00 xxxxxxxxxx
  4.830 RB    0.1039 E+01 xxxxxxxxxxxxxxxxxxxxxxxxxxxxxxxxxxxxx
  4.860 RB    0.1288 E+01 xxxxxxxxxxxxxxxxxxxxxxxxxxxxxxxxxxxxxxxxxxxxxxxxxxxxxxx
  4.880 RB    0.7151 E+00 xxxxxxxxxxxxxxx
  4.930 RB    0.9364 E+00 xxxxxxxxxxxxxxxxxxxxxxxxxxxxxx
  4.960 RB    0.6282 E+00 xxxxxxxxx
  4.980 RB    0.9186 E+00 xxxxxxxxxxxxxxxxxxxxxxxxxxxxx
  5.020 RB    0.8644 E+00 xxxxxxxxxxxxxxxxxxxxxxxxx
  5.060 RB    0.1409 E+01 xxxxxxxxxxxxxxxxxxxxxxxxxxxxxxxxxxxxxxxxxxxxxxxxxxxxxxxxxxxxxxx
  5.080 RB    0.1336 E+01 xxxxxxxxxxxxxxxxxxxxxxxxxxxxxxxxxxxxxxxxxxxxxxxxxxxxxxxxxx
  5.130 RB    0.1019 E+01 xxxxxxxxxxxxxxxxxxxxxxxxxxxxxxxxxxxx
  5.150 RB    0.1054 E+01 xxxxxxxxxxxxxxxxxxxxxxxxxxxxxxxxxxxxxxx
  5.180 RB    0.5110 E+00 x
  5.220 RB    0.6122 E+00 xxxxxxxx
  5.250 RB    0.8099 E+00 xxxxxxxxxxxxxxxxxxxxx
  5.280 RB    0.8081 E+00 xxxxxxxxxxxxxxxxxxxxx
  5.310 RB    0.6599 E+00 xxxxxxxxxxx
  5.350 RB    0.5571 E+00 xxxx
  5.390 RB    0.6512 E+00 xxxxxxxxxx
  5.430 RB    0.7495 E+00 xxxxxxxxxxxxxxxxx
  5.550 RB    0.9409 E+00 xxxxxxxxxxxxxxxxxxxxxxxxxxxxxxx
  5.580 RB    0.7932 E+00 xxxxxxxxxxxxxxxxxxxx
  5.620 RB    0.1399 E+01 xxxxxxxxxxxxxxxxxxxxxxxxxxxxxxxxxxxxxxxxxxxxxxxxxxxxxxxxxxxxxxx
  5.650 RB    0.1534 E+01 xxxxxxxxxxxxxxxxxxxxxxxxxxxxxxxxxxxxxxxxxxxxxxxxxxxxxxxxxxxxxxxxxxxxxxxx
  5.680 RB    0.1408 E+01 xxxxxxxxxxxxxxxxxxxxxxxxxxxxxxxxxxxxxxxxxxxxxxxxxxxxxxxxxxxxxxx
  5.730 RB    0.1221 E+01 xxxxxxxxxxxxxxxxxxxxxxxxxxxxxxxxxxxxxxxxxxxxxxxxxx
  5.760 RB    0.7694 E+00 xxxxxxxxxxxxxxxxxxx
  5.790 RB    0.1412 E+01 xxxxxxxxxxxxxxxxxxxxxxxxxxxxxxxxxxxxxxxxxxxxxxxxxxxxxxxxxxxxxxxx
  5.820 RB    0.8458 E+00 xxxxxxxxxxxxxxxxxxxxxxxx
  5.850 RB    0.1029 E+01 xxxxxxxxxxxxxxxxxxxxxxxxxxxxxxxxxxxxx
  5.880 RB    0.1388 E+01 xxxxxxxxxxxxxxxxxxxxxxxxxxxxxxxxxxxxxxxxxxxxxxxxxxxxxxxxxxxxxx
                          |---+---|---+---|---+---|---+---|---+---|---+---|---+---|---+---|---+---|---+---|
                     0.5110 E+00     0.7396 E+00     0.9683 E+00     0.1197 E+01     0.1426 E+01     0.1654 E+01
```

Figure 5.11 Variation of h_{ec} along the Road Section

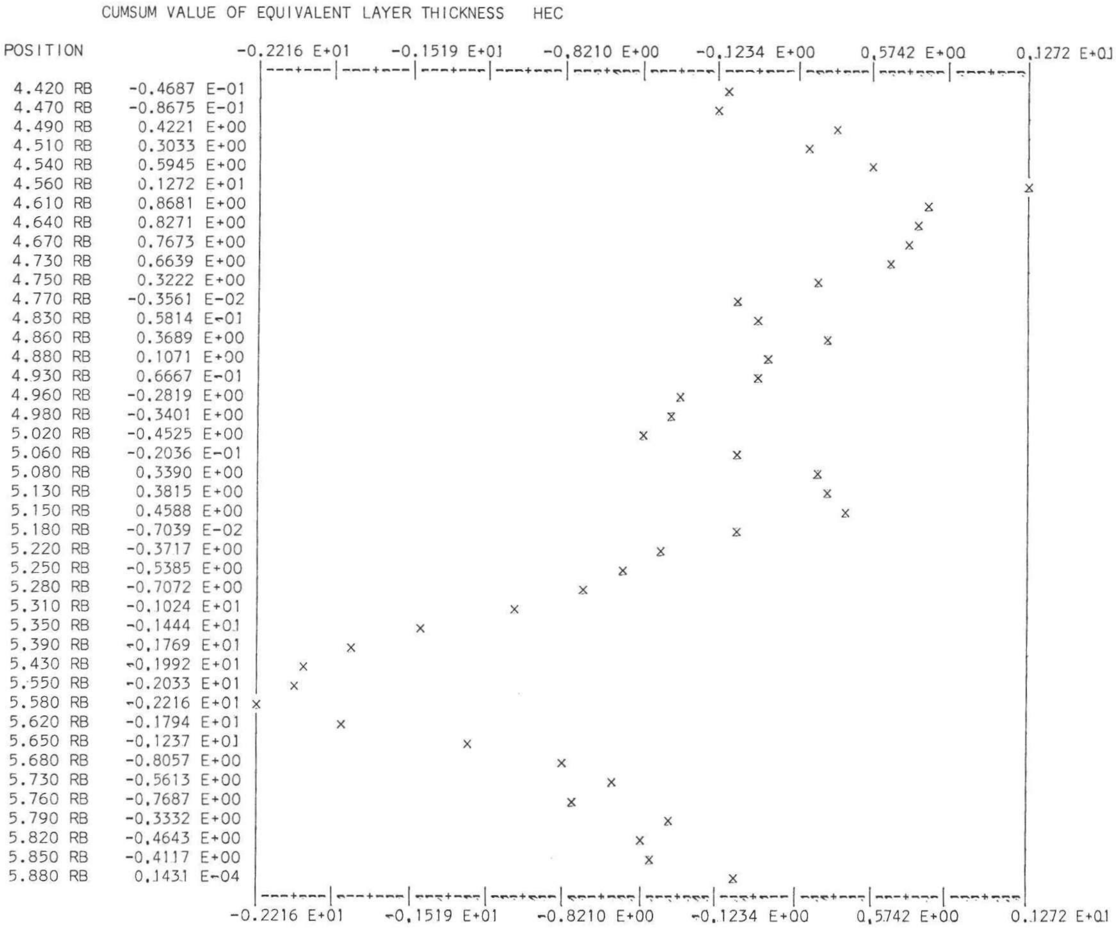

```
                         CUMSUM VALUE OF EQUIVALENT LAYER THICKNESS   HEC

POSITION                 -0.2216 E+01   -0.1519 E+01   -0.8210 E+00   -0.1234 E+00   0.5742 E+00   0.1272 E+01

 4.420 RB   -0.4687 E-01
 4.470 RB   -0.8675 E-01
 4.490 RB    0.4221 E+00
 4.510 RB    0.3033 E+00
 4.540 RB    0.5945 E+00
 4.560 RB    0.1272 E+01
 4.610 RB    0.8681 E+00
 4.640 RB    0.8271 E+00
 4.670 RB    0.7673 E+00
 4.730 RB    0.6639 E+00
 4.750 RB    0.3222 E+00
 4.770 RB   -0.3561 E-02
 4.830 RB    0.5814 E-01
 4.860 RB    0.3689 E+00
 4.880 RB    0.1071 E+00
 4.930 RB    0.6667 E-01
 4.960 RB   -0.2819 E+00
 4.980 RB   -0.3401 E+00
 5.020 RB   -0.4525 E+00
 5.060 RB   -0.2036 E-01
 5.080 RB    0.3390 E+00
 5.130 RB    0.3815 E+00
 5.150 RB    0.4588 E+00
 5.180 RB   -0.7039 E-02
 5.220 RB   -0.3717 E+00
 5.250 RB   -0.5385 E+00
 5.280 RB   -0.7072 E+00
 5.310 RB   -0.1024 E+01
 5.350 RB   -0.1444 E+01
 5.390 RB   -0.1769 E+01
 5.430 RB   -0.1992 E+01
 5.550 RB   -0.2033 E+01
 5.580 RB   -0.2216 E+01
 5.620 RB   -0.1794 E+01
 5.650 RB   -0.1237 E+01
 5.680 RB   -0.8057 E+00
 5.730 RB   -0.5613 E+00
 5.760 RB   -0.7687 E+00
 5.790 RB   -0.3332 E+00
 5.820 RB   -0.4643 E+00
 5.850 RB   -0.4117 E+00
 5.880 RB    0.1431 E-04

                         -0.2216 E+01   -0.1519 E+01   -0.8210 E+00   -0.1234 E+00   0.5742 E+00   0.1272 E+01
```

Figure 5.12 Variation of the Cumulative Sums of h_{ec} along the Road Section

VARIABLE	NO. OF DATA	MEAN	MEDIAN	STANDARD DEVIATION	SKEWNESS	KURTOSIS	MINIMUM	MAXIMUM
LOADING FORCE	42	0.475 E+02	0.475 E+02	0.805 E+00	0.095	0.911	0.456 E+02	0.498 E+02
DEFLECTION GEOPHONE 1	42	0.158 E+03	0.154 E+03	0.358 E+02	0.556	0.689	0.840 E+02	0.259 E+03
DEFLECTION GEOPHONE 2	42	0.139 E+03	0.131 E+03	0.322 E+02	0.337	-0.241	0.740 E+02	0.215 E+03
DEFLECTION GEOPHONE 3	42	0.120 E+03	0.117 E+03	0.254 E+02	0.235	-0.500	0.680 E+02	0.173 E+03
DEFLECTION GEOPHONE 4	42	0.865 E+02	0.860 E+02	0.149 E+02	-0.256	-0.786	0.520 E+02	0.114 E+03
DEFLECTION GEOPHONE 5	42	0.603 E+02	0.625 E+02	0.903 E+01	-0.119	-0.730	0.420 E+02	0.810 E+02
DEFLECTION GEOPHONE 6	42	0.450 E+02	0.450 E+02	0.738 E+01	0.016	-1.095	0.320 E+02	0.590 E+02
SUBGRADE MODULUS	42	0.155 E+03	0.152 E+03	0.268 E+02	0.347	-0.974	0.114 E+03	0.213 E+03
SCI FALLING WEIGHT	42	0.382 E+02	0.340 E+02	0.154 E+02	1.631	3.059	0.160 E+02	0.890 E+02
SCI FALLING WEIGHT (F =50KN)	42	0.402 E+02	0.365 E+02	0.162 E+02	1.575	2.838	0.166 E+02	0.921 E+02
LOG(SCI) FALLING WEIGHT (F=50KN)	42	0.157 E+01	0.156 E+01	0.159 E+00	0.251	0.587	0.122 E+01	0.196 E+01
SCI DUAL WHEEL (F=50KN)	42	0.231 E+02	0.192 E+02	0.145 E+02	2.086	4.522	0.607 E+01	0.736 E+02
LOG(SCI) DUAL WHEEL (F=50KN)	42	0.130 E+01	0.128 E+01	0.231 E+00	0.251	0.587	0.783 E+00	0.187 E+01
EQUIVALENT LAYER THICKNESS HES	42	0.171 E+01	0.162 E+01	0.438 E+00	0.632	0.369	0.883 E+00	0.284 E+01
EQUIVALENT LAYER THICKNESS HEST	42	0.170 E+01	0.162 E+01	0.437 E+00	0.601	0.329	0.869 E+00	0.282 E+01
EQUIVALENT LAYER THICKNESS HEC	42	0.194 E+01	0.189 E+01	0.518 E+00	0.700	0.940	0.959 E+00	0.338 E+01
TENSILE ASPHALT STRAIN	42	0.118 E-04	0.770 E-05	0.110 E-04	2.430	5.677	0.146 E-05	0.514 E-04
COMPRESSIVE SUBGRADE STRAIN	42	0.874 E-04	0.775 E-04	0.453 E-04	1.894	3.919	0.294 E-04	0.241 E-03
ELASTIC SURFACE DEFORMATION	42	0.157 E+03	0.150 E+03	0.339 E+02	0.393	0.310	0.850 E+02	0.243 E+03

STANDARD DEVIATION OF THE LOGARITHM OF THE NO. OF 100KN SINGLE AXLE LOADS	0.960

TABLE WITH STATISTICAL PARAMETERS

Figure 5.13 Main Results of the Deflection Measurements taken on the Area between the Wheel Paths

5.9.2 Assessment of Future Permanent Deformation

A pavement section is considered on which regularly rut depth measurements have been taken. The results of these measurements are shown in table 5.5. The pavement is 10 years in service and one likes to know the rut depth that might occur after 15 years. Unfortunately no axle load data are available but from traffic counts it is known that the traffic growth is 4% per year. The normalized cumulative number of load repetitions calculated from the traffic growth rate is also given in table 5.5.

Table 5.5 Ruth Depth Data to be used in the Example Problem

Year of Service	Ruth depth |mm|	Normalized Cumulative Number of Load Repetitions
1	4	1.04
4	9	4.37
8	13	9.55
10	15	12.45
15	?	20.79

From the data given in table 5.5, the following rut depth model was derived

$$\log RD = 0.599 + 0.531 \log n \qquad \text{eq. 5.23}$$

where RD = rut depth |mm|
n = normalized cumulative number of load repetitions

From equation 5.23 , it can easily be shown that the rut depth after 15 years of service will be

$$RD_{15} = RD_{10}/(\frac{n_{10}}{n_{15}})^{0.531} = 20 \text{ mm} \qquad \text{eq. 5.24}$$

where the indices 10 and 15 denote the magnitude of the variable after 10 resp. 15 years of service.

Next, a three layered pavement with a 0.3 m thick unbound base is considered. Here the observed rut depth is 18 mm, unfortunately no records on rut depth development are available. One million equivalent 100 kN single axles have been applied to the pavement. The question is "what will be the rut depth after 3.10^6 load repetitions".
In order to solve this question, deflection measurements are taken by means of a falling weight deflectometer. The most important results of these measurements are given in table 5.6. This table also shows the elastic deformations at the interfaces between the different layers as calculated by means of equations 5.12, 5.13 and 5.3.

Table 5.6 Deflection and calculated Vertical Elastic Displacement at the Layer Interfaces to be used in the Example Problem

Falling Weight Data			Vertical Elastic Displ. at Interface |µm|	
maximum deflection	|µm|	381	surface	344
surf. curvature index	|µm|	197	top layer/base	324
E_3 |MPa|		150	base/subgrade	234

By means of the interface displacements given in table 5.6 and table 5.4 one arrives to the following rut depths.

asphalt layer: $u_p = 20.10^{-6} * 4.49 * (10^6)^{0.25} = 2.84 \; . \; 10^{-3}$ m

base : $u_p = 90.10^{-6} * 2 * (10^6)^{0.2} = 2.85 \; . \; 10^{-3}$ m

subgrade : $u_p = 234.10^{-6} * 2 * (10^6)^{0.3} = \underline{29.53 \; . \; 10^{-3}}$ m

rut depth $\simeq$ 35 mm

The observed rut depth is 18 mm so the correction factor that should be applied on the calculated values is 0.51.

In the same way, the rut depth after 3.10^6 load applications is calculated and corrected with the above mentioned factor using equation 5.15. This results in a rut depth of 25 mm.

References

|1| SPIEGEL, M.R.
Theory and Problems of Statistics
Schaum's Outline Series
McGraw Hill Book Company; New York - 1972

|2| STUDY CENTRE FOR ROAD CONSTRUCTION
Quality Control in Road Construction (in Dutch)
SCW Report 22
Arnhem - 1970

|3| VEVERKA, V.
"Evaluation of Rutdepth in Flexible Pavements (in French and Dutch)
La Technique Routiere", Vol.24, no.3 - 1979

|4| VERSTRAETEN, J.; VEVERKA, V.; FRANCKEN, L.
Rational and Practical Designs of Asphalt Pavements to avoid Cracking and Rutting
"Proceedings 5th Int. Conf. Structural Design of Asphalt Pavements"
Delft - 1982

|5| LYTTON, R.L.; MICHALAK, C.H.; SCULLION, T.
The Texas Flexible Pavement Design System
"Proceedings 5th Int. Conf. Structural Design of Asphalt Pavements"
Delft - 1982

|6| LYTTON, R.L.
Personal Communication
Texas A & M University - 1982

Chapter 6

FRACTURE AND CRACK GROWTH CHARACTERISTICS OF ASPHALT CONCRETE MIXES

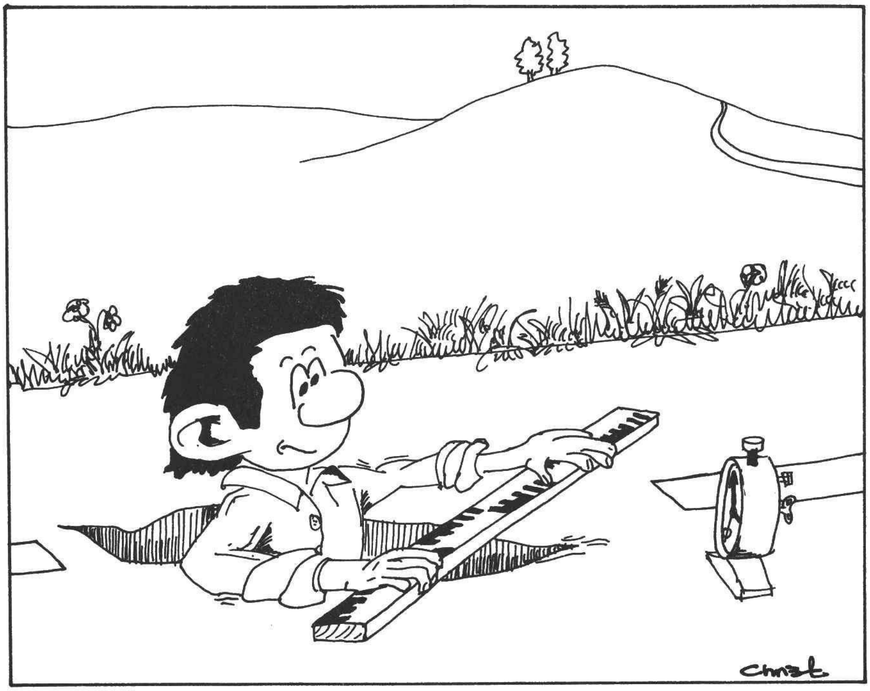

TABLE OF CONTENTS

6.1 Introduction

It needs hardly any argumentation that cracking is a major type of distress. In the previous chapters it has been shown how cracking influences the structural performance of pavements. It has been shown that cracking is influenced by the stress and strain level within the pavement as well as the ultimate and fatigue strength characteristics of the materials used.
In chapters 3 and 5 considerable attention has been paid to the analysis of stresses and strains that are introduced in the pavement structure by traffic loads. In this chapter attention will be paid to the fracture and crack growth characteristics of asphalt concrete mixes. The characterization of the fracture and crack growth properties will be done by using fracture mechanics principles.
In the subsequent sections, first of all the author will go into the question why fracture mechanics principles should be used.
Then a short literature review will be given in which special attention is paid to the crack growth theories developed by Schapery. This will be followed by the description of the experimental program that was carried out to determine the fracture and crack growth properties. Next the results of these tests will be discussed, and finally it will be shown how the crack growth characteristics can be estimated by means of simple static tests.

6.2 Application of Fracture Mechanics to the (Overlay) Design of Asphalt Pavements

As has been indicated in the previous parts of this study, that normally the phenomenological approach is used to the (overlay) design of asphalt pavements. This means that the calculated bending strain level is related to the pavement life.
Although this approach is simple in use, it is not really applicable. It has been shown that crack propagation from the stabilized base to the asphaltic top layer or from the cracked pavement to the asphalt overlay, cannot be analysed by using this classical phenomenological approach. This is considered to be a serious drawback of this method since crack reflection can reduce the overlay and pavement life to an unexpected and considerable extent. This in turn might have undesired influence on the maintenance budget.
Although the problem of reflection cracking and the inability of the phenomenological approach to analyse this problem is known over a long period of time, only a limited number of researchers have studied the possibilities of the application of fracture mechanics in solving these problems. To the knowledge of the author only three research institutes have paid a considerable amount of attention to the incorporation of fracture mechanics into the solving of reflection crack problems. They are the Ohio State University |1-9|, the University of California at Berkeley|10-12| and the Texas A & M University |13-17|. Also research performed at the LCPC organization in France has been reported |18|.
Although the fracture mechanics approach has the potential to be an excellent tool in solving the reflection crack problem, it has not gained very much popularity. In fact it can be stated that it is still a research tool and that its practical application is limited to only a few cases.
The reasons for this somewhat adverse attitude towards this approach might be that:

a. The fracture mechanics approach is not attractive to be used on a routine base, due to the high costs for running finite element programs and due to the more complex material testing if compared with the testing needed in the phenomenological approach.

b. Little agreement seems to exist between the crack properties of asphalt mixes obtained by means of crack growth tests as reported by different researchers. Also disagreement seems to exist on aspects like for instance position of initiation of reflection cracking. Furthermore opinions differ as to the relative importance of the different fracture models.

The adverse attitude towards the fracture mechanics approach to reflection cracking is perhaps illustrated at best by a statement made by Coetzee |11|.
"The proposed method of analysis for evaluating pavement overlays in terms of reflection cracking should ideally be
(i) simple to use and understand
(ii) able to consider the various alternatives which may retard or eliminate crack reflection
(iii) consistent with theoretical predictions.
A primary requirement for the evaluation is some estimate of stress levels in the overlay, and the effects that various overlay design alternatives may have on these stress levels. This obviously requires a stress analysis which focuses on the cracks in the existing pavement and the effect that these have on the overlay. As indicated, fracture mechanics provides some tools for approaching the problem, but as yet no exact solution exists for a cracked multi-layered system under complex stress conditions. Further, the average highway pavement engineer responsible for overlay design is not likely to be well versed in the field of fracture mechanics, making this approach unlikely as an everyday design method until such time as extremely simplified procedures, such as design charts based on fracture mechanics, become available".
Nevertheless it is believed that application of fracture mechanics concepts in overlay design and reflection crack problems is justified because it gives at least a better insight in the cracking behaviour of pavement materials and structures. It should be repeated again that this is not possible by using the phenomenological approach since this only gives a reasonable accurate indication where cracking may initiate in structures which show no cracking. Therefore it was decided that efforts should be made to incorporate fracture mechanics concepts in this study in order to get a better grasp on the reflection crack problems which have been mentioned in the previous parts of this study.
This part of the study will describe the research on crack growth behaviour of common Dutch asphalt mixes as carried out by, and under supervision of the author.
Furthermore it will be shown how these results can be used in order to estimate the appearance of reflection cracks in overlays.

First of all however a short review of the available literature will be given in order to set the scope of this study.

6.3 Literature Survey

6.3.1 Basic Principles

Basicly distinction can be made between three fracture modes. These modes are shown in figure 6.1. Considering the mode I cracking, which is common to cracking due to tensile stresses perpendicular to the crack, the stress conditions near the crack tip can be calculated by

$$\begin{vmatrix} \sigma_{xx} \\ \sigma_{yy} \\ \sigma_{xy} \end{vmatrix} = \frac{K_I}{\sqrt{2\pi r}} \cos\left(\frac{\phi}{2}\right) \begin{vmatrix} 1 - \sin\frac{\phi}{2}\sin\frac{3\phi}{2} \\ 1 + \sin\frac{\phi}{2}\sin\frac{3\phi}{2} \\ \sin\frac{\phi}{2}\cos\frac{3\phi}{2} \end{vmatrix} \qquad \text{eq. 6.1}$$

where K_I = stress intensity factor

σ_{xx}, σ_{yy} = normal stresses in the marked direction

σ_{xy} = shear stress in the marked direction.

Figure 6.2 shows the used coordinate axis and explains the variables r and ϕ.

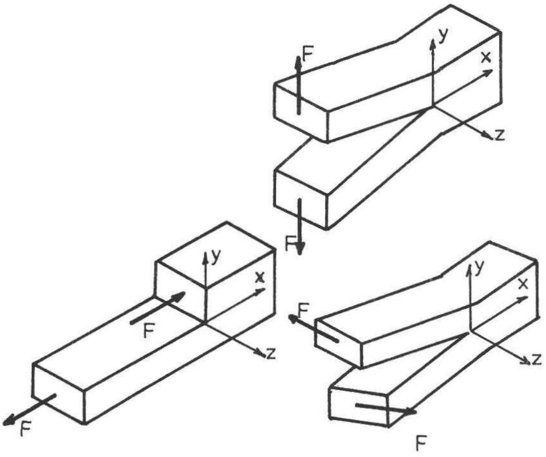

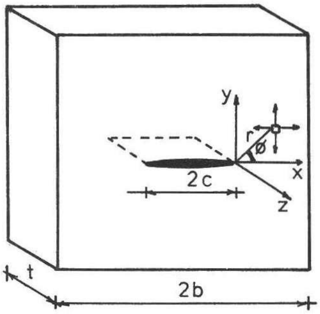

Figure 6.1 *Cracking Modes*

Figure 6.2 *Coordinate System*

Fracture will occur if the value for K_I, the stress intensity factor, has reached a certain critical value K_{IC}. This critical value is called the fracture toughness. It can be considered as a material property. K_{IC} can be determined by means of tensile tests, indirect tensile tests and three point bending tests. According to the ASTM procedure |19| K_{IC} follows from three point bending tests by

$$K_{IC} = \frac{P \cdot l}{bh^{3/2}} \; f\,(c/h) \qquad \text{eq. 6.2}$$

where K_{IC} = fracture toughness |N/mm|

$$f(c/h) = 2.9(c/h)^{0.5} - 4.6(c/h)^{1.5} + 21.8(c/h)^{2.5} - 37.6(c/h)^{3.5} + 38.7(c/h)^{4.5} \qquad \text{eq. 6.3}$$

P = fracture load |N|

l, b, h = length, width, height of the specimen |mm|

c = crack length |mm|

6.3.2 Multi Mode Cracking

There will be no doubt that in most cases all three cracking modes will occur. For instance in pavements, mode I and mode II cracking will prevail. The question now arises how this multi mode cracking should be treated or, in other words, how can we derive the direction of cracking from multi mode cracking conditions. In order to overcome this problem, Sih |20| has postulated his multimode fracture theory.
From the energy dW per unit of volume dV in an elastic material

$$dW = \frac{1}{2E} \left| \sigma_x{}^2 + \sigma_y{}^2 + \sigma_z{}^2 - 2\nu(\sigma_y\sigma_z + \sigma_z\sigma_x + \sigma_x\sigma_y) + 2(1+\nu)(\tau_{yz}^2 + \tau_{zx}^2 + \tau_{xy}^2) \right| dV \qquad \text{eq. 6.4}$$

he arrived to

$$\frac{dW}{dV} = \frac{1}{r}\,(a_{11}K_1{}^2 + 2a_{12}K_1K_2 + a_{22}K_2{}^2 + a_{33}K_3{}^2) \qquad \text{eq. 6.5}$$

where $a_{11} = \frac{1}{16\mu}\,|(3-4\nu-\cos\phi)(1+\cos\phi)|$

$a_{12} = \frac{1}{16\mu}\,2\,\mathbf{\sin\phi}\,|\cos\phi-(1-2\nu)|$

$a_{22} = \frac{1}{16\mu}\,|4(1-\nu)(1-\cos\phi)+(1+\cos\phi)(3\cos\phi-1)|$

$a_{33} = \frac{1}{4\mu}$

$\mu = \frac{E}{2(1+\nu)}$

E = elastic modulus
ν = Poisson's ratio
$K_1 = K_I/\sqrt{\pi}$
$K_2 = K_{II}/\sqrt{\pi}$
$K_3 = K_{III}/\sqrt{\pi}$

K_I, K_{II}, K_{III} = stress intensity factor associated with mode I, II, III cracking respectively.

r, ϕ = as indicated in figure 6.2.

The part in parentheses in equation 6.5 gives the amplitude of the elastic energy at a distance r of the cracktip. This factor is defined as the strain energy density factor S.

$$S = a_{11}K_1{}^2 + 2a_{12}K_1K_2 + a_{22}K_2{}^2 + a_{33}K_3{}^2 \qquad \text{eq. 6.6}$$

Sih hypothesized that the cracks would grow in the direction of the minimum strain energy density which equals the direction of the maximum potential energy introduced into the system due to the applied loads.
Mathematically this can be written as:

$$Up = -S\,\frac{dUp}{d\phi} = 0 \qquad \text{eq. 6.7}$$

The direction of cracking will be $\phi = \phi_0$

$$\text{if } \frac{dS}{d\phi} = 0 \text{ and } \frac{d^2S}{d\phi^2} > 0 \qquad \text{eq. 6.8}$$

Using this approach, Sih showed that for mode I cracking ϕ_0=0 while for mode II cracking ϕ_0 depends on Poisson's ratio (figure 6.3, table 6.1)

Table 6.1 *Direction of Mode II Cracking in relation to Poisson's Ratio*

ν	ϕ_o
0	-70.5°
0.1	-75.6°
0.2	-79.3°
0.3	-83.3°
0.4	-87.2°
0.5	-90.0°

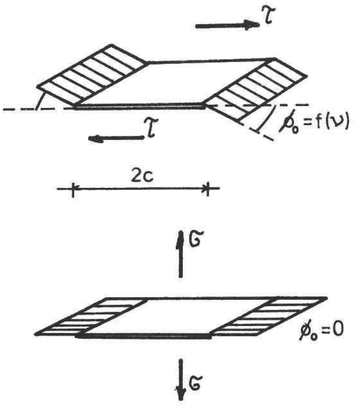

Figure 6.3 *Direction of Cracking in relation to the Cracking Mode and Poisson's Ratio.*

Since cracking will occur at a critical value of S, called S_{cr}, it can be shown that

$$S_{cr} = \frac{(1+\nu)(1-2\nu)}{2\pi E} K_{Ic}^2 \qquad \text{eq. 6.9}$$

Furthermore it can be shown by supposing

$$S_{cr_{\text{mode I}}} = S_{cr_{\text{mode II}}} \qquad \text{eq. 6.10}$$

that $$K_{IIc}^2 = \frac{3(1-2\nu)}{2(1-\nu)-\nu^2} \cdot K_{Ic}^2 \qquad \text{eq. 6.11}$$

6.3.3 Crack Propagation Laws

In 1963, Paris and Erdogan |21| found from experimental data that the crack propagation rate dc/dN was proportional to the stress intensity factor K raised to the power n

$$\frac{dc}{dN} = AK^n \qquad \text{eq. 6.12}$$

where dc/dN = increase in crack length per loading cycle
K = stress intensity factor
A, n = constants depending on the material

Paris and Erdogan stated that n was about 4. Majidzadeh et al. |2, 3, 4, 5| concluded from their experiments on sand asphalt that a value of about 4 was indeed a reasonable value for n. For asphaltic concrete mixes however n was close to 3. Also n = 4 values were reported by Monismith et al. |10|. Furthermore Majidzadeh showed a dependency of n on temperature. In general n increased with decreasing temperature. This makes sense since at lower temperatures asphalt mixes behave more brittle which should be reflected in the value of n.

In later publications Majidzadeh et al. |6, 7, 8| reported that the crack growth relation between log (dc/dN) and log K, is not linear in general. They concluded that a four term model described the experimental data much better. This four term model looked like

$$\frac{dc}{dN} = A_1K + A_2K^2 + A_3K^4 + A_4K^6 \qquad \text{eq. 6.13}$$

Furthermore Majidzadeh concluded that if the one term model was used (eq. 6.12), the power n was dependent on the loading conditions. For low loads, high cycle fatigue, n would be somewhere between 4 and 8 while for high loads low cycle fatigue, n would be equal to or smaller than 2. He also concluded that if n=2, the constant A could be estimated from mechanical mix properties by

$$A * 10^{9} = 0.231 + 2.613\ (\frac{\sigma_m}{E^*} * 10^{3}) + 3.233\ (K_{Ic} * 10^{-4}) \qquad \text{eq. 6.14}$$

where σ_m = tensile strength (psi) (σ = 1200 psi/s)
E^* = dynamic modulus (psi) (f = 10 Hz)
K_{Ic} = fracture toughness (lbs/in $^{1.5}$) (σ = 1200 psi/s)

Since the loading conditions influenced the value of n, Majidzadeh concluded that a two term crack growth law could be used to cover all loading conditions. This model looked like

$$\frac{dc}{dN} = A_1K^2 + A_2K^4 \qquad \text{eq. 6.15}$$

Here A_1 and A_2 could be estimated from mechanical properties by

$$A_1 * 10^{10} = 7.02 + 77.9\ (\frac{\sigma_m}{E^*} * 10^{3})^2 - 6.09\ (K_{Ic} * 10^{-3})^3 \qquad \text{eq. 6.16}$$

$$A_2 * 10^{16} = 31.36 - 1132.4\ (\frac{\sigma_m}{E^*} * 10^{3})^3 - 43.32\ (K_{Ic} * 10^{-3})^3 \qquad \text{eq. 6.17}$$

From Majidzadeh's work one could come to the conclusion that Paris'law cannot be used for crack growth predictions. However, it will be shown that this conclusion is not correct.

In spite of the above mentioned objections, theoretical justification of Paris' law can be found by considering Schapery's work |13|. He derived an equation relating the velocity of a crack in a visco-elastic material due to mode I displacements, to the properties of that material.

$$\frac{dc}{dN} = AK^n \qquad \text{eq. 6.18}$$

$$A = \frac{\pi}{6\sigma_m^{\,2} I_1^{\,2}}\ \left| \frac{(1-\nu^2)D_2}{2\Gamma} \right|^{1/m} \left| \int_0^{\Delta t} w(t)^{2(1+1/m)} dt \right| \qquad \text{eq. 6.19}$$

$$n = 2(1 + 1/m) \qquad \text{eq. 6.20}$$

where σ_m = maximum tensile stress the material can withstand before failure

I_1 = a factor depending on the stress conditions at the crack tip, the failure stress of the material and the length of the failure zone

D_2 = the compliance of the material considered at t=1 sec.
ν = Poisson's ratio

Γ = fracture energy, defined as the work done on a material to produce a unit area of crack surface
$w(t)$ = the pulse shape of the stress intensity factor
m = the slope of the compliance curve.

In equation 6.19 all factors except I_1 and $w(t)$ are solely dependent on the type of material. Considering the magnitude of I_1, Germann and Lytton |15| have stated that *"reasonable values of I_1 can be taken any value between one and two"*. In this way they justified the choice of 1.5 as used in their study.

Observation of Schapery's equation shows that this theoretically derived equation is basicly the same as the Paris relation.
Comparison of the regression equations to estimate the magnitude of A as derived by Majidzadeh et al, with the equation for A as given by Schapery, leads to the conclusion that for fixed loading conditions it is indeed possible to estimate A from routine material tests.
Furthermore it can be concluded that Majidzadeh's statement n being dependent on the loading conditions is valid if we consider the elastic or stiffness moduli of asphaltic materials to be stress dependent. This is certainly the case at higher temperatures (or lower load frequencies) (fig. 6.4 |22|).

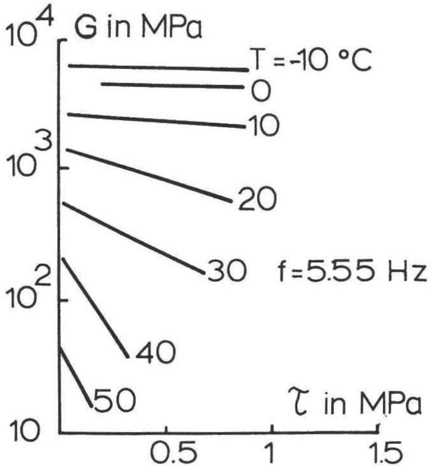

Note: $G = E/2(1 + \nu)$

Figure 6.4 *Dependency of the Shear Modulus on the Magnitude of the Shear Stress.*

It can easily be shown that m increases at higher temperatures (or lower load frequencies) if the stress level increases. This would, according to equation 6.20 result in lower values for n.
However it might be doubted whether these low n values (< 2) as reported by Majidzadeh will occur in practice since normally the pavement is not designed to sustain 10^4 load cycles but at least 10^6 load cycles.
Nevertheless almost all specimens tested by Majidzadeh failed at less than 5.10^4 cycles while most of them failed after 10^4 load repetitions. So in practice, low load high cycle fatigue conditions resulting in unreduced n values, will probably prevail.

Recently Schapery has extended his theory in order to be able to describe the fracture in nonlinear viscoelastic composite materials |23, 24|.
He assumed a nonlinear behaviour which can be described by (fig. 6.5)

$$\frac{\sigma}{\sigma_o} = b_o \, \varepsilon^{b_1} \qquad \text{eq. 6.21}$$

where σ = applied stress level
σ_o = yield stress
b_o, b_1 = constants.

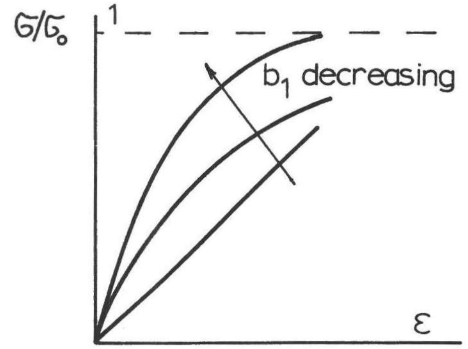

Figure 6.5 Nonlinear Stress - Strain Relations used by Schapery.

By using a generalized J integral theory he arrived to the following expressions for the exponent of the crack growth law n

If σ_m and Γ take a constant value then

$$n = 2(1 + \frac{1}{m}) \qquad \text{eq. 6.22}$$

If the length of the fracture zone α and Γ take a constant value then

$$n = 2(\frac{1}{m}) \qquad \text{eq. 6.23}$$

If the length of the fracture zone α and the crack opening displacement u take a constant value, then

$$n = 2(\frac{1}{m(1+b_1)}) \qquad \text{eq. 6.24}$$

For the sake of completeness α and u are defined in figure 6.6.

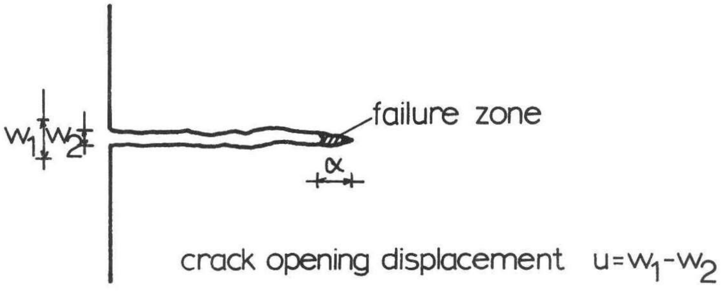

Figure 6.6 Definition of α and u.

Schapery's developments have the following implications.
If we assume m = 0.5 and we also assume $b_1 = 1$, then n = 6 if the crack growth properties were derived by means of a constant stress type of test, and n = 4 if the test was a constant displacement type of test.

Application of Schapery's theory seems very attractive since it shows theoretically that there exist possibilities to determine the constants A and n from simple tests and nomographs.

From the foregoing it is concluded that Paris' law as extended by Schapery can be used for crack propagation calculations with a rather high degree of confidence.
Furthermore it is concluded that Paris' law can also be used for the analysis of multi mode cracking conditions since, as has been indicated in the previous paragraph, K can easily be replaced by S.

6.3.4 Calculation Techniques

Calculation on crack propagation in pavement structures involves the use of finite element programs in order to be able to calculate the stresses and stress intensity factors in the area surrounding the crack tip. In order to avoid accuracy errors, a fine element mesh has to be created around the crack tip. Furthermore cracking is a typical three dimensional phenomenon so in fact 3D programs should be used. These types of programs however do require a large storage capacity and a large amount of computation time. Therefore their use is restricted to special problems.
In order to overcome this problem a two dimensional plain strain approach is usually adopted while sometimes a quasi 3D program is used which incorporates prismatic elements |25|.
Just recently, two 2-D finite element programs incorporating special crack tip elements have become available which allows the user to define a much coarser element mesh around the crack tip. Chang, Lytton and Carpenter |14| have reported such a program that has been shown to be very efficient and highly accurate even when a coarse element mesh is used.
Figure 6.7 gives an example of the finite element representation of a cracked pavement incorporating the special crack tip element as used in their study.

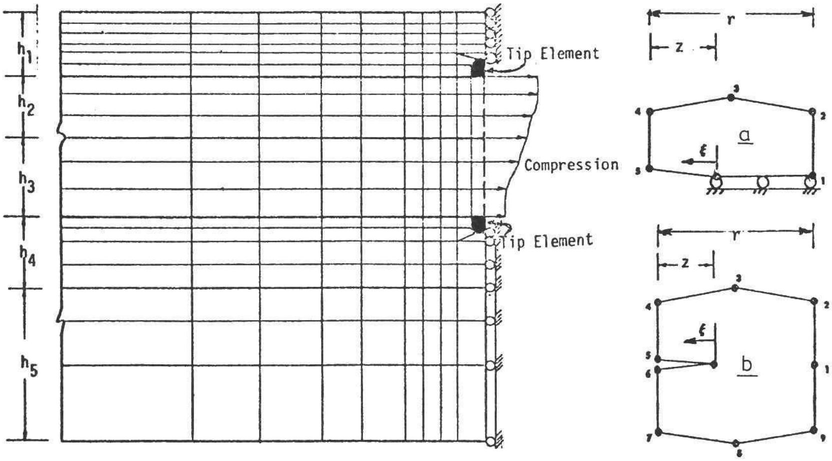

Figure 6.7 *Finite Element Representation of a Pavement Structure,*
a) Five-Node Tip Element for Symmetric Case
b) Nine-Node Tip Element for Non Symmetric Case |14|

Marchand and Goacolon |18| reported the development of the BIFIS program which incorporates a crack tip element as shown in figure 6.8.
Both the Chang and Marchand program produce K_1 and K_2 values at the crack tip.

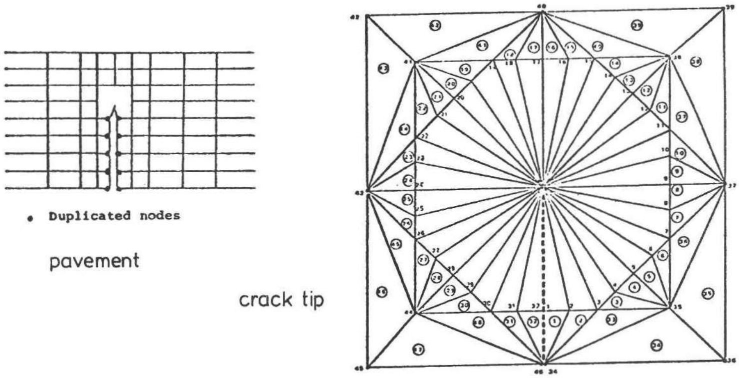

Figure 6.8 Finite Element Representation of a Pavement Structure and the Crack Tip Element as used by Marchand et al. |18|

Coetzee in his study |11| used a finite element program to calculate the effective stress contours instead of K values in the surrounding of the crack tip. The effective stress is defined by

$$\sigma_{eff} = \frac{1}{\sqrt{2}} \sqrt{\ } \left|(\sigma_1 - \sigma_2)^2 + (\sigma_2 - \sigma_3)^2 + (\sigma_3 - \sigma_1)^2\right| \qquad \text{eq. } 6.25$$

He motivated his choice for calculating σ_{eff} instead of K by stating
"The use of the effective stress allows consideration of a given state of stress in the pavement in terms of a parameter that can be compared with that of a different stress condition to determine the relative effects of the stress states on the pavement. Further, unlike generally applied pavement design techniques which use horizontal tensile strains at the base of the surface layer as a failure criterion, effective stress considerations can accomodate the detrimental effect of compressive stresses in the overlay over the existing crack."
However it should be noted that failure predictions based on the effective stress are only valid if the material follows the von Mises failure criterion. This is not the case for asphaltic materials. Here the failure conditions can be described better by the Mohr-Coulomb criterion. This involves that the first stress invariant should also be taken into account.
Based on the foregoing the author decided that for the stress intensity calculations the program reported by Chang et al. could be used |14|.

6.4 Experimental Program

In order to obtain the fracture and crack growth characteristics of common Dutch mixes, an experimental program on both subjects was carried out.
Also this program should result in relations between the fracture characteristics, as determined by means of static tests and crack growth properties which are the result of repeated load tests.
By means of these relation one would be able to estimate the dynamic properties by means of routine testing. The author believes, that the development of such relations should be encouraged, since in this way application of fundamental sound approaches which give an insight in the reflection cracking problem, would be promoted.

The experimental program consisted of

- a: static tests;
  - a1: indirect tensile tests to determine the tensile strength of the mixes considered
  - a2: three point bending tests on notched beam specimens to determine the fracture toughness and stiffness of the mix
- b: dynamic tests;
  - b1: dynamic tensile tests on notched beam specimens at higher load levels and various frequencies and temperatures to determine the crack growth characteristics
  - b2: dynamic tensile and compressive tests on beams at low load levels and various frequencies and temperatures to determine the mix stiffness (compliance) characteristics (D_2 and m, see equation 6.19).

In the subsequent sections these tests and their results will be described.

First of all however attention will be paid to the mix compositions and preparation of the test specimens.

6.4.1 Mix Compositions, Preparation of the Test Specimens

Basicly four mix types were considered in the dynamic test program while in the static test program five mixes were considered. Within three mix types the type of bitumen as well as the gradation was varied which resulted in three to four variant mix compositions. All mixes can be considered to be typical Dutch mixes. The typical aspect of Dutch mixes is that they contain factory made fillers because, among other reasons, the natural mineral aggregate contains very little inherent filler. The fillers are specified according to their "strength", which is the capacity of the filler to absorb bitumens, into very weak, weak and medium fillers.
Table 6.2 gives the composition of each mix. Figure 6.9 shows the gradation of the aggregate as used in each mix.
Table 6.2 also gives information on the void content of the mixes after compaction. Because Marshall compacted densities were available for most mixes, it was possible to calculate the degree of compaction; table 6.2 also contains this information.
Furthermore the table gives an indication in which part of the asphalt structure the mixes are used.

Since it was decided to use beam specimens for most of the static and all dynamic tests, slabs were made having a size of 0.9 * 0.26 * 0.095 m (length * width * height).
After casting the material into a mold, having the above mentioned internal dimensions, the material was compacted by means of a roller, with a width of 0.26 m. The roller was moved along the material by hand.
First 10 passes were applied using an unloaded roller (m=38 kg) after which 10 passes were applied using a loaded roller (m=74 kg). The sandasphalt slabs were compacted by hand since use of the roller resulted in shoving of the mix.

The beam specimens were sawn from the slabs in the following way. First the edges of the slab were cut off and after that the beams were sawn at their desired length. Next the top and bottom of each beam were cut off in order to avoid edge effects.

Cores were taken from the slabs in order to obtain specimens for the indirect tensile tests. Again the top and bottom of each core were cut off and the remaining parts were sawn in two disks each having a height of about 0.025 m.

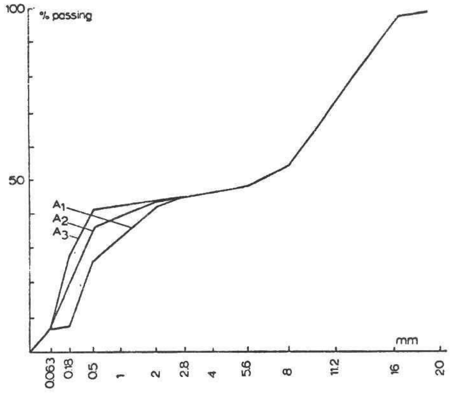

Figure 6.9a Gradation of Mix A_1, A_2, A_3

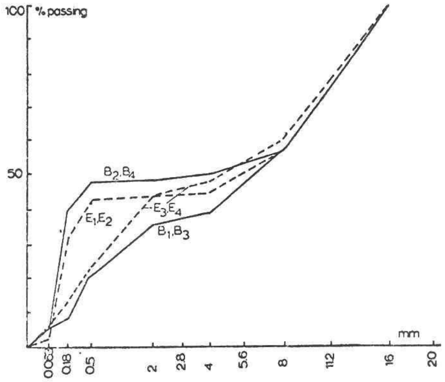

Figure 6.9b Gradation of Mix B_1, B_2, B_3, B_4, E_1, E_2, E_3, E_4

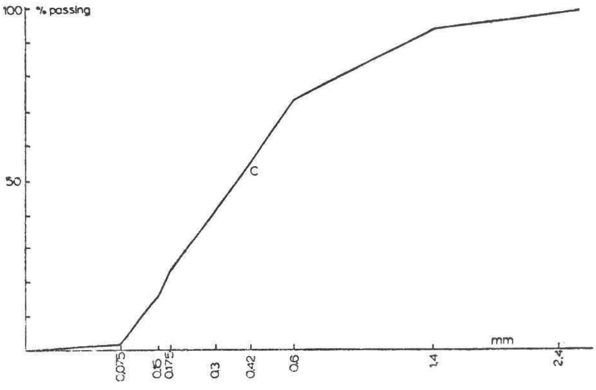

Figure 6.9c Gradation of Mix C

Table 6.2 Composition of the Mixes studied

Mix	Gravel Sand Asphalt			Open Asphaltic Concrete				Sand Asphalt	Dense Asphaltic Concrete				Cold Asphalt
Composition (Percentage by weight)	A_1	A_2	A_3	B_1	B_2	B_3	B_4	C	E_1	E_2	E_3	E_4	F
Gravel	55	55	55	--	--	--	--	--	--	--	--	--	--
Crushed gravel	--	--	--	62	62	62	62	--	57	57	57	57	60
Riversand	39	19.5	9	31	--	31	--	63	--	--	9	9	--
Fore shore sand	--	19.5	30	--	31	--	31	31	35	35	--	--	--
Crushed riversand	--	--	--	--	--	--	--	--	--	--	26	26	31
Filler DF18 (weak)	6	6	6	7	7	7	7	--	--	--	--	--	--
Filler K40 (weak)	--	--	--	--	--	--	--	6	--	--	--	--	--
Filler Duras (medium)	--	--	--	--	--	--	--	--	8	8	8	8	--
Filler	--	--	--	--	--	--	--	--	--	--	--	--	9
Bitumen 45/60	5	5	5	--	--	5	5	4	6.4	--	6.4	--	--
Bitumen 80/100	--	--	--	5	5	--	--	--	--	6.4	--	6.4	--
Bitumen 80/100+ fluxoil	--	--	--	--	--	--	--	--	--	--	--	--	7.5
Mean Void Content (%)	5.94	7.57	10.01	4.95	9.98	3.72	9.09	20.5	7.08	6.84	2.9	4.39	8
Degree of Compaction (%)	97.2	97.1	96.5	97.7	96.5	99.0	97.5	97.0	95.4	96.4	98.7	97.2	
Location in Structure	Base			Binder Temporary Top layer				Subbase	Top layer				Top layer

6.5 Static Tests to determine the Fracture Toughness, Tensile Strength and Stiffness Characteristics

In this section the static tests which were carried out in order to determine the fracture toughness, tensile strength and stiffness characteristics will be described. Many of these results have already been published elsewhere |26|.

Three point beam bending tests were performed to determine the fracture toughness and mix stiffness characteristics. The tensile strength of the mixes was evaluated by means of the indirect tensile test.

6.5.1 Fracture Toughness Tests

Three point bending tests (fig. 6.10) were performed in order to obtain fracture toughness values for the different mixes. The dimensions of the tested beams were $l \times w \times h = 0.45 \times 0.05 \times 0.05$ m. At midspan an initial crack was sawn with a depth of about 0.01 m. The width of the artificial crack was about 5 mm, the radius of the crack tip about 2.5 mm.

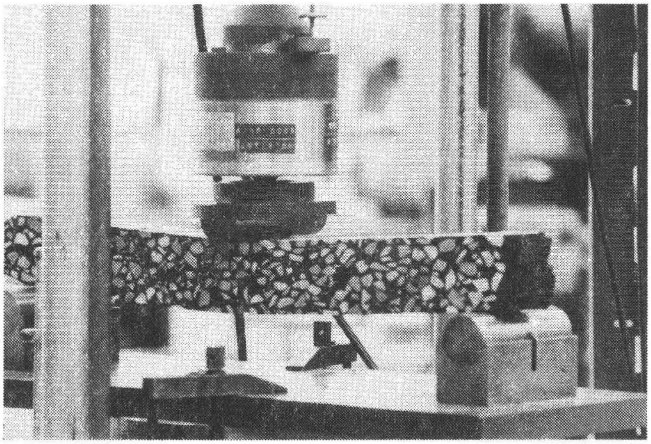

Figure 6.10 Three Point Bending Test

It was decided to perform the fracture toughness tests on a Marshall testing device since this piece of equipment is available in each pavement material testing laboratory. Using the Marshall device means that a stroke controlled type of test is used (vertical deformation speed = 0.85 mm/sec).

In order to get fracture toughness results at different mix stiffnesses, the tests were performed at temperatures of -15, -5, 5 and 15°C. Table 6.3 shows the mean fracture toughness values and standard deviation around the mean as determined for the different mixes. It should be noted that all K_{Ic} values are calculated from the fracture load.

The ASTM procedure |19| (see appendix 6A) was used, in order to check whether the K_{Ic} values calculated in this way could be considered to be "valid".

From this it was concluded that all 15°C results and some of the 5°C results were "invalid". Candidate K_{Ic} values were then calculated and these are given

Table 6.3 *Fracture Toughness Values (K_{Ic}) as determined for the Mixes considered* |$N/mm^{1.5}$|

Mix	Temperature |°C| -15		-5		5		15	
	K_{Ic}	vc	K_{Ic}	vc	K_{Ic}	vc	K_{Ic}	vc
A_1	17.39	8	19.1	2.2	15.45(17.97)	6.2	11.1 (14.8)	2.9
A_2	15.08	9	16.4	13.6	13.66(14.85)	6.1	3.98(6.99)	18.8
A_3	13.32	16	13.56	7.4	10.48(11.04)	11.7	2.49(2.49)	5.4
B_1	22.02	10.8	22.38	10.	11.64(18.77)	4.1	5.95(9.01)	7.1
B_2	10.45	12.3	10.37	5.5	5.8 (8.66)	7.5	2.73(4.14)	18.9
B_3	20.74	2.5	25.38	13.9	16.77(17.11)	4.6	11.82(16.89)	6.2
B_4	13.48	5.3	9.72	25.2	10.39(11.95)	8.8	8.19(8.19)	5.4
C	6.12	4	6.34	5.2	9.15	1.9	6.18(8.03)	3.8
E_1	4.1	7.4	4.77	7.1	3.85	9.1	1.65(2.89)	6.1
E_2			4.39	9.0	5.33(6.66)	23.1	1.41(2.87)	2.9
E_3	6.98	8.6	7.38	6.5	6.87	5.	3.6 (6.2)	2.8
E_4	6.91	6.4	7.67	3.2	6.44	5.6	1.34(3.52)	2.1
F	12.4	1.7	8.22(9.79)	1.22	2.72(4.39)	0.3	(0°C data)	

Note: vc = coefficient of variation |%|
The K_{Ic} values in parentheses are calculated from the fracture load, the other values are calculated according to the described ASTM procedure (appendix 6A).

Table 6.4 *Tangent Modulus (S_{mix}) of the Mixes determined from the Fracture Toughness Tests* |*MPa*|

Mix	Temperature |°C| -15		-5		5		15	
	S_{mix}	vc	S_{mix}	vc	S_{mix}	vc	S_{mix}	vc
A_1	6458	15	5141	6	2527	16	1754	9
A_2	5654	13	4565	15	2530	15	1214	32
A_3	5266	7	5096	32	1719	11	784	35
B_1	9095	15	5935	8	3034	3	1474	4
B_2	4052	18	3017	16	1292	4	689	16
B_3	8176	17	7817	10	3619	10	2157	7
B_4	4975	11	3793	17	2131	6	1495	13
C	3406	15	2936	18	1522	7	1081	4
E_1	1853	6	1564	6	706	7	337	9
E_2			1118	16	919	21	675	17
E_3	2818	14	2173	7	1558	5	658	15
E_4	2465	9	2063	8	850	17	334	12
F	2731	18	1334	36	469	38	(0°C data)	

Note: vc = coefficient of variation |%|

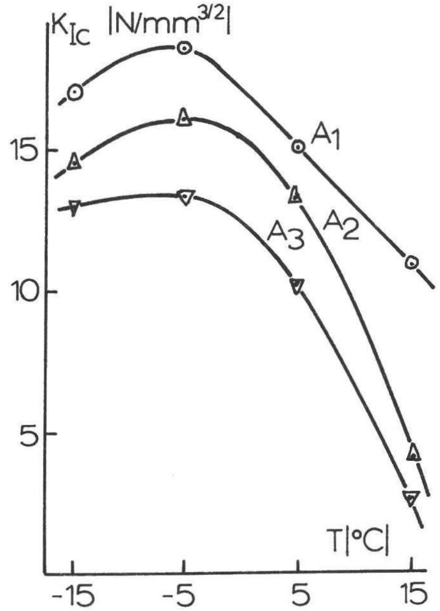

Figure 6.11a *Fracture Toughness Values for the Gravel Sand Asphalt Mixes*

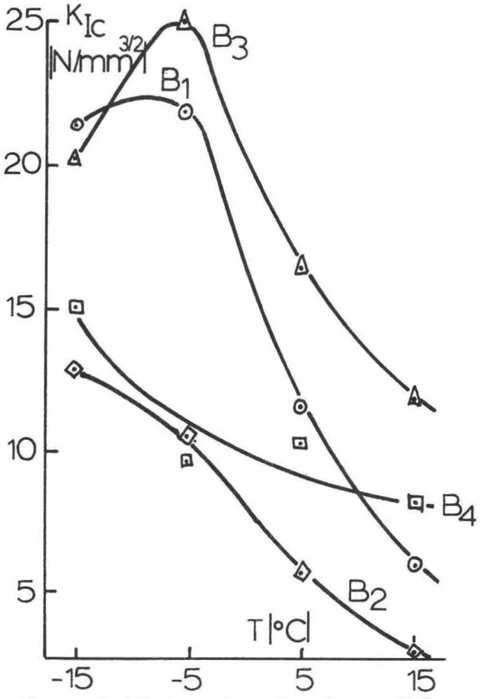

Figure 6.11b Fracture Toughness Values for the Open Asphaltic Concrete Mixes

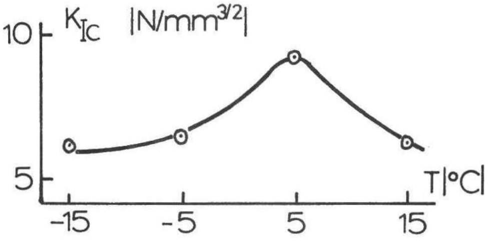

Figure 6.11c Fracture Toughness Values for the Sand Asphalt Mix

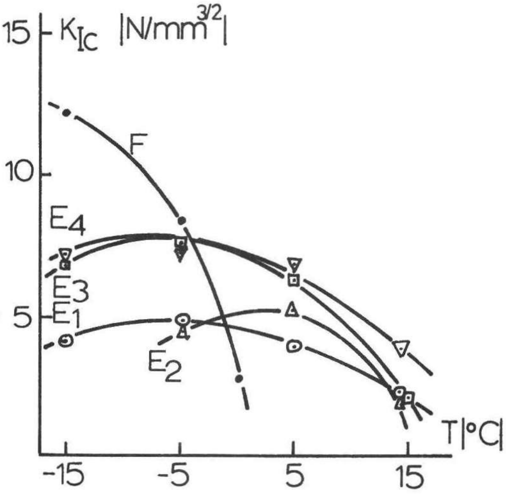

Figure 6.11d Fracture Toughness Values for the Cold Asphalt and Dense Asphaltic Concrete Mixes

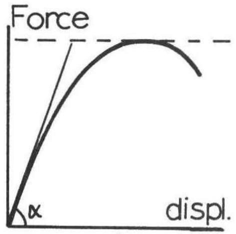

S_{mix} = $l^3 \tan\alpha / 48I$
S_{mix} = mix stiffness |MPa|
l = beam length |mm|
I = $bh^3/12$
b = beam width |mm|
h = beam height |mm|
α = indicated in graph

Figure 6.12 Schematical Representation of the Calculation of the Tangent Modulus

in table 6.3 too (values in parentheses).
The terms "valid", "invalid" and "candidate" are explained in appendix 6A. Figure 6.11 shows the results of the K_{Ic} measurements in a graphical way. Furthermore the tangent stiffness modulus of each specimen was calculated from the load displacement curves (fig. 6.12). These results are given in table 6.4 and figure 6.13.

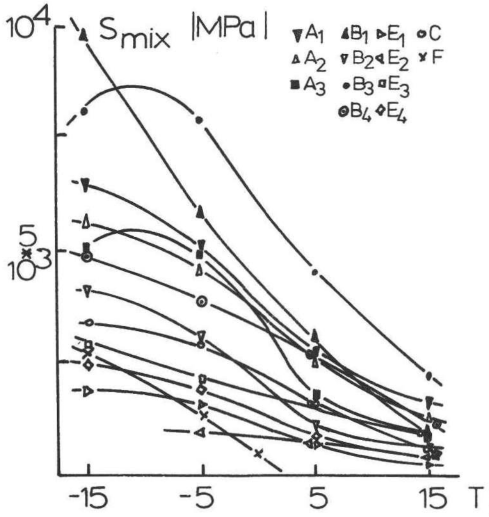

Figure 6.13 Tangent Modulus (S_{mix}) as determined for the Mixes considered

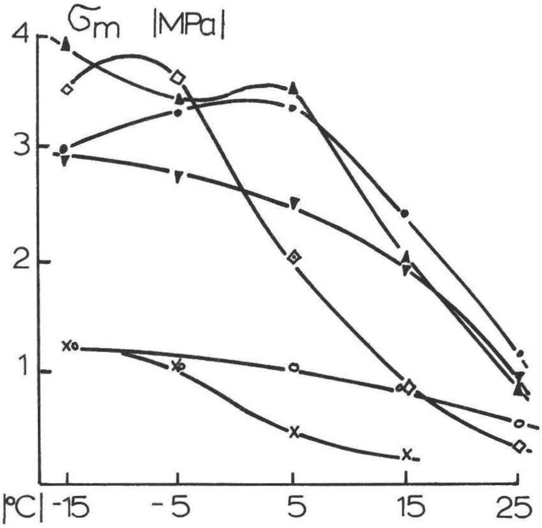

Figure 6.14 Tensile strength (σ_m) as determined for the Mixes considered

6.5.2 Indirect Tensile Tests

Indirect tensile tests were performed in order to obtain tensile strength values for the different mixes. Only those mixes were considered which were also tested in the crack growth experiments. These indirect tensile tests were performed too on a Marshall testing device. The testing temperatures were -15, -5, 5, 15 and 25°C. The tensile strength values of each mix in relation to the testing temperature are shown in figure 6.14.

6.5.3 Discussion on the Static Test Results

In this subsection, the results of the static tests will be discussed. First of all the attention will be focussed on the fracture toughness results, subsequently the stiffness moduli will be discussed and finally attention will be paid to the indirect tensile test results.

6.5.3.1 Fracture Toughness

As could be expected, temperature has a large influence on the test results (fig. 6.11). This influence is most pronounced for the gravel sand asphalt and open asphaltic concrete mixes. Also a dramatic decrease of the K_{Ic} with respect to temperature can be observed for the cold asphalt mix. Furthermore a large influence of the type of sand used in the mix can be observed. Foreshore sand results in lean mixes which have a high void content (compare A_1 with A_2 and A_3, B_1 with B_2 and B_3 with B_4). Figure 6.15 nicely shows the influence of the void content on the K_{Ic} for the gravel sand asphalt mixes.

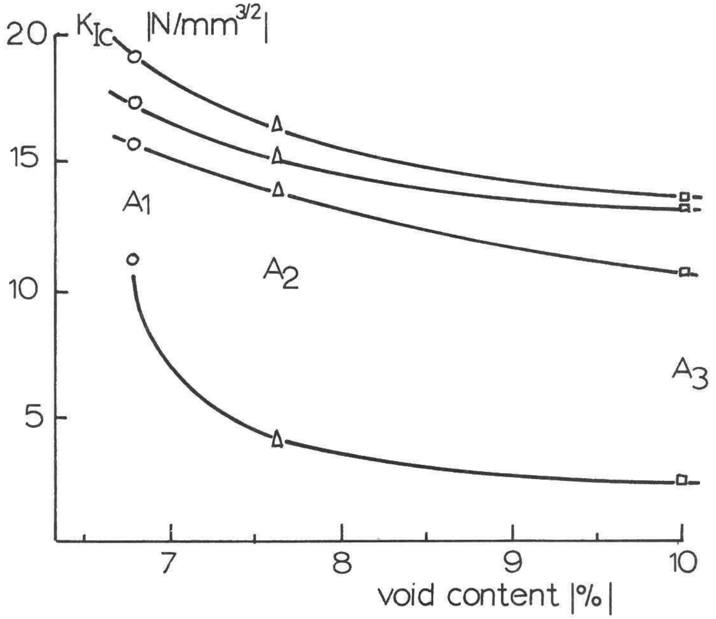

Figure 6.15 Influence of Void Content and Temperature on the Fracture Toughness of Gravel Sand Asphalt Mixes

Also the influence of the type of bitumen, or perhaps better the influence of the characteristics of the bitumen/filler mortar, can be recognized. Especially at higher temperatures the mixes having a 45/60 bitumen produce higher K_{Ic} values than comparable mixes containing a 80/100 bitumen (compare B_1 with B_3, B_2 with B_4 and E_3 with E_4, fig. 6.11b and 6.11d)
Furthermore it should be noted that all dense asphaltic concrete mixes showed low K_{Ic} values. This is contributed to the higher bitumen content of this mix. The rather constant values of K_{Ic} as obtained for the sand asphalt mix is contributed to the high void content of this mix.

6.5.3.2 Mix Stiffness

The mix stiffness as obtained from the fracture toughness tests (fig. 6.13) do not give rise to special comments. The stiffness increases with decreasing temperature and the mixes containing a harder bitumen (lower pen.) produce higher stiffnesses than comparable mixes having softer bitumens tested at the same temperature. Also the effect of the void content on the mix stiffness can be observed (compare for instance mix B_1 with B_2 and B_3 with B_4, fig. 6.11b)
From the mix stiffnesses and mix composition, the appropriate bitumen stiffnesses were back calculated using the modified Shell S_{bit} - S_{mix} nomograph |27|. The calculated S_{bit} values are given in table 6.5.

Table 6.5 Calculated S_{bit} values |MPa|

Mix Type	Temperature |°C|			
	-15	-5	5	15
A_1	100	72	23	14
A_2	72	52	23	9
A_3	110	100	23	6.3
B_1	73	42	15	0.9
B_2	73	43	14	5
B_3	100	90	29	15
B_4	80	50	22	13
C	120	100	36	20
E_1	30	23	15	3
E_2		17	12	7
E_3	23	18	12	3.5
E_4	21.5	19	6.5	1.8
F	23	8.5	1.7 (0°C)	

6.5.3.3 Tensile Strength

From the tensile strength values as given in figure 6.14 it can be concluded that especially at temperatures below 0°C the dense asphaltic concrete mix compares favorably with the open asphaltic and gravel sand asphalt mixes. This might be considered as an unexpected result since the tangent modulus as well as the K_{Ic} values of this mix are rather low compared to the values obtained for the gravel sand asphalt and open asphaltic concrete mixes. This leads to the conclusion that a high tensile strength does not always mean that the mix also has a high stiffness or a high K_{Ic}.
From this it is concluded that in order to determine the fracture properties of asphalt mixes, one should not only take into account the tensile strength of the material but also the stiffness of the material.

6.6 Dynamic Tensile Tests to characterize the Crack Growth Behaviour of Asphalt Concrete Mixes

In order to obtain values for the constants A and n from Paris' crack growth law (eq. 6.12) it was decided to carry out repeated load tests on the mixes A_1, B_1, B_3, E_4 and F. The first question which had to be solved was, which type of test should be selected for these experiments. This section will therefore first deal with the selection of the type of test, and secondly with the experimental program and its results.

6.6.1 Selection of the Type of Test

A number of tests can be used to evaluate the fatigue and crack growth properties of asphalt mixes, for example (fig. 6.16)

a. three or four point beam bending tests
b. beam on elastic foundation tests
c. pure shear tests
d. indirect tensile tests

e. direct tensile tests.

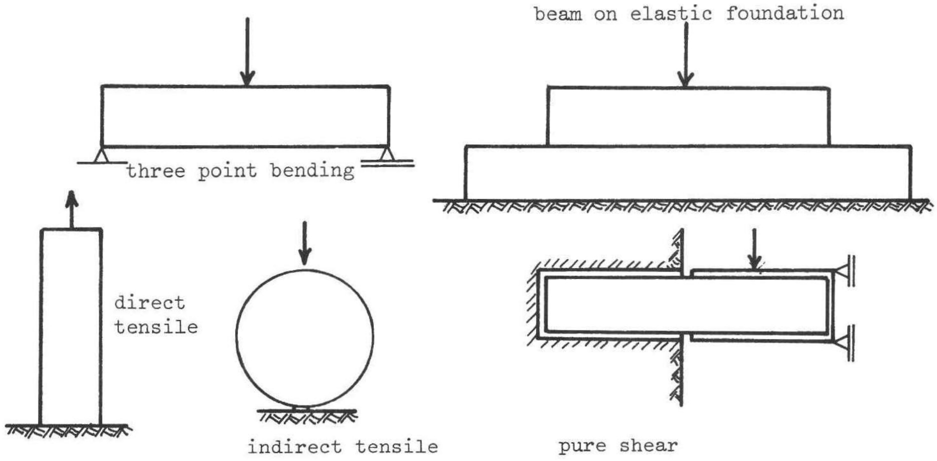

Figure 6.16 Schematical Representation of the different Test Types

Furthermore distinction can be made between constant load tests and constant displacement tests.
The selection of which test should be used for crack growth experiment should be based on two criteria

a. the simplicity of the test
b. the possibility to calculate the stress intensity factor and crack length from the increase of the measured displacements.

By the first criterion it is meant whether or not the test equipment is readily available, whether or not the test is easy to run, and whether or not the specimen preparation is simple.
The latter criterion is an important one since it is very hard to do accurate crack length measurements on asphalt concrete specimens. Therefore the crack length must be determined from the increase in the measured displacements.
In order to determine whether or not it would be possible to calculate the crack length from the measured displacements, the five above mentioned tests were analysed by means of the finite element program described by Chang et al. |14|. A detailed description of this analysis is given in appendix 6B.

From this analysis it was concluded that for each test it is possible to calculate the crack length and stress intensity factor from the increase of the measured displacements.
However for the beam on elastic foundation test, the K profile was considered to be rather complicated. Furthermore it was noticed that exact knowledge on the degree of adhesion between the asphaltic beam and the rubber subgrade was necessary in order to be able to make proper estimations of K.
Another result of the analysis was that constant load tests should be preferred. This is because of the fact that at constant displacement tests, the applied load (the magnitude of which should be measured) will drop to such a low level that instability of the loading system used, might occur. Therefore this type of test was thought to be inappropriate.
For reasons of simplicity the pure shear test was rejected. For this type of test a very stiff and strong frame is needed. Furthermore the preparation of the test specimens was considered to be complicated.

The three and four point bending test was rejected since in this test the dead weight of the specimen can have a significant influence on the K value. The indirect tensile test was not thought to be appropriate since it was observed that "rocking" of the specimen could occur. This rocking movement has of course an influence on the stress conditions. Furthermore it was quite often observed that the edges of the loading strips incised into the specimen. This of course will influence the stress condition as well as the cracking behaviour.

Incision by the loading strips might be overcome by placing a rubber strip between the specimen and the loading strip. This however hinders the measurements of the vertical displacement.

From the above mentioned considerations the author concluded that the direct tensile test was the most appropriate one for crack growth experiments. It should be noted that in this test special attention should be paid to a proper alignment of the specimen. Also considerable care should be given to the fastening of the specimen to the loading frame.

6.6.2 Test Set-Up and Experimental Program

As described in the previous subsection,the direct tensile test was selected for the crack growth experiments. A sketch of the test set-up as used,is given in figure 6.17. Figure 6.18 is a picture of the set-up |28|.

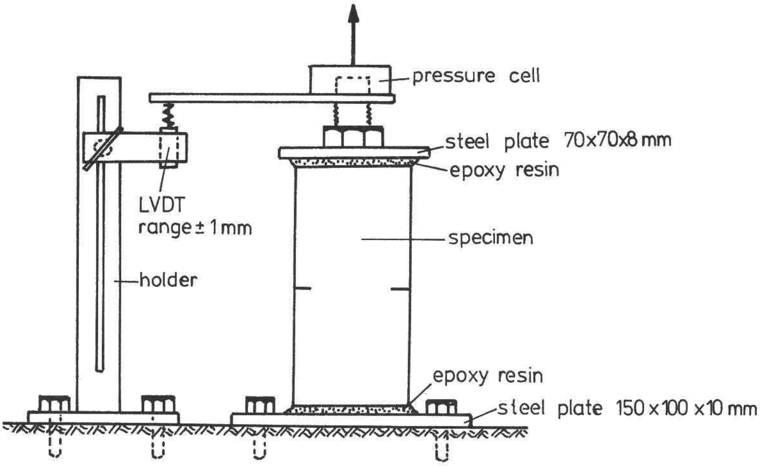

Figure 6.17 Test Set-Up

The specimens were about 0.15 m long and the cross section was about 0.05 x 0.05 m. At midlength of two opposite sides, an artificial crack was sawn which has a depth of about 0.005 m.

The beam specimens were sawn from slabs which were prepared in the way as described before. An epoxy resin was used to glue the specimens to the top and bottom loading plate. To ensure a proper alignment of the specimens, hardening of the glue took place while the beam was positioned under the ram of the dynamic loading system.

Use was made of a MTS hydraulic loading system. Figure 6.19 gives a view on the system control and recording equipment.

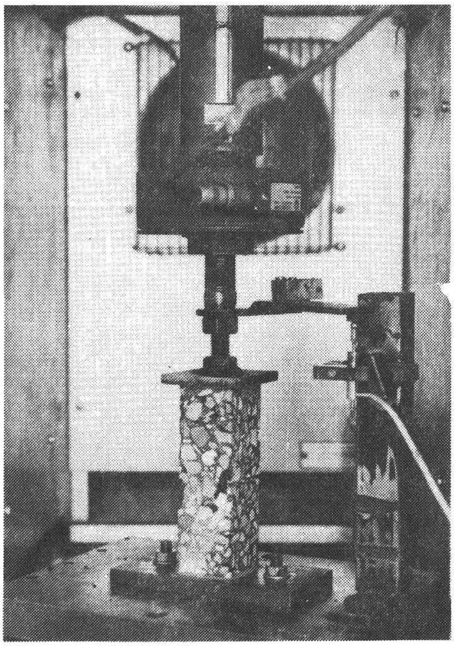

Figure 6.18 *Picture of the Test Set-Up*

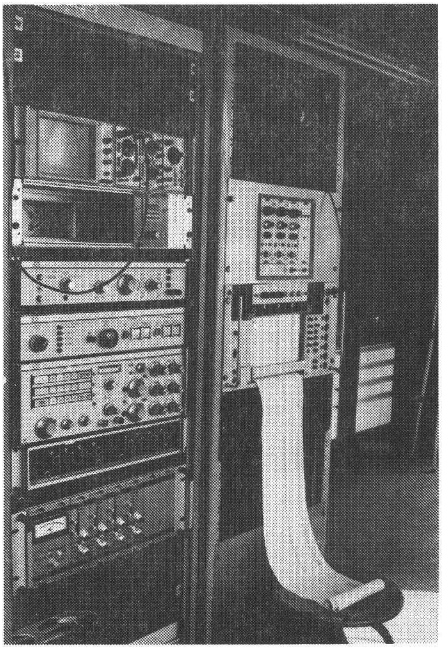

Figure 6.19 *Picture of the System Control and Recording Equipment*

The shape of the load pulse was a haversine and a load to rest period ratio of 1 to 7 was used. During the tests the elastic vertical displacement was continuously recorded (fig. 6.20). Furthermore recordings were made at regular instances of the load displacement curves by means of a x-y recorder (fig. 6.21). However it should be noted that due to limitations of the equipment, this latter was only possible at a loading frequency of 1 Hz.

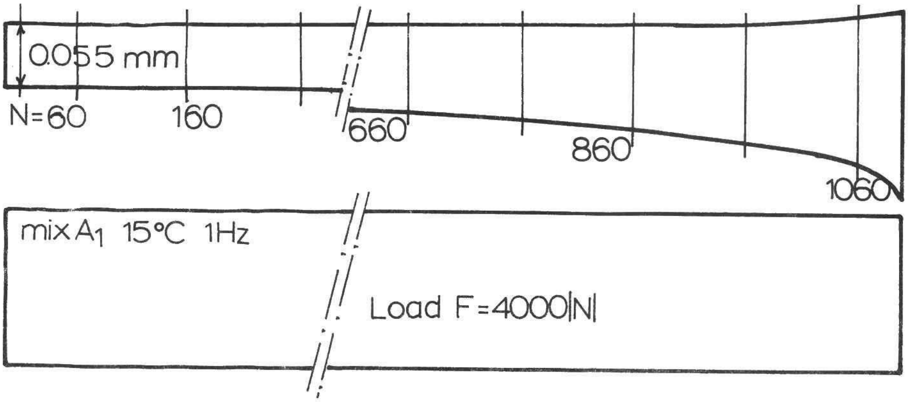

Figure 6.20 *Example of the Continuous Recording of the Elastic Vertical Displacement*

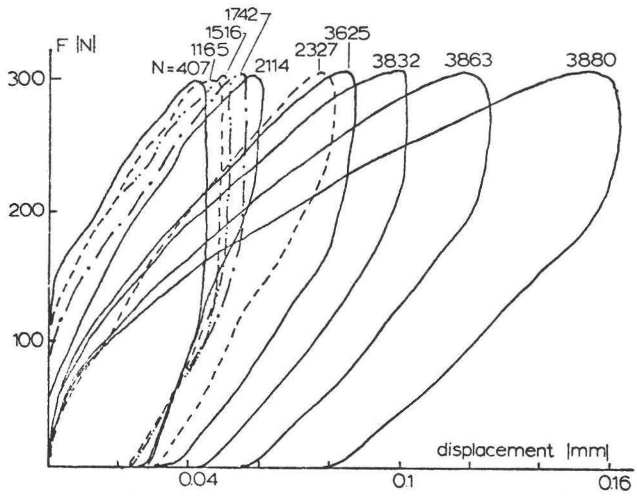

Figure 6.21 Example of the Load vs Displacement Recordings

From the recordings of the elastic vertical deformation, the crack length and associated stress intensity factor was calculated. These calculations will be described in the next section. From the load vs displacement recordings, the amount of energy introduced into the specimen was determined.

Considering the testing program, the following remarks can be made.
From Schapery's visco-elastic crack growth law (eq. 6.18, 6.19, 6.20), it becomes apparent that the so called constants A and n are dependent to a large extent on mix properties, loading frequency and temperature. Considering Schapery's crack growth law one can see that if tests are carried out at a given temperature but at various loading frequencies, only the constant A will be influenced. If however the tests are carried out at a given loading frequency but at various temperatures, especially n and to some extent A will be influenced.
In order to determine the dependency of A and n on temperature and loading frequency, the author decided to carry out the experiments at several frequency and temperature conditions. These are shown in table 6.6.

Table 6.6 Test Conditions used in the Crack Growth Experiments

Mix	5°C/10 Hz	15°C/10 Hz	15°C/1 Hz	25°C/1 Hz
A_1	X	X	X	X
B_1		X	X	
B_3	X		X	
E_4		X	X	
F	X		X	

6.6.3 Calculation of Crack Length and Stress Intensity Factor from the Elastic Vertical Displacement

Appendix 6B contains a detailed description of how the crack length and stress intensity factor can be determined from the increase in elastic deformation. The procedure which has been outlined there, can be resumed as follows:

a. determine the increase in elastic deformation d_n in relation to the number of load application n (fig. 6.20)

b. determine the ratio d_n/d_o; d_o is the elastic deformation on the first load

c. determine the ratio crack length (c) to beam width (b) from the ratio d_n/d_o, by using figure 6.22

d. determine the stress intensity factor K from the ratio d_n/d_o, by using figure 6.23

e. since figure 6.23 is based on a stress level of 1.6 N/mm², the K value as determined in step d. should be corrected for the applied stress level σ according to

$$K_{corrected} = \frac{\sigma}{1.6} * K \qquad \text{eq. 6.26}$$

f. from the increase in crack length in relation to the number of load applications as determined from steps a. to c. and the stress intensity factor at a given crack length, as determined from steps a., b., d. and e., the relation d_c/d_n vs K is determined.

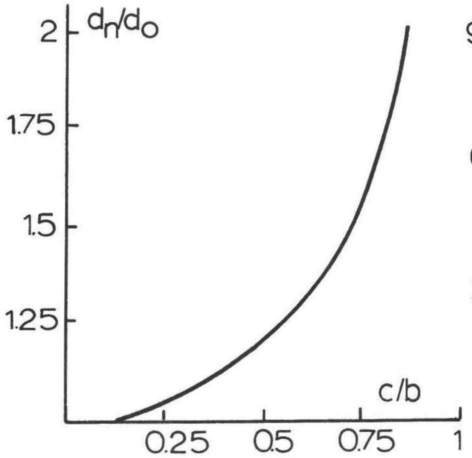

Figure 6.22 Relation between the Displacement Ratio (d_n/d_o) and the Crack Length over Beam Width Ratio (c/b)

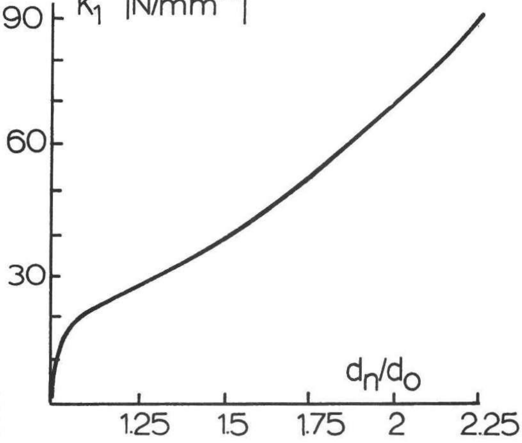

Figure 6.23 Relation between the Displacement Ratio and the Stress Intensity Factor (K_1)

6.6.4 Test Results:

From the applied stress level, the measured initial elastic deformation, the recorded load vs displacement diagrams and the number of load applications, the following fatigue relations were determined.

$$\log N = k_1 + n_1 \log \varepsilon \qquad \text{eq. 6.27}$$
$$\log N = k_2 + n_2 \log \sigma \qquad \text{eq. 6.28}$$
$$\log N = k_3 + n_3 \log W \qquad \text{eq. 6.29}$$

where N = number of load applications to failure
ε = initial strain level as determined from the elastic deformation recorded during the early portions of the crack growth tests
σ = applied stress level (N/mm²)
W = amount of energy introduced into the specimen during the early portions of the crack growth tests as determined from the load vs displacement recordings (N mm)
n_i, k_i, i= 1-3 = constants.

Next to the above mentioned fatigue relations, the stiffness of each mix as occuring under the prevailing loading conditions was calculated.
From the calculated crack lenghts and K values together with the associated number of load applications, the constants A and n from Paris' crack growth law could be determined by means of regression analysis.
We recall Paris' crack growth law

$$dc/dN = AK^{n} \qquad \text{eq. 6.30}$$

where K = stress intensity factor $|N/mm^{3/2}|$
dc/dN = increase in crack length per loading cycle $|mm|$

Table 6.7 summarizes the results obtained in this way.
For the sake of completeness also the mean void content and its coefficient of variation are given.
Typical test results are shown in figures 6.24 to 6.27. To estimate the amount of fracture energy Γ which is needed to produce a unit area of crack, results depicted from figures 6.25 and 6.27 were used. We recall that this parameter Γ is one of the factors which, according to Schapery, governs the magnitude of A (equation 6.19). This will be discussed in detail in the next sections.

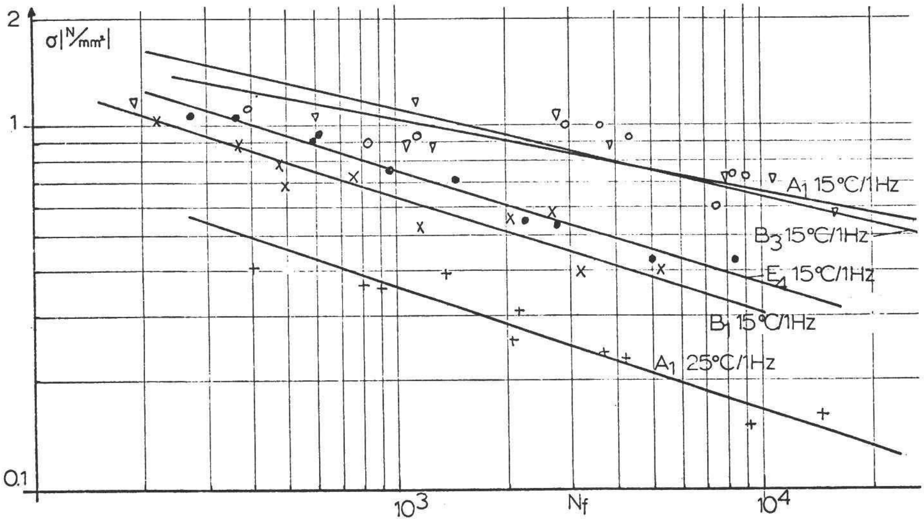

Figure 6.24 *Examples of the Stress based Fatigue Relations obtained from the Crack Growth Experiments*

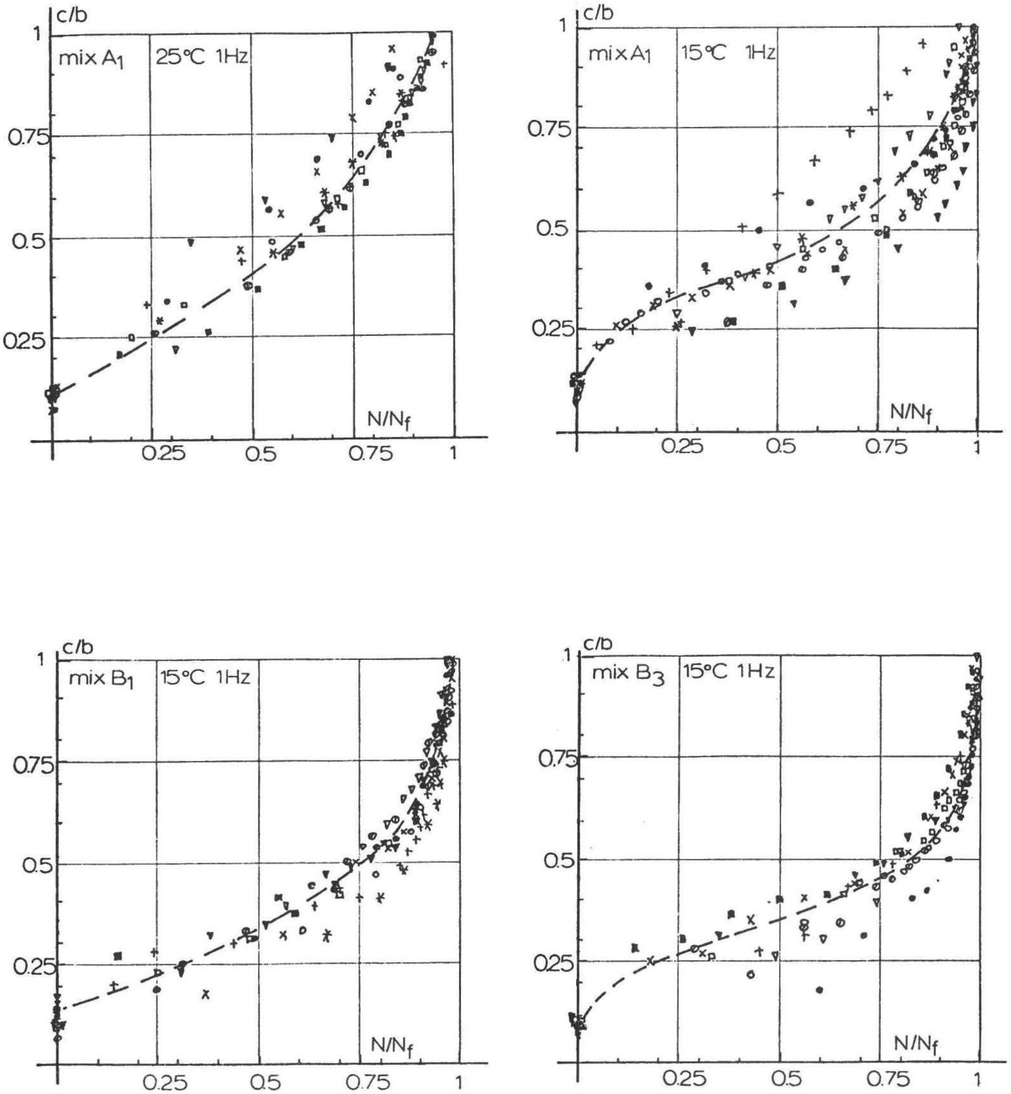

Figure 6.25 *Increase of the Crack Length ÷ Beam Width Ratio (c/b) in relation to the Ratio Applied Number of Load Repetitions (N) ÷ Number of Load Repetitions to Failure (N_f)*

Table 6.7 Results of the Crack Growth Experiments

Mix	temp |°C|	freq |Hz|	E |MPa|	c.v.	log k_1	n_1	log k_2	n_2	k_3	n_3	A	n	void content |%|	c.v.
A_1	25	1	1939	15.6	- 4.386	-2.02	1.686	-2.957	4.798	-1.281	6.394E- 5	2.889	5.76	13.7
	15	1	4084	27.0	- 7.670	-3.014	3.581	-4.246	6.549	-2.387	8.984E- 8	4.026	5.85	12.8
	15	10	8426	31.7	- 9.657	-3.571	4.245	-3.546			1.009E- 9	4.367	5.57	12.9
	5	10	8937	32.2	-12.917	-4.348	4.088	-4.63			5.035E- 9	3.086	6.58	5.6
B_1	15	1	2730	8.1	- 6.997	-2.756	2.392	-3.145	5.43	-1.539	1.673E- 6	3.787	4.72	22.5
	15	10	7951	34.6	- 9.701	-3.308	3.436	-2.611			9.183E- 7	2.882	5.17	11.8
B_3	15	1	4260	12.7	-13.206	-4.487	2.795	-4.876	6.459	-2.175	1.546E- 8	4.767	3.87	16
	5	10	17449	32.2	-17.908	-5.405	5.823	-6.803			2.612E-16	8.696	3.57	15.5
E_4	15	1	2612	11.9	- 6.692	-2.744	2.605	-3.194	5.775	-1.548	3.059E- 6	3.239	4.53	15.1
	15	10	4963	21.2	- 5.82	-2.342	2.799	-2.392			1.403E- 6	2.571	4.24	12.7
F	15	1	238	20.6	- 3.909	-1.842	-0.209	-2.328	3.591	-1.216	4.91 E- 3	2.994		
	5	10	2404	21.5	- 4.682	-1.938	1.778	-1.965			5.161E- 4	1.255		

Note: c.v. = coefficient of variation

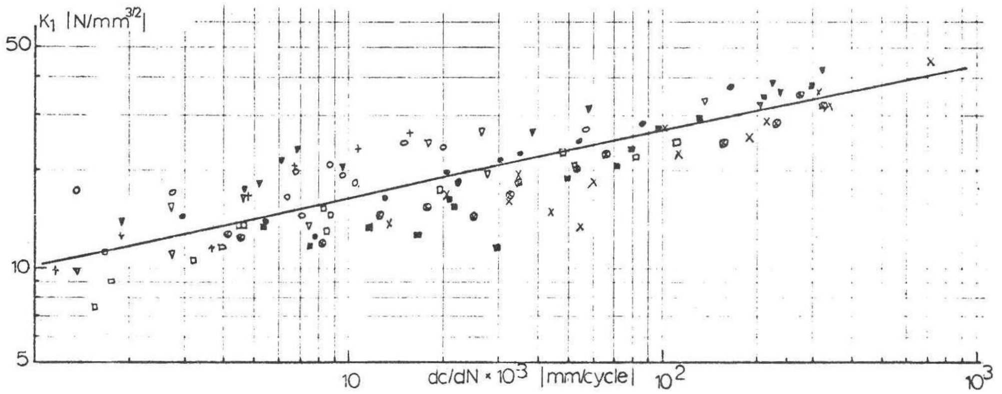

Figure 6.26 *Stress Intensity Factor (K) vs Crack Growth (dc/dN) Relation for Open Asphaltic Concrete (45/60, T = 15°C, f = 1 Hz)*

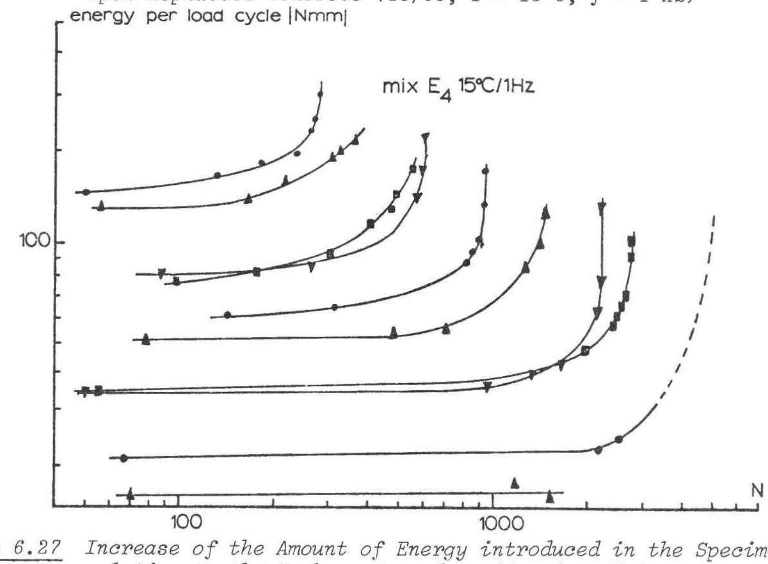

Figure 6.27 *Increase of the Amount of Energy introduced in the Specimen in relation to the Number of Load Applications (N)*

6.6.5 Discussion of the Results

Considering the fatigue and crack growth relations determined from the crack growth tests, it can be observed that in general the absolute values of the factors k_1, n_1, k_2, n_2, A and n increase with increasing stiffness. This is illustrated in figures 6.28, 6.29 and 6.30.
As can be observed k_1, n_1, k_2 and A do correlate reasonable well with the elastic (stiffness) modulus of the mix. The correlation between E and n_2 is much less developed. Hardly no correlation can be observed between E and n.

Very often relations between k_1 and n_1 or k_2 and n_2 can be found in literature |29-35|. Figure 6.31 shows the k_1 vs n_1 relation as determined by means of the experiments described here. Also data points which were taken from other sources are included in figure 6.31. As can be seen from figure 6.31, the data obtained from this study agree well with the data taken from literature.

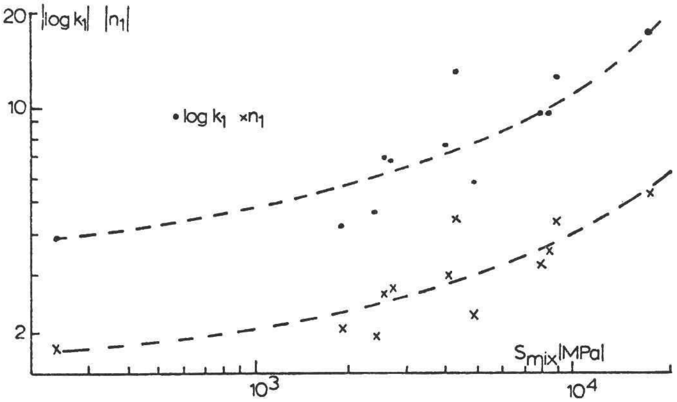

Figure 6.28 Relation between S_{mix} and $|n_1|$, $|log\ k_1|$ resp.

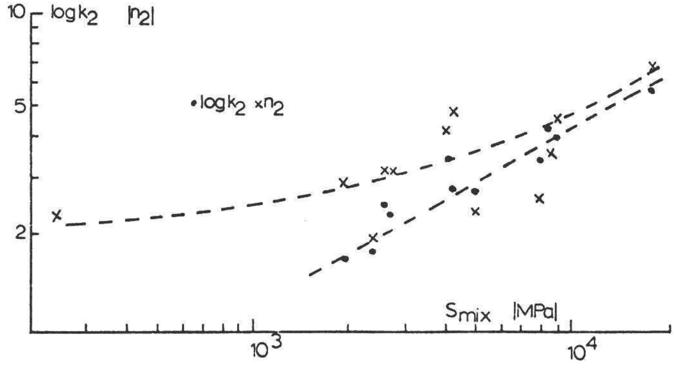

Figure 6.29 Relation between S_{mix} and $|n_2|$, $log\ k_2$ resp.

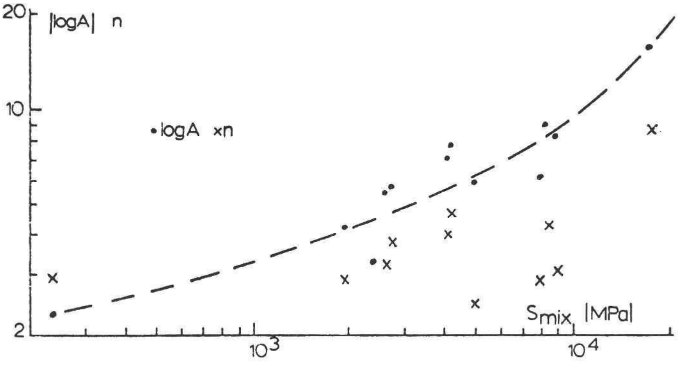

Figure 6.30 Relation between S_{mix} and $|log\ A|$, n resp.

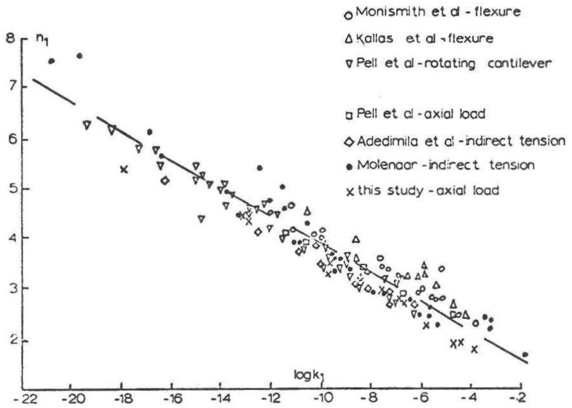

Figure 6.31 *Relation between log k_1 and n_1*

6.6.6 Relation between the Fatigue and Crack Growth Parameters

If we consider the crack growth law

$$\frac{dc}{dN} = A\ K_1^n \qquad \text{eq. 6.31}$$

and we assume a constant load type of test, then equation 6.31 can be rewritten to

$$\frac{dc}{dN} = A\ (\sigma\sqrt{c})^n \qquad \text{eq. 6.32}$$

This is because in a constant load type of test

$$K_1 = \sigma\sqrt{c} \qquad \text{eq. 6.33}$$

From equation 6.32 one obtains

$$\int_1^{N_f} dN = \int_0^b \frac{dc}{A\sigma^n c^{n/2}} \qquad \text{eq. 6.34}$$

and finally one arrives to

$$N_f = \left(\frac{b^{e_o} + c}{e_o\ A}\right)\left(\frac{1}{\sigma}\right)^n \qquad \text{eq. 6.35}$$

where N_f = number of load repetitions to failure
A, n = constant from the crack growth law
b = specimen height
e_o = $(2-n)/2$
c = integration constant

Equation 6.35 is identical to the equation used to describe the fatigue relation based on the applied stress level. Therefore the constants k_2 and n_2 of this fatigue relation can be calculated from

$$k_2 = \frac{b^{e_o} + c}{e_o\ A} \qquad \text{eq. 6.36}$$

and

$$n_2 = n \qquad \text{eq. 6.37}$$

Equation 6.35 can be rewritten to

$$N_f = \left(\frac{b^{e_o} + c}{e_o \; A \; E^n}\right) \left(\frac{1}{\varepsilon}\right)^n \qquad \text{eq. 6.38}$$

which is identical to the expression used to describe the fatigue relation based on applied strain level. Therefore the constants k_1 and n_1 of this fatigue relation can be calculated from

$$k_1 = \frac{b^{e_o} + c}{e_o \; A \; E^n} \qquad \text{eq. 6.39}$$

and

$$n_1 = n \qquad \text{eq. 6.40}$$

From equation 6.36 and 6.40 one arrives to

$$k_1 = k_2/E^n \qquad \text{eq. 6.41}$$

From the derivations given above the following conclusions can be drawn:

<u>a.</u> the exponents of the stress based fatigue relation, strain based fatigue relation and crack growth law should be equal to each other

<u>b.</u> the constant of the stress based fatigue relation is partly dependent on the constant and exponent of the crack growth law and the size of the specimen

<u>c.</u> the constant of the strain based fatigue relation is equal to the constant of the stress based fatigue relation multiplied by a constant which is dependent on the stiffness and the crack growth properties.

In order to illustrate the conclusions mentioned above, figure 6.32 was derived from the available data. This figure shows the correspondence between n_1 and n. Figure 6.33 shows the correspondence between n_2 and n. As can be observed, the agreement between the different n values is reasonable. The n_2 values show a somewhat better agreement with n than the n_1 values.
Figure 6.34 shows the relation between the absolute values of log k_1 as derived from the tests and the log k_1 values calculated by means of equation 6.41.

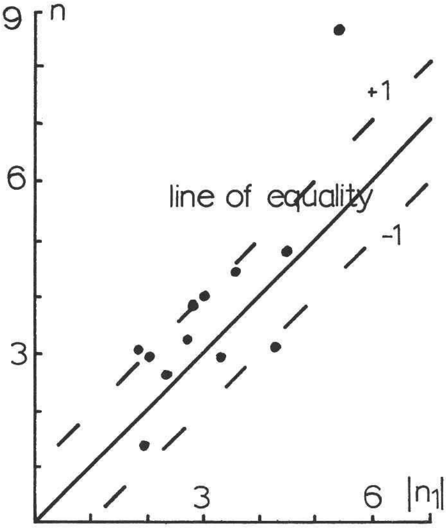

Figure 6.32 *Relation between n_1 and n*

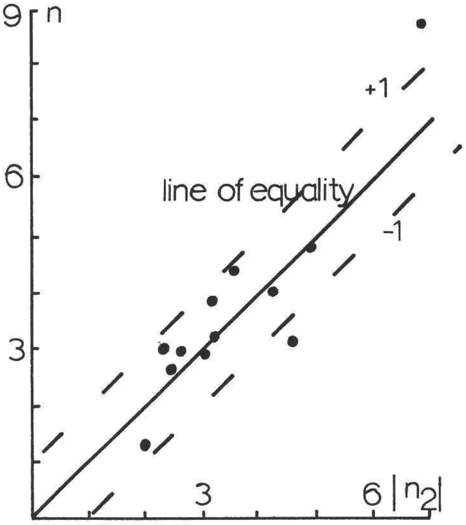

Figure 6.33 *Relation between n_2 and n*

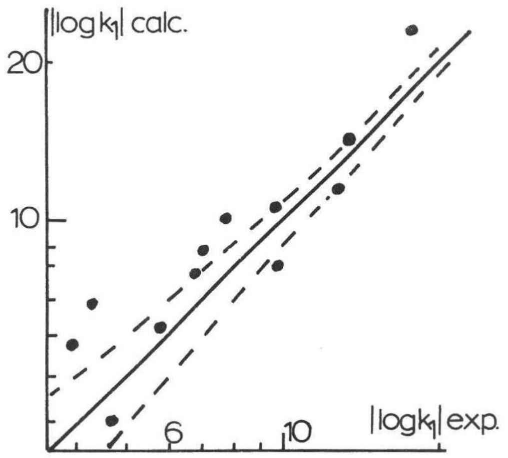

Figure 6.34 *Relation between $k_{1_{experimental}}$ and $k_{1_{calculated}}$ (equation 6.41)*

6.7 Estimation of the Parameters of the Crack Growth Law from Simple Static Tests and Nomographs

It will be obvious that estimating the constants of the crack growth law by means of repeated load testing, is a time consuming and costly affair. In order to be able to use the fracture mechanics approach in the routine practice of for instance overlay design, the assessment of the constants of the crack growth law from simple static testing and/or nomographs is a necessity.
Let us recall the equations developed by Schapery to calculate the constants A and n:

$$A = \frac{\pi}{6\sigma_m{}^2 I_1^2} \left| \frac{(1-\nu^2)D_2}{2\Gamma} \right|^{1/m} \left| \int_0^{\Delta t} w(t)^{2(1+1/m)}\, dt \right| \qquad \text{eq. 6.42}$$

$$n = 2(1+{}^1/m) \qquad \text{eq. 6.43}$$

where σ_m = tensile strength
I_1 = 1.5
Γ = energy needed to produce a unit surface of fracture
D_2 = compliance at t=1 sec
m = slope of the compliance curve
$W(t)$ = wave shape of the stress intensity factor
ν = Poisson's ratio

Values of D_2 and m can be obtained by using the bitumen and mix stiffness nomographs as developed by researchers of Shell Oil Company |27, 36|. Furthermore the tensile strength of the material at the test conditions considered (loading frequency, temperature) can be estimated by means of e.g. indirect tensile tests performed at different temperatures. The tensile strength values should be related to the stiffness of the bitumen (fig. 6.35 |37|) which can be back calculated from the stiffness of the mix. Reversely the bitumen stiffness can be calculated from the loading and temperature conditions. By means of figure 6.35 the appropriate tensile strength can then be determined.

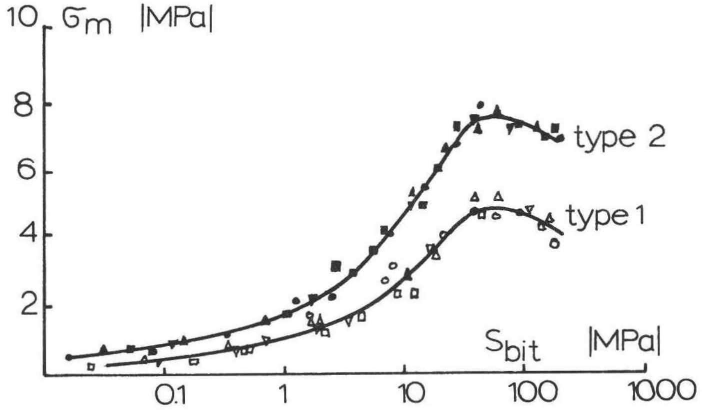

Figure 6.35 *Tensile Strength of Mixes as a Function of the Stiffness Modulus of the Asphalt Cement*

In the subsequent sections the assessment of n by means of nomographs or stiffness modulus tests will be discussed,and it will be shown which correction factors should be applied on these assessed values in order to let them coincide with the experimental values. Next the assessment of A by means of Schapery's equation (eq. 6.42) will be described. Also regression equations which have been developed to estimate A will be presented.

6.7.1 Assessment of n and D_2 from Mix Compliance calculated from Nomographs and determined by means of Repeated Load Tensile and Compressive Tests

By using the van der Poel |36| and modified S_{bit} vs S_{mix} nomograph |27|, the dependency of the mix stiffness on the loading time at given temperatures was determined. From this D_2 and n were calculated. The results are given in table 6.8.

In order to check whether the nomographs produced reliable stiffness estimates, complex modulus test in tension were carried out too. For this the same test set-up was used as in the crack growth tests. However no initial cracks were sawn in the specimens.
The tests were carried out at temperatures of 5, 15, 25 and 35°C, starting at the lowest temperature, and by using a loading frequency schedule of 20, 10, 5, 1, 0.5 Hz. The applied stress level was about 25% of the split tensile strength at the test temperature considered. The number of load repetitions applied at each loading frequency was kept as small as possible in order to prevent fatigue of the specimens. The same specimens were used throughout the whole testing scheme.
From the test results,values for D_2 and n were calculated, and these are given in table 6.9.

Since in many cases the complex modulus tests are carried out in compression, because this type of test is much easier to run, it was of interest to know whether the results of these compressive tests would result in acceptable estimates for D_2 and n. A comparison of these values and those determined by means of the nomographs or the tensile complex modulus test, is given in table 6.10.

Table 6.8 Results of the Nomograph Predictions to determine the Stiffness Modulus

	-5°C			5°C			15°C			25°C			35°C		
	D	m	n	D	m	n	D	m	n	D	m	n	D	m	n
Gravel Sand Asphalt															
A_1	9.911	0.203	11.86	9.665	0.24	10.3	9.345	0.288	8.95	8.912	0.346	7.77	8.268	0.43	6.65
A_2	9.866	0.209	11.58	9.614	0.248	10.08	9.287	0.295	8.79	8.846	0.354	7.65	8.19	0.438	6.57
A_3	9.752	0.224	10.91	9.485	0.264	9.58	9.142	0.312	8.41	8.68	0.372	7.38	7.997	0.457	6.38
Open Asphaltic Concrete															
B_1	9.951	0.186	12.78	9.581	0.256	9.8	9.109	0.336	7.95	8.53	0.422	6.74	7.967	0.451	6.43
B_2	9.712	0.215	11.29	9.296	0.291	8.86	8.773	0.375	7.33	8.14	0.464	6.31	7.532	0.491	6.07
B_3	10.024	0.187	12.69	9.792	0.225	10.9	9.49	0.27	9.4	9.078	0.328	8.1	8.461	0.41	6.88
B_4	9.793	0.219	11.14	9.531	0.258	9.75	9.193	0.306	8.54	8.738	0.366	7.47	8.066	0.45	6.44
Sand Asphalt															
C	9.477	0.261	9.66	9.176	0.302	8.62	8.793	0.352	7.69	8.284	0.413	6.84	7.543	0.5	6
Dense Asphaltic Concrete															
E_1	9.73	0.227	10.79	9.46	0.267	9.49	9.113	0.315	8.35	8.647	0.375	7.33	7.96	0.461	6.34
E_2	9.701	0.217	11.23	9.282	0.293	8.82	8.757	0.377	7.31	8.122	0.466	6.29	7.511	0.493	6.06
E_3	9.939	0.199	12.06	9.969	0.237	10.44	9.38	0.284	9.05	8.952	0.342	7.85	8.314	0.425	6.7
E_4	9.901	0.192	12.43	9.522	0.264	9.58	9.039	0.344	7.81	8.448	0.431	6.64	7.875	0.46	6.35

Note: the regression equation is $\log S_{mix} = D - m \log t$ $\qquad |S_{mix}| = |Pa|$

$$D_2 = \frac{1}{10^D} \qquad |t| = |s|$$

$$n = 2(1 + \frac{1}{m})$$

Table 6.9 Results of the Repeated Load Tensile Tests to determine the Stiffness Modulus

	-5°C			5°C			15°C			25°C			35°C		
	D	m	n	D	m	n	D	m	n	D	m	n	D	m	n
Gravel Sand Asphalt															
A_1				9.828	0.208	11.59	9.488	0.239	10.36	8.903	0.435	6.6	7.958	0.7	4.86
A_2				9.625	0.196	12.2	9.281	0.344	7.81	8.63	0.535	5.74	7.808	0.62	5.22
A_3				9.509	0.241	10.31	9.001	0.358	7.59	8.474	0.487	6.11	7.566	0.574	5.48
Open Asphaltic Concrete															
B_1				9.764	0.139	16.37	9.289	0.319	8.27	8.522	0.63	5.17	7.583	0.669	4.99
B_2				9.325	0.227	9.38	8.864	0.392	7.1	7.946	0.619	5.23	6.901	0.786	4.55
B_3				9.831	0.226	10.86	9.445	0.371	7.39	8.758	0.557	5.59	7.902	0.748	4.68
B_4				9.718	0.174	13.52	9.149	0.471	6.25	8.426	0.625	5.2	7.596	0.716	4.8
Dense Asphaltic Concrete															
E_1				9.959	0.204	11.82	9.359	0.366	7.46	8.607	0.612	5.27	7.703	0.707	4.83
E_2				-	-	-	-	-	-	-	-	-	-	-	-
E_3				9.924	0.13	17.36	9.492	0.478	6.19	8.618	0.634	5.16	7.589	0.762	4.63
E_4				9.641	0.201	11.94	8.981	0.519	5.85	8.145	0.683	4.93	7.643	0.684	4.93
Sand Asphalt															
C				9.635	0.125	17.95	9.324	0.305	8.55	8.739	0.545	6.4	7.982	0.585	5.41
CARPAVE															
F	9.226	0.376	7.32	8.428	0.569	5.52	7.401	0.782	4.56						

Note: the regression equation is $\log S_{mix} = D - m \log t$ $|S_{mix}| = |Pa|$

$D_2 = \frac{1}{10^D}$ $|t| = |s|$

$n = 2(1 + \frac{1}{m})$

Table 6.10 Comparison between the values of D and n as predicted by means of the Nomographs and as determined by means of Repeated Load Tensile and Compressive Tests (nomograph : tensile : compressive)

Gravel Sand Asphalt		5°C	15°C	25°C	35°C
A_1	A	0.687 : 1 : 1.102	0.719 : 1 : 0.953	1.021 : 1 : 1.035	2.042 : 1 : 2.588
	n	0.889 : 1 : 1.553	0.864 : 1 : 1.328	1.117 : 1 : 1.168	1.368 : 1 : 1.42
A_2	A	0.975 : 1 : 0.908	1.014 : 1 : 0.785	1.644 : 1 : 1.466	2.41 : 1 : 3.954
	n	0.826 : 1 : 1.445	1.125 : 1 : 1.241	1.333 : 1 : 1.256	1.259 : 1 : 1.519
A_3	A	0.946 : 1 : 0.723	1.384 : 1 : 1.156	1.607 : 1 : 1.324	2.698 : 1 : 5.047
	n	0.929 : 1 : 1.348	1.108 : 1 : 1.195	1.208 : 1 : 1.098	1.164 : 1 : 1.38
Open Asphaltic Concrete					
B_1	A	0.656 : 1 : 0.695	0.661 : 1 : 1.371	1.019 : 1 : 1.871	2.421 : 1 : 6.18
	n	0.599 : 1 : 1.667	0.961 : 1 : 0.959	1.304 : 1 : 1.315	1.289 : 1 : 1.337
B_2	A	0.935 : 1 : 1.225	0.811 : 1 : 1.39	1.563 : 1 : 3.226	4.276 : 1 : 20.749
	n	0.945 : 1 : 2.845	1.032 : 1 : 1.217	1.207 : 1 : 1.272	1.334 : 1 : 1.695
B_3	A	0.914 : 1	1.198 : 1 : 1.53	2.089 : 1 : 2.371	3.622 : 1 : 4.093
	n	1.004 : 1	1.272 : 1 : 1.468	1.449 : 1 : 1.165	1.47 : 1 : 1.459
B_4	A	0.65 : 1 : 0.471	1.107 : 1 : 1.483	2.051 : 1 : 1.671	2.951 : 1 : 5.61
	n	0.721 : 1 : 1.868	1.366 : 1 : 1.995	1.437 : 1 : 1.427	1.346 : 1 : 1.635
Sand Asphalt					
C	A	0.348 : 1	0.294 : 1 : 0.699	0.351 : 1 : 1.028	0.364 : 1 : 1.914
	n	0.48 : 1	0.899 : 1 : 1.242	1.069 : 1 : 1.383	1.109 : 1 : 1.734
Dense Asphaltic Concrete					
E_1	A	0.317 : 1 : 0.308	0.599 : 1 : 0.8	1.096 : 1 : 1.309	0.553 : 1 : 3.342
	n	0.803 : 1 : 1.667	1.119 : 1 : 1.345	1.391 : 1 : 1.376	1.313 : 1 : 1.59
E_2		-	-	-	-
E_3	A	0.59 : 1	0.773 : 1 : 0.499	2.158 : 1 : 1.489	4.217 : 1 : 2.931
	n	0.601 : 1	1.462 : 1 : 5.006	1.521 : 1 : 1.312	1.447 : 1 : 1.652
E_4	A	0.76 : 1 : 0.631	1.143 : 1 : 1.315	2.009 : 1 : 2.655	1.706 : 1 : 2.799
	n	0.802 : 1 : 1.894	1.335 : 1 : 1.214	1.347 : 1 : 1.205	1.288 : 1 : 1.588
CARPAVE					
F	A	1 : 0.94	1 : 4.064		
	n	1 : 1.761	1 : 1.408		

Note: the D values stand for S_{mix} at t=1s. The comparisons are based on the real D values and not on the logarithmic values.

From table 6.10 it can be concluded that the n values estimated from the compressive complex modulus tests are always over estimated. The n values as determined by means of the nomographs are much closer to the n values determined from the tensile complex modulus test. However a systematic deviation can be observed,since at lower values the nomograph determined n values are somewhat underpredicted while at higher temperatures this n value is somewhat overpredicted.

The best agreement between the experimentally determined n values (both compressive and tensile test results) and the values determined by means of the nomographs is obtained at a testing temperature of 15°C.

Much larger deviations are observed between the experimentally determined and nomograph predicted D_2 values. At higher temperatures, especially the "compressive" D_2 values differ considerably from the "tensile" values.

Finally it is concluded from table 6.10 that candidate values of n can be determined with reasonable accuracy by using nomographs. However care should be taken with the D_2 values assessed by means of the nomographs,since they can differ considerably from the "tensile" D_2 values especially at temperatures other than "room temperature" (= 18°C).
It is advised not to use the results of compressive complex modulus tests to estimate D_2 and n since in most cases this results in values which are too high.

6.7.2 Comparison of Estimated and Experimentally determined n Values

Although the n values estimated from nomographs and calculated from tensile complex modulus tests are in rather good agreement, they do differ considerably from the n values as calculated from the crack growth experiments. Table 6.11 gives an overview of the n values together with the mean void content of the mixes tested in the crack growth test. It is believed that the differences between the experimentally and estimated n values, should be contributed to the difference between theory and practice mainly. Although Schapery derived his theory for visco-elastic materials it is not fully applicable to asphaltic mixes since these contain voids, aggregate particles which in most cases force the crack to propagate around the particles etc. Especially the void content seems to have an influence on the crack growth rate since most of the difference between the experimentally determined and estimated n values could be explained by this factor (figure 6.36). The correction factor,by which the n values as determined from the tensile complex modulus test need to be divided to obtain n values which might be obtained from crack growth tests, can be calculated by

$$\text{C.F.} = -0.93 + 0.65\ \text{V.C.} \qquad r = 0.93 \qquad \text{eq. } 6.44$$

C.F. = correction factor
V.C. = void content (%)

It should be noted that the data point marked with a question mark (mix F tested at 15°C/1 Hz) was not taken into account in deriving the above mentioned regression equation. The reason why this data point doesn't fit in the relation should, to the opinion of the author, be contributed to the uncommon properties of this mix. It is recalled that this mix has a very high flexibility which is caused by the additives that are mixed with the bitumen. From the developed regression equation, it can be concluded that at void content ratio's of 3% and lower,no correction factor needs to be applied on the estimated n values.

Table 6.11 *Comparison of Experimentally determined and Estimated Values of n*

Mix	V.C.(%)	T(%)	f(Hz)	n_{cg}	n_n	$\frac{n_n}{n_{cg}}$	n_{tcm}	$\frac{n_{tcm}}{n_{cg}}$
A_1	5.77	25	1	2.89	7.77	2.69	6.6	2.28
	5.85	15	1	4.03	8.95	2.22	10.36	2.57
	5.57	15	10	4.37	8.95	2.05	10.36	2.37
	6.58	5	10	3.09	10.3	3.33	11.59	3.75
B_1	4.72	15	1	3.79	7.95	2.1	8.27	2.18
	5.17	15	10	2.88	7.95	2.76	8.27	2.87
B_3	3.87	15	1	4.77	9.4	1.97	7.39	1.55
	3.57	5	10	8.70	10.9	1.25	10.86	1.25
E_4	4.53	15	1	3.24	7.81	2.41	5.85	1.81
	4.24	15	10	2.57	7.81	3.04	5.85	2.28
F	*	15	1	2.99			4.56	1.53
		5	10	1.26			5.52	4.38

Note: V.C. = void content
* V.C. ≅ 8% (according to producer)
n_{cg} = n as determined from crack growth tests
n_n = n as determined from nomographs
n_{tcm} = n as determined from tensile complex modulus tests

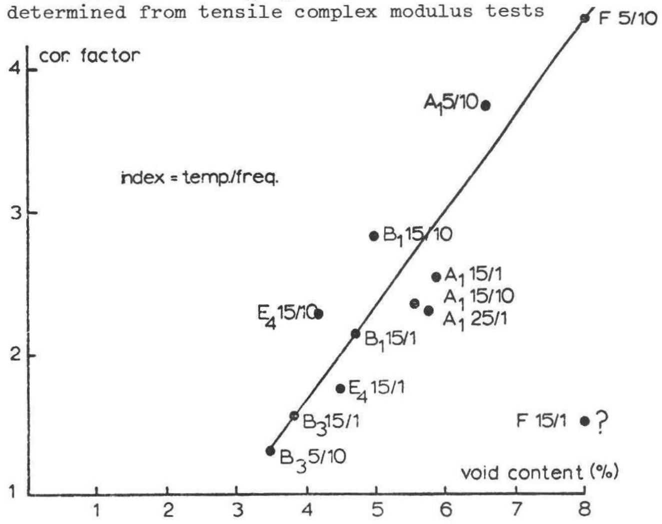

Figure 6.36 *Relation between the Void Content and the Correction Factor which should be applied on Values of n determined from Nomographs or Stiffness Modulus Tests*

6.7.3 Estimation of A using Nomographs and Static Tests

As has been shown before, the constant A of the crack growth law, is dependent on a large number of factors. They are

Γ = energy to produce a unit surface of fracture
σ_m = tensile strength
D_2 = compliance at t=1 sec
ν = Poisson's ratio, which is set at 0.35
$w(t)$ = shape of the stress intensity pulse
I = constant which is set at 1.5
m = slope of the creep compliance curve

In the following sections, it will be shown how each of these factors can be estimated from nomographs or static tests and it will also be shown to what extent the constant A,as derived using the above mentioned factors, matches the A factor which is derived using the results of the crack growth tests.

6.7.3.1 Estimation of Γ

First of all Γ was calculated using the load vs displacement curves which were recorded during the crack growth experiments carried out at 15°C and 1 Hz. This was realised in the following way.
The increase in dissipated energy during the tests was, according to figure 6.27, described by

$$\log W_n/W_o = a_o + a_1 \log (1-n/N) \qquad \text{eq. 6.45}$$

where W_n = energy dissipated at the nth loading cycle
W_o = energy dissipated at the first loading cycle
a_o, a_1 = constants

Then the increase in crack length during the tests was, according to figure 6.25 described by

$$\log c/b = a_o + a_1 \log n/N \qquad \text{eq. 6.46}$$

or

$$\log c/b = a_o + a_1 \log (1-n/N) \qquad \text{eq. 6.47}$$

where c = crack length
b = beam width
n = applied number of load applications
N = number of load applications to failure
a_o, a_1 = constants

The choice of the model to be used was dependent on the magnitude of the correlation coefficient.
By assuming a value of N, the increase of energy per load cycle of W (ΔW) and c (Δc) could be calculated. The increase in cracked surface per load cycle was calculated by multiplying Δc with two times the width of the specimen b. It will be clear that Γ follows from

$$\Gamma = \frac{\Delta W}{2b\Delta c} \qquad \text{eq. 6.48}$$

Table 6.12 summarizes the Γ values obtained in this way.

In order to be able to estimate Γ from nomographs and static tests, a relation was developed between Γ and σ_m, E and n because these parameters represent the strength, deformation and crack growth characteristics of the material.

Table 6.12 *Values of Γ as determined from the Crack Growth Experiments*

Mix	T|°C|	f|Hz|	Γ|Nmm/mm²|
A_1	25	1	7.625 E-4
	15	1	1. E-2
B_1	15	1	1.101 E-2
B_3	15	1	1.937 E-2
E_4	15	1	1.674 E-3
F	15	1	1.259 E-4

Having studied several equations, the author decided that best estimates for Γ could be obtained from

$$\log \Gamma = -6.181 + 0.938 \log E.\sigma_m.n \qquad r= 0.98 \qquad \text{eq. 6.49}$$

(Γ) = |Nmm/mm²|

n = exponent of the crack growth law corrected for influence of void content

σ_m = tensile strength of the material given the loading conditions (see par. 6.7.3.2) |MPa|

E = stiffness modulus of the material given the loading condition. |MPa|

This relation is given in figure 6.37. The used data are given in table 6.13.

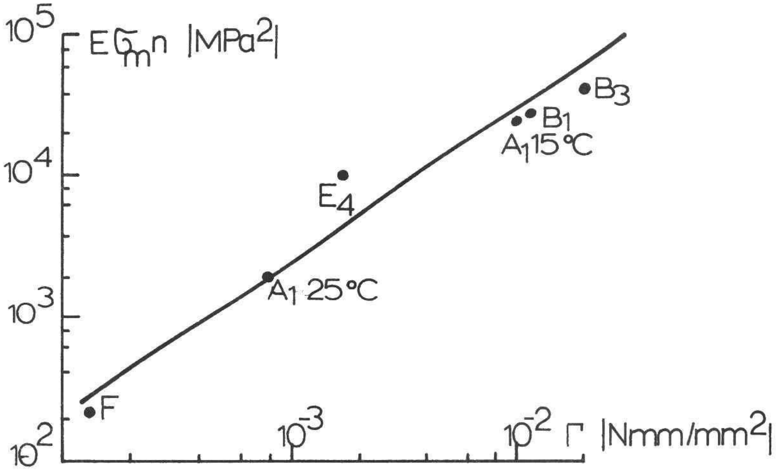

Figure 6.37 *Relation between the product $E.\sigma_m.n$ and Γ*

Table 6.13 *Data used to develop the $E.\sigma_m.n$ vs Γ Relation*

Mix	T|°C|	f|Hz|	Γ|Nmm/mm²|	E|MPa|	σ_m|MPa|	n_{exp}
A_1	25	1	7.625 E-4	1939	0.35	2.89
	15	1	1. E-2	4084	1.5	4.03
B_1	15	1	1.101 E-2	2730	2.6	3.79
B_3	15	1	1.937 E-2	4260	2	4.77
E_4	15	1	1.674 E-3	2612	1.15	3.24
F	15	1	1.259 E-4	238	0.30	2.99

Resuming the foregoing, it can be stated that for normal asphaltic concrete mixes, Γ can be estimated by means of nomographs and simple static tests.

6.7.3.2 Estimation of σ_m

As has been indicated before, σ_m can be obtained from indirect tensile tests performed at different temperature levels. From the test conditions, S_{bit} can be determined and then a relation between S_{bit} and σ_m can be developed. This relation can be used to estimate σ_m at given loading frequencies and temperatures. Figure 6.38 shows the S_{bit} vs σ_m relations as determined for the mixes considered here.

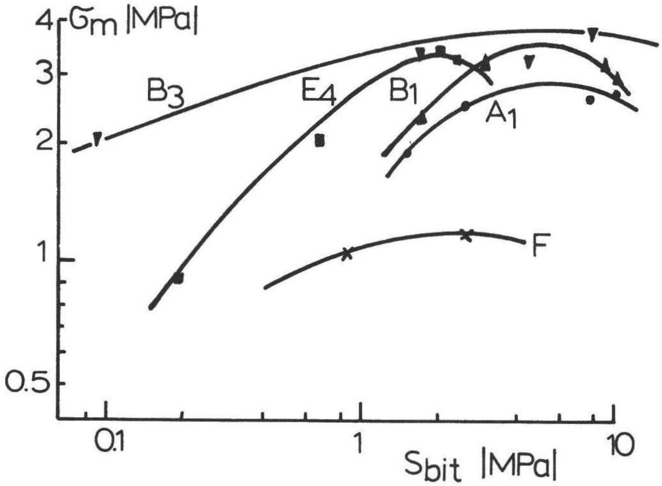

Figure 6.38 Relation between S_{bit} and σ_m

6.7.3.3 Estimation of D_2 and m

The estimation of D_2 and m from nomographs has already been discussed in section 6.7.1.

6.7.3.4 Estimation of $\int|w(t)|^n dt$

Since the shape of the load pulse was a haversine, the shape of the stress intensity function $|w(t)|$ is a haversine too. The way in which the function $|w(t)|^n$ is influenced by the magnitude of n is illustrated in figure 6.39. For load pulses having a frequency of 1 Hz and 10 Hz the area enclosed by the $|w(t)|^n$ curve was calculated for several values of n. It showed that the magnitude of this area was dependent on n in the following way

$$\log \int|w(t)|^n \, dt = -0.2696 - 0.1825 \log n. \quad (\ 1\ \text{Hz}) \qquad \text{eq. } 6.50$$

$$\log \int|w(t)|^n \, dt = -1.2696 - 0.1825 \log n. \quad (10\ \text{Hz}) \qquad \text{eq. } 6.51$$

6.7.3.5 Estimation of A from Nomographs and Static Test Results Comparison with the Experimentally derived Values

The relations derived in the previous sections were used to calculate tne A values for the mixes considered in the crack growth test program. These values were then compared with the A values as obtained from the results of the crack growth tests themselves. The results are shown in table 6.14.

Table 6.14 *Comparison of the A Values calculated from the Nomographs etc. and A Values obtained from Crack Growth Experiments*

Mix	T|°C|	f|Hz|	S_{bit} |MPa|	σ_m |MPa|	v.c. |%|	n_{nom}	n_{cor}	$\int w(t)^n dt$	I_1	S_{mix} |MPa|	Γ|Nmm/mm²|	D_2|mm²/N|	ν	$\frac{1}{m}$	A_{calc}	A_{exp}
A_1	25	1	2	0.35	6.79	7.77	2.23	0.464	1.5	1038	3.53 E-4	1.23 E-3	0.35	2.89	2.98	6.39 E-5
	15	1	10	1.5	6.79	8.95	2.57	0.452	1.5	2702	3.87 E-3	4.52 E-4	0.35	3.47	1.55 E-6	8.98 E-8
	15	10	40	2.7	6.79	8.95	2.57	0.0452	1.5	5244	1.25 E-2	4.52 E-4	0.35	3.47	8.17 E-10	1.01 E-9
	5	10	150	2.7	6.79	10.3	2.98	0.0441	1.5	9489	2.49 E-2	2.16 E-4	0.35	4.17	1.16 E-13	5.04 E-9
B_1	15	1	3	2.6	5.44	7.95	3.05	0.439	1.5	1622	4.71 E-3	7.78 E-4	0.35	2.98	6.04 E-8	1.67 E-6
	15	10	15	3.2	5.44	7.95	3.05	0.0439	1.5	3526	1.18 E-2	7.78 E-4	0.35	2.98	2.55 E-8	9.19 E-7
B_3	15	1	10	2	4.82	9.4	4.27	0.412	1.5	3726	1.1 E-2	3.24 E-4	0.35	3.70	2.42 E-9	1.55 E-8
	5	10	150	2.7	4.82	10.9	4.95	0.0401	1.5	12154	5.11 E-2	1.61 E-4	0.35	4.44	2.6 E-16	2.61 E-16
E_4	15	1	3	1.15	4.53	7.81	3.87	0.442	1.5	1389	2.37 E-3	9.14 E-4	0.35	2.91	4.39 E-4	3.06 E-6
	15	10	15	3.3	4.53	7.81	3.87	0.0442	1.5	3066	1.34 E-2	9.14 E-4	0.35	2.91	3.47 E-8	1.4 E-6
F	15	1	0.37	0.3	8	4.56	1.07	0.531	1.5	200	9.5 E-5	3.97 E-2	0.35	1.28		4.91 E-3
	5	10	20	1.1	8	7.4	1.73	0.0486	1.5	2100	8.6 E-4	3.73 E-3	0.35	1.76	2.86 E-2	5.16 E-4

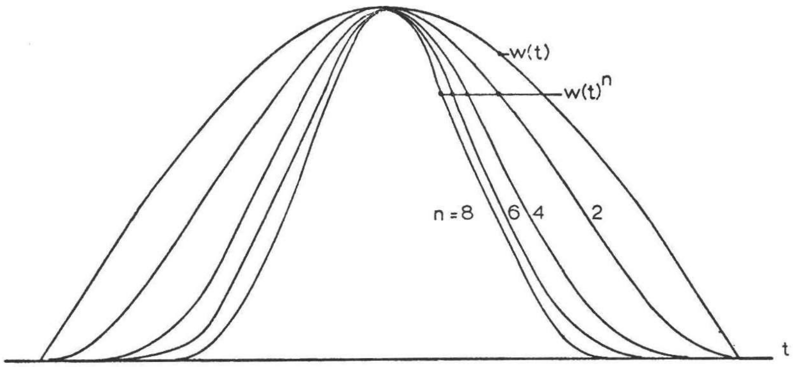

Figure 6.39 $|w(t)|^n$ *in relation to n*

It should be noted that S_{bit} is estimated from the test conditions and σ_m is estimated from the derived S_{bit} vs σ_m relations. The void content was the mean value of all specimens tested under static and dynamic loading conditions. The n_{nom} values were taken from table 6.8 while the corrected n values were obtained by using equation 6.44. Values for $\int|w(t)|^n$ dt were obtained by using equations 6.50 and 6.51. The S_{mix} values were obtained from the loading conditions together with table 6.8. The fracture energy was calculated from equation 6.49. The creep compliance at t=1 sec was obtained from table 6.8 as was the case for the 1/m values.
The relation between log A as calculated in this way and log A as determined from the experimental results is shown in figure 6.40. As can be seen from this figure the agreement is not very good.

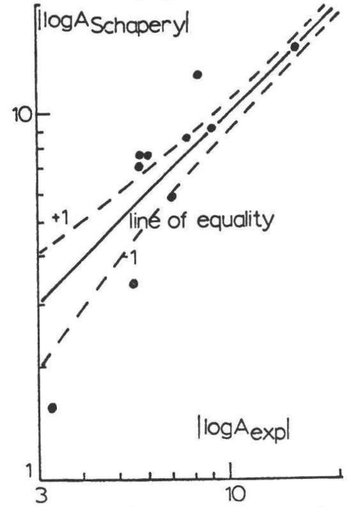

Figure 6.40 *Relation between* $|log\ A_{exp}|$ *and* $|log\ A|$ *as determined by means of Schapery's Equation*

6.7.4 Estimation of A by means of Regression Equations

Since the calculation of A by means of Schapery's equation is more or less complicated and since the agreement between A_{exp} and A_{calc} is not very good, it was decided to develop regression equations for the estimation of A. The first equation which was developed is a relation between the exponent of the crack growth law n,and A. This relation is

$$|\log A| = 0.977 + 1.628\, n \qquad r = 0.94 \qquad \text{eq. } 6.52$$

A graphical representation is given in figure 6.41. The relation is of the same shape as the one between n_1 and log k_1 as shown in figure 6.31.

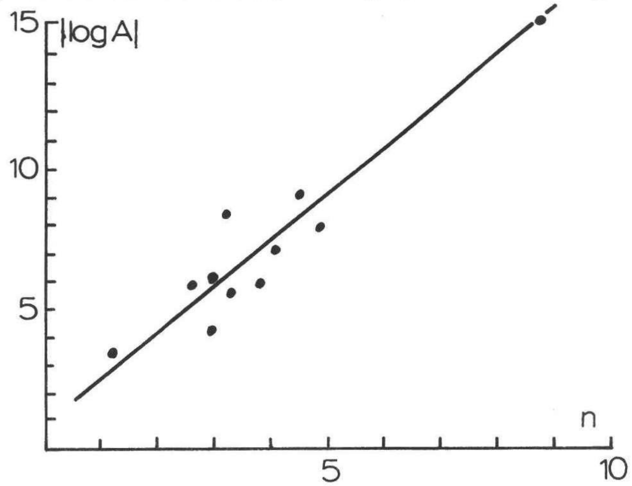

Figure 6.41 *Relation between n and log A*

Also an equation was developed by which it is possible to estimate A from nomographs and static tests. This equation is

$$\log A = 4.389 - 2.52 \log E.\sigma_m.n \qquad r = -0.96 \qquad \text{eq. } 6.53$$

where A = constant of the crack growth law
σ_m = tensile strength of the material at the given loading conditions |MPa|
n = exponent of the crack growth law
E = stiffness modulus of the material at the given loading conditions |MPa|

To develop this equation, the data as given in table 6.13 were used together with the experimentally derived A values as given in table 6.7. A graphical representation of the equation is given in figure 6.42.

The capabilities of equation 6.53 to predict acceptable A values was tested by means of the remaining data given in table 6.7. The E and n values for the 15°C/10 Hz and 5°C/10 Hz tests together with the appropriate σ_m values were introduced in equation 6.53. The A values calculated in this way were compared with the experimentally determined values. The results are shown in figure 6.43 and table 6.14.

From this comparison it was concluded that equation 6.53 predicts A values with a reasonable accuracy.
From table 6.15 it can also be concluded that there is no need to modify the regression equation in order to take into account the shape of the stress intensity wave.

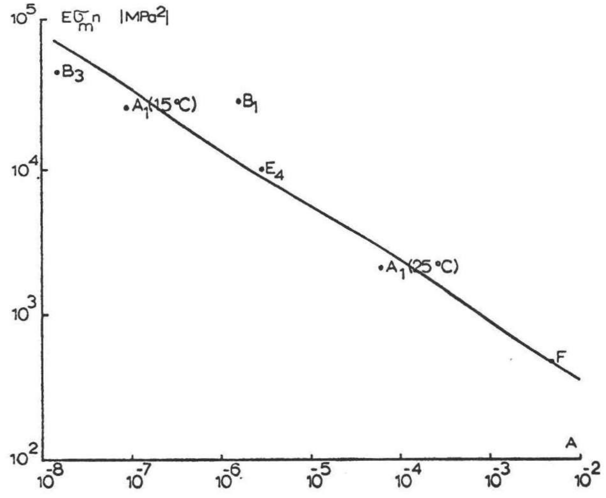

Figure 6.42 *Relation between $E.\sigma_m.n$ and A*

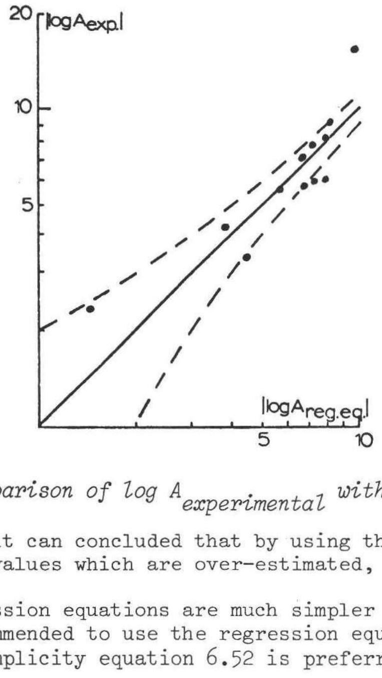

Figure 6.43 *Comparison of log $A_{experimental}$ with log $A_{regr.\ equation}$*

From table 6.15 it can concluded that by using the regression equation one obtains usually A values which are over-estimated, so A values which are on the "safe side".
Since both regression equations are much simpler in use than Schapery's equation, it is recommended to use the regression equations for the assessment of A. Due to its simplicity equation 6.52 is preferred over equation 6.53.

6.7.5 Conclusions on the Assessment of A and n from Nomographs and Static Tests

From the material presented in section 6.7, it can be concluded that the constants A and n can indeed be estimated from nomographs and simple static tests.

Table 6.15 Comparison of the Experimentally determined A values with those calculated by means of the Regression Equation (eq. 6.53)

Mix	T|°C|	f|Hz|	$A_{exp.}$	$A_{reg.eq.}$
A_1	25	1	6.39 E-5	1.23 E-4
	15	1	8.98 E-8	2.09 E-7
		10	1.01 E-9	6.25 E-9
	5	10	5.04 E-9	1.29 E-8
B_1	15	1	1.67 E-6	1.68 E-7
		10	9.18 E-7	1.34 E-8
B_3	15	1	1.55 E-8	5.96 E-8
	5	10	2.61 E-16	1.76 E-10
E_4	15	1	3.06 E-6	2.18 E-6
		10	1.40 E-6	5.44 E-8
F	15	1	4.91 E-3	3.29 E-2
	5	10	5.16 E-4	3.28 E-5

The nomographs to be used are the van der Poel nomograph and the S_{bit} vs S_{mix} nomographs as developed by researchers of Shell Oil Company. The static tests involved are indirect tensile tests performed at several temperatures in order to obtain S_{bit} vs σ_m relations. From the results presented it becomes obvious that the mix properties and especially the void content, do have a pronounced influence on the results. Since the predictions are rather sensitive to changes in void content, special care should be taken in preparing test specimens and assuming mix properties for nomograph predictions. Both the assumed composition and the composition of the test specimens, should match closely the mix composition in the field.

6.8 Summary and Conclusions

In this chapter the need for the application of fracture mechanics in the design of overlays has been described. Furthermore attention has been paid to the assessment of the fracture behaviour of common Dutch asphaltic mixes tested both under dynamic and static loading conditions. Special consideration has been given to the assessment of crack growth properties using nomographs and static test results,since the availability of such relations would stimulate the use of fracture mechanics principles in designing pavements and overlays related to the cracking behaviour of asphalt mixes.

From the experimental work it can be concluded that

a. Crack growth characteristics of asphalt mixes are heavily dependent on the mix composition.

b. Schapery's crack growth theory, which can be seen as a theoretical justification of the empirical Paris'crack growth law, can be used to estimate the constants A and n from the crack growth law provided that the effect of voids is taken into account.

c. For practical purposes A can also be estimated by means of a regression equation which relates A to n and an equation which relates A to σ_m, E and n.

d. Although fracture toughness tests give a better insight in the fracture properties of asphalt mixes than the indirect tensile tests, this latter test is recommended since it is much easier to perform and since it enables testing of cores taken from the pavement. Furthermore the indirect tensile test provides data which enable the estimation of A.

e. Since the estimates of A and n are rather sensitive to changes in mix compositions, special attention should be given to the conformity of the designed mix to the mix in the field.

Appendix 6A

Description of the ASTM Procedure to Determine K_{Ic} Values from Three Point Bending Tests

6.A.1 Description of the ASTM Procedure to Determine K_{Ic} Values from Three Point Bending Tests

ASTM has developed a procedure |19| to determine the K_{Ic} values from direct tensile as well as from beam bending tests. This procedure will be described hereafter.

Let us assume a load displacement graph like the one given in figure 6.A.1. The secant line OP_x is drawn with a slope which is less steep than the slope of line OA. The slope of line OP_x is dependent on the ratio crack depth (c) over specimen height (b) and on the type of test (fig. 6.A.2).

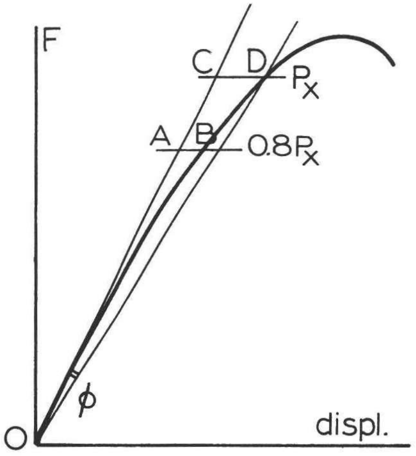

Figure 6.A.1 *Procedure to calculate K_{Ic} Values*

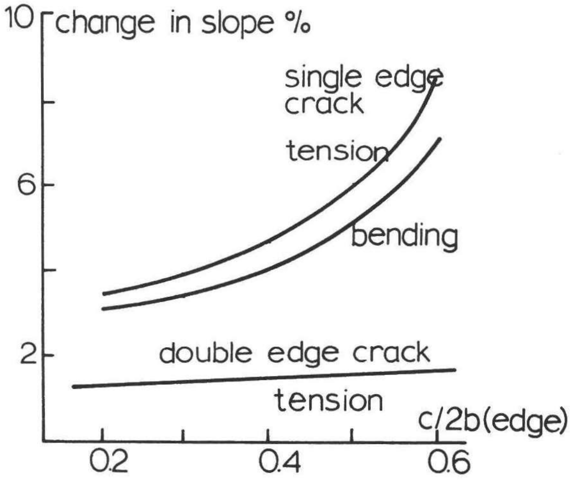

Figure 6.A.2 *Dependency of ϕ on Ratio c/b and Test Conditions*

Next a horizontal line is drawn at $F=0.8\ P_x$. In order to obtain a "valid" K_{Ic}, distance AB should be less or equal to 0.25 times the distance CD.

Then K_ϕ is calculated from P_x (see equation 6.2). It should be checked whether or not

$$2.5(K_\phi/\sigma_e)^2 < t$$

and

$$2.5(K_\phi/\sigma_e)^2 < 2a$$

where σ_e = yield stress
t = specimen thickness
$2a$ = crack length
K_ϕ = candidate fracture toughness value

When these conditions are fulfilled, then

$$K_{Ic} = K_\phi$$

If one of these conditions is not fulfilled or when the test should be considered to be invalid then K_ϕ is a candidate value for K_{Ic} |6|.

Appendix 6B

Evaluation of Five Types of Test on their Applicability for Crack Growth Experiments

6.B.1 Introduction

In this appendix the results will be given of a theoretical analysis on the applicability of different types of tests to be used in a crack growth experiment. The analysis was carried out by means of the finite element program described in |14|. Subsequently, the following tests will be discussed

a. three point bending test
b. beam on elastic foundation test
c. pure shear test
d. indirect tensile test
e. direct tensile test.

It will be shown how the results of the analysis can be used in order to determine the crack length and stress intensity factor from the increase of the measured elastic displacements.

6.B.2 Three Point Bending Test

An example of the finite element mesh which was used to simulate the three point bending test is given in figure 6.B.1. Calculations were made for the uncracked beam and for cracked beams with different crack lengths. A constant load type of test was assumed. Figure 6.B.2 shows the increase in deflection at mid span in relation to the crack length (c) over beam height (b) ratio. Figure 6.B.3 shows the increase in the K value in relation to the increase of the c/b ratio. Figure 6.B.4 shows the increase of the normalized value $K_I/\sigma\sqrt{b}$ in relation to the increase of the c/b ratio as calculated by means of the finite element program. This figure also shows the $K_I/\sigma\sqrt{b}$ vs c/d relation as calculated by means of equation 6.2. The agreement between both relations is considered to be good. Although this type of test might be considered for use in crack growth experiments, it was not selected in this research program since it was believed that the dead weight of the specimen, which is neglected so far, has a marked influence on the K values.

6.B.3 Beam on Elastic Foundation Test

An example of the finite element mesh which was used to simulate the beam on elastic foundation test is given in figure 6.B.5. Again calculations were made for the uncracked specimen as well as for cracked specimens with different crack lengths. As indicated in figure 6.B.5, both bending as well as shearing load conditions were studied. Also here a constant load type of test was assumed. Figure 6.B.6 shows the increase in deflection as well as the increase in curvature in relation to the crack length ÷ beam height ratio. One should note the S shaped increase of the maximum deflection and the surface curvature index! It is believed that these results give evidence to the structural performance model which was stipulated in chapter 3. Figure 6.B.7 shows the variation of the K_1 and K_2 values in relation to the c/d ratio. As could be expected, the K_2 rapidly increases with increasing crack length. The K_1 values are decreasing if the c/d ratio is larger than 0.5. This is because the crack tip reaches the compressive zone. It should be noted that the K_1 vs c/d ratio as developed here is very different from the one assumed by Majidzadeh et al. in their analysis of the crack growth in a number of mixes |6, 7|. They assumed that for beams on elastic foundation tests the relation K_1 vs c/d could be described by means of figure 6.B.4. This figure can only be used if full slip conditions occur at the interface between the asphaltic beam and the rubber subgrade. It is believed that although precautions are taken, full slip conditions are not likely to occur. Therefore it is strongly advised to glue the asphaltic beam to the rubber subgrade in order to be sure that perfect adhesion occurs as was assumed in the calculations performed here.

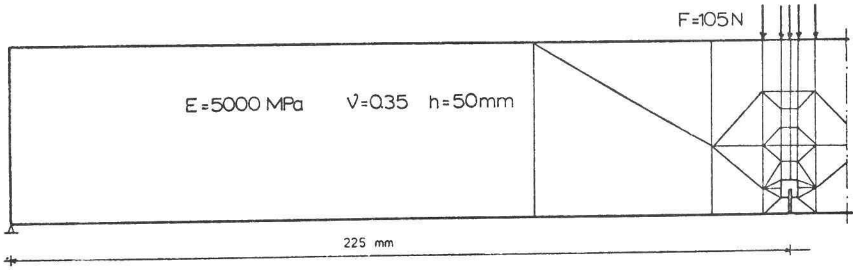

Figure 6.B.1 *Finite Element Mesh used in the Simulation of the Three Point Bending Test*

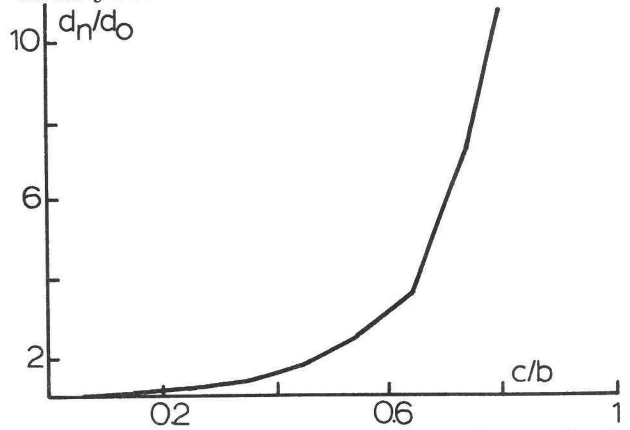

Figure 6.B.2 *Increase of Deflection Ratio in relation to the Increase of the Crack Length Ratio (c/b)*

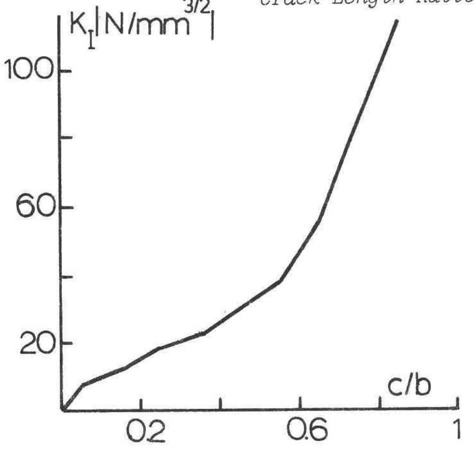

Figure 6.B.3 *Increase of K_I in relation to the c/b Ratio*

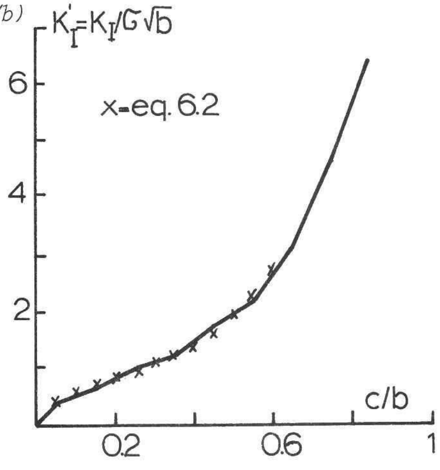

Figure 6.B.4 *Relation between the c/b Ratio and the normalized K_I (K'_I)*

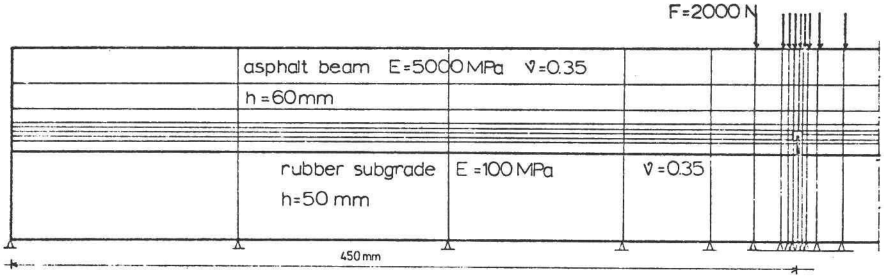

Figure 6.B.5 *Finite Element Mesh used in the Simulation of the Beam on Elastic Foundation Test*

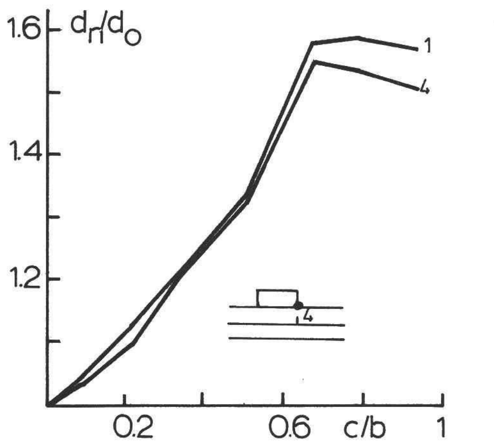

Figure 6.B.6a *Increase of the Deflection Ratio in relation to the c/b Ratio*

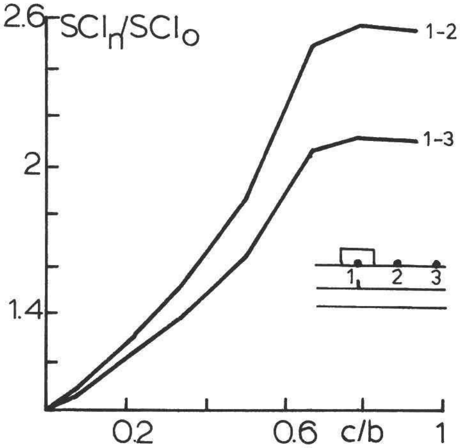

Figure 6.B.6b *Increase of the Curvature Ratio in relation to the c/b Ratio*

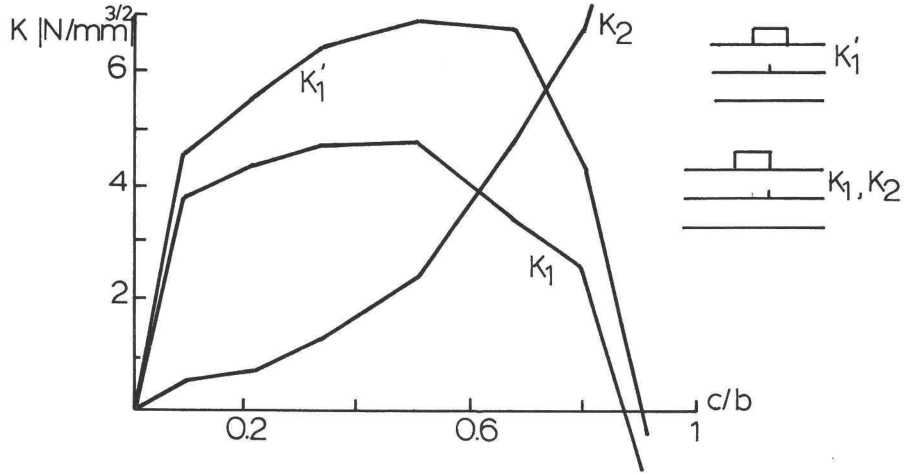

Figure 6.B.7 *Variation of K_1 and K_2 in relation to the c/b Ratio*

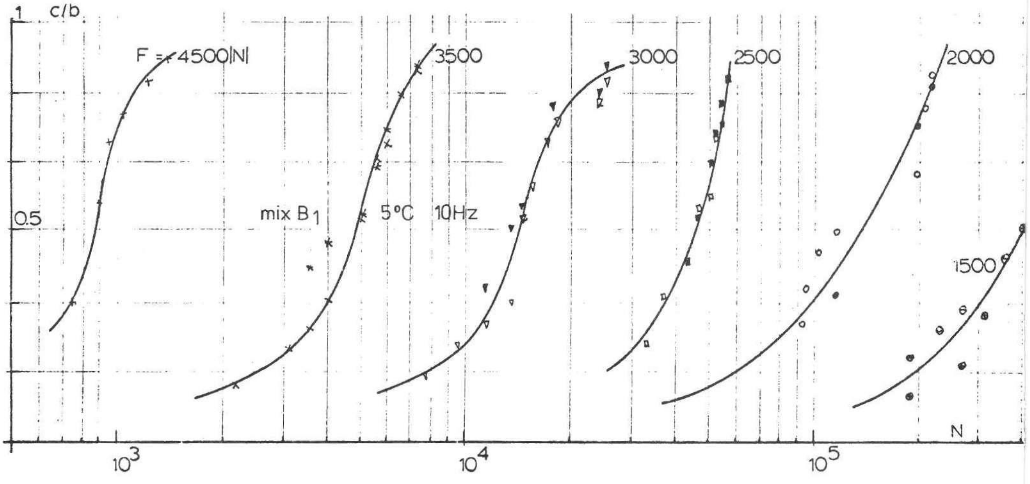

Figure 6.B.8 *Ratio c/b in relation to the Number of Load Repetitions (N)*

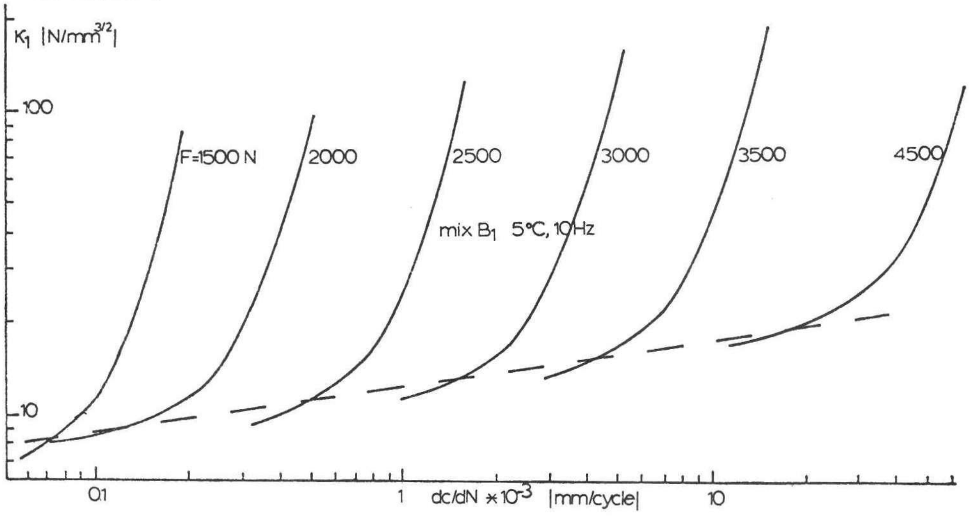

Figure 6.B.9 *Crack Growth Rate in relation to K, assuming full slip between Beam and Subgrade*

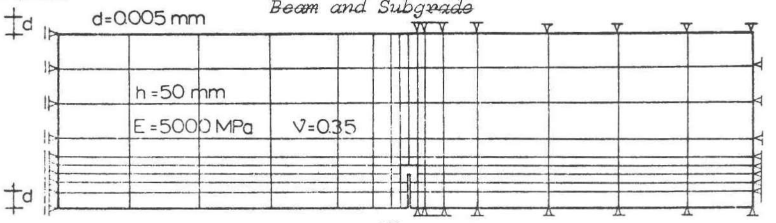

Figure 6.B.10 *Finite Element Mesh used in the Simulation of the Pure Shear Test*

The effect of a wrong assumption on the interface conditions has been shown by Thewessen and this author |28|. By using a test set-up similar to that described in figure 6.B.5, they obtained results like those given in figure 6.B.8. From this figure it can already be observed that the rate of crack propagation decreased if the c/b was 0.6 or larger.
The stress intensity factors were calculated by means of figure 6.B.4. This resulted in K vs dc/dN graphs like the one given in figure 6.B.9. These results can, to put it mildly, be considered as remarkable. If however figure 6.B.7 was used to assess the K_1 values, a K_1 vs dc/dN relation was obtained as indicated by the dashed line in figure 6.B.9.

From the discussion on the beam on elastic foundation test which was given here, it was decided that, although realistic support conditions exist, this type of test should not be used in the experimental program.

6.B.4 Pure Shear Test

Pure shear tests are considered to be important since they enable to determine crack growth relations of the shape.

$$\left(\frac{dc}{dN}\right)_{\text{shear}} = A\ K_2^n \qquad \text{eq. 6.B.1}$$

It might be argued that these relations can be derived from the relation

$$\left(\frac{dc}{dN}\right)_{\text{bending}} = A\ K_1^n \qquad \text{eq. 6.B.2}$$

because, according to Sih, K_1 and K_2 are related to each other in the following way

$$K_2^2 = \frac{3(1-2\nu)}{2(1-\nu)-\nu^2}\ K_1^2 \qquad \text{eq. 6.B.3}$$

For ν=0.35 equation 6.B.3 reduces to

$$K_2 = 0.87\ K_1 \qquad \text{eq. 6.B.4}$$

Nevertheless it is thought worthwhile to check the transformation of K_2 to K_1 as indicated in equation 6.B.3. This can be done by means of this type of test.

The test, which was analysed by means of the finite element program, was a constant displacement type of test. In this type of test, the crack length and stress intensity factor should be assessed from the decrease of the associated load.

Figure 6.B.10 shows the finite element mesh, while figure 6.B.11 shows the decrease of the load in relation to the c/b ratio. Figure 6.B.12 shows the variation of K_2 in relation to the c/b ratio.

From figure 6.B.11 it can be concluded that the load decreases almost linearly with increasing crack length. On the other hand K_2 stays almost constant over a rather large c/b range. This would mean that only a limited number of dc/dN vs K_2 combinations can be obtained from this test. Therefore a considerable amount of tests should be run in order to be able to determine the constants from the crack growth law as given in equation 6.B.2.

This, together with the fact that it is a rather difficult test (one needs to have a very stiff frame in order to avoid bending; specimen preparation might be difficult), has lead to the conclusion that this type of test should not be used in order to determine the crack growth properties.

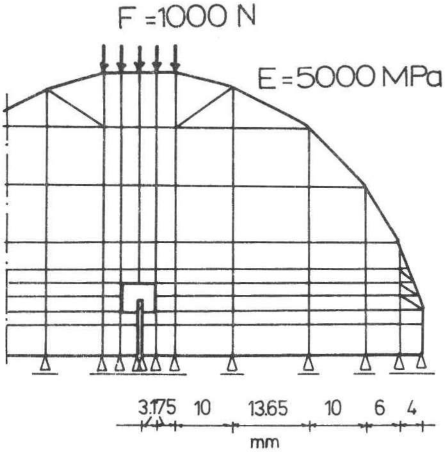

Figure 6.B.13 Finite Element Mesh used in the Simulation of the Indirect Tensile Test

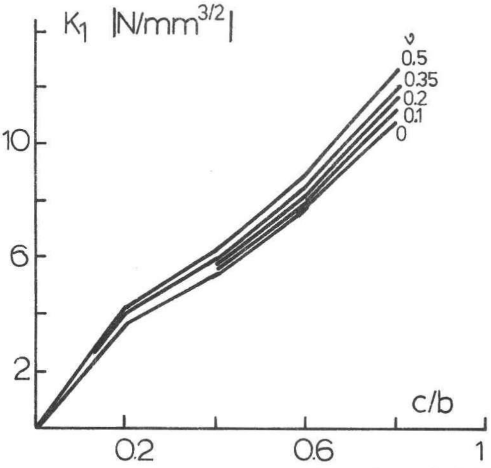

Figure 6.B.14 Increase of K_1 in relation to the Ratio c/b and ν

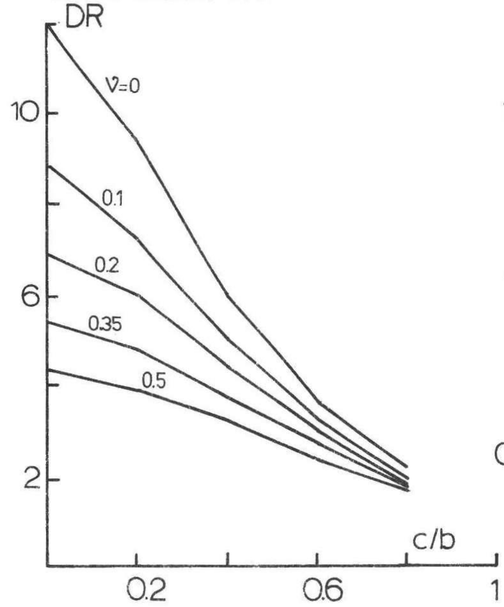

Figure 6.B.15 Decrease of DR in relation to the Ratio c/b

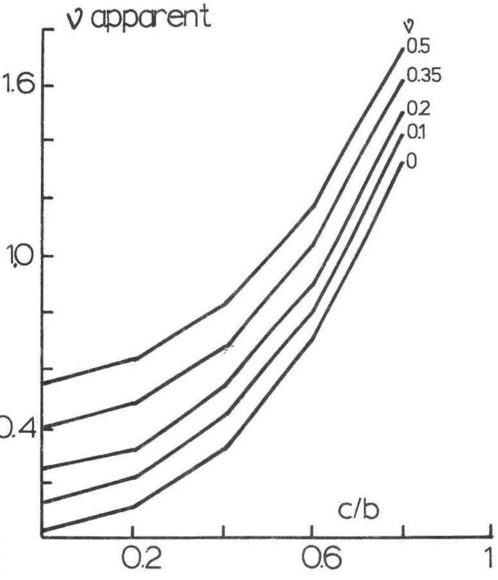

Figure 6.B.16 Increase of the apparent Poisson's Ratio in relation to the Ratio c/b

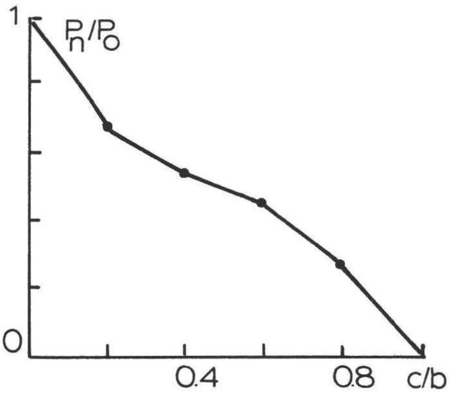

Figure 6.B.11 Decrease of the Ratio Pn/P_0 in relation to the Increase of the Ratio c/b

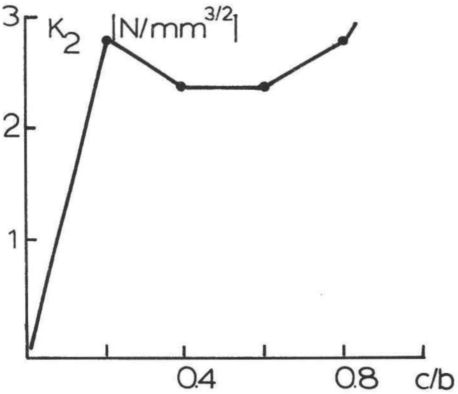

Figure 6.B.12 Variation of K_2 in relation to the Ratio c/b

6.B.5 Indirect Tensile Test

The indirect tensile test or split test, is normally used for the testing of brittle materials. During the last 10 years this test is also recognized as a valuable type of test to be used on asphaltic materials. Its use on this type of material however, is subjected to a large amount of criticism which is mainly caused by the fact that quite often one seems to get unrealistic results. Especially the magnitude of Poisson's ratio, calculated from the measured vertical and horizontal displacements takes unrealistic values like e.g. 1.5.
In spite of this criticism it is still believed that the indirect tensile test is a valuable test since it gives the possibility to determine the strength characteristics of cores taken in the field. Because of this, it is felt that this type of test is a very practical one and therefore it was studied in this analysis in order to determine its applicability for crack growth experiments.
The finite element mesh which was used for the calculations is given in figure 6.B.13. Some results are shown in figure 6.B.14, 6.B.15 and 6.B.16.
Figure 6.B.14 shows the increase in K_1 in relation to the ratio c/b. Also its dependency on the magnitude of Poisson's ratio is shown. Figure 6.B.15 shows the decrease of the value of DR. This factor is defined as

$$DR = \frac{\text{vertical displacement}}{\text{horizontal displacement}} \qquad \text{eq. 6.B.5}$$

From DR, the value of Poisson's ratio can be calculated from

$$\nu = \frac{0.0673DR - 0.8954}{-0.2494DR - 0.0156} \qquad \text{eq. 6.B.6}$$

The constants in equation 6.B.6 are dependent on the diameter of the specimen and the width of the loading strip. A complete picture of the variation of these constants with varying specimen diameter is given in |38|. Equation 6.B.6 is valid for specimens having a diameter of 100 mm, the width of the loading strip should be 12.7 mm.
Equation 6.B.6 was used to calculate apparent Poisson's ratios from the DR values given in figure 6.B.15. The results are shown in figure 6.B.16. From this figure it can immediately be observed that apparent Poisson's ratios can be obtained that are much larger than 0.5. This should be contributed to the existance of cracks and flaws in the specimen.
From the analysis presented here it can be concluded that the indirect tensile test is also a very useful test for the assessment of crack growth properties.

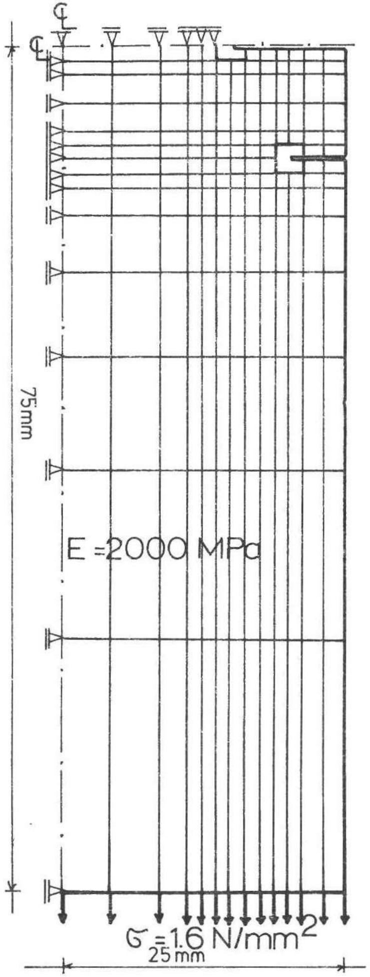

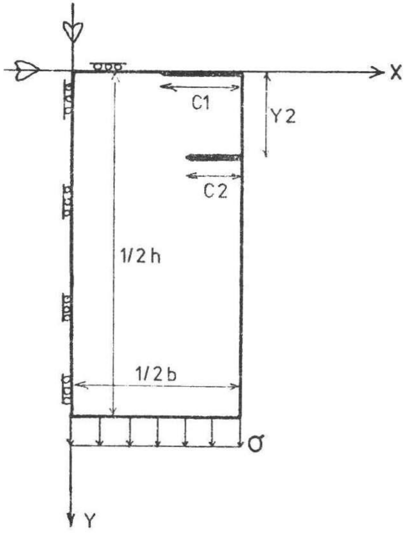

Figure 6.B.19 Quarter Beam used in the Finite Element Calculations

Figure 6.B.18 Finite Element Mesh used in the Simulation of the Direct Tensile Test

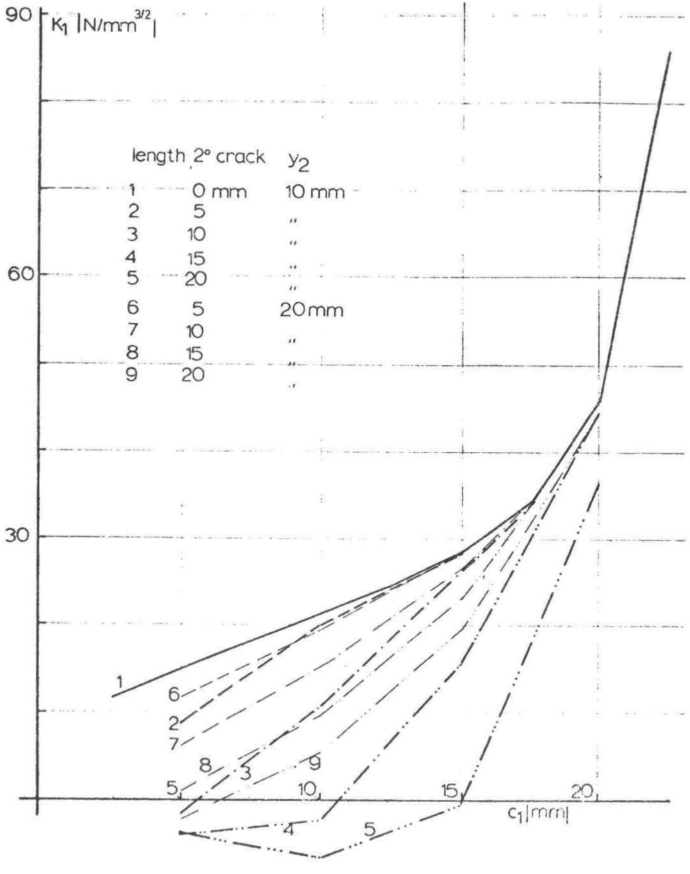

Figure 6.B.20 K_1 in relation to c_1, c_2 and y_2

As an example, figure 6.B.17 is given which shows the increase of Poisson's ratio as determined by means of the repeated load indirect tensile tests. The data were obtained from |33|.

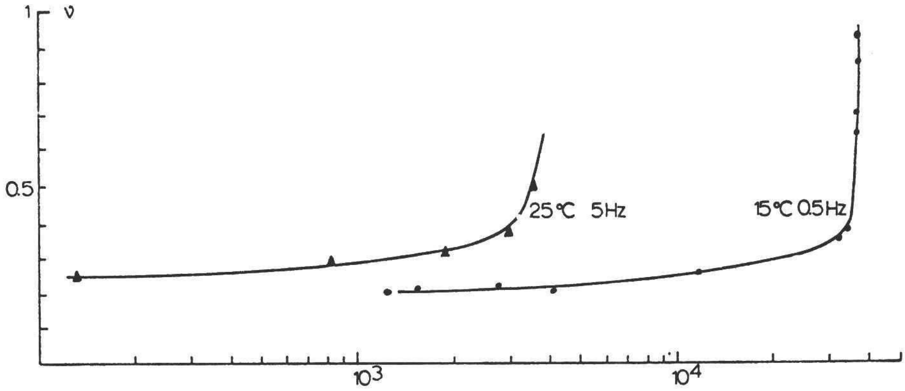

Figure 6.B.17 *Increase in Poisson's Ratio during a Repeated Load Indirect Tensile Test (mix A_1, Marshall compaction, void content=3.5%)*

Although the test seems very attractive from a theoretical point of view, there are some practical inconveniences that can occur during the test.
During the testprogram described in |33, 34, 35| regularly rocking of the specimen was observed because the loading strips were pressed somewhat skew into the specimen. This rocking will of course influence the stress distribution and displacement. Furthermore the stainless steel loading strips incised in the specimen causing cracking near the edges of the strips. This of course will also influence the stress, displacement and crack growth behaviour of the specimen. It is believed however that both inconveniences might be overcome by placing a thin strip of rubber between the specimen and the loading strip. In that case special care should be given to the measurements of the vertical displacements of the specimen.
Due to these inconveniences, this test was not selected to be used for the crack growth experiments.

6.B.6 Direct Tensile Test

As indicated in chapter 6, the direct tensile test was selected for the crack growth experiments. The main reason for its selection was that the tests are relatively easy to perform and that, as will be indicated here, the crack length and stress intensity factor can easily be obtained from the increase in elastic deflection.

The finite element mesh that was used in the calculations is shown in figure 6.B.18. Both the constant load and constant displacement test were simulated.

6.B.6.1 Constant Load Test

Figure 6.B.19 shows the quarter beam which has been considered in the finite element calculations. Typical calculation results are shown in figures 6.B.20 and 6.B.21. The multiple cracking conditions were simulated since this type of cracking was observed several times during the testing of the E_4 and F mix at 15°C and 1 Hz.

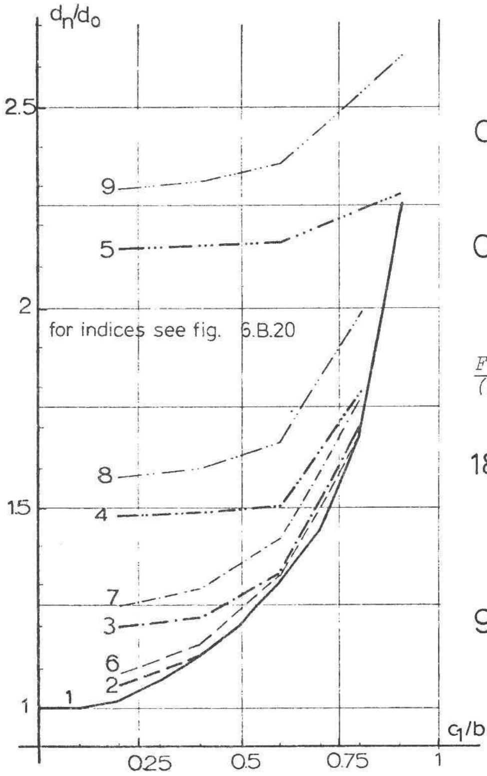

Figure 6.B.21 Deflection Ratio (d_n/d_0) in relation to the Ratio c/b

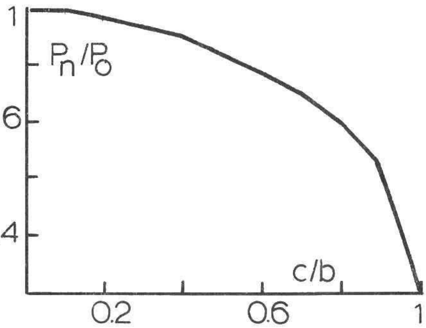

Figure 6.B.22 Decrease of the Load Ratio (P_n/P_0) in relation to the Ratio c/b

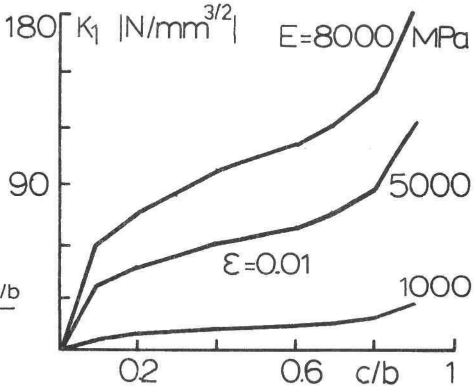

Figure 6.B.23 Increase in K_1 in relation to the Ratio c/b

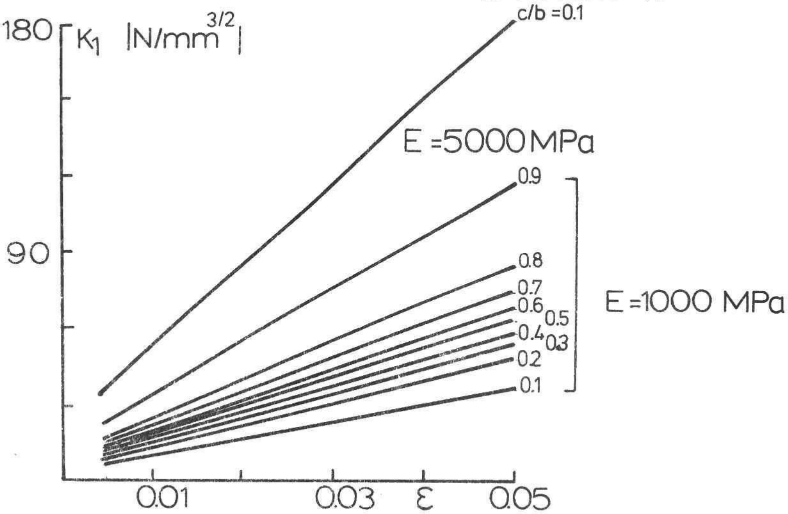

Figure 6.B.24 Increase in K_1 in relation to the applied Deformation (ε) and the Mix Stiffness

As can be seen from figure 6.B.20 and 6.B.21, both the crack length and the stress intensity factor of crack number 1 can be assessed with reasonable accuracy from the $c_2=0$ curves as long as c_2 is smaller than c_1. These curves ($c_2=0$) have therefore been selected for the evaluation of the crack growth tests.

6.B.6.2 Constant Displacement Test

Figure 6.B.22 shows how the load decreases with increasing crack length. The increase of K_1 with respect to the crack length is shown in figure 6.B.23. Based on this figure, figure 6.B.20 has been developed which enables the assessment of K_1 for different applied strain levels and elastic moduli.

6.B.7 Summary

In this appendix the results are presented of a theoretical analysis on the applicability of different types of test for crack growth experiments.
In general it can be concluded that each type of test considered, can be used for the experiments. For reasons of simplicity, the direct tensile test and the indirect tensile test are preferred. For the experiments which were carried out in this study, the direct tensile test was selected.

References

|1| MAJIDZADEH, K.; RAMSAMOOJ, D.V.; FLETCHER, T.A.
Analysis of Fatigue of a Sand Asphalt Mixture
"Proceedings Association of Asphalt Paving Technologists", Vol. 39-1969

|2| MAJIDZADEH, K; KAUFMANN, E.M.; RAMSAMOOJ, D.V.
Application of Fracture Mechanics in the Analysis of Pavement Fatigue
"Proceedings Association of Asphalt Paving Technologists", Vol. 41-1971

|3| RAMSAMOOJ, D.V.; MAJIDZADEH, K.; KAUFMANN, E.M.
The Analysis and Design of the Flexibility of Pavements
"Proceedings 3rd Int. Conf. Structural Design of Asphalt Pavements"
London - 1972

|4| MAJIDZADEH, K.; RAMSAMOOJ, D.V.
Mechanistic Approach to the Solution of Cracking in Pavements
Special Report 140; Transportation Research Board
Washington D.C. - 1973

|5| MAJIDZADEH, K.; KAUFMANN, E.M.; CHANG, C.W.
Verification of Fracture Mechanics Concepts to Predict Cracking of Flexible Pavements
Report FHWA-RD-73-91; Federal Highway Administration
Washington D.C. - 1973

|6| MAJIDZADEH, K.; BURANAROM, C.; KARAKOUZIAN, M.
Application of Fracture Mechanics for Improved Design of Bituminous Concrete. Vol. I: Plan of Research; State of the Art and Mathematical Investigations
Report FHWA-RD-76-91; Federal Highway Administration
Washington D.C. - 1976

|7| MAJIDZADEH, K.; DAT, M.; MADISI-ILYAS, F.
Application of Fracture Mechanics for Improved Design of Bituminous Concrete. Vol. II: Evaluation of Improved Mixture Formulations and the Effect of Temperature Conditions on Fatigue Models
Report FHWA-RD-76-92; Federal Highway Administration
Washington D.C. - 1976

|8| MAJIDZADEH, K.; TALBERT, L.O.; KARAKOUZIAN, M.
Development and Field Verification of a Mechanistic Structural Design System in Ohio
"Proceedings 4th Int. Conf. Structural Design of Asphalt Pavements"
Ann Arbor - 1977

|9| KARAKOUZIAN, M.
A Simplified Method for Material Testing and Design of Pavement Systems
Ph. D. Dissertation, Ohio State University
Columbus - 1978

|10| MONISMITH, C.L.; HICKS, R.G.; SALAM, Y.M.
Basic Properties of Pavement Components
Report FHWA-RD-72-19; Federal Highway Administration
Washington D.C. - 1971

|11| COETZEE, N.F.
Some Considerations on Reflection Cracking in Asphalt Concrete Overlay Pavements
Ph. D. Dissertation; University of California
Berkeley - 1979

|12| MONISMITH, C.L.; COETZEE, N.F.
Reflection Cracking: Analysis, Laboratory Studies and Design Considerations
"Proceeding Association of Asphalt Paving Technologists", Vol. 50-1980

|13| SCHAPERY, R.A.
A Theory of Crack Growth in Visco-Elastic Media
Report MM 2764-73-1; Mechanics and Materials Research Centre
Texas A & M University - 1973

|14| CHANG, H.S.; LYTTON, R.L.; CARPENTER, H.
Prediction of Thermal Reflection Cracking in West Texas
RR 18-3; Texas Transportation Institute
Texas A & M University - 1976

|15| GERMANN, F.P.; LYTTON, R.L.
Methodology for Predicting the Reflection Cracking Life of Asphalt Concrete Overlays
RR 207-5; Texas Transportation Institute
Texas A & M University - 1979

|16| SHANMAUGHAM, U.L.
Prediction of Thermal Fatigue Cracking using Fracture Mechanics
MSc. Thesis; Texas A & M University
College Station - 1980

|17| LYTTON, R.L.; SHANMUGHAM, U.L.
Analysis and Design of Pavements to Resist Thermal Cracking using Fracture Mechanics
"Proceedings 5th Int. Conf. Structural Design of Asphalt Pavements"
Delft - 1982

|18| MARCHAND, J.P.; GOACOLON, H.
Cracking in Wearing Courses
"Proceedings 5th Int. Conf. Structural Design of Asphatl Pavements"
Delft - 1982

|19| BROWN, W.F.; STRAWLEY, J.E.
Plain Strain Crack Toughness Testing of High Strength Metallic Materials
ASTM STP 410; American Society for Testing and Materials - 1967

|20| SIH, G.C.
A Special Theory of Crack Propagation, in Methods of Analysis and Solutions to Crack Problems
Edited by G.C. Sih
Wolters-Noordhoff Publishing Company - 1972

|21| PARIS, P.C.; ERDOGAN, F.
A Critical Analysis of Crack Propagation Laws
Transactions of the ASME, "Journal of Basic Engineering",
Series D, Vol. 85 No. 3 - 1963

|22| LEMPE, U.
Dynamic Shear Modulus and Resistance to Fatigue of Bituminous Bound Materials (in German)
"Strassenbau und Strassenverkehrstechnik", Heft 130; Bonn - 1972

|23| SCHAPERY, R.A.
Non-Linear Fracture Analysis of Visco-Elastic Composite Materials based on a Generalized J Integral Theory
"Proceedings Japan-USA Conference on Composite Materials"
Tokyo - 1981

|24| SCHAPERY, R.A.
On Visco-Elastic Deformation and Failure Behavior of Composite Materials with Distributed Flaws
"1981 Advances in Aerospace Structures and Materials AD-01"
Edited by S.S. Wang and W.J. Renton
The American Society of Mechanical Engineers; New York - 1981

|25| WILSON, E.L.
Analysis of Prismatic Solids
Unpublished Report; Department of Civil Engineering
University of California; Berkeley - 1967

|26| THEWESSEN, H.P.M.; MOLENAAR, A.A.A.
Determination of the Fracture Toughness and its Relation to other Material Characteristics of some Bituminous Mixes commonly used in the Netherlands (in Dutch)
Report 7-82-115-26; Department of Civil Engineering; Lab. for Road and Railroad Research; Delft University of Technology - 1981

|27| BONNAURE, F.; GEST, G.; GRAVOIS, A.; UGÉ, P.
A New Method of Predicting the Stiffness of Asphalt Paving Mixtures
"Proceedings Association of Asphalt Paving Technologists", Vol. 47-1977

|28| THEWESSEN, H.P.M.; MOLENAAR, A.A.A.
Investigation into the Crack Growth Behavior of some Bituminous Mixes commonly used in the Netherlands (in Dutch)
Report 7-82-115-27; Department of Civil Engineering; Lab. for Road and Railroad Research; Delft University of Technology - 1981

|29| MONISMITH, C.L.; EPPS, J.A.; KASIANCHUK, D.A.; McLEAN, D.B.
Asphalt Mixture Behavior in Repeated Flexure
Report TE-70-5; Office of Research Services
University of California, Berkeley - 1970

|30| KALLAS, B.F.; PUZINAUSKAS, V.P.
Flexural Fatigue Tests on Asphalt Paving Mixtures
RR-72-5; The Asphalt Institute
College Park - 1972

|31| PELL, P.S.; COOPER, K.E.
The Effect of Testing and Mix Variables on the Fatigue Performance of Bituminous Materials
"Proceedings Association of Asphalt Paving Technologists", Vol. 45-1975

|32| ADEDIMILA, A.S.; KENNEDY, T.W.
Fatigue and Resilient Characteristics of Asphalt Mixtures by Repeated Load Indirect Tensile Test
RR 183-5; Center for Highway Research
University of Texas at Austin - 1975

|33| MOLENAAR, A.A.A.
Behavior of Three Gravel Sand Asphalt Mixes under Repeated Loading (in Dutch)
Report 7-79-113-3; Department of Civil Engineering; Lab. for Road and Railroad Research; Delft University of Technology - 1979

|34| MOLENAAR, A.A.A.
Behavior of a Sand Asphalt Mix under Repeated Loading (in Dutch)
Report 7-80-113-4; Department of Civil Engineering; Lab. for Road and Railroad Research; Delft University of Technology - 1980

|35| MOLENAAR, A.A.A.
Behavior of Open Asphaltic Concrete under Static and Repeated Loading (in Dutch)
Report 7-80-113-5; Department of Civil Engineering; Lab. for Road and Railroad Research; Delft University of Technology - 1980

|36| VAN DER POEL, C.
A General System describing the Visco-Elastic Properties of Bitumens and its Relation to Routine Test Data
"Journal of Applied Chemistry", Vol. 4, Part 5 - 1954

|37| HEUKELOM, W.
Observations on the Rheology and Fracture of Bitumens and Asphalt Mixes
"Proceedings Association of Asphalt Paving Technologists", Vol. 36-1966

|38| GONZALES, G.; KENNEDY, T.W.; ANAGNOS, J.N.
Evaluation of the Resilient Elastic Characteristics of Asphalt Mixtures using the Indirect Tensile Test
RR 183-6; Center for Highway Research
University of Texas at Austin - 1975

Chapter 7

DESIGN OF ASPHALT CONCRETE OVERLAYS

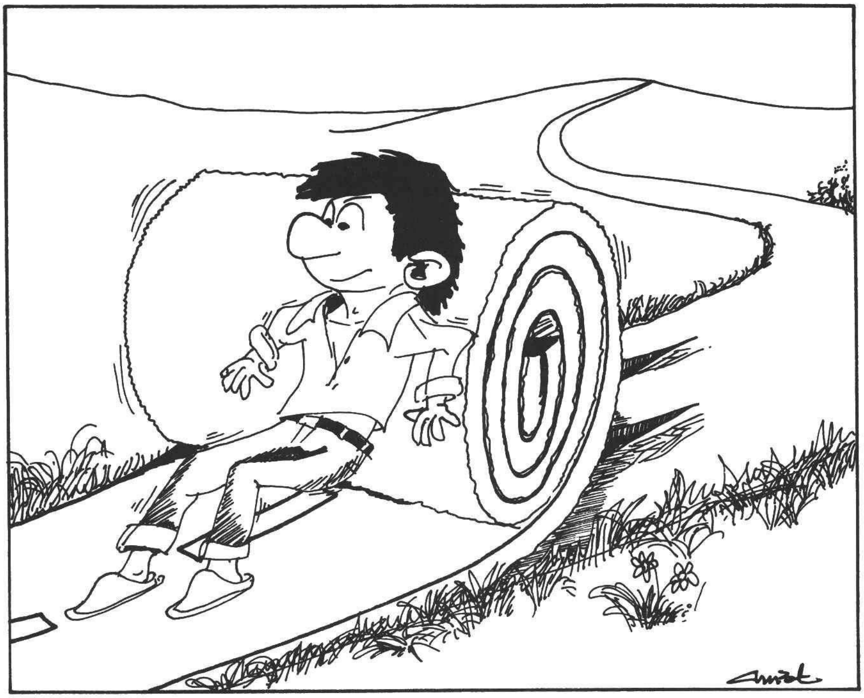

TABLE OF CONTENTS

7.1 Introduction

If the pavement structure reaches the condition that a safe and fast public and commercial transportation cannot be garanteed any longer, maintenance should take place in order to restore the pavement condition to such a level that it can serve as transportation surface for another number of years. Maintenance activities can be such as filling cracks, levelling of the surface or surface treatments. If however the structural condition should be improved, those relatively simple maintenance techniques are not sufficient. In those conditions overlays with a thickness of 0.05 to 0.15 m should be placed on the existing pavement.
For the thickness design of these overlays, empirical as well as mechanistic methods have been developed. The same advantages and disadvantages apply for these methods, as for the empirical and mechanistic design methods which were described in chapter 3. The author believes that, as was the case for the design methods for new pavements, mechanistic overlay design methods are in advantage over the empirical methods, since they have better predictive capabilities. Nevertheless the capabilities of existing mechanistic methods should be improved since they have still a number of shortcomings.

In this chapter a new overlay design procedure will be presented. It is based on the models and material characterization that were described in the previous chapters. The author believes that the presented procedure overcomes the main imperfections of the existing methods.
In order to obtain a better understanding for the rationale of the new overlay design procedure, this chapter will start with a short description of the basic principles of the current mechanistic methods and a discussion on their applicability and imperfections.

7.2 Current Mechanistic Overlay Design Methods

A rather complete picture of current overlay desing methods using a mechanistic approach, can be found in the proceedings of the 4th and 5th International Conference Structural Design of Asphalt Pavements |1, 2|. This section summarizes the basic assumptions used in most of the methods presented there.
All current overlay design methods use measured surface deflections as input. Departing from these deflections two main types of design methods can be discerned. In the methods of the first type, the elastic moduli of the different pavement layers (both cracked and uncracked) are calculated from the measured deflections and the layer thicknesses which are obtained by means of coring. These moduli are used together with the layer thicknesses as input into a computer program to calculate the stresses and strains in the multi layered pavement system. From the calculated stresses and strains, and using an appropriate fatigue relation, usually this relation is taken from literature, the number of load applications to failure can be calculated. This number, together with the number of loads applied to the pavement (n), which is obtained from traffic and axle load data, Miner's ratio (n/N) is calculated. Depending on the magnitude of this ratio it is decided whether an overlay should be applied or not. Then the stresses and strains in the existing pavement as well as in the overlay, are calculated for different overlay thicknesses and a new number of load applications to failure (N_n) is calculated. The number of loads which still can be applied (n_d) is calculated from

$$\frac{n_d}{N_n} = 1 - \frac{n}{N} \qquad \text{eq. 7.1}$$

In the methods of the second type, deflection measurements are used to calculate an effective layer thickness. An example of such a method is the one developed by researchers of the Shell laboratories |3|. This approach is different from the one described above in that way that now an effective thickness of the asphaltic top layer is calculated assuming this layer has an elastic modulus equal to that of new material.
The effective layer-thickness approach is an attractive one since this thickness can be compared directly with the original thickness. It will be obvious that structural damage has occurred if the ratio $h_{effective} \div h_{original}$ is smaller than 1. The effective layer thickness and the applied and expected number of load repetitions are then used as input in the design method for new pavements to determine the overlay thickness |3|.

7.3 Imperfections of Current Mechanistic Overlay Design Methods and Suggestions for Improvement

Basicly six major imperfections and/or disadvantages can be formulated against the current mechanistic overlay design procedures. They are:

a. difficulties in the calculation of the elastic moduli of the pavement layers,
b. the application of Miner's ratio in overlay thickness estimation,
c. selection of a proper fatigue relation,
d. estimation of the loading history,
e. inability to take into account the presence of cracks in the existing pavement on the behavior of the overlay,
f. the non-existance of relations between visual observed distress and structural deterioration as determined from the deflection measurements.

These disadvantages will be discussed in the following paragraphs.

Re a. The calculation of elastic moduli from known layer thicknesses and measured deflections gives no problems for two layer pavement structures. Sound mathematical solitions have been provided in the shape of graphs |4| tables |5| and computer programs |6|. The calculation of the moduli of three layered pavement systems is possible if the modulus of the asphaltic top layer is estimated from nomographs |3| and the subgrade modulus is estimated from the deflection measured at a certain distance of the load |1,7|. Using these moduli values, the elastic modulus of the base can be estimated rather easily. Elastic moduli of multi layered pavement systems can only be estimated in an iterative way assuming starting values for the moduli |8|. This method however is rather cumbersome, costly and time consuming and one also needs to have a good knowledge of the layer thicknesses since they have a major influence on the calculated moduli. This means that a rather large amount of cores needs to be taken which is not very attractive.

Re b. Although Miner's law is applicable to the development of one crack, further extension of cracks is dependent on the redistribution of the stresses, and in this case Miner's law may not be fully applicable. Furthermore Miner's law defines a clear failure condition which occurs at e.g. the fracture of a test specimen. Such a failure point does not exist in the case of pavements. A 100 percent cracked pavement surface can still be used as a reasonable driving surface unless large deformations and/or potholes occur. Therefore a straight forward use of Miner's law in the estimation of overlay thicknesses is not considered to be a proper approach, since this will result in an unrealistic overlay design especially in those cases where Miner's ratio comes close to one.

Re c. The selection of the proper fatigue relation is of major concern since this affects highly the results of the pavement life calculations. Fatigue relations can be determined experimentally in the laboratory but they should be corrected with a proper factor in order to take into account benificial effects of e.g. rest periods. However this will make the fatigue relation rather diffuse. It is therefore much better to determine the fatigue relation from the in situ behavior of the pavement, since then a realistic relation including the beneficial effects is determined. Unfortunately the current design methods don't have options to assess such an in situ fatigue relation.

Re d. Especially the information on traffic loads is in most cases very poor or even not available at all. This is because the collection of this type of data is rather costly. It is expected that no substantial improvement of the quality of these data will be obtained in the coming years. It is therefore suggested that research should be undertaken in order to be able to make reasonable estimations of the axle load spectrum what has been applied to the pavement and that, what might be expected in future.

Re e. Visible cracks in the existing pavement will influence the behavior or the overlay, because they will act as a crack initiator unless special precautions have been taken. This influence can be that pronounced that this will result in a substantial reduction of the life of the overlay. Up to now all mechanistic design methods, which are readily available, do not take into account this important aspect.

Re f. The deterioration or distress of the pavement can be observed visually and can be detected by means of deflection measurements. Up to now the mechanistic overlay design methods rely heavily on the results of the deflection measurements. This is thought to be a valid approach if deflection measurements are taken on a regular basis, this however will seldom be the case. Usually deflection measurements are only taken if maintenance activities are thought to be necessary. In that case visual condition surveys should be performed in order to obtain additional information. This means that the relation between these two aspects, visual condition and deflection, should be improved in order to be able to make better overlay thickness designs.

From the above mentioned disadvantages, it can be concluded that considerable modifications should be applied to most of the existing overlay design methods. A number of these modifications have already been discussed in the previous chapter.

In chapter 3 it has been discussed how the stress and strain level in pavement structures can be assessed rather easily by means of deflection measurements. The equations presented there overcome the problems of calculating elastic moduli as mentioned under item a. Furthermore a structural performance model has been described in chapter 3. This model overcomes the problem of describing the pavement condition even in those cases where Miner's ratio is larger than one. It will also be possible to make realistic overlay thickness designs in these cases by means of this model. This in turn means that the question raised under item b. has been solved.

In chapter 5 it has been shown how the remaining life of the pavement can be assessed without any knowledge on the number of load applications applied to the pavement. It has been shown that knowledge on the traffic intensity is sufficient to make reasonable accurate estimates on the remaining life. This means that the presented method overcomes the difficulties which have been mentioned under item d. Of course the accuracy of the remaining life assessments will increase if accurate data on the amount and magnitude of the traffic loads are available.
In chapter 5 also relations have been developed between the structural condition of the pavement,as determined by means of deflection measurements,and the distress which can be observed visually. It has even been shown how the structural condition can be estimated by means of visual condition surveys in those cases where deflection measurements fail to do so. This means that the problems mentioned under item f. have been overcome.

Chapter 6 described the important aspect of crack propagation in bituminous materials. The results given in that chapter, together with a calculation of the stress intensity factor in overlays due to cracks in the underlying existing pavement, will solve the problems mentioned under item e.

From the previous paragraphs it can be concluded that all imperfections but one (item c.) have been dealt with in one of the previous chapters. The assessment of an in situ fatigue relation will be discussed in this chapter.

7.4 New Overlay Design Method

Departing from the improvements as suggested in the previous section, the author has developed a new overlay design method that incorporates the methods and techniques developed and described in the previous chapters.
In this new method three design options are distinguished. They are
a. design of unbonded overlays
b. design of bonded overlays with special emphasis placed on the upgrading of the structural condition of the existing pavement
c. design of bonded overlays with special emphasis placed on the reduction of reflection cracking.

Re a. In certain circumstances, e.g. a badly cracked pavement, it is desirable to place the overlay in such a way that reflection of cracking from the existing pavement into the overlay is prevented. Such conditions can be created by applying a bond breaker between the overlay and the existing pavement. Ideally the application of a bond breaker creates a condition where the overlay can be considered as a slab resting on another slab and where no shear stresses are transmitted from the overlay to the existing pavement.
Since the overlay and the existing pavement are not behaving like a single slab but like two separate slabs, the overlay should primarily be designed on the tensile strain that occurs at the bottom of the overlay. It will be obvious that the strain reduction in the existing pavement due to an unbonded overlay is less than the strain reduction due to

a bonded overlay. Nevertheless the desired strain reduction in the existing pavement should be one of the constraints in the selection of the overlay thickness. Figure 7.1 shows schematically the design principle of unbonded overlays

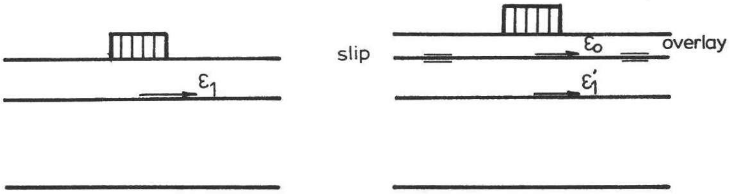

Figure 7.1 *Design Principle of Unbonded Overlays*

Re b. The main objective of a bonded overlay is, to reduce the stress and strain level in the existing pavement to such an extent that the structural life of the existing pavement is extended considerably. Since the overlay lies above the neutral axis, the stresses and strains in the overlay itself will be compressive.
Figure 7.2 shows schematically the design principle of bonded overlays.

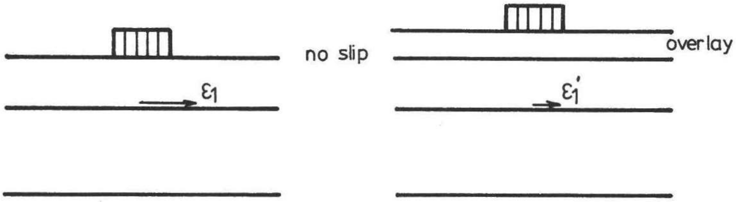

Figure 7.2 *Design Principle of Bonded Overlays*

Re c. In the design of bonded overlays, performed according to the principles described above, the effect of cracks in the existing pavement on the performance of the overlay is not taken into account. It is a well known fact however that the influence of these cracks is rather pronounced. Bonded overlay designs should therefore be checked on the propagation rate of reflection cracks through the overlay.
Figure 7.3 shows schematically the reflection cracking process through overlays.

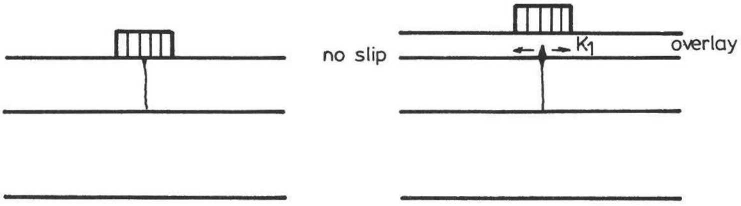

Figure 7.3 *Reflection Cracking of Overlays*

In the following sections, methods will be described that enable the design of overlays according to options described above.

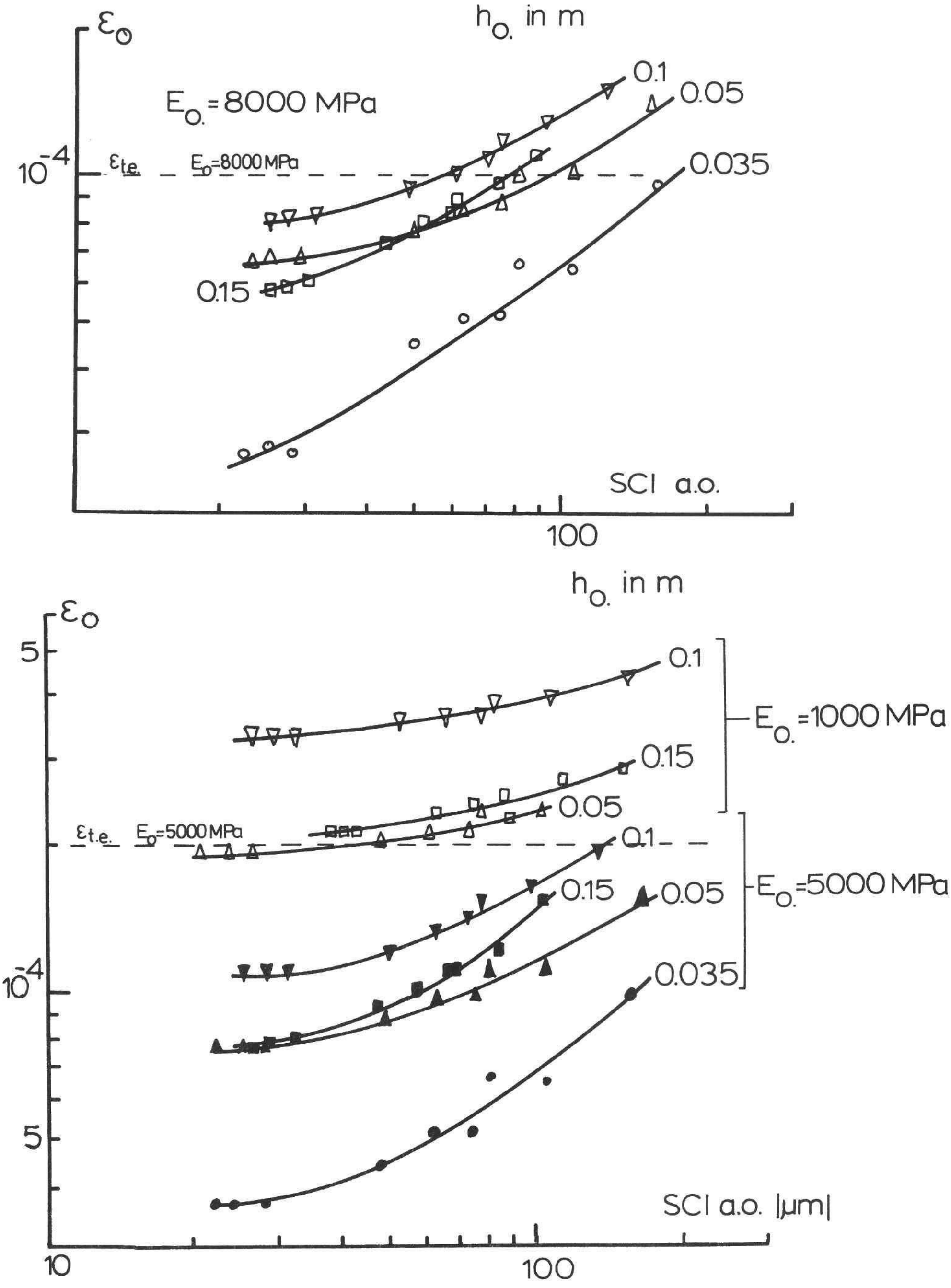

Figure 7.5 Strain Level in the Unbonded Overlay (ε_0) in relation to the SCI after Overlaying ($SCI_{a.o.}$)

7.4.1 Design of Unbonded Overlays

The effect of unbonded overlays on the structural behavior of pavements has been studied by the author by means of a number of calculations on four layered pavement systems using the CIRCLY computer program |9|. These calculations have resulted in relations between the SCI after overlaying on one hand and the maximum tensile strain in the overlay on the other.
Figure 7.4 shows the layered systems which were analysed. Figure 7.5 shows the results of the calculations.

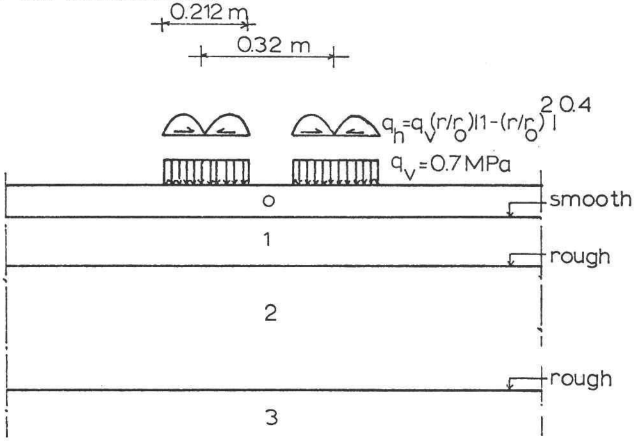

$E_0 = 1000, 5000, 8000$ MPa $\quad h_0 = 0.02, 0.035, 0.05, 0.1, 0.15$ m

$E_1 = 5000$ MPa $\quad h_1 = 0.1, 0.15, 0.2$ m

$E_2 = 400, 1200, 6000$ MPa $\quad h_2 = 0.3$ m

$E_3 = 150$ MPa $\quad \mu_1 = \mu_2 = \mu_3 = \mu_0 = 0.35$

Figure 7.4 *Layered Systems analysed to determine the Effect of Unbonded Overlays*

In figure 7.5 the strain values for the 0.02 m thick overlays are omitted since in these cases the strain in the overlay was compressive.

Figure 7.6 shows the relation between the SCI before overlaying and the SCI after overlaying for different overlay thicknesses and stiffnesses.

From figure 7.5 it can be concluded that thin overlays are in advantage over thick overlays. Especially overlay thicknesses of 0.1 m exhibit high strain values.

Special care should be given to the selection of the overlay thickness in relation to its stiffness for the following reasons. As has been mentioned in chapter 3, the tensile strain the pavement surface due to inward shear forces ($\varepsilon_{t.e.}$) can be estimated by means of

$$\log \varepsilon_{t.e.} = 4.822 \times 10^{-2} - 1.049 \log E_1 \qquad \text{eq. 7.1}$$

where E_1 = stiffness of the top layer (in this case the overlay) |MPa|

Due to the lack of adhesion between the existing pavement and the overlay, the tensile strains at the surface of the overlay appeared to be 13% to 20% higher than the strain value estimated by means of equation 7.1.

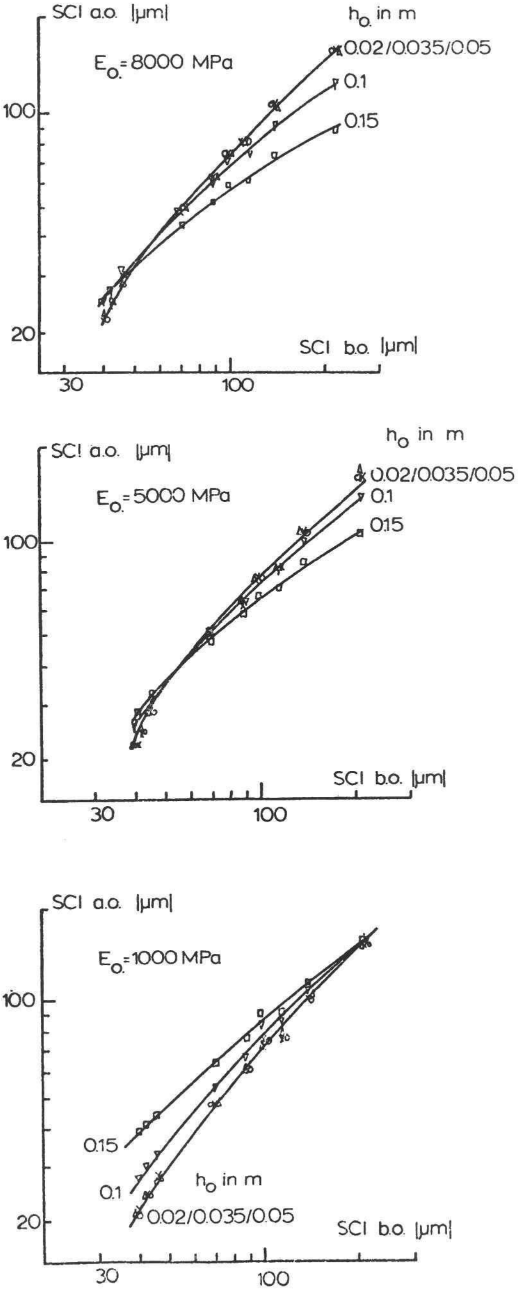

Figure 7.6 *Relation between the SCI before Overlaying ($SCI_{b.o.}$) and the SCI after Overlaying ($SCI_{a.o.}$) for Unbonded Overlays*

These tensile strains at the pavement surface are in most cases higher than the tensile strains at the bottom of the overlay (compare the dashed lines in figure 7.5 with the solid lines). Therefore cracking that grows from bottom to top is very likely to occur. If the overlay is thin, there will be a big chance that these cracks will reach the interface between the overlay and the existing pavement. Since there is hardly any bonding between the overlay and the existing pavement, loose parts will develop which might result in potholes.

From the results of the calculations, it can also be concluded that the reduction of the strain level in the existing pavement as a result of the unbonded overlay is only limited. The amount of reduction is shown in figures 7.7 and 7.8. Especially if the overlay has a thickness of 0.05 m or less, and the $SCI_{b.o.}$ is less than 100 µm, there is hardly any strain reduction in the existing pavement. This leads to the conclusion that an unbonded overlay acts more or less like a sealant and does not reduce the deterioration rate of the existing pavement.

The thickness of the unbonded overlay is designed in the following way.

<u>a.</u> first of all the future number of load applications (N) should be estimated

<u>b.</u> from this number, the design strain level in the overlay can be calculated by means of

$$\log \varepsilon = \frac{\log N - a_o}{a_1}$$

where a_o and a_1 represent the intercept and slope of the fatigue relation of the overlay material.

<u>c.</u> then ε is introduced in figure 7.5 and the needed $SCI_{a.o.}$ is determined for various overlay thicknesses and stiffnesses.

<u>d.</u> the $SCI_{a.o.}$ values are introduced in figure 7.6 together with the measured $SCI_{b.o.}$ value; this results in the needed overlay thickness and stiffness.

7.4.2 Design of Bonded Overlays with Special Emphasis on the Upgrading of the Structural Condition of the Existing Pavement

The method which has been developed for the design of bonded overlays has been outlined basicly in |10, 11, 12, 13, 14|. Here the most important aspects of this method will be summarized.

As has been shown in chapter 3, the number of load applications N_{P_1}, the pavement can sustain until the pavement has reached a probability of survival level P_1, can be calculated from

$$\log N_{P_1} = a_o + a_1 b_o + a_1 b_1 \log h_{e_1} - u_1 S_{\log N} \qquad \text{eq. 7.2}$$

where h_{e_1} = equivalent layer thickness of the construction
u_1 = standardised normal deviate associated to a probability P_1
$S_{\log N}$ = standard deviation of the logarithm of the number of load repetitions to failure
a_o, a_1 = constants from the relation $\log N = a_o + a_1 \log \varepsilon$
b_o, b_1 = constants from the relation $\log \varepsilon = b_o + b_1 \log h_e$

If the pavement life has to be extended to $(N+\Delta N)_{P_2}$, the needed equivalent layer thickness can be calculated from

$$\log (N+\Delta N)_{P_2} = a_o + a_1 b_o + a_1 b_1 \log h_{e_2} - u_2 S_{\log N+\Delta N} \qquad \text{eq. 7.3}$$

where $h_{e_2} = h_{e_1} + \Delta h_e$
Δh_e = increase in equivalent layer thickness due to the overlay
P_2 = desired reliability level of the construction at the end of the design life of the overlay
u_2 = standardised normal deviate associated to a probability P_2

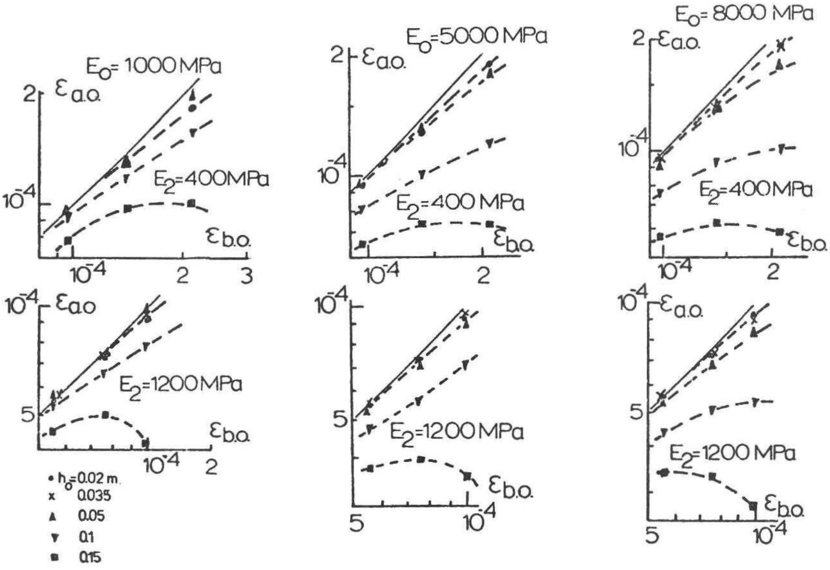

Figure 7.7 *Strain Level in the Existing Pavement after Overlaying* ($\varepsilon_{a.o.}$) *in relation to the Strain Level before Overlaying* ($\varepsilon_{b.o.}$) *and the Thickness* (h_0) *and Stiffness* (E_0) *of the Unbonded Overlay*

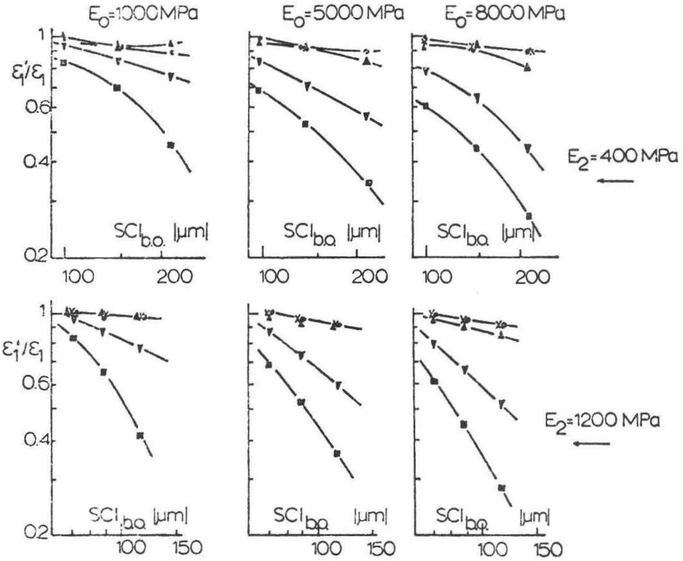

Figure 7.8 *Reduction of the Strain Level in the Existing Pavement* ($\varepsilon_1'/\varepsilon_1$) *in relation to the Thickness* (h_0) *and Stiffness* (E_0) *of the Unbonded Overlay*

$S_{\log N+\Delta N}$ = standard deviation of the logarithm of the number of load applications to failure of the overlaid pavement

By subtracting equation 7.3 from equation 7.2 one obtains

$$\log \frac{N_{P_1}}{(N+\Delta N)_{P_2}} = a_1 b_1 \log \frac{h_{e1}}{h_{e2}} - u_1 S_{\log N} + u_2 S_{\log N+\Delta N} \qquad \text{eq. 7.4}$$

by writing $\frac{N_{P_1}}{(N+\Delta N)_{P_2}} = \frac{1}{X}$ eq. 7.5

$$J_1 = 10^{u_1 S_{\log N}} \qquad \text{eq. 7.6}$$

$$J_2 = 10^{u_2 S_{\log N+\Delta N}} \qquad \text{eq. 7.7}$$

one arrives to

$$\log \frac{1}{X} = a_1 b_1 \log \frac{h_{e1}}{h_{e2}} - \log J_1 + \log J_2 \qquad \text{eq. 7.8}$$

which can be rewritten into

$$h_{e_2} = h_{e1} \sqrt[a_1 b_1]{\frac{XJ_2}{J_1}} \qquad \text{eq. 7.9}$$

The overlay thickness can be calculated from

$$h_o = \frac{1.11\ (h_{e2} - h_{e1})}{\sqrt[3]{E_o/E_3}} \qquad \text{eq. 7.10}$$

where h_o = overlay thickness |m|
E_o = stiffness of the overlay |MPa|
E_3 = stiffness of the subgrade |MPa|

One should note that only information on the amount of traffic is needed in terms of ratio past to future traffic. In |14| it has been shown that this ratio can be determined from traffic counts; an exact knowledge on the axle load spectrum is not strictly necessary.

Furthermore one should note that only the slope of the asphalt fatigue relation needs to be known. It has been shown in sections 6.6.6 and 6.7.2 that these values can be assessed by means of the Shell mix stiffness nomographs and knowing the void content of the mix. In this way the problems of selecting an appropriate fatigue relation (see section 7.3 item c) are overcome.

The same type of equations can be developed using the relations between SCI and ε instead of the h_e vs ε relations. Using the SCI one obtains:

$$\log N_{P_1} = a_o + a_1 c_o + a_1 c_1 \log SCI - u_1 S_{\log N} \qquad \text{eq. 7.11}$$

where c_o, c_1 = constants from the relation $\log \varepsilon = c_o + c_1 \log SCI$

By using the same approach one arrives to:

$$SCI_{a.o.} = SCI_{b.o.} \sqrt[a_1 c_1]{\frac{XJ_2}{J_1}} \qquad \text{eq. 7.12}$$

where $SCI_{a.o.}$ = surface curvature index after overlaying
$SCI_{b.o.}$ = surface curvature index before overlaying

Van Gurp |15| has shown that the overlay thickness can now be obtained from:

$$\log SCI_{a.o.} = b_0 + b_2 \log SCI_{b.o.} + (b_1 + b_3 \log SCI_{b.o.} + b_4 E_0) h_0$$
$$r^2 = 0.96 \qquad \text{eq. 7.13}$$

where $b_o = -0.205$
$b_1 = -11.795$
$b_2 = 0.951$
$b_3 = -2.589$
$b_4 = -1.653 * 10^{-10}$
E_o = mix stiffness of the overlay |Pa|
h_o = thickness of the overlay |m|

As can be observed from equations 7.9 and 7.12, one needs to know values for $S_{\log N}$ and $S_{\log N+\Delta N}$ in order to be able to make overlay thickness estimations. In chapter 3 it has been shown that $S_{\log N}$ can be calculated from $S_{\log SCI_{b.o.}}$ by

$$S^2_{\log N} = a_1^2 c_1^2 S^2_{\log SCI_{b.o.}} + 0.16 \qquad \text{eq. } 7.14$$

A value for $S_{\log N+\Delta N}$ can be obtained in the following way.

From equation 7.13 one can derive the $S_{\log SCI_{a.o.}}$ by

$$S^2_{\log SCI_{a.o.}} = (b_2 + b_3 h_o)^2\, S^2_{\log SCI_{b.o.}} + b_4^2 h_o^2 S^2_{E_o} + (b_1 + b_4 E_o + b_3 \log SCI_{b.o.})^2\, S^2_{h_o} \qquad \text{eq. } 7.15$$

Application of equation 7.14 here, results in

$$S^2_{\log N+\Delta N} = a_1^2 c_1^2 S^2_{\log SCI_{a.o.}} + 0.16 \qquad \text{eq. } 7.16$$

Considering equation 7.16, one will notice that the $S_{\log N}$ after overlaying will be larger than the $S_{\log N}$ before overlaying. In reality however, one will notice that, in most cases, $S_{\log N}$ will decrease after an overlay has been applied, rather than increase. Also it will be observed that for overlaid pavements, $S_{\log N}$ will increase in time and finally one will obtain values which are larger than those before overlaying. Evidence of this latter statement has been given in chapter 3. There it has been shown that the $S_{\log N}$ values as determined on overlaid pavements are larger than the $S_{\log N}$ values of pavements that have not yet been overlaid.

7.4.3 Design of Bonded Overlays with Special Emphasis on the Reduction of Reflection Cracking

As has been mentioned in the introduction of section 7.4, cracks in the existing pavement have a large influence on the performance of the overlay. The effectivity of the overlay might be reduced to a considerable extent if cracks from the existing pavement are reflecting through the overlay. Therefore the bonded overlays, designed according to the principles described in the previous section, should be checked on the occurence of premature reflection cracking. This section describes the overlay design method that can be used to reduce reflection cracking.

In chapter 6 the assessment of the crack growth characteristics of asphalt concrete mixes has been described by means of the fracture mechanics principles. It has been shown that the crack growth can be described by

$$\frac{dc}{dN} = AK^n \qquad \text{eq. } 7.17$$

where dc/dN = increase in crack length per loading cycle |mm/cycle|
A, n = constants (see chapter 6)
K = stress intensity factor, due to the applied load $|N/mm^{1.5}|$

From equation 7.17, the life of the overlay expressed in a number of load repetitions (N) can be calculated using:

$$N = \int_{o}^{h_o} \frac{dc}{A(K(c))^n} \qquad \text{eq. 7.18}$$

where h_o = thickness of the overlay |mm|

The stress intensity factor K in relation to the crack length c should be known in order to solve equation 7.18. For pavement systems, K should be determined by means of a finite element program. This however reduces the applicability of the fracture mechanics concepts in the design of overlays, for the practising engineers. In order to overcome this problem, a large number of calculations by means of the finite element program reported in |16|,have been made by the author that should result in graphs which enable the practising engineer to estimate K in a rather simple way.

Figure 7.9 shows the finite element mesh that was used in the calculations. Also in this figure the loading geometry and the layer properties are given. As can be observed both bending and shearing conditions were studied. It should be noted that only the crack conditions as indicated in figure 7.9 were studied. This is because from the calculations on beams on elastic foundations (see chapter 6), it became apparent that no dramatic increase in the stress intensity factors could be expected if the crack depth over beam height ratio had reached a value of 0.8. For pavements this ratio is crack length over thickness of the bound layers. Figure 7.10 shows the K/K_{max} ratio in relation to the crack length over bound layer thickness ratios which were analysed here.

The results of the performed calculations are summarized in figure 7.11.

As can be observed from the results, the shear loading conditions are governing the reflection cracking process. Especially in cases where the base has a reasonable stiffness (i.e. 1200 MPa), the bending loading conditions are not important at all.

Furthermore one will notice that the thickness and stiffness of the overlay have a large influence on the magnitude of the stress intensity factors. This effect is most pronounced at the thin overlays. One will also observe that in cases where the base is cracked too, the K_2 values seem hardly to be affected by the properties of the existing pavement. Also the influence of the stiffness of the overlay is less pronounced in these cases than in cases where only the top layer of the existing pavement is cracked.

Another important result of the calculations is,that especially if rather thin overlays are used, low stiffness overlays might be in advantage over stiff overlays. This is not a very surprising result since quite often a disappointing behavior of stiff overlays can be observed in the field. It should be noted however, that a superior behavior of low stiffness bonded overlays cannot be shown by means of the classical theory,in which overlay design is based on limiting the strain in the existing pavement. For instance equation 7.13 shows that in case of bonding, high stiffness overlays should be preferred!

7.5 Summary

This chapter has been dealing with the design of bonded and unbonded overlays. Graphs and equations have been presented to assess the strain levels and values for the stress intensity factors in the existing pavement as well as in the overlay. Also it has been indicated how the overlay thickness can be determined from these values. It has been shown that the selection of the thickness and stiffness of the overlay is affected to a large extent by the adhesion conditions at the interface between overlay and existing pavement. Emphasis has been placed on the fact that bonded overlays, that are designed to upgrade the structural condition of the existing pavement, should be checked on whether premature reflection cracking might occur or not.

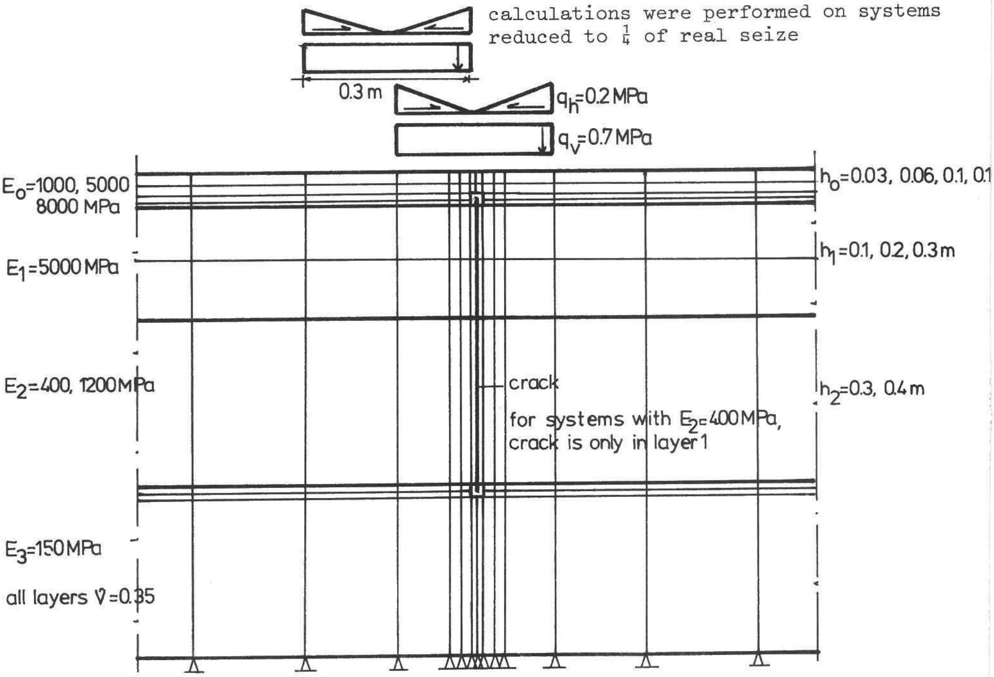

Figure 7.9 Finite Element Mesh used in the Analysis of Cracked Pavements

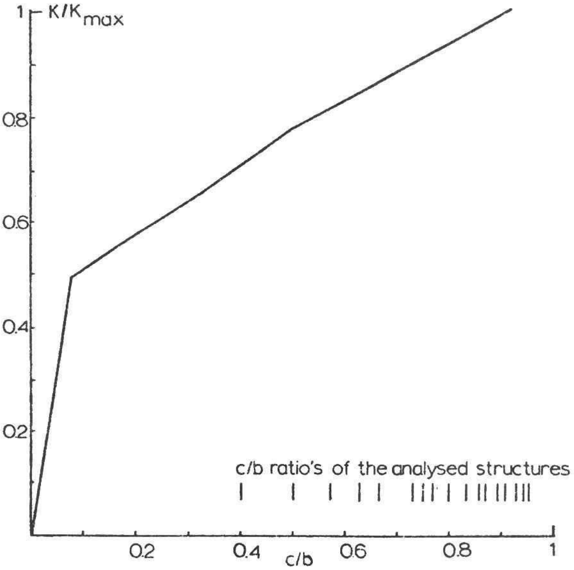

Figure 7.10 Ratio K/K_{max} in relation to the Ratio c/b

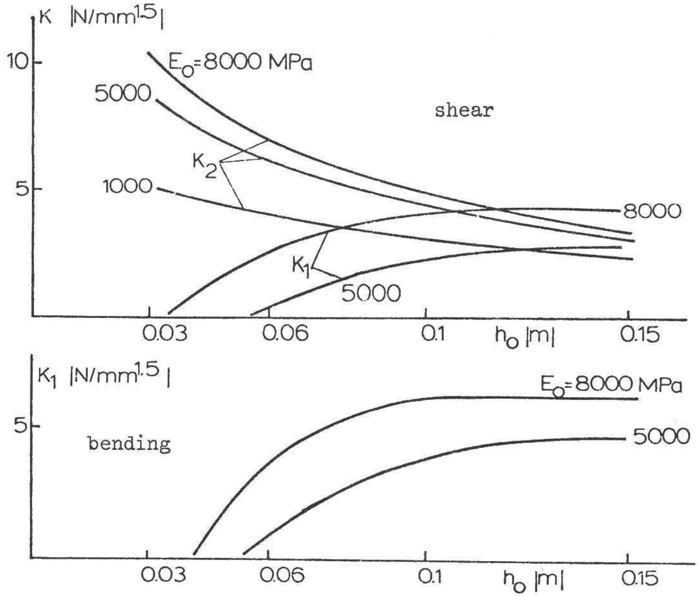

Figure 6.11a *K_1 and K_2 in relation to Overlay Thickness and Stiffness*
h_1 = 0.1 m, h_2 = 0.3 m, E_2 = 400MPa

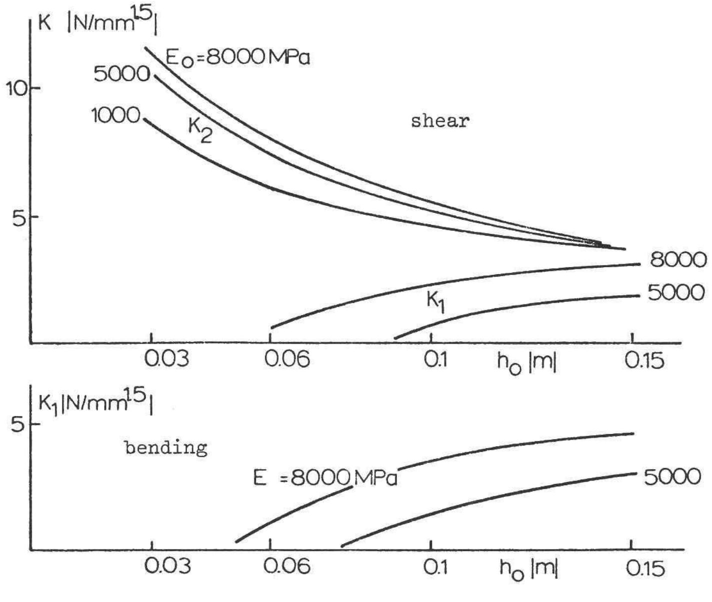

Figure 6.11b *K_1 and K_2 in relation to Overlay Thickness and Stiffness*
h = 0.1 m, h = 0.3 m, E = 1200 MPa

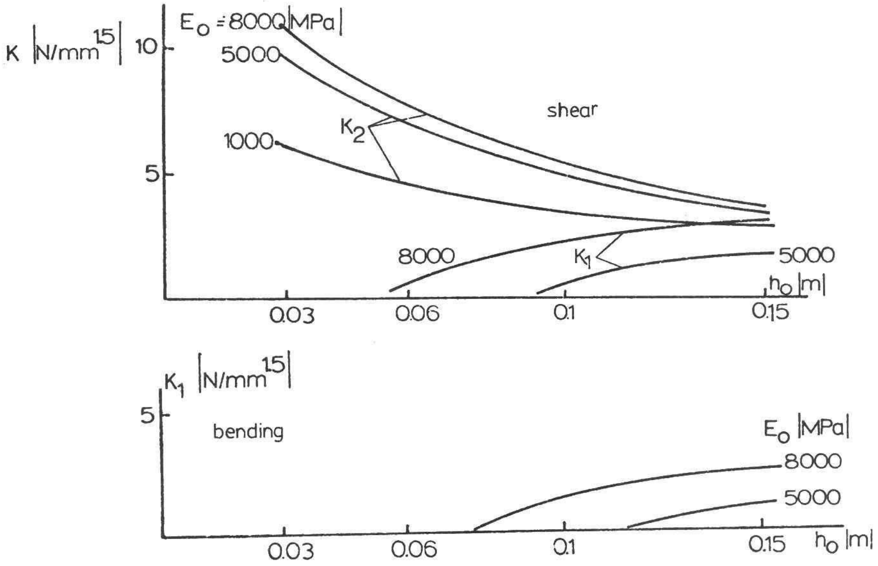

Figure 6.11c K_1 *and* K_2 *in relation to Overlay Thickness and Stiffness*
$h_1 = 0.2$ *m,* $h_2 = 0.3$ *m,* $E_2 = 400$ *MPa*

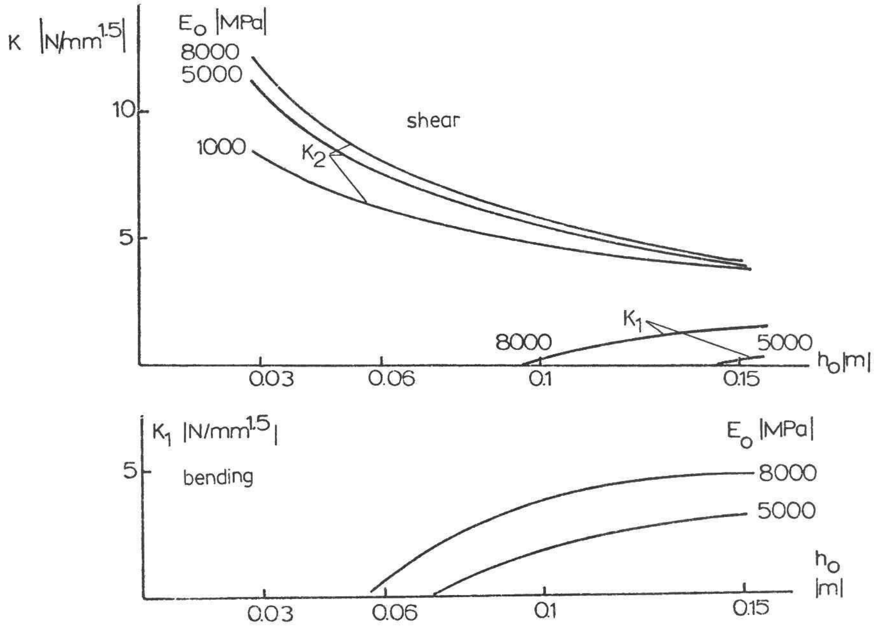

Figure 6.11d K_1 *and* K_2 *in relation to Overlay Thickness and Stiffness*
$h_1 = 0.2$ *m,* $h_2 = 0.3$ *m,* $E_2 = 1200$ *MPa*

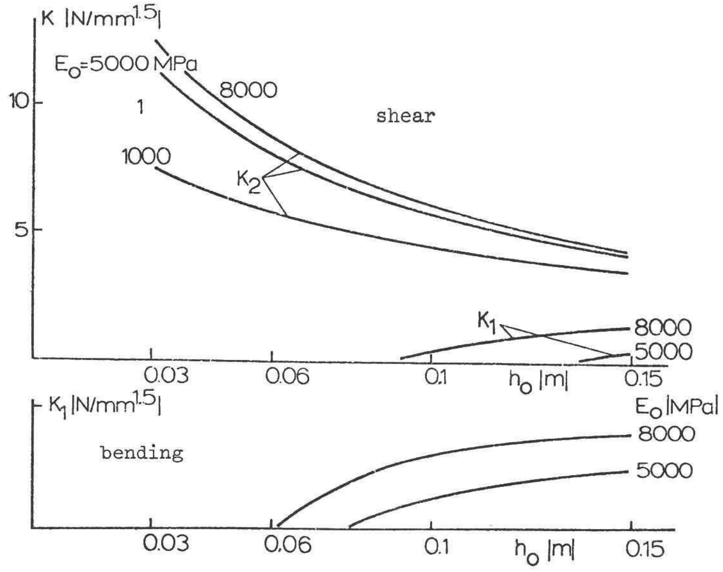

Figure 6.11e K_1 and K_2 in relation to Overlay Thickness and Stiffness
$h_1 = 0.3$ m, $h_2 = 0.3$ m, $E_2 = 400$ MPa

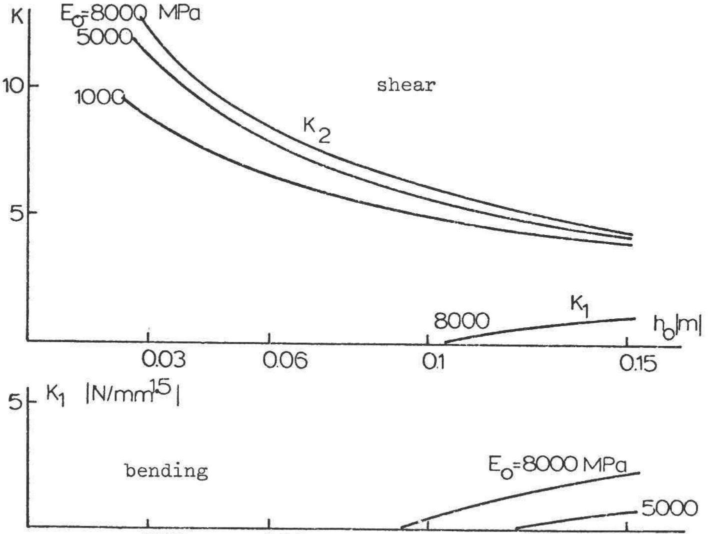

Figure 6.11f K_1 and K_2 in relation to Overlay Thickness and Stiffness
$h_1 = 0.2$ m, $h_2 = 0.4$ m, $E_2 = 1200$ MPa

it has also been shown that thick stiff overlays are not always in advantage over overlays, the thickness and stiffness of which are less.
Furthermore it is shown that in the design of overlays, the axle load spectrum of the vehicles which have trafficked the pavement, need not necessarily to be known.
Finally it is noted that, according to the procedure for the design of bonded overlays presented here, only the slope of the fatigue relation applicable to the existing pavement needs to be known. This value can be determined rather easily.

7.6 Examples

In order to illustrate the way in which the presented graphs and equations should be used, each design option will be illustrated by means of an example.

7.6.1 Unbonded Overlay

It is decided to design an unbonded overlay for a pavement the SCI of which is 120 μm. The overlay should be able to sustain 10^4 load repetitions of a dual wheel 100kN single axle. Two types of overlay material are selected the properties of which are given in table 7.1.

Table 7.1 Properties of the Overlay Materials

	material 1	material 2
E |MPa|	8.000	5.000
log k_1	-9.701	-5.82
n_1	3.308	2.342
A	9.183×10^{-7}	1.403×10^{-6}
n	2.882	2.571

By means of the fatigue relation

$$\log N = \log k_1 - n_1 \log \varepsilon \qquad \text{eq. 7.19}$$

the allowable strain levels can be calculated. For material 1 this is $\varepsilon = 7.2 \times 10^{-5}$, for material 2 the allowable strain level is $\varepsilon = 6.41 \times 10^{-5}$.
By means of figure 7.5 one can determine that an overlay thickness of 0.035 m would be sufficient for both materials if the SCI is reduced to 100 μm. By means of figure 7.6 one can determine that an overlay thickness of 0.035 m will indeed decrease the SCI from 120 μm to 100 μm.
Material 1 is selected for the overlay since it has a higher resistance to surface cracking than material 2.
From figures 7.7 and 7.8 it can be observed that the overlay will not reduce the structural deterioration of the existing pavement.

7.6.2 Bonded Overlay

A pavement with an h_{eco} of 1.0 m has deteriorated to P = 0.75. An overlay should be designed in such a way that the pavement is capable of carrying the same amount of traffic as it has been done in the past. The design level of reliability is 0.9. The characteristics of the existing pavement and the overlay which need to be known for the overlay thickness calculations, are given in table 7.2.

Table 7.2 Input for the Design Example of a Bonded Overlay

$S_{logSCI} = 0.139$

$a_1 = 4$

$c_1 = 0.943$

$b_1 = 1.963$

$(\frac{\bar{x}}{\sigma})_{E_o} = 0.1$

$(\frac{\bar{x}}{\sigma})_{h_o} = 0.1$

$P_{actual} = 0.75$

$P_{design} = 0.9$

$\frac{N}{N+\Delta N} = \frac{1}{X} = \frac{1}{2}$

$h_{e1} = 1.0$ m

$E_3 = 150$ MPa

$u_1 = 0.68$

$u_2 = 1.28$

It should be noted that the slope of the fatigue realtion which is applicable for the existing pavement (a_1) is equal to 4.
First of all the S_{logN} of the existing pavement is calculated. This is done by means of equation 7.14. Next the S_{logN} values of the overlaid pavement are calculated. This is done by means of equations 7.14, 7.15 and 7.16. In these calculations two stiffnesses for the overlay were assumed. Furthermore it was assumed that $h_o = 0.1$ m. The results of these calculations are shown in table 7.3.

Table 7.3 Results of the Example Problem of the Bonded Overlay Design

	S_{logN}	J_i	$\frac{h_{e2}}{h_{e1}}$	$h_o\|m\|$
existing pavement	0.659	2.806	--	--
overlaid pavement $E_o = 8000$ MPa	0.743	8.934	1.267	0.08
overlaid pavement $E_o = 5000$ MPa	0.730	8.598	1.260	0.09

The needed increase in equivalent layer thickness was calculated by means of equation 7.9. The input was obtained from tables 7.2 and 7.3. From the required increase in h_e, the overlay thickness was calculated by means of equation 7.10. The results are given in table 7.3.
From these results it can be concluded that the thickness of the overlay with the lower stiffness must be little more than the thickness of the stiff overlay.

7.6.3 Selection of the Type of Overlay Material to Reduce Reflection Cracking

The 0.2 m thick top layer of a pavement, with a base built up from unbound granular materials, shows a considerable amount of cracking. It is decided to apply an overlay in order to prevent the intrusion of water. The thickness of the overlay is limited to 0.03 m. For the overlay,two types of material are available, the properties of which are given in table 7.1. The question is which material should be selected.
From figure 7.11 the stress intensity factors which will occur are determined. The crack growth rate is calculated by means of equation 7.17. Since the K values will be reasonable constant with increasing crack length, the number of load cycles to failure (N_f) is calculated by means of

$$N_f = \frac{h_o}{2\,\frac{dc}{dN}} \qquad \text{eq. 7.20}$$

The overlay thickness is divided by twice the crack growth rate since the shear loading conditions do occur twice per one wheel passage.
The results of the calculations are given in table 7.4.

From this table it can be concluded that the lower stiffness overlay should be selected since it lasts longer.

Table 7.4 *Results of the Example Problem of Selecting an Overlay Material to Reduce Reflection Cracking*

E_o |MPa|	K|$N/mm^{3/2}$|	dc/dN	N
5000	9.8	4.964×10^{-4}	30216
8000	10.75	8.624×10^{-4}	17393

References

|1| ————————————
Sessions VI and VII
"Proceedings 4th Int. Conf. Structural Design of Asphalt Pavements"
Ann Arbor - 1977

|2| ————————————
Sessions III and V
"Proceedings 5th Int. Conf. Structural Design of Asphalt Pavements"
Delft - 1982

|3| SHELL INTERNATIONAL PETROLEUM COMPANY LTD
Shell Pavement Design Manual - Asphalt Pavements and Overlays for Road Traffic
London - 1978

|4| MOLENAAR, A.A.A.; ELZENAAR, J.
Graphs for the Assessment of the Stiffness Moduli and Stress and Strain Conditions in Two Layered Systems (in Dutch)
Report 7-79-115-7; Department of Civil Engineering; Lab. for Road and Railroad Research; Delft University of Technology - 1979

|5| MOLENAAR, A.A.A.; VAN DER VELDEN, G.
Tables for the Assessment of Stiffness Moduli from Deflection Measurements (in Dutch)
Report 7-77-115-2; Department of Civil Engineering; Lab. for Road and Railroad Research; Delft University of Technology - 1977

|6| SCRIVNER, F.M.; MICHALAK, C.H.; MOORE, W.M.
Calculation of the Elastic Moduli of a Two Layered Pavement System from Measured Surface Deflections
RR 123-6; Texas Transportation Institute
Texas A & M University - 1971

|7| MOLENAAR, A.A.A.
A Theoretical Study on the Assessment of the Structural Condition of Pavements using Deflection Measurements (in Dutch)
Report WB-9 (7-77-6-115-1); Department of Civil Engineering; Lab. of Road and Railroad Research; Delft University of Technology - 1977

|8| YIH YOU, Th.
Evaluation of Layered Material Properties from Measured Surface Deflections
Ph. D. Dissertation; University of Utah
Salt Lake City - 1977

|9| WARDLE, L.J.
Program CIRCLY, a Computer Program for the Analysis of Multiple Complex Circular Loads on Anisotropic Media
CSIRO; Australia - 1977

|10| MOLENAAR, A.A.A., VAN GURP, Ch.A.P.M.
Optimization of the Thickness of Asphalt Concrete
"Proceedings 10th Australian Road Research Board Conf." Vol. 10 (2)
Sidney - 1980

|11| MOLENAAR, A.A.A.; VAN GURP, Ch.A.P.M.
Verification of a Model for the Prediction of the Structural Deterioration of Pavements (in Dutch)
"Wegen", Vol. 55 no. 8 - 1981

|12| MOLENAAR, A.A.A.; VAN GURP, Ch.A.P.M.
Structural Performance Model and Overlay Design Method for Asphalt Concrete Pavements
Paper presented at the 1982 Annual Meeting of the Transportation Research Board; Washington D.C. - 1982

|13| MOLENAAR, A.A.A.; VAN GURP, Ch.A.P.M.
A Pavement Management System for Provincial Roads in the Netherlands
"Proceedings 5th Int. Conf. Structural Design of Asphalt Pavements"
Delft - 1982

|14| MOLENAAR, A.A.A.; VON DEVIVERE, M.
A New Method for the Structural Evaluation of Airfield Pavements
"Proceedings Int. Symp. on Bearing Capacity of Roads and Airfields"
Trondheim - 1982

|15| VAN GURP, Ch.A.P.M.
Personal Communication
Department of Civil Engineering; Lab. for Road and Railroad Research
Delft University of Technology - 1982

|16| CHANG, H.S.; LYTTON, R.L.; CARPENTER, S.H.
Prediction of Thermal Reflection Cracking in West Texas
RR 18-3; Texas Transportation Institute
Texas A & M University - 1976

Chapter 8

SUMMARY, CONCLUSIONS,
AND
RECOMMENDATIONS

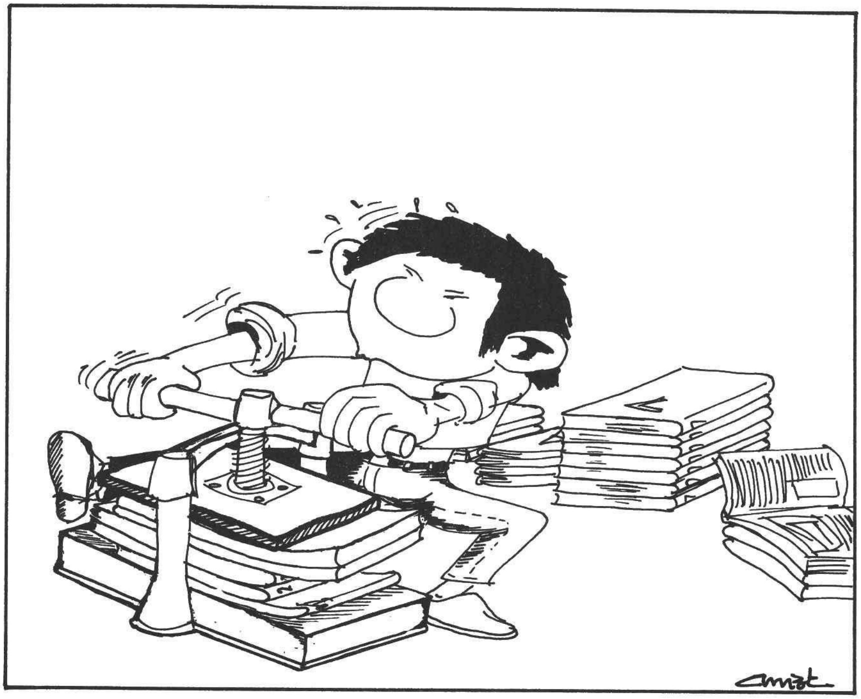

8.1 Summary

In this report, the development of a structural performance and design system for flexible road constructions and asphalt concrete overlays is described. In this overall system, five subsystems are recognized. They are:

a. Design and Performance of Flexible Road Constructions
b. Visual Condition Surveys and Planning of Maintenance
c. Deflection Testing and Analysis, Assessment of Remaining Structural Life and Future Permanent Deformation
d. Fracture and Crack Growth Characteristics of Asphalt Concrete Mixes
e. Design of Asphalt Concrete Overlays

The development of each subsystem is based on theoretical analyses of layered pavement systems, field observations on the structural behavior of in service pavements, and a fundamentally sound characterization of the cracking behavior of asphalt concrete mixes.
Special care has been given to the comprehensibility and applicability of the subsystems. Although the various equations might seem complicated, they are in fact rather simple and can be used easily by the practising engineer.
Emphasis has also been placed on how the system can be used in the development of pavement maintenance policies.
Since the various subsystems are described in separate chapters, the accomplishments will be summarized chapter by chapter.

In *chapter 3*, the development of a *new design method for flexible road constructions* has been described. This method is based on a characterization of the load carrying capacity of pavements by means of Odemark's equivalent layer thickness concept, and on relations which have been developed between the equivalent layer thickness and the maximum tensile strain in the asphaltic top layer of a three layered pavement system.
Furthermore a *structural performance model* has been developed, by which it is possible to assess the future deterioration of the pavement as a whole. This model has been verified and validated by means of in situ measurements on the load carrying capacity of pavements.
Finally a method has been presented to assess the *future permanent deformation* of pavements.
The various models and equations have been illustrated by means of examples.

Chapter 4 describes the *visual condition survey system* that has been used in this study in order to assess the structural condition of pavements in time. Furthermore *visual condition performance models* have been described which are based on condition surveys carried out on a number of sections over a five year period. Also the development of *minimum acceptance levels* for the visual condition have been described. These levels are related to the risks of increased maintenance needs due to winter damage.
Finally this chapter describes how the condition survey method can be used in conjunction with the developed performance model in the *planning of maintenance and rehabilitation.*
Examples have been given to illustrate the presented procedures.

Chapter 5 describes how the *structural condition index* and the *structural remaining life* of pavements can be determined by means of *deflection measurements*. It is shown in this chapter, that a precise knowledge on the applied number of load repetitions is not a necessity in the assessment of the remaining life. Furthermore it is described how the *shape of the structural performance model* can be determined also by means of deflection measurements.
A considerable amount of attention has been paid to those conditions where the

structural condition index cannot be determined by means of deflection measurements. It has been shown how in this case, this value can be obtained from the results of visual condition surveys.
A method has been presented to assess the *future development of permanent deformations by means of deflection measurements.* Next to a more or less classical method, a general permanent deformation model has been presented that can be used to evaluate the permanent deformation behavior of pavements.
Also in this chapter, examples have been given to illustrate the presented procedures.

In *chapter 6*, the results are presented of a study on the *fracture and crack growth characteristics of asphalt mixes.* In the introduction of this chapter, it is discussed that the problem of reflection cracking can only be analysed properly by application of the principles of fracture mechanics. After a short introduction to fracture mechanics,attention is paid to the crack growth laws that heve been developed. Special emphasis is placed on Schapery's theory since it explains how and to what extent,the so called constant of the crack growth law, are dependent on other material properties like stiffness and strength.
By means of Schapery's theory, it is shown that the constants of the crack growth law can be estimated by means of nomographs and static tests.
Furthermore this chapter describes and discusses the results of fracture toughness tests and crack growth experiments, that were performed to characterize the cracking behavior of asphalt concrete mixes. Emphasis has been placed on the relations that exist between the constants of the stress and strain based fatigue relations, and the constants of the crack growth law. Furthermore special emphasis is placed on the assessment of the *constants of the crack growth law from mix stiffness nomographs and simple static tests.*

A description of the methods that have been developed for the *design of unbonded and bonded asphalt concrete overlays,* has been given in *chapter 7.* It has been shown that the design of unbonded overlays should be based on limiting the tensile strain at the bottom of the overlay. It has been shown that the strain reduction in the existing pavement is limited if unbonded overlays are applied. Furthermore it has been shown that thin overlays are in advantage over thick overlays.
In the design of *bonded overlays*, distinction is to be made in designing overlays the primary goal of which is to *reduce the strain level in the existing pavement*, and designing overlays to *prevent reflection cracking.*
All three overlay design options are illustrated by means of an example.

8.2 Conclusions

From the results as obtained from the various parts of this study, a number of conclusions can be drawn. As has been done in the previous section, these conclusions will be given chapter by chapter.

From the work presented in chapter 3 *"Design and Performance of Flexible Road Constructions"*, the following main conclusions have been drawn:

a. The stress and strain conditions in pavements can be assessed by means of simple equations that describe the relation between the equivalent layer thickness and the maximum tensile strain in the asphalt layer.
b. Pavement deterioration is determined by the variation in layer thickness and stiffness of the various materials used in the structure, and the slope of the fatigue relation of the bound materials used.
c. Cracking which is often observed at the pavement surface and which only progresses to a limited depth into the pavement, can be explained by taking

into account the effect of inward shear forces which are normally neglected in pavement design.

d. Miner's fatigue law is considered to be applicable for the prediction of pavement cracking but not for the prediction of pavement failure. This is because pavements do not collapse in the same way as can be observed at civil engineering structures like buildings and bridges.

e. The presented design method for flexible road constructions is considered to be applicable and reliable, since the method consists of fairly simple equations, and since the performance model has been verified and validated by means of in situ measurements on the load carrying capacity of pavements.

From the results presented in chapter 4 "*Visual Condition Surveys and Planning of Maintenance*", the following conclusions have been drawn.

a. Visual condition surveys as performed in the way described in this report, are a powerful tool in the determination of the pavement condition.

b. The performance models developed in this study to describe the deterioration of the visual condition, are an extremely valuable tool in the planning of maintenance.

c. The visual condition survey method and the performance models are considered to be reliable since they are based on observations taken on a number of road sections over a five year period. Furthermore a full scale test on a 160 km long pavement netweork, has proven the applicability of the methods and models presented.

From the achievements reported in chapter 5 of this study "*Deflection Testing and Analysis; Assessment of Remaining Structural Life and Future Permanent Deformation*", the following conclusions have been drawn.

a. It is strongly recommended to perform deflection measurements immediately after the construction has been built or overlaid, in order to determine the initial equivalent layer thickness.

b. If these initial measurements are not available, then the initial equivalent layer thickness, which is needed to determine the structural condition index, can be determined by means of measurements taken between the wheelpaths.

c. The structural condition index of pavements can be determined by taking the ratio of the equivalent layer thickness as determined in the wheelpaths over the initial equivalent layer thickness.

d. If the structural condition index cannot be determined in the above described way, then a reasonable accurate estimate for this factor can be obtained using the results of visual condition surveys.

e. Depending on its stiffness, the construction can considered to be failed if the structural condition index has dropped to values between 0.65 and 0.75.

f. For the assessment of the remaining life, it is not necessary to have detailed information on the number of load repetitions to the time of measurement, in terms of equivalent single 100 kN axles. Reasonable reliable estimates can be made also if only traffic intensity data are available.

g. Due to its simplicity, the method is considered to be applicable. The method is considered to be reliable since the structural performance model that is used in the assessment of the remaining life, is verified and validated by means of in situ measurements on the load carrying capacity of pavements.

From the results of the work presented in chapter 6 "*Analysis of the Fracture and Crack Growth Characteristics of Asphalt Concrete Mixes*", the following conclusions have been drawn:

a. The principles of fracture mechanics are applicable to describe the cracking behavior of asphalt concrete mixes.

b. The constants A and N in Paris' crack growth law can be determined by means of simple static tests and available mix stiffness nomographs.

c. The exponent of the crack growth law as estimated from the slope of the compliance curve, should be corrected by a factor which depends on the air void content. For the mixes tested, the mean value for this correction factor was 2.38, its standard deviation was 0.6.

d. The exponent of the crack growth law is equal to the exponent of the stress and strain based fatigue relations, if those are determined by means of constant stress fatigue testing.

e. The type of material characterization is considered to be reliable and applicable. The presented method to assess the crack growth characteristics can be used very easily to check whether the mixes as laid in situ, will behave as was expected from tests on laboratory manufactured specimens.

The main conclusions that have been drawn from the results of chapter 7 *"Design of Asphalt Concrete Overlays"*, are as follows.

a. The design of asphalt concrete overlays should be based on two aspects which are the preservation of the condition of the existing pavement, and the prevention of cracking of the overlay itself.

b. Unbonded overlays do reduce the strain level in the existing pavement only to a limited extent.

c. In case of bonded overlays, the strain reduction in the existing pavement is the largest if the stiffness of the overlay increases.

d. In case of bonded overlays, the stress intensity factor at the tip of the crack entering the overlay, decreases if the stiffness of the overlay decreases and if its thickness increases.

e. The overlay design method is considered to be applicable and reliable. This conclusion is drawn since the method presented does give a better insight in the factors which cause the overlay to crack, and which cause a further development of deterioration of the existing pavement.

8.3 Recommendations

Considering the results of this study and considering the conclusions that have been drawn, a large number of recommendations can be given. The author however, likes to restrict himself to the most important ones.

a. First of all it is recommended to use the developed methods and models as presented in this report. Especially the visual condition performance model as well as the structural performance model, both are based on observations taken over a number of years, enable the pavement engineer to assess the future condition of the pavement network.
It is therefore recommended that these models should be used in the planning of maintenance and rehabilitation as well as in optimization programs.

b. Furthermore it is recommended to characterize the cracking behavior of pavements by means of the principles of fracture mechanics, and to use these concepts also in the design of overlays. Only by means of these concepts one will be able to solve the reflection cracking problem.

c. It is recommended that deflection measurements and visual condition surveys are conducted more detailed and carefully, in order to get a continuous updating and improving of the presented models.

d. Further research of a detailed nature should be conducted on the fracture, creep and healing properties of asphalt mixes, in order to obtain new means of extending the life of flexible road constructions and asphalt concrete overlays.

9. Het strikt hanteren van normen bij het bepalen van het al dan niet acceptabel zijn van de conditie van wegverhardingen en de planning van het onderhoud is onjuist. Niet zozeer de norm is van belang doch veel meer de periode welke ligt tussen het moment van aanleg en het moment van het bereiken van de norm.

10. Bij het dimensioneren van overlagen is het een dwingende voorwaarde dat men daarbij de levensduur van de overlaag zelf mede in de beschouwing betrekt. Voor het analyseren van het gedrag van overlagen, zijn de gebruikelijke lineair elastische meerlagenmodellen ongeschikt. Toevlucht zal daarom moeten worden gezocht in toepassing van principes uit de breukmechanica.

11. Een belangrijke voorwaarde van het door de Minister van Onderwijs en de Colleges van Bestuur zo gestimuleerde derde geldstroom onderzoek is dat het verrichten van dergelijk onderzoek financieel aantrekkelijk moet zijn voor de betrokken laboratoria. Dit moet betekenen dat:
    a. de verdiende gelden voor het grootste gedeelte ten goede moeten komen aan de betrokken laboratoria,
    b. bij de toewijzing van budgetten uit de algemene middelen de "geldverdienende" laboratoria niet evenredig aan het verdiende worden gekort,
    c. er gereserveerd kan worden voor onderhoud cq vervanging van de voor het derde geldstroom onderzoek benodigde apparatuur.

12. Daar kennis snel veroudert en Universiteiten en Hogescholen hun bestaansrecht alleen kunnen danken aan een hoge kwaliteit van onderwijs en onderzoek, zou op elke jonge wetenschappelijk medewerker in vaste dienst sterke aandrang moeten worden uitgeoefend zijn onderzoek zodanig in te richten en uit te voeren, dat het leidt tot het schrijven van een proefschrift.

13. Ten aanzien van de financiering van administratie, bestuur en beheer van het bijzonder lager en kleuteronderwijs is er geen sprake van een volgens de wet geregelde gelijkstelling met het openbaar onderwijs. Deze ongelijkheid plaatst besturen van scholen voor bijzonder onderwijs bij voorbaat in een nadelige onderhandelingspositie ten opzichte van de gemeentelijke overheid.

14. De wijze waarop gedurende de laatste jaren door binnen- en buitenlandse politici het "vijandsbeeld" nieuw leven is ingeblazen moet worden veroordeeld daar dit heeft geleid tot een agressieve defensiepolitiek.

15. De door een aantal "scenarioschrijvers" ingenomen stelling dat een kernoorlog ondanks "X Megadoden" zou zijn te winnen, is onjuist, werkt moraal en moreel vervuilend en dient derhalve te worden verworpen en bestreden.

16. De mate waarin door fietsers en voetgangers het rode verkeerslicht wordt genegeerd is recht evenredig met de mate waarin het door hen als overbodig wordt geacht.

17. Het aardige van tennis is, dat een beginneling na het enkele malen succesvol retourneren van de hem toegespeelde bal, zich reeds als een topspeler op het centre court waant.

Stellingen behorende bij het proefschrift:
"Structural Performance and Design of Flexible Road Constructions and Asphalt Concrete Overlays" van A.A.A. Molenaar

Delft, 10 mei 1983

STELLINGEN

1. Het vertalen van ingewikkelde reken- en materiaalmodellen tot voor de praktijk handzame en inzichtelijke formules, grafieken en tabellen, is een absolute voorwaarde teneinde een geaccepteerde synthese tussen theorie en praktijk in de wegbouwkunde te kunnen realiseren.

2. De oorzaak van de soms grote verschillen tussen het berekende en waargenomen gedrag van wegverhardingen is niet zozeer te wijten aan de soms vergaande schematisering van het werkelijke mechanica- en materiaalmodel, doch veel meer aan een vaak te rigoreuze schematisering van de in werkelijkheid geldende randvoorwaarden.

3. Het feit dat zeer weinig bekend is over de verschillen in karakteristieken tussen proefstukken van een bitumineus mengsel in het laboratorium vervaardigd danwel aan "het werk" ontleend, leidt tot de conclusie dat:
   a. meer onderzoek moet worden verricht teneinde de aard, omvang en oorzaak van deze verschillen vast te stellen,
   b. grote voorzichtigheid moet worden betracht bij het toepassen van vermoeiingskarakteristieken welke in het laboratorium zijn bepaald.

4. Het gebruik van in de literatuur gegeven regressievergelijkingen voor het bepalen van vermoeiingsrelaties leidt, uitgaande van dezelfde mengselkarakteristieken, tot grote verschillen. Dit wettigt de conclusie dat deze vergelijkingen het werkelijke vermoeiingsgedrag onvoldoende beschrijven. Het verdient dan ook aanbeveling dit soort vergelijkingen te baseren op die parameters waarvan door Schapery, langs theoretische weg, de invloed op het scheur- cq vermoeiingsgedrag is aangetoond.
   (Finn et al., Proc. Fourth Int. Conf. Struct. Design of Asph. Pav. 1977; Brown et al., Proc. Fourth Int. Conf. Struct. Design of Asph. Pav. 1977; Bonnaure et al., Proc. A.A.P.T. Vol. 49 1980; Schapery, Report MM 2764-73-1 Texas A&M University)

5. Het strikt toepassen van de schaderegel van Miner in de bepaling van de restlevensduur van bestaande verhardingen en de dimensionering van overlagen leidt tot op zijn minst merkwaardige conclusies, indien deze regel niet bezien wordt in relatie tot het werkelijke gedrag van wegverhardingen.

6. Het bij de oplevering uitgevoerde asfaltonderzoek zou naast een controle op het materiaal (mengselsamenstelling, holle ruimte en Marshall eigenschappen) een controle moeten inhouden van die karakteristieken die het gedrag en de levensduur van de constructie beheersen. Met name wordt hierbij gedacht aan een controle op de vervormingseigenschappen alswel een controle op de breuk- en scheurgroei-eigenschappen zoals aangenomen bij het ontwerp.

7. Het verdient sterke aanbeveling deflectiemetingen te verrichten op pas aangelegde wegconstructies en op constructies welke pas zijn overlaagd. Met behulp van deze metingen wordt een inzicht verkregen in de kwaliteit van de constructie zoals gebouwd en in het toekomstig gedrag van de verharding. Op deze wijze wordt de zo noodzakelijke koppeling gelegd tussen ontwerp en toekomstig onderhoud.

8. Het belang van globale visuele inspecties moet niet worden overschat. Gezien de kwaliteit van de globale visuele inspectiedata kunnen deze slechts in beperkte mate worden gebruikt voor de planning van het onderhoud. Dergelijke inspecties zijn vooral bedoeld als selectie van die wegvakken waarop gedetailleerde inspecties en/of metingen dienen te worden verricht.